NEUROIMAGING FINDINGS IN SLEEP DISORDERS AND CIRCADIAN DISRUPTION

EDITED BY: Xi-Jian Dai, Hengyi Rao and Kai Spiegelhalder
PUBLISHED IN: Frontiers in Neurology and Frontiers in Psychiatry

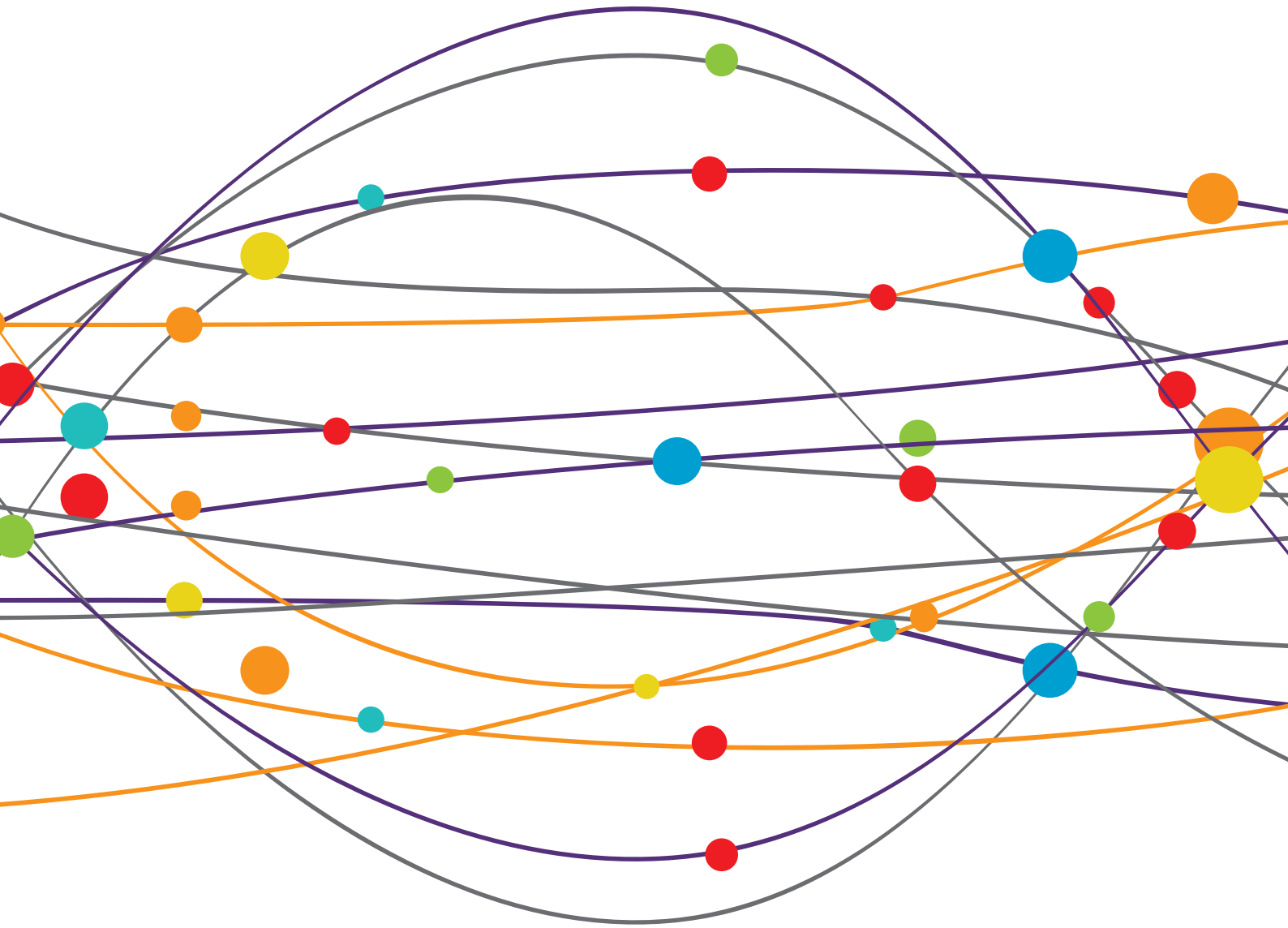

frontiers Research Topics

frontiers

ISSN 1664-8714
ISBN 978-2-88945-859-2
DOI 10.3389/978-2-88945-859-2

About Frontiers

Frontiers is more than just an open-access publisher of scholarly articles: it is a pioneering approach to the world of academia, radically improving the way scholarly research is managed. The grand vision of Frontiers is a world where all people have an equal opportunity to seek, share and generate knowledge. Frontiers provides immediate and permanent online open access to all its publications, but this alone is not enough to realize our grand goals.

Frontiers Journal Series

The Frontiers Journal Series is a multi-tier and interdisciplinary set of open-access, online journals, promising a paradigm shift from the current review, selection and dissemination processes in academic publishing. All Frontiers journals are driven by researchers for researchers; therefore, they constitute a service to the scholarly community. At the same time, the Frontiers Journal Series operates on a revolutionary invention, the tiered publishing system, initially addressing specific communities of scholars, and gradually climbing up to broader public understanding, thus serving the interests of the lay society, too.

Dedication to Quality

Each Frontiers article is a landmark of the highest quality, thanks to genuinely collaborative interactions between authors and review editors, who include some of the world's best academicians. Research must be certified by peers before entering a stream of knowledge that may eventually reach the public - and shape society; therefore, Frontiers only applies the most rigorous and unbiased reviews.
Frontiers revolutionizes research publishing by freely delivering the most outstanding research, evaluated with no bias from both the academic and social point of view. By applying the most advanced information technologies, Frontiers is catapulting scholarly publishing into a new generation.

What are Frontiers Research Topics?

Frontiers Research Topics are very popular trademarks of the Frontiers Journals Series: they are collections of at least ten articles, all centered on a particular subject. With their unique mix of varied contributions from Original Research to Review Articles, Frontiers Research Topics unify the most influential researchers, the latest key findings and historical advances in a hot research area! Find out more on how to host your own Frontiers Research Topic or contribute to one as an author by contacting the Frontiers Editorial Office: researchtopics@frontiersin.org

NEUROIMAGING FINDINGS IN SLEEP DISORDERS AND CIRCADIAN DISRUPTION

Topic Editors:
Xi-Jian Dai, Nanjing University, China
Hengyi Rao, University of Pennsylvania,United States
Kai Spiegelhalder, University of Freiburg, Germany

Each of us spends almost a third of our life asleep. Sleep is important for normal life processes including blood, metabolism, immune, endocrine, and brain activity. Neuroimaging studies of sleep disorders have not received as much attention as other psychiatric diseases. Here, we introduce some new findings in neuroimaging field of sleep disorders from five chapters in different aspects.

Citation: Dai, X.-J., Rao, H., Spiegelhalder, K., eds. (2019). Neuroimaging Findings in Sleep Disorders and Circadian Disruption. Lausanne: Frontiers Media.
doi: 10.3389/978-2-88945-859-2

Table of Contents

SECTION 2
RESTLESS LEGS SYNDROME

SECTION 3
CIRCADIAN DISRUPTION

frontiers in Neurology

EDITORIAL
published: 21 March 2019
doi: 10.3389/fneur.2019.00249

Editorial: Neuroimaging Findings in Sleep Disorders and Circadian Disruption

Xi-Jian Dai[1]*, *Hengyi Rao*[2] and *Kai Spiegelhalder*[3]

[1] Department of Medical Imaging, Jinling Hospital, Medical School of Nanjing University, Nanjing, China, [2] Division of Sleep, Perelman School of Medicine, University of Pennsylvania, Philadelphia, PA, United States, [3] Department of Psychiatry and Psychotherapy, Faculty of Medicine, Medical Center – University of Freiburg, Freiburg, Germany

Keywords: insomnia, obstructive sleep apnea, sleep deprivation, functional magnetic resonance imaging, sleep disorders, circadian rhythm

Editorial on the Research Topic

Neuroimaging Findings in Sleep Disorders and Circadian Disruption

Each of us spends almost a third of our life asleep. Thus, obviously, sleep is a necessary physical need in human life. After sleep, the tired nerve cells and the biological characteristics of long-distance signal transmission recover to normal physiological function. In general, precise control of the sleep process is the basis of normal life processes including blood, metabolism, immune, endocrine, and brain activity, and is key to plasticity formation, information processing, and function implementation [(1–5); Dai et al.].

Sleep has played a minor role as object of research for a long time. Yet, recently there is a growing public interest in sleep. Sleep disorders are a major public health problem and widespread in today's society. In modern society, more and more people undergo an increased curtailment of daily sleep because of work overtime, exam preparation, shift working and long-term working or driving, resulting in an increased incidence of sleep disorders. The disturbed and/or interrupted sleep may be associated with a number of clinical conditions and has a detrimental effect on attention, working memory, executive functioning, emotion, or even metabolism. Nowadays, important challenges are posed to sleep disorders for which approved treatments are of limited efficacy.

Although there is surprising upsurge in neuroimaging findings in addressing the brain structural and functional changes associated with sleep disorders and circadian disruption, it is still difficult to glean a consistent story about its neuropathology of brain alterations. Therefore, a more comprehensive understanding of brain structural and functional changes associated with sleep disorders and circadian disruption are needed. The aim of this Research Topic is to contribute to a better understanding of the link between brain and sleep disorders, and offer an up-to-date view on how sleep affects our brain.

PRIMARY INSOMNIA

This specific issue includes two studies focusing on insomnia. In one study by Li et al. the authors found decreased effective connectivity from right ventral and dorsal anterior insula to the precuneus, postcentral gyrus, and cerebellum posterior lobe, which negatively correlated with Pittsburgh Sleep Quality Index and Insomnia Severity Index scores.

OPEN ACCESS

Edited by:
Jan Kassubek,
University of Ulm, Germany

Reviewed by:
Menno Michiel Schoonheim,
VU University Medical Center,
Netherlands

***Correspondence:**
Xi-Jian Dai
daixjdoctor@126.com

Specialty section:
This article was submitted to Applied Neuroimaging, a section of the journal Frontiers in Neurology

Received: *02 February 2019*
Accepted: *25 February 2019*
Published: *21 March 2019*

Citation:
Dai X-J, Rao H and Spiegelhalder K (2019) Editorial: Neuroimaging Findings in Sleep Disorders and Circadian Disruption. Front. Neurol. 10:249. doi: 10.3389/fneur.2019.00249

In another study by Dai et al. the authors found that acute sleep deprivation (SD) and chronic insomnia showed widespread changes in gray matter volumes (GMVs) with shared but also distinct neurobiological representation in brain morphology. Acute SD may be associated with inhibition in sensory-informational processing with decreased GMVs in the somatosensory areas to compensate for the effects of sleep loss on advanced cognitive function, while primary insomnia may be associated with increased GMVs in several brain areas, which may be key a core predisposing or perpetuating factor of ultimately hampering the ability to initiate or maintain sleep.

SD

This specific issue also includes four studies focusing on SD and one study on narcolepsy. In one study by Satterfield et al. the authors reported that increased baseline responsiveness within reward regions are more vulnerable to SD-induced overeating. Functional activation within the ventral striatum during the multi-source interference task (MSIT) and n-back task positively correlated with total caloric and carbohydrate intake during the final 6 h (06:00–12:00) of acute SD. Activation within the middle and superior temporal gyri during the MSIT also correlated with total carbohydrates consumed.

In the second study by Dai et al. these authors found prolonged acute SD hours (20, 24, 32, 36 h SD) exhibit accumulative brain atrophic effects and recovering plasticity (after one night sleep recovery) on brain morphology, in line with the behavioral changes on attentional and working memory tasks, which may provide the neurobiological basis for attention and memory impairments following sleep loss.

The last two studies focus on finding potential indicators. Chen et al. and Kong et al. found that the amplitude of low-frequency fluctuation and short-range and long-range functional connectivity density may be potential biomarkers to describe the altered regional brain cortical activities and intrinsic brain functional organization disturbed by acute SD with high discriminating performances.

OBSTRUCTIVE SLEEP APNEA

One study by Chen et al. examined topological changes in obstructive sleep apnea and found decreased functional connectivity within the default mode network, which may contribute to the observed topological reorganization of clustering coefficient, path length, global efficiency, and Montreal cognitive assessment score. These findings may provide evidence of cognitive deficits in obstructive sleep apnea.

NARCOLEPSY WITH CATAPLEXY

One study by Fulong et al. found that both adult and juvenile narcolepsy had lower fractional low-frequency fluctuations (fALFF) values in bilateral medial superior frontal gyrus, bilateral inferior parietal lobule and supra-marginal gyrus, and higher fALFF values in bilateral sensorimotor cortex and middle temporal gyrus. The right medial superior frontal gyrus discriminated between narcolepsy and healthy controls with high degree of sensitivity (100%) and specificity (88.9%), which may suggest that the fALFF may be a helpful imaging biomarker.

RESTLESS LEGS SYNDROME

One study by Hermesdorf et al. evaluated the relationship between the genetic risks and subcortical volumes for restless legs syndrome, but neither of them gave rise to the GMV changes in the hippocampal and subcortical shapes.

CIRCADIAN DISRUPTION

The ninth study by McGlashan et al. investigated whether BOLD-fMRI activation of human suprachiasmatic area in response to light in a 30 s block-paradigm of lights on (100 lux) and lights off (<1 lux) is related to a functional outcome. They found a positive correlation between this activation and melatonin suppression, which may help to better understand the clinical vulnerability influenced by circadian disruption.

CONCLUSIONS

Together, this issue features articles that address the relationships between sleep-related disorders and the brain structure and function using neuroimaging methods. We hope this special issue will contribute to a better understanding of the link between brain and sleep disorders and offer an up-to-date view on how sleep affects our brain. We believe that this special issue will stimulate discussions in a wider public involving not only those working in the field, since both conditions cause an extreme impairment of quality of life, in particular in those patients suffering from both conditions.

AUTHOR CONTRIBUTIONS

All authors listed have made a substantial, direct and intellectual contribution to the work, and approved it for publication.

FUNDING

This work was supported by National Natural Science Foundation of China (grant No. 81701678).

REFERENCES

1. Ohayon MM, Smolensky MH, Roth T. Consequences of shiftworking on sleep duration, sleepiness, and sleep attacks. *Chronobiol Int*. (2010) 27:575–89. doi: 10.3109/07420521003749956

2. Dai XJ, Liu CL, Zhou RL, Gong HH, Wu B, Gao L, et al. Long-term total sleep deprivation decreases the default spontaneous activity and connectivity pattern in healthy male subjects: a resting-state fMRI study. *Neuropsychiatr Dis Treat*. (2015) 11:761–72, doi: 10.2147/NDT.S78335

3. Tsigos C, Chrousos GP. Hypothalamic-pituitary-adrenal axis, neuroendocrine factors and stress. *J Psychosom Res.* (2002) 53:865–71. doi: 10.1016/S0022-3999(02)00429-4
4. Dai XJ, Gong HH, Wang YX, Zhou FQ, Min YJ, Zhao F, et al. Gender differences in brain regional homogeneity of healthy subjects after normal sleep and after sleep deprivation: a resting-state fMRI study. *Sleep Med*. (2012) 13:720–7. doi: 10.1016/j.sleep.2011.09.019
5. Walker MP, Stickgold R. Sleep, memory, and plasticity. *Annu Rev Psychol*. (2006) 57:139–66. doi: 10.1146/annurev.psych.56.091103.070307

Conflict of Interest Statement: The authors declare that the research was conducted in the absence of any commercial or financial relationships that could be construed as a potential conflict of interest.

frontiers in Neurology

ORIGINAL RESEARCH
published: 08 May 2018
doi: 10.3389/fneur.2018.00317

Aberrant Effective Connectivity of the Right Anterior Insula in Primary Insomnia

*Chao Li, Mengshi Dong, Yi Yin, Kelei Hua, Shishun Fu and Guihua Jiang**

Department of Medical Imaging, Guangdong Second Provincial General Hospital, Guangzhou, China

Objective: Daytime cognitive impairment is an essential symptom of primary insomnia (PI). However, the underlying neural substrate remains largely unknown. Many studies have shown that the right anterior insula (rAI) as a key node of salience network (SN) plays a critical role in switching between the executive control network (ECN) and the default mode network (DMN) for better performance of cognitively demanding tasks. Aberrant effective connectivity (directional functional connectivity) of rAI with ECN or DMN may be one reason for daytime cognitive impairment in PI patients. Up to now, no effective connectivity study has been conducted on patients with PI during resting state. Our aim is to investigate the effective connectivity between the rAI and the other voxels in the whole brain in PI.

Materials and methods: Fifty drug-naive patients with PI and forty age- and sex-matched healthy controls were scanned using resting-state functional MRI. Seed-based Granger causality analysis was used to examine effective connectivity between the rAI, including ventral and dorsal part, and the whole brain. The effective connectivity was compared between the two groups and was correlated with clinical characteristics.

Results: Compared with controls, patients showed decreased effective connectivity from the rAI to the bilateral precuneus, the left postcentral gyrus (extending to bilateral precuneus) and the bilateral cerebellum posterior lobe, and decreased effective connectivity from the bilateral orbitofrontal cortex (OFC) to the rAI (single voxel $P < 0.001$, AlphaSim corrected with $P < 0.01$). In addition, effective connectivity from the ventral rAI to the left postcentral gyrus and from the left OFC to the ventral rAI were significantly negatively correlated with Insomnia Severity Index scores ($r = -0.28/P = 0.046$ and $r = -0.29/P = 0.038$, respectively).

Conclusion: The present study is the first to reveal aberrant effective connectivity between the SN hub (rAI) and the posterior DMN hub (precuneus) as well as decision-making region (OFC) and sensori-motor region in PI. These findings suggest an aberrant salience processing system of the rAI in PI patients.

Keywords: primary insomnia, functional magnetic resonance imaging, effective connectivity, insular cortex, executive function, cognitive impairment

OPEN ACCESS

Edited by:
Xi-jian Dai,
Medical School of Nanjing University, China

Reviewed by:
Zhen Yuan,
University of Macau, Macau
Axel Steiger,
Max-Planck-Institut für Psychiatrie, Germany

***Correspondence:**
Guihua Jiang
jiangguihua1970@163.com

Specialty section:
This article was submitted to Sleep and Chronobiology, a section of the journal Frontiers in Neurology

Received: *28 January 2018*
Accepted: *23 April 2018*
Published: *08 May 2018*

Citation:
Li C, Dong M, Yin Y, Hua K, Fu S and Jiang G (2018) Aberrant Effective Connectivity of the Right Anterior Insula in Primary Insomnia. Front. Neurol. 9:317. doi: 10.3389/fneur.2018.00317

INTRODUCTION

Primary insomnia (PI) is one of the most common health problems. It is characterized by difficulties in falling asleep, maintaining sleep, or early awakening for at least 1 month (1). The worldwide prevalence of insomnia symptoms is approximately 30–35% and approximately 10% of people are diagnosed with PI (2, 3). Insomnia is associated with cognitive impairment, daytime fatigue, and

mood disruption (4, 5). Among a series of adverse consequences caused by insomnia, daytime cognitive impairment is an essential symptom with regard to working memory, episodic memory, and some aspects of executive functioning (4, 6). However, the underlying neural substrate is incompletely understood.

Neuroimaging techniques provided a new avenue to study the pathophysiological mechanisms underlying many psychiatric disorders (7–12). With regard to PI, PET, functional, and structural MR imaging have shown abnormal glucose metabolism (13), activation (14, 15), spontaneous activity (16–18), functional or structural connectivity (19–25), or atrophic structure (26–28) related to the cognitive system, especially the salience network (SN) (11, 21), executive control network (ECN), and default mode network (DMN) (22, 29).

It is worth noting that failed reducing activities of DMN is an important feature of PI during cognitively demanding tasks, such as during working memory task (15). During working memory task, with increasing task difficulty PI patients not only showed reduced activation in task-positive regions but also showed reduced deactivation in task-negative regions (DMN) (15). This study suggested that it was not simply the failure to recruit ECN that was associated with the reduced cognitively demanding task performance, but there was a conjoint failure to deactivate the DMN. However, very little is known about the neural mechanism behind this phenomenon.

The right anterior insula (rAI) as a key node of SN can modulate activity in the ECN and the DMN in healthy individuals for better performance of cognitively demanding tasks (30, 31). It is worth noting that the modulating function of anterior insula is right lateralized. So, we only choose the right side as the seed region but not left insula. Present theory holds that one fundamental mechanism underlying cognitive control is a transient signal from the right fronto-insular cortex, which engages the brain's attention, working memory, and higher-order control processes while disengaging other systems (such as DMN) that are not immediately task relevant (30, 32). Therefore, aberrant directed functional connectivity (FC) (effective connectivity) of rAI over ECN or DMN may be one reason of daytime cognitive impairment in PI patients. Previous studies have found altered FC in the right insula in PI patients (20–22, 33–35). However, there is no research to study the effective connectivity of the rAI.

In contrast to FC, which is zero time-lagged correlation between time series at spatially distinct regions of brain, the effective connectivity is the time-lagged correlation between time series. Effective connectivity from a region *X* to another region *Y* implies that the neuronal activity in region *X* precedes and predicts the neuronal activity that occurs in region *Y*. As mentioned above, some FC studies have already been performed to study the right insula (including rAI). However, there is still no research to study the directional FC (effective connectivity) in PI. Investigation of effective connectivity in PI patients may deepen our understanding of neurologic mechanism of PI.

We employed Granger causality analysis (36–38) in resting-state functional MR imaging to investigate the rAI-centered effective connectivity. Granger causal influence from a region *X* to another region *Y* implies that the neuronal activity in region *X* precedes and predicts the neuronal activity that occurs in region *Y* (38). Thus, the whole-brain Granger causal analysis is a useful approach to study the effective connectivity that may exist across networks. In contrast to undirected FC which does not support inferences about directed (causal) brain connections, effective connectivity refers to the influence that one neural system exerts over another and quantifies the directed coupling among brain regions. In addition to Granger causal analysis, there are also several ways to capture the directional brain dynamics, such as dynamic causal modeling and structural equation modeling. Granger causal analysis has been widely used to study effective connectivity in normal brains (30), schizophrenia (38), and major depressive disorders (37). To date, to the best of our knowledge, no studies have been published reporting effective connectivity in PI patients. The purpose of this study was to analyze the effective connectivity between the rAI and the whole brain in PI patients using first-order Granger causality analysis and its association with sleep and emotion scales of PI. We hypothesized that the effective connectivity between rAI and ECN or DMN was disrupted.

MATERIALS AND METHODS

Participants

This prospective study was approved by the ethics committee of the Guangdong Second Provincial General Hospital. All PI patients were recruited from the Department of Neurology at Guangdong Second Provincial General Hospital, Guangzhou, China from April 2010 to May 2016. Written informed consent was obtained from all patients. The inclusion criteria for PI patients were (a) all patients must meet Diagnostic and Statistical Manual of Mental Disorders, Fourth Edition (DSM-IV) for diagnosis of PI; (b) patients had been complaining of difficulty falling asleep, maintaining sleep, or early awakening for at least 1 month; (c) patients had no other sleep disorders such as hypersomnia, parasomnia, sleep-related movement disorder, or other psychiatric disorders; (d) patients were younger than 60 years old; (e) free of any psychoactive medication at least 2 weeks prior to and during the study; and (f) patients were right-hand dominant as assessed with the Edinburgh Handedness Inventory. Exclusion criteria were as follows: (a) patients had an abnormal signal in any region of the brain verified by conventional T1-weighted or T2-fluid-attenuated inversion recovery MR imaging; (b) the insomnia disorder was caused by organic disease or severe mental disease such as secondary to depression or generalized anxiety; (c) other sleep disorder; (d) women who were pregnant, nursing, or menstruating; and (e) head motion more than or equal to 1.5 mm or 1.5° during MR imaging. Then three patients were discarded. Finally, 50 PI patients who met the requirements were included in the study.

A total of 40 age-, gender-, and education-matched healthy control (HC) subjects were recruited (17 men, 23 women; mean age, 39.38 ± 9.26 years) from the local community by using advertisements. Each HC subject gave written informed consent. HCs must met the following criterion: (a) Insomnia Severity Index (ISI) score was less than 7; (b) no history of swing shifts, shift work, or sleep complaints; (c) no medication or substance abuse

such as caffeine, nicotine, or alcohol; (d) no brain lesions or prior substantial head trauma, which was verified by conventional T1-weighted or T2-fluid-attenuated inversion recovery MR imaging; (e) no history of psychiatric or neurological diseases; (f) head motion less than 1.5 mm or 1.5° during MR scan; and (g) right-hand dominant. Three controls were discarded due to head motion.

Sleep and Emotion Scales

Several questionnaires were filled out by study participants. These questionnaires included the ISI (39), the Pittsburgh Sleep Quality Index (PSQI) (40), the Self-rating Anxiety Scale (SAS) (41), and the Self-rating Depression Scale (SDS) (42).

MR Imaging

Resting-state functional MR imaging data were acquired using a 1.5 T MR scanner (Achieva Nova-Dual; Philips, Best, the Netherlands) in the Department of Medical Imaging, Guangdong Second Provincial General Hospital. To minimize head movements, a belt and foam pads were used. During the scanning, subjects were instructed to rest with their eyes closed and remain still but emphatically without falling asleep. The functional MR images were acquired in about 10 min using a gradient-echo planar imaging sequence as follows: interleaved scanning, repetition time = 2,500 ms, echo time = 50 ms, matrix = 64 × 64, field of view = 224 mm × 224 mm, flip angle = 90°, section thickness = 4 mm, gap = 0.8 mm, 27 axial slices, and 240 volumes.

Data Preprocessing

The Data Processing Assistant for Resting-State Functional MR Imaging toolbox[1] (version 2.3) was used to process the resting-state functional MR imaging data. Volumes at the first 10 time points were discarded so that magnetization reached a steady state and subjects had adapted to the MR scanning noise. The slice timing and realignment for head motion correction were conducted on the remaining images. Then, the realigned images were spatially normalized to the Montreal Neurological Institute template by applying the EPI template, and each voxel was resampled to 3 mm × 3 mm × 3 mm. We spatially smoothed the spatially normalized images with a 6-mm full-width half-maximum isotropic Gaussian kernel. In order to reduce effects of low-frequency drift and high-frequency noise, we processed the data to remove linear trends and filtered temporally (band-pass, 0.01–0.08 Hz). Nine nuisance covariates, including cerebrospinal fluid signals, white matter signals, global brain signal, and six head motion parameters were regressed from the imaging data. The residuals of these regressions were used for the following analysis.

Granger Causality Analysis

We calculated the effective connectivity of the time series of the dorsal and ventral rAI on every voxel in the whole brain (X to Y) and the effective connectivity of the time series of every voxel in the whole brain on the dorsal and ventral rAI (Y to X). The mean temporal-domain bold signals for the dorsal and ventral rAI are displayed in Figure S10 in Supplementary Material. Regions of interest (ROI) in the dorsal and ventral rAI were selected based on the brain atlas based on connectional architecture (43).[2] Bivariate first-order coefficient-based voxel-wise Granger causality analysis was performed using REST-GCA (44). We followed Chen's (37) extended model as following:

$$Y_t = \sum_{i=1}^{p} A_i X_{(t-i)} + \sum_{i=1}^{p} B_i Y_{(t-i)} + CZ_t + \varepsilon_t$$

$$X_t = \sum_{i=1}^{p} A_i' Y_{(t-i)} + \sum_{i=1}^{p} B_i' X_{t-i} + C' Z_t + \varepsilon_t'$$

where Y_t is the BOLD time series of one voxel in the brain at time t; X is the BOLD time series of seed region; Z_t is a $q \times 1$ vector containing exogenous variables (covariates or confounds) at time t; ε_t is the error term; p and q are the number of lags and confounds, respectively; A_i is the signed path coefficient at time lag i ($i = 1, \ldots, p$); B_i is the autoregression coefficient. In the present study, the number of lags $p = 1$ (1 TR = 2.5 s).

Explanation of the coefficient was the same as the previous study (38). The positive coefficient is referred as excitatory influence and *vice visa*.

Statistical Analysis

Differences in age, education level, ISI, PSQI, SAS, and SDS scores between PI patients and HCs were compared by using two-sample t tests. Differences associated with gender between the two groups were assessed by using chi-squared tests.

First, the effective connectivity maps were analyzed using one-sample t-test for the entire sample (both PI patients and HCs) with an uncorrected $P < 0.001$, cluster size = 50. Then, between-group differences in effective connectivity were compared by using two-sample t tests in a voxel-by-voxel fashion with age, sex, and education level imported as covariates. Multiple comparisons were corrected by an AlphaSim method implemented in the DPABI software [DPABI version 2.3, Data Processing & Analysis for (Resting-State) Brain Imaging] (45) and using significant corrected thresholds of $P < 0.01$ with combined with single voxel $P < 0.001$. The estimated FWHM (x–y–z) for the 4T maps (from ventral rAI, from dorsal rAI, to ventral rAI, and to dorsal rAI) were 6.9857–7.1202–7.9652, 5.8353–5.9840–6.7710, 9.1891–9.4015–9.4269, and 5.0546–5.1626–5.8403. The cluster size thresholds for the 4T maps were 22, 16, 48, and 26.

Besides, we used permutation threshold-free cluster enhancement (TFCE) correction method to perform statistical analysis (46, 47). The permutation TFCE correction method implements correction through a permutation testing approach which controls family-wise error rate by comparing voxel-wise statistics (TFCE) to the maximal statistics obtained from repeating the analysis with randomized data. The Matlab scripts for the permutation TFCE correction have been made available online: https://github.com/markallenthornton. ROI were defined as 6-mm-diameter spheres centered on voxels that exhibited the

[1] http://www.restfMRI.net/forum/DPARSF (Accessed: July, 2017).

[2] http://atlas.brainnetome.org/ (Accessed: July, 2017).

largest absolute *t* value in each of the significant clusters in the *t* map of between-group differences in effective connectivity. Then, effective connectivity was calculated for each subject by averaging the values of effective connectivity across all voxels within each of the ROI and correlated with the sleep and emotion scales using Pearson's correlation analysis.

RESULTS

Sleep and Emotion Scales

As **Table 1** shown, the PI patients and the controls showed no significant differences in age ($P = 0.37$), sex ($P = 0.81$), and education level ($P = 0.28$). PI patients had higher ISI, PSQI, SAS, and SDS scores than those of HCs (all $P < 0.001$).

Effective Connectivity

One-sample *t*-test showed that the rAI exerted excitatory influence on the bilateral dorsolateral prefrontal cortex (DLPFC), the inferior parietal regions, the cingulate gyrus, and the left cerebellar crus. Inhibitory influence of the rAI was noted on the left precentral gyrus, the postcentral gyrus, and the bilateral occipital lobe. Furthermore, the bilateral DLPFC, the inferior parietal regions, and the cingulate gyrus, in turn, had inhibitory influence on the rAI, and in the same way, the bilateral occipital lobe had excitatory influence on the rAI. It is worth noting that the results of one-sample *t*-test were very similar to those of previous study (38). The results of the one-sample *t* tests are presented in Figures S4–S7 in Supplementary Material.

Compared with HCs, patients with PI showed negative effective connectivity (inhibitory influences) from the ventral rAI to the left precuneus, the left postcentral gyrus extending to the bilateral precuneus, and bilateral cerebellum posterior lobe including the bilateral cerebelum_crus1 and left cerebelum_6 (**Figure 1A**), and negative effective connectivity from the dorsal rAI to the bilateral precuneus and left postcentral gyrus extending to the left precuneus (**Figure 1B**). Also, patients with PI showed negative effective connectivity from bilateral orbitofrontal cortex (OFC) to ventral rAI (**Figure 1C**) (single voxel $P < 0.001$, corrected by AlphaSim correction with cluster $P < 0.01$). All above results of between-group differences in effective connectivity are shown in **Table 2**. Figures S1–S3 in Supplementary Material showed the bar graphs demonstrating the mean effective connectivity values in the ROI defined as 6-mm-diameter spheres centered on voxels that exhibited the largest absolute *t* value in each of the significant clusters in the *t* map.

Results from permutation TFCE correction (5,000 times permutation, default parameters, FWE corrected, $P < 0.05$) were very similar to those derived from our parameter statistical method (two-sample *t* test with AlphaSim correction). Therefore, we only discussed these results. Figure S8 in Supplementary Material showed the *P* map of the permutation TFCE correction.

TABLE 1 | Demographic, sleep, and emotional scales of all participants.

Variable	PI group ($n = 50$)	HC group ($n = 40$)	*P* value
Sex (M/F)	20/30	17/23	0.81[a]
Age (years)	40.06 ± 8.52	39.38 ± 9.26	0.37[b]
Duration (months)	40.31 ± 44.09	N/A	N/A
Education (years)	7.56 ± 3.24	8.32 ± 3.43	0.28[b]
PSQI	12.55 ± 2.95	5.68 ± 2.46	<0.001[b]
ISI	19.44 ± 3.18	5.78 ± 2.34	<0.001[b]
SAS	51.83 ± 9.27	41.69 ± 5.61	<0.001[b]
SDS	56.03 ± 7.83	42.75 ± 2.64	<0.001[b]

Unless otherwise noted, data are mean ± SD.
PSQI, Pittsburgh Sleep Quality Index; ISI, Insomnia Severity Index; SAS, Self-rating Anxiety Scale; SDS, Self-rating Depression Scale; PI, primary insomnia.
[a]*The P value was obtained by using chi-square test.*
[b]*The P value was obtained by using two-sample t tests.*

Relationships Between Effective Connectivity and Sleep and Emotion Scales

As **Figure 2** shown, effective connectivity from the ventral rAI to the left postcentral gyrus extending to the bilateral precuneus and from the left OFC to the ventral rAI were significantly negatively correlated with ISI scores in PI group ($r = -0.28/P = 0.046$ and $r = -0.29/P = 0.038$, respectively).

Effective connectivity from the ventral rAI to the left precuneus was significantly negatively correlated with PSQI and ISI scores in HC group ($r = -0.31/P = 0.047$ and $r = -0.32/P = 0.045$, respectively). Figure S9 in Supplementary Material shows the results of the correlation analysis of the HC group.

DISCUSSION

The present study investigated the effective connectivity between the rAI and the whole brain in PI patients. Our findings showed aberrant effective connectivity of rAI (a key node of SN) with the posterior DMN hub (precuneus) as well as regions involved in decision-making (OFC) and regions involved in sensori-motor function in PI. In addition, effective connectivity from the ventral rAI to the left postcentral gyrus extending to the bilateral precuneus and from the left OFC to the ventral rAI were significantly negatively correlated with ISI scores in PI group.

In contrast to FC which does not support inferences about directional brain connections, effective connectivity refers to the influence that one neural system exerts over another and quantifies the directional connectivity among brain regions (38). Consequently, effective connectivity may provide new insight into the neurological mechanism of insomnia.

The important findings in the current study were aberrant effective connectivity from the ventral rAI to the left precuneus and from the dorsal rAI to the bilateral precuneus at resting state. The rAI was a hub node of SN which is involved in detecting and orienting to both external and internal salient stimuli and events (31, 32). The precuneus was a hub node of DMN which is involved in self-referential/internally oriented processes (48). Previous study using chronometry and Granger causality analysis confirmed that rAI plays a critical and causal role in switching between the ECN and the DMN during visual attention tasks, oddball tasks, and even resting state (30). Furthermore, the present theory holds that one fundamental mechanism underlying cognitive control is a transient signal

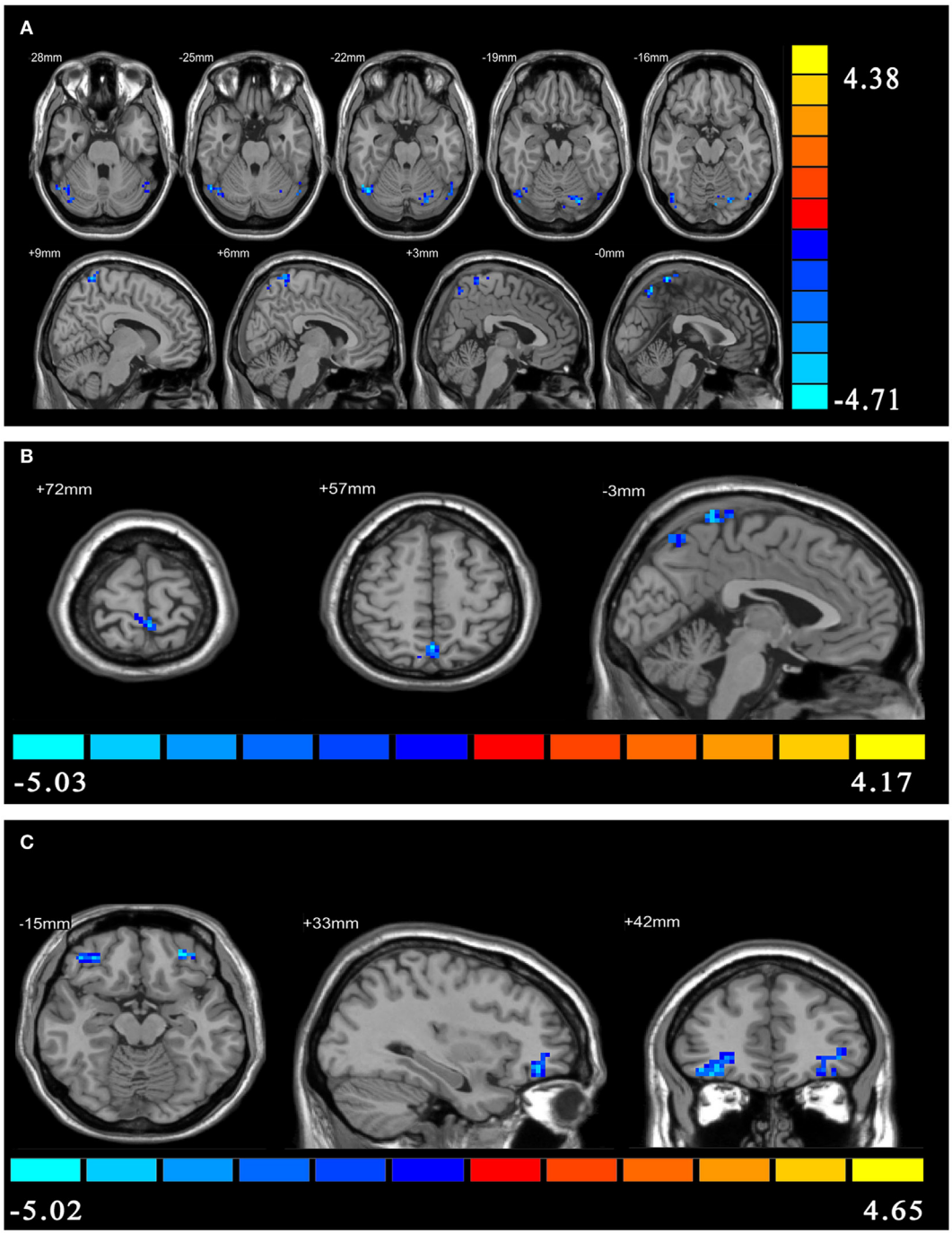

FIGURE 1 | The between-group differences in effective connectivity. **(A)** The between-group differences in effective connectivity from ventral right anterior insula (rAI) to the whole brain. **(B)** The between-group differences in effective connectivity from dorsal rAI to the whole brain. **(C)** The between-group differences in effective connectivity from the whole brain to ventral rAI.

from the right fronto-insular cortex, which engages the brain's attentional, working memory, and higher-order control processes while disengaging other systems (such as DMN) that are not immediately task relevant (30, 32). Interestingly, a recent study found that PI patients showed both reduced activation in task-related working memory regions and reduced deactivation in regions of the DMN with increasing task difficulty (15). This finding demonstrated a failed disengagement from DMN during working memory tasks in PI patients. It is a complement to previous studies that only found decreased metabolism or decreased activation in cognitive or task-related regions (13, 14). In our study, although we did not found any altered effective

TABLE 2 | Between-group differences in Granger causal influences.

Brain regions	MNI coordinates (mm)	Cluster size (voxels)	*T* values (peak)	Mean values of causal influences in ROI	
				PI group	HC group
From ventral rAI to following regions					
Left precuneus	(0 −63 57)	35	−4.61	−0.21 ± 0.33	0.09 ± 0.35
Left postcentral gyrus (extending to bilateral precuneus)	(−3 −45 72)	68	−4.94	−0.12 ± 0.24	0.26 ± 0.48
Left cerebelum_Crus1	(−48 −72 −15)	34	−4.28	−0.07 ± 0.20	0.09 ± 0.23
Right cerebelum_Crus1	(48 −66 −21)	72	−4.97	−0.17 ± 0.31	0.08 ± 0.24
Left cerebelum_6	(−24 −78 −18)	37	−4.66	−0.08 ± 0.20	0.13 ± 0.21
From dorsal rAI to following regions					
Bilateral precuneus	(0 −63 57)	45	−5.35	−0.33 ± 0.45	0.14 ± 0.41
Left postcentral gyrus (extending to left precuneus)	(−3 −45 72)	28	−4.94	−0.13 ± 0.30	0.26 ± 0.43
From following regions to ventral rAI					
Left orbitofrontal cortex	(−30 45 −15)	90	−5.34	−0.04 ± 0.04	0.00 ± 0.02
Right orbitofrontal cortex	(33 42 −15)	86	−4.93	−0.04 ± 0.05	0.00 ± 0.02

ROI, regions of interest, which was defined as 6-mm-diameter spheres centered on voxels that exhibited the largest absolute t value in each of the significant clusters in the t map of between-group differences in Granger causal influences.
PI, primary insomnia; HC, healthy control, rAI; right anterior insula.

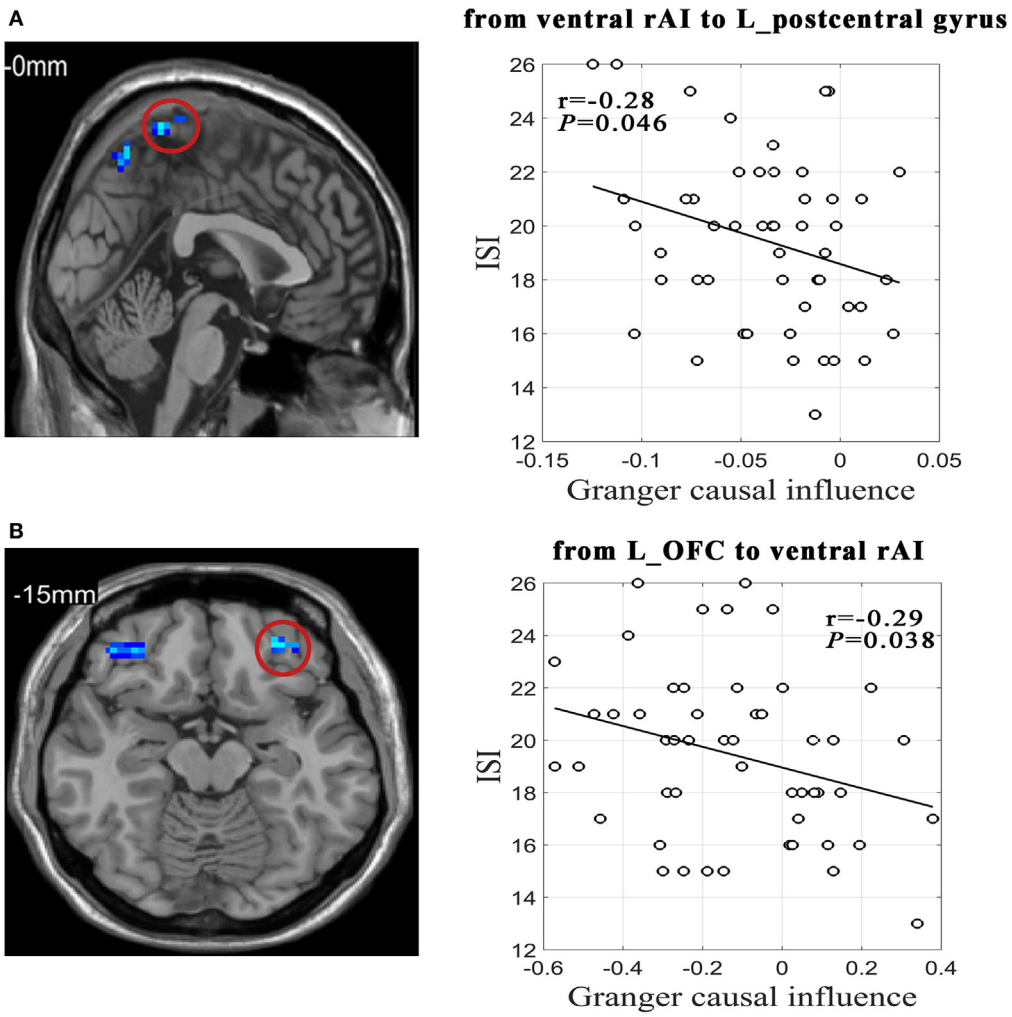

FIGURE 2 | Relationships between effective connectivity and sleep and emotion scales in primary insomnia group. **(A)** Scatter plot shows correlation between effective connectivity value from ventral right anterior insula (rAI) to left postcentral gyrus extending to bilateral precuneus and Insomnia Severity Index (ISI) scores. **(B)** Scatter plot shows correlation between effective connectivity value from left orbitofrontal cortex (L_OFC) to ventral rAI and ISI.

connectivity from rAI to ECN, we found aberrant effective connectivity from the rAI to regions of DMN at resting state or baseline condition. Our findings offer a parsimonious explanation for failed disengagement from DMN during cognitively demanding tasks (especially the working memory task) in PI patients.

Another finding was that PI patients showed aberrant effective connectivity from the bilateral OFC to the ventral rAI. Besides, the effective connectivity from left OFC to ventral rAI was significantly negatively correlated with ISI scores in PI group. The OFC is an important brain area responsible for emotion and decision-making (49). Previous study showed that PI patients' speed are slower than controls on a vigilance task which only need decision-making (50). Impaired decision-making may also lead to a lack of ability to solve problems in the insomnia patients (51). Indeed, PI patients showed reduced orbitofrontal gray matter volume or density (27, 28). Recent studies found that rAI also acted as a main outflow hub within SN for easier decision-making task (52). Together with previous studies, our findings suggest an abnormal OFC-rAI circuit in PI patients, which might be one of underlying substrate of impaired decision-making observed in PI patients.

We also found that PI patients showed aberrant effective connectivity from the rAI to the left postcentral gyrus (extending to bilateral precuneus) and the bilateral cerebellum posterior lobe. In addition, effective connectivity from ventral rAI to the left postcentral gyrus was significantly negatively correlated with ISI scores in the PI group. The postcentral gyrus and the cerebellum are locations of primary somatosensory cortex and motor control area, respectively. In recent years, several studies have also frequently reported abnormal spontaneous brain activity in the cerebellum posterior lobe as well as the postcentral gyrus in PI (16, 17, 53). On the other hand, existing evidence suggests the anterior insula and the anterior cingulate cortex serve as complementary limbic sensory and motor regions. They work together, similar to the somatosensory and motor cortices (54, 55). Relative to rAI, which is high on the level of the hierarchy due to its function of switching between other large-scale networks, the postcentral gyrus and the cerebellum is lower in the hierarchy (32, 56). Therefore, our findings that aberrant effective connectivity from the rAI to the left postcentral gyrus and the bilateral cerebellum posterior lobe may reflect aberrant top-down sensory and motor control of rAI in PI patients.

Our study had several limitations. First, it was a cross-sectional study, and we cannot directly identify the causal relation between PI and the abnormal effective connectivity. Longitudinal studies may help address this question. Second, we did not directly investigate the inter-network effective connectivity among SN, ECN, and DMN using independent component analysis, even though selected seed regions of rAI for Granger causality analysis was the widely recognized hub node of SN. Future researchers can use independent component analysis to study inter-network effective connectivity in PI. Third, analyses of combination of mental chronometry and Granger causality analysis will increase our understanding of PI. However, we did not do these analyses for technical reasons. Future study is suggested to do these analyses. Finally, the activity of the brain at resting state is not static but is a highly dynamic system. Therefore, static effective connectivity may not be enough to fully characterize the human brain. Future study is suggested to use dynamic FC to investigate the brain in PI.

In summary, we for the first time found aberrant effective connectivity of rAI (a key node of SN) with the posterior DMN hub (precuneus) as well as regions involved in decision-making (OFC) and regions involved in sensori-motor function in PI. These findings suggest an aberrant salience processing system of the rAI, which may be a candidate substrate for cognitive impairment, especially the impairment of working memory and decision-making in PI patients.

ETHICS STATEMENT

This study was carried out in accordance with the recommendations of "ethics committee of the Guangdong Second Provincial General Hospital" with written informed consent from all subjects. All subjects gave written informed consent in accordance with the Declaration of Helsinki. The protocol was approved by the "ethics committee of the Guangdong Second Provincial General Hospital."

AUTHOR CONTRIBUTIONS

Study concepts/study design or data acquisition, manuscript drafting for important intellectual content, and approval of final version of submitted manuscript: all authors; literature research: CL, YY, KH, SF, and GJ; clinical studies: CL, MD, and GJ; experimental studies: CL and GJ; statistical analysis: CL and SF; and manuscript editing: CL, MD, and GJ.

FUNDING

This study has received funding by the National Natural Science Foundation of China (grant no.: 81471639); the National Natural Science Foundation of China (grant no.: 81771807); the Natural Science Foundation of Guangdong Provincial (grant no.: 2015-A030313723); the Science and Technology Foundation of Guangdong Province (grant no.: 2016A020215125; 2017A020215077); and the Science and Technology Foundation of Guangzhou City (grant no.: 201607010056).

SUPPLEMENTARY MATERIAL

The Supplementary Material for this article can be found online at https://www.frontiersin.org/articles/10.3389/fneur.2018.00317/full#supplementary-material.

FIGURE S1 | The bar graphs demonstrating the mean effective connectivity values in the regions of interest defined as 6-mm-diameter spheres centered on voxels that exhibited the largest absolute *t* value in each of the significant clusters in the *t* map. Error bars indicate SD. Abbreviations: L_CER_crus1, left cerebelum_crus1; R_CER_crus1, right cerebelum_crus1; L_CER_6, left cerebelum_6; L_precuneus, left precuneus; L_postcentral gyrus, left postcentral gyrus (extending to bilateral precuneus).

FIGURE S2 | The bar graphs demonstrating the mean effective connectivity values in the regions of interest defined as 6-mm-diameter spheres centered on voxels that exhibited the largest absolute *t* value in each of the significant clusters in the *t* map. Error bars indicate SD. Abbreviations: Bi_precuneus, bilateral precuneus; L_postcentral gyrus, left postcentral gyrus (extending to left precuneus).

FIGURE S3 | The bar graphs demonstrating the mean effective connectivity values in the regions of interest defined as 6-mm-diameter spheres centered on voxels that exhibited the largest absolute *t* value in each of the significant clusters in the *t* map. Error bars indicate SD. Abbreviations: R_OFC, right orbitofrontal cortex; L_OFC, left orbitofrontal cortex.

FIGURE S4 | The effective connectivity from ventral right anterior insula to the whole brain.

FIGURE S5 | The effective connectivity from dorsal right anterior insula to the whole brain.

FIGURE S6 | The effective connectivity from the whole brain to ventral right anterior insula.

FIGURE S7 | The effective connectivity from the whole brain to dorsal right anterior insula.

FIGURE S8 | The statistical results of the permutation threshold-free cluster enhancement correction (5,000 times permutation, default parameters, FWE corrected, $P < 0.05$). **(A)** Between-group differences in effective connectivity from ventral right anterior insula (rAI) to the whole brain. **(B)** Between-group differences in effective connectivity from dorsal rAI to the whole brain. **(C)** Between-group differences in effective connectivity from the whole brain to ventral right anterior insula.

FIGURE S9 | Relationships between effective connectivity and sleep and emotion scales in healthy control group.

FIGURE S10 | Temporal-domain bold signals for seed regions.

REFERENCES

1. Gmitrowicz A, Kucharska A. [Developmental disorders in the fourth edition of the American classification: diagnostic and statistical manual of mental disorders (DSM IV – optional book)]. *Psychiatr Pol* (1994) 28(5):509–21.
2. Morin CM, Drake CL, Harvey AG, Krystal AD, Manber R, Riemann D, et al. Insomnia disorder. *Nat Rev Dis Primers* (2015) 1:15026. doi:10.1038/nrdp.2015.26
3. Ohayon MM. Epidemiology of insomnia: what we know and what we still need to learn. *Sleep Med Rev* (2002) 6(2):97–111. doi:10.1053/smrv.2002.0186
4. Fortier-Brochu É, Beaulieu-Bonneau S, Ivers H, Morin CM. Insomnia and daytime cognitive performance: a meta-analysis. *Sleep Med Rev* (2012) 16(1):83–94. doi:10.1016/j.smrv.2011.03.008
5. Roth T, Roehrs T. Insomnia: epidemiology, characteristics, and consequences. *Clin Cornerstone* (2003) 5(3):5–15. doi:10.1016/S1098-3597(03)90031-7
6. Fulda S, Schulz H. Cognitive dysfunction in sleep disorders. *Sleep Med Rev* (2001) 5(6):423–45. doi:10.1053/smrv.2001.0157
7. Liu F, Guo W, Fouche JP, Wang Y, Wang W, Ding J, et al. Multivariate classification of social anxiety disorder using whole brain functional connectivity. *Brain Struct Funct* (2015) 220(1):101–15. doi:10.1007/s00429-013-0641-4
8. Liu F, Guo W, Liu L, Long Z, Ma C, Xue Z, et al. Abnormal amplitude low-frequency oscillations in medication-naive, first-episode patients with major depressive disorder: a resting-state fMRI study. *J Affect Disord* (2013) 146(3):401–6. doi:10.1016/j.jad.2012.10.001
9. Sommer IEC, Ramsey NF, Kahn RS. Language lateralization in schizophrenia, an fMRI study. *Schizophr Res* (2001) 52(1):57–67. doi:10.1016/S0920-9964(00)00180-8
10. Chen CH, Suckling J, Lennox BR, Ooi C, Bullmore ET. A quantitative meta-analysis of fMRI studies in bipolar disorder. *Bipolar Disord* (2011) 13(1):1–15. doi:10.1111/j.1399-5618.2011.00893.x
11. Khazaie H, Veronese M, Noori K, Emamian F, Zarei M, Ashkan K, et al. Functional reorganization in obstructive sleep apnoea and insomnia: a systematic review of the resting-state fMRI. *Neurosci Biobehav Rev* (2017) 77:219–31. doi:10.1016/j.neubiorev.2017.03.013
12. Sheng J, Shen Y, Qin Y, Zhang L, Jiang B, Li Y, et al. Spatiotemporal, metabolic, and therapeutic characterization of altered functional connectivity in major depressive disorder. *Hum Brain Mapp* (2018) 39(5):1957–71. doi:10.1002/hbm.23976
13. Nofzinger EA, Buysse DJ, Germain A, Price JC, Miewald JM, Kupfer DJ. Functional neuroimaging evidence for hyperarousal in insomnia. *Am J Psychiatry* (2004) 161(11):2126. doi:10.1176/appi.ajp.161.11.2126
14. Altena E, Yd VDW, Sanzarigita EJ, Voorn TA, Rombouts SA, Kuijer JP, et al. Prefrontal hypoactivation and recovery in insomnia. *Sleep* (2008) 31(9):1271. doi:10.5665/sleep/31.9.1271
15. Drummond SP, Walker M, Almklov E, Campos M, Anderson DE, Straus LD. Neural correlates of working memory performance in primary insomnia. *Sleep* (2013) 36(9):1307. doi:10.5665/sleep.2952
16. Dai XJ, Nie X, Liu X, Pei L, Jiang J, Peng DC, et al. Gender differences in regional brain activity in patients with chronic primary insomnia: evidence from a resting-state fMRI study. *J Clin Sleep Med* (2015) 12(3):363. doi:10.5664/jcsm.5586
17. Li C, Ma X, Dong M, Yin Y, Hua K, Li M, et al. Abnormal spontaneous regional brain activity in primary insomnia: a resting-state functional magnetic resonance imaging study. *Neuropsychiatr Dis Treat* (2016) 12:1371–8. doi:10.2147/NDT.S109633
18. Dai XJ, Peng DC, Gong HH, Wan AL, Nie X, Li HJ, et al. Altered intrinsic regional brain spontaneous activity and subjective sleep quality in patients with chronic primary insomnia: a resting-state fMRI study. *Neuropsychiatr Dis Treat* (2014) 10:2163–75. doi:10.2147/NDT.S69681
19. Wang T, Yan J, Li S, Zhan W, Ma X, Xia L, et al. Increased insular connectivity with emotional regions in primary insomnia patients: a resting-state fMRI study. *Eur Radiol* (2017) 27(9):3703–9. doi:10.1007/s00330-016-4680-0
20. Li C, Dong M, Yin Y, Hua K, Fu S, Jiang G. Abnormal whole-brain functional connectivity in patients with primary insomnia. *Neuropsychiatr Dis Treat* (2017) 13:427–35. doi:10.2147/NDT.S128811
21. Lu FM, Liu CH, Lu SL, Tang LR, Tie CL, Zhang J, et al. Disrupted topology of frontostriatal circuits is linked to the severity of insomnia. *Front Neurosci* (2017) 11:214. doi:10.3389/fnins.2017.00214
22. Pang R, Zhan Y, Zhang Y, Guo R, Wang J, Guo X, et al. Aberrant functional connectivity architecture in participants with chronic insomnia disorder accompanying cognitive dysfunction: a whole-brain, data-driven analysis. *Front Neurosci* (2017) 11:259. doi:10.3389/fnins.2017.00259
23. Huang Z, Liang P, Jia X, Zhan S, Li N, Ding Y, et al. Abnormal amygdala connectivity in patients with primary insomnia: evidence from resting state fMRI. *Eur J Radiol* (2012) 81(6):1288–95. doi:10.1016/j.ejrad.2011.03.029
24. Lu FM, Dai J, Couto TA, Liu CH, Chen H, Lu SL, et al. Diffusion tensor imaging tractography reveals disrupted white matter structural connectivity network in healthy adults with insomnia symptoms. *Front Hum Neurosci* (2017) 11:583. doi:10.3389/fnhum.2017.00583
25. Lu Z, Wang E, Zhang X, Sherif K, Budhachandra K, Zhang H, et al. Cortical structural connectivity alterations in primary insomnia: insights from MRI-based morphometric correlation analysis. *Biomed Res Int* (2015) 2015(3):1–23. doi:10.1155/2015/817595
26. Suh S, Kim H, Dang-Vu TT, Joo E, Shin C. Cortical thinning and altered cortico-cortical structural covariance of the default mode network in patients with persistent insomnia symptoms. *Sleep* (2016) 39(1):161–71. doi:10.5665/sleep.5340
27. Altena E, Vrenken H, Van Der Werf YD, van den Heuvel OA, Van Someren EJ. Reduced orbitofrontal and parietal gray matter in chronic insomnia: a voxel-based morphometric study. *Biol Psychiatry* (2010) 67(2):182–5. doi:10.1016/j.biopsych.2009.08.003
28. Stoffers D, Moens S, Benjamins J, van Tol MJ, Penninx BW, Veltman DJ, et al. Orbitofrontal gray matter relates to early morning awakening: a neural correlate of insomnia complaints? *Front Neurol* (2012) 3:105. doi:10.3389/fneur.2012.00105
29. Nie X, Shao Y, Liu SY, Li HJ, Wan AL, Nie S, et al. Functional connectivity of paired default mode network subregions in primary insomnia. *Neuropsychiatr Dis Treat* (2015) 11:3085–93. doi:10.2147/NDT.S95224
30. Sridharan D, Levitin DJ, Menon V. A critical role for the right fronto-insular cortex in switching between central-executive and default-mode

networks. *Proc Natl Acad Sci U S A* (2008) 105(34):12569–74. doi:10.1073/pnas.0800005105
31. Seeley WW, Menon V, Schatzberg AF, Keller J, Glover GH, Kenna H, et al. Dissociable intrinsic connectivity networks for salience processing and executive control. *J Neurosci* (2007) 27(9):2349–56. doi:10.1523/JNEUROSCI.5587-06.2007
32. Menon V, Uddin LQ. Saliency, switching, attention and control: a network model of insula function. *Brain Struct Funct* (2010) 214(5–6):655–67. doi:10.1007/s00429-010-0262-0
33. Chen MC, Chang C, Glover GH, Gotlib IH. Increased insula coactivation with salience networks in insomnia. *Biol Psychol* (2014) 97:1–8. doi:10.1016/j.biopsycho.2013.12.016
34. Li X, Guo S, Wang C, Wang B, Sun H, Zhang X. Increased interhemispheric resting-state functional connectivity in healthy participants with insomnia symptoms: a randomized clinical consort study. *Medicine (Baltimore)* (2017) 96(27):e7037. doi:10.1097/MD.0000000000007037
35. Liu X, Zheng J, Liu BX, Dai XJ. Altered connection properties of important network hubs may be neural risk factors for individuals with primary insomnia. *Sci Rep* (2018) 8(1):5891. doi:10.1038/s41598-018-23699-3
36. Roebroeck A, Formisano E, Goebel R. Mapping directed influence over the brain using Granger causality and fMRI. *Neuroimage* (2005) 25(1):230–42. doi:10.1016/j.neuroimage.2004.11.017
37. Hamilton JP, Chen G, Thomason ME, Schwartz ME, Gotlib IH. Investigating neural primacy in major depressive disorder: multivariate Granger causality analysis of resting-state fMRI time-series data. *Mol Psychiatry* (2011) 16(7):763–72. doi:10.1038/mp.2010.46
38. Palaniyappan L, Simmonite M, White TP, Liddle EB, Liddle PF. Neural primacy of the salience processing system in schizophrenia. *Neuron* (2013) 79(4):814–28. doi:10.1016/j.neuron.2013.06.027
39. Bastien CH, Vallieres A, Morin CM. Validation of the Insomnia Severity Index as an outcome measure for insomnia research. *Sleep Med* (2001) 2(4):297–307. doi:10.1016/S1389-9457(00)00065-4
40. Buysse DJ, Reynolds CR, Monk TH, Berman SR, Kupfer DJ. The Pittsburgh Sleep Quality Index: a new instrument for psychiatric practice and research. *Psychiatry Res* (1989) 28(2):193–213. doi:10.1016/0165-1781(89)90047-4
41. Zung WW. A rating instrument for anxiety disorders. *Psychosomatics* (1971) 12(6):371–9. doi:10.1016/S0033-3182(71)71479-0
42. Zung WW. A self-rating depression scale. *Arch Gen Psychiatry* (1965) 12:63–70. doi:10.1001/archpsyc.1965.01720310065008
43. Fan L, Li H, Zhuo J, Zhang Y, Wang J, Chen L, et al. The human Brainnetome Atlas: a new brain atlas based on connectional architecture. *Cereb Cortex* (2016) 26(8):3508–26. doi:10.1093/cercor/bhw157
44. Zang ZX, Yan CG, Dong ZY, Huang J, Zang YF. Granger causality analysis implementation on MATLAB: a graphic user interface toolkit for fMRI data processing. *J Neurosci Methods* (2012) 203(2):418–26. doi:10.1016/j.jneumeth.2011.10.006
45. Yan CG, Wang XD, Zuo XN, Zang YF. DPABI: data processing & analysis for (resting-state) brain imaging. *Neuroinformatics* (2016) 14(3):339–51. doi:10.1007/s12021-016-9299-4
46. Smith SM, Nichols TE. Threshold-free cluster enhancement: addressing problems of smoothing, threshold dependence and localisation in cluster inference. *Neuroimage* (2009) 44(1):83–98. doi:10.1016/j.neuroimage.2008.03.061
47. Nichols TE, Holmes AP. Nonparametric permutation tests for functional neuroimaging: a primer with examples. *Hum Brain Mapp* (2002) 15(1):1–25. doi:10.1002/hbm.1058
48. Greicius MD, Krasnow B, Reiss AL, Menon V. Functional connectivity in the resting brain: a network analysis of the default mode hypothesis. *Proc Natl Acad Sci U S A* (2003) 100(1):253–8. doi:10.1073/pnas.0135058100
49. Bechara A, Damasio H, Damasio AR. Emotion, decision making and the orbitofrontal cortex. *Cereb Cortex* (2000) 10(3):295–307. doi:10.1093/cercor/10.3.295
50. Altena E, Van Der Werf YD, Strijers RL, Van Someren EJ. Sleep loss affects vigilance: effects of chronic insomnia and sleep therapy. *J Sleep Res* (2008) 17(3):335–43. doi:10.1111/j.1365-2869.2008.00671.x
51. Wicklow A, Espie CA. Intrusive thoughts and their relationship to actigraphic measurement of sleep: towards a cognitive model of insomnia. *Behav Res Ther* (2000) 38(7):679–93. doi:10.1016/S0005-7967(99)00136-9
52. Chand GB, Dhamala M. The salience network dynamics in perceptual decision-making. *Neuroimage* (2016) 134:85–93. doi:10.1016/j.neuroimage.2016.04.018
53. Zhou F, Huang S, Zhuang Y, Gao L, Gong H. Frequency-dependent changes in local intrinsic oscillations in chronic primary insomnia: a study of the amplitude of low-frequency fluctuations in the resting state. *Neuroimage Clin* (2017) 15:458–65. doi:10.1016/j.nicl.2016.05.011
54. Augustine JR. Circuitry and functional aspects of the insular lobe in primates including humans. *Brain Res Brain Res Rev* (1996) 22(3):229–44. doi:10.1016/S0165-0173(96)00011-2
55. Craig AD. How do you feel – now? The anterior insula and human awareness. *Nat Rev Neurosci* (2009) 10(1):59–70. doi:10.1038/nrn2555
56. Chen T, Cai W, Ryali S, Supekar K, Menon V. Distinct global brain dynamics and spatiotemporal organization of the salience network. *PLoS Biol* (2016) 14(6):e1002469. doi:10.1371/journal.pbio.1002469

Conflict of Interest Statement: The authors declare that the research was conducted in the absence of any commercial or financial relationships that could be construed as a potential conflict of interest.

frontiers in Psychiatry

ORIGINAL RESEARCH
published: 27 June 2018
doi: 10.3389/fpsyt.2018.00266

Plasticity and Susceptibility of Brain Morphometry Alterations to Insufficient Sleep

Xi-Jian Dai[1,2], Jian Jiang[2], Zhiqiang Zhang[1], Xiao Nie[2,3], Bi-Xia Liu[4], Li Pei[2], Honghan Gong[2], Jianping Hu[1], Guangming Lu[1] and Yang Zhan[5]**

[1] Department of Medical Imaging, Medical School of Nanjing University, Jinling Hospital, Nanjing, China, [2] Department of Radiology, The First Affiliated Hospital of Nanchang University, Nangchang, China, [3] Department of Radiology, Yiyang Central Hospital, Yiyang, China, [4] Department of ICU, Jiangxi Cancer Hospital, Nanchang, China, [5] Brain Cognition and Brain Disease Institute, Shenzhen Institutes of Advanced Technology, Chinese Academy of Sciences, Shenzhen, China

Background: Insufficient sleep is common in daily life and can lead to cognitive impairment. Sleep disturbance also exists in neuropsychiatric diseases. However, whether and how acute and chronic sleep loss affect brain morphology remain largely unknown.

Methods: We used voxel-based morphology method to study the brain structural changes during sleep deprivation (SD) at six time points of rested wakefulness, 20, 24, 32, 36 h SD, and after one night sleep in 22 healthy subjects, and in 39 patients with chronic primary insomnia relative to 39 status-matched good sleepers. Attention network and spatial memory tests were performed at each SD time point in the SD Procedure. The longitudinal data were analyzed using one-way repeated measures ANOVA, and *post-hoc* analysis was used to determine the between-group differences.

Results: Acute SD is associated with widespread gray matter volume (GMV) changes in the thalamus, cerebellum, insula and parietal cortex. Insomnia is associated with increased GMV in temporal cortex, insula and cerebellum. Acute SD is associated with brain atrophy and as SD hours prolong more areas show reduced GMV, and after one night sleep the brain atrophy is restored and replaced by increased GMV in brain areas. SD has accumulative negative effects on attention and working memory.

Conclusions: Acute SD and insomnia exhibit distinct morphological changes of GMV. SD has accumulative negative effects on brain morphology and advanced cognitive function. The altered GMV may provide neurobiological basis for attention and memory impairments following sleep loss.

STATEMENT OF SIGNIFICANCE

Sleep is less frequently studied using imaging techniques than neurological and psychiatric disorders. Whether and how acute and chronic sleep loss affect brain morphology remain largely unknown. We used voxel-based morphology method to study brain structural changes in healthy subjects over multiple time points during sleep deprivation (SD) status and in patients with chronic insomnia. We found that prolonged acute SD together with one night sleep recovery exhibits accumulative atrophic effect and

OPEN ACCESS

Edited by:
Thomas Pollmächer, Klinikum Ingolstadt, Germany

Reviewed by:
Axel Steiger, Max-Planck-Institut Für Psychiatrie, Germany
Thomas Penzel, Charité Universitätsmedizin Berlin, Germany

****Correspondence:***
Guangming Lu
cjr.luguangming@vip.163.com
Yang Zhan
yang.zhan@siat.ac.cn

Specialty section:
This article was submitted to Sleep and Chronobiology, a section of the journal Frontiers in Psychiatry

Received: *31 March 2018*
Accepted: *31 May 2018*
Published: *27 June 2018*

Citation:
Dai X-J, Jiang J, Zhang Z, Nie X, Liu B-X, Pei L, Gong H, Hu J, Lu G and Zhan Y (2018) Plasticity and Susceptibility of Brain Morphometry Alterations to Insufficient Sleep. Front. Psychiatry 9:266. doi: 10.3389/fpsyt.2018.00266

recovering plasticity on brain morphology, in line with behavioral changes on attentional tasks. Furthermore, acute SD and chronic insomnia exhibit distinct morphological changes of gray matter volume (GMV) but they also share overlapping GMV changes. The altered GMV may provide structural basis for attention and memory impairments following sleep loss.

Keywords: insomnia, sleep deprivation, voxel-based morphometry, gray matter, attention network test, spatial working memory

INTRODUCTION

We spend a third of our lives in sleep, yet sleep is less frequently studied using imaging techniques than many neurological and psychiatric disorders. Sleep is increasingly found to have far more health impact than what was previously thought. The precise control of sleep process is the basis of normal life process such as blood, metabolism, immune, endocrine, brain activity, and is the key of plasticity forming, information processing and function implementation (1–4). Sleep deprivation (SD) is associated with a series of maladaptive changes in alertness, judgment, emotion, memory, learning, immunity and central nervous system (5–12). Short-time SD may influence the expression of certain genes (13) while long-term SD can result in genetic changes (14). Insomnia as a general sleep disorder affects nearly 10–15% of the adult population (15). Insufficient sleep can lead to cognitive impairment, emotional change, brain dysfunction, psychomotor retardation and metabolic dysregulation (7, 8, 10, 12, 16–21). Despite the adverse socioeconomic impact of insufficient sleep, its neurobiological substrates are still elusive. Evidence suggests that chronic insomnia is accompanied by brain structural and functional changes (20–31). Elucidating brain-morphological changes of insufficient sleep can gain insights on the cognitive and emotional impacts by the sleep loss and bridges the gap between insufficient sleep and neurological or psychiatric disorders. Although SD is a frequently used protocol to investigate the functional consequences and behavioral changes associated with sleep loss (32, 33), what the brain structure changes temporally during the course of acute SD and what the brain structure changes after SD compare to those in patients with chronic primary insomnia remains unknown.

Sleep is associated with increased brain expression of genes involved in regulating macromolecule biosynthesis (34–37), and elevated transcription of genes involved in synthesis and maintenance of cell membrane lipids and myelin in the brain (34, 38, 39). Nevertheless, these structures might be particularly susceptible to insufficient sleep (39, 40). Recently a emerging view that structural brain gray matter and white matter changes can be observed within brief periods of time, from hours to days, following short-term learning (41) or neurotransmitter blockade (42). SD was associated with disturbed level of neurotransmitters (43), neuropeptides (44) and various kinds of cytokines (45) in the brain. In the longer term, rodent studies have shown that chronic sleep restriction and chronic stress are associated with brain structural changes (46, 47). The reported structural changes reflect the underlying pathology of the disease and may determine clinical phenomenology (48). Given the neurochemical changes by the SD and the link between the brain morphology and the neurochemical manipulation, we tested whether the brain structures exhibit changes as a result of insufficient sleep. First, we asked whether SD at different length of time could contribute to the changes in brain morphometry and its plasticity. Second, we examined the brain morphometry in patients with insomnia to understand whether short-term and chronic sleep loss may underlie shared structural basis.

Previous studies suggest that the reported structural changes reflected the underlying pathology of the disease and may determine clinical phenomenology (48). Voxel-based morphometry (VBM) method uses refined image registration and segmentation and provides sensitive measurements on the structural gray matter and white matter changes (49–51). In this study we applied VBM method to explore the dynamic evolution procedure of whole brain morphometry changes in the longitudinal data of 36-h acute SD and in a large sample of patients with insomnia. In the 36 h SD procedure, we performed repeated MRI sessions at 20, 24, 32, and 36 h after the SD started. We also performed one MRI session before the SD started and another one after one-night sleep recovery. Along with each MRI session, attentional network test (ANT) and spatial working memory task (SWM) were performed to evaluate the cognitive vulnerability to SD. In the insomnia study, we collected MRI data from patients with insomnia together with good sleepers (GSs).

Abbreviations: SD, Sleep deprivation; GMV, Gray matter volume; VBM, Voxel-based morphometry; ANT, Attentional network test; SWM, Spatial working memory; ROIs, Regions of interest; GSs, Good sleepers; RW, Rested wakefulness; PSQI, Pittsburgh Sleep Quality Index; HAMD, Hamilton Depression Rating Scale; HAMA, Hamilton Anxiety Rating Scale; DSM-IV, Diagnostic and Statistical Manual of Mental Disorders, version 4; ISI, Insomnia Severity Index; SDS, Self-Rating Depression Scale; SAS, Self Rating Anxiety Scale; SRSS, Self-Rating Scale of Sleep; POMS, Profile of Mood States; SPM12, Statistical Parametric Mapping 12; DICOM, Digital Imaging and Communications in Medicine; CSF, Cerebrospinal fluid; DARTEL, Diffeomorphic Anatomical Registration Through Exponentiated Lie algebra; MNI, Montreal Neurological Institute; TIV, Total intracranial volume; FWE, Family-wise error; WMV, White matter volume.

MATERIALS AND METHODS

Subjects

This study was approved by the Medical Research Ethical Committee of Jinling Hospital and the First Affiliated Hospital of Nanchang University in accordance with the Declaration of Helsinki. The MRI and behavioral data were collected from two studies with a total of 100 subjects including an acute SD study and a chronic insomnia study. In the acute SD study, a total of 22 healthy university students (13 female, 9 male;

mean age, 21.91 ± 1.38 years, mean ± standard deviation) participated an experiment of 36h SD design. In the chronic insomnia study, 39 patients with chronic primary insomnia (29 female, 10 male; mean age 48.92 ± 11.38 years, mean ± standard deviation) and 39 age-, sex-, and education-matched GSs (26 female, 13 male; mean age, 47.87 ± 9.15 years, mean ± standard deviation) were recruited. All volunteers participated voluntarily and were informed of the purposes, methods, and potential risks of this study, and signed an informed consent form. Twenty-one patients with insomnia (4 males, 17 females) were not the first-time visitors and previously had taken hypnotic or psychoactive medications. The other eighteen patients with insomnia (6 males, 12 females) were drug-naive and had never taken any medications before. The medication history duration was 1 month to 5 years. To avoid the possible effect of the medications, the patients with insomnia were kept medications-free for at least 2 weeks prior to the data collection and for the duration of this study, except that three patients with insomnia were medications-free for only 2–4 days. The mean duration of insomnia for patients with insomnia was 6.52 ± 5.65 (years, mean ± standard deviation).

Patients with insomnia met the relevant diagnostic criteria of the International Classification of Sleep Disorders, Second Edition(52), duration of insomnia > 1 year, Pittsburgh Sleep Quality Index (PSQI) score > 5, and sleep diary for >2 weeks duration. Furthermore, they had to report a total sleep time ≤ 6.5 h and (a) sleep onset latency > 45 min or (b) wake after sleep onset > 45 min or (c) total wake time during the sleep period (sleep latency + wake after sleep onset) > 60 min. To evaluate their sleep status, all subjects were asked to wear a Fitbit Flex tracker (http://help.fitbit.com) (20). These data were primarily used to verify sleep-wake diary information and not for independent assessment of inclusion and exclusion criteria.

All GSs and the 22 healthy university students met the following criteria: good sleeping habits, good sleep onset (<30 min) and/or maintenance (without easily wakened or morning awakening symptom) and regular dietary habits as measured by the Fitbit Flex tracker and sleep diary; no consumption of any stimulants, hypnotic or psychoactive medication, during or prior to the study for ≥3 months; PSQI score < 5, and Hamilton Depression Rating Scale (HAMD) and Hamilton Anxiety Rating Scale (HAMA) < 7. All subjects were right-handed. The exclusion criteria for all subjects comprised pathological brain magnetic resonance imaging (MRI) findings; inborn or other acquired diseases; any foreign implants in the body; BMI >32 or <19.8; present or past psychiatric or neurological disorders, substance dependency or substance abuse (including heroin, nicotine, or alcohol addiction); foreign implants in the body; any history of swing shift, night shift, or other shift work within the preceding year; any history of sleep complaints, or other sleep disorders, including hypersomnia, parasomnia, sleep related breathing disorder, sleep related movement disorder, or circadian rhythm sleep disorder, confirmed by overnight polysomnography; any history of significant head trauma or loss of consciousness >30 min; current smoking of more than 10 cigarettes per day; and consumption of >2 caffeinated beverages or potent tea per day.

SD Procedure

In the acute SD study, the SD Procedure started from 20:00 in the first day and lasted until 8:00 in the fourth day (**Figure 1**). All subjects were asked to arrive the lab at 19:00 in the first day (the day before the SD process) and underwent an MRI session as a base-line. All subjects were asked to sleep in the laboratory at the same time as usual. During this process, the subjects who had poor sleep quality were excluded. The 36 h SD Procedure started at 8:00 in the morning in the second day and lasted until 20:00 in the third day. The participants were required to stay awake during the entire time of the SD procedure. All subjects were not allowed to lie down and do some vigorous exercise, and they were not allowed to continue to do one thing for a long time, such as read and talk about an exciting topic. The food and water were provided during the SD procedure. Specially, all subjects eat the same food at every meal during the SD procedure to control the food intake, but the water are not controlled. The temperature of the room was maintained between 23 and 27°C. The staffs of the research team took charge of monitoring in turns through video monitors to make sure that the participants did not fall asleep during the SD procedure. If there were any signs of falling asleep, the participants were awakened by an alarm clock immediately.

Each subject underwent MRI sessions at the following time points: the start of the experiment during rested wakefulness (RW), 20, 24, 32, and 36 h after the experiment started (**Figure 1**). The subjects then spent one night of sleep for recovery and underwent another MRI session at 8:00 in the next morning in the fourth day. Furthermore, each subject underwent the long-term task of ANT and short-term simple task of SWM at each measurement time point before each of those MRI scans.

Insomnia Procedure

An experienced psychiatrist evaluated the patients with insomnia with the Diagnostic and Statistical Manual of Mental Disorders, version 4 (DSM-IV) (53) for the life history of psychiatric disorders, as well as an unstructured clinical interview for the history of medicine and sleep disorders. The patients with insomnia and status-matched GSs were asked to complete a number of questionnaires, including PSQI (54), Insomnia Severity Index (ISI) (55), Self-Rating Depression Scale (SDS) (56), Self Rating Anxiety Scale (SAS) (57), HAMD (58), HAMA (59), Self-Rating Scale of Sleep (SRSS) and Profile of Mood States (POMS) (60). The POMS questionnaire contains of 7 indexes, including 5 negative emotion indexes (nervousness, wrath, fatigue, depression and confusion) and 2 positive emotion indexes (energy and self-esteem). Then the patients with insomnia and the status-matched GSs each underwent the MRI scan once between 19:00 and 20:00.

Attention Network Test (ANT)

The ANT, adapted from Fan et al.'s study (61, 62), contains of three cue conditions (no cue, center cue, spatial cue) and two target conditions (congruent and incongruent). The visual stimuli consisted of a row of 5 horizontal black arrows pointing leftward or rightward with the target arrow in the center. The participants responded to the direction of central arrow by pressing the left or right buttons of the computer mouse. The task measures alerting, orienting and conflict effects by calculate time

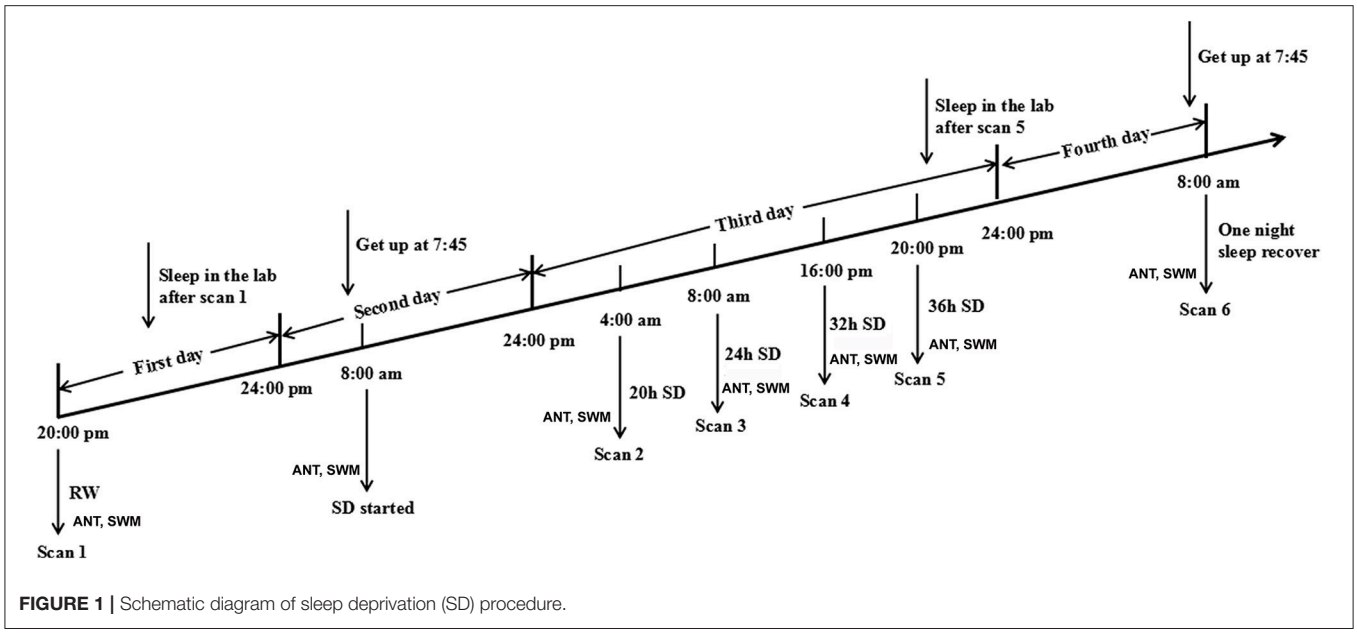

FIGURE 1 | Schematic diagram of sleep deprivation (SD) procedure.

difference between the response time and the presentation time under three different cue conditions.

The accuracy rate using corrected recognition, reaction time using only trials with correct responses, and lapse rate using missing recognition, were calculated. Finally, the intraindividual coefficient of variation was calculated for each participant by dividing the mean value of accuracy rate or correct reaction time by that of standard deviation.

Spatial Working Memory Test (SWM)

The SWM was based on visual recognition of a series of 6 × 6 smaller squares filled in a large square with size of 7.2*7.2 mm^2 (**Figure 2**). All these 36 small squares were filled with white. First, there was only shown a single small square filled with black in one location among these 36 smaller square. Next, the second and third small square was filled with black in another location respectively. Then, the fourth square will be filled with black immediately once the first small black square was recovered from black to white. At this time, the subjects were asked to make a keypress response to determine whether the location of the fourth black square was in the same location with the first black square, or subsequent the fifth black square was in the same location with the second black square, and so on. If they are in the same location, the subjects were asked to press the right button, conversely, the left button was conducted. The accuracy rate using corrected recognition, reaction time using only trials with correct responses, and lapse rate using missing recognition, were calculated. Finally, the intraindividual coefficient of variation was calculated for each participant by dividing the mean value of accuracy rate or correct reaction time by that of standard deviation.

MRI Parameter

The MRI scan was performed on a 3-Tesla MR scanner (Trio, Siemens, Erlangen, Germany). High-resolution T1-weighted anatomical images were acquired with a three-dimensional spoiled gradient-recalled sequence in sagittal orientation: 176 images (repetition time = 1,900 ms, echo time = 2.26 ms, thickness = 1.0 mm, gap = 0.5 mm, acquisition matrix = 256 × 256, field of view = 250 × 250 mm, flip angle = 9^0) were obtained. A simple questionnaire was administered immediately after the ∼3-min MRI scan to ask whether the subjects were awake during the scan. The data of subjects who fell asleep during the scan were excluded.

Voxel-Based Morphometry (VBM)

MRIcro software (www.MRIcro.com) was used to ensure data quality. The data pre-processing was conducted using the available CAT12 toolbox (http://dbm.neuro.uni-jena.de/cat12/) which is based on Statistical Parametric Mapping 12 (SPM12, http://www.fil.ion.ucl.ac.uk/spm). First, the Digital Imaging and Communications in Medicine (DICOM) standard images were transformed into NIFIT format and were realigned into sagittal orientation. The images were corrected for bias field inhomogeneity by linear (12-parameter affine) and nonlinear transformations. Next, the structural images were segmented into gray matter, white matter, and cerebrospinal fluid (CSF). Diffeomorphic Anatomical Registration Through Exponentiated Lie algebra (DARTEL) segmentation procedure was performed in the present study. The 36 h SD Procedure were analyzed using segment procedures for the longitudinal data. The original unwrapped individual gray matter and white matter segmentations were warped to a newly constructed template with a combination of linear and nonlinear registration.

Then the data were spatially normalized using East Asian brain template to the Montreal Neurological Institute (MNI; http://www.mni.mcgill.ca/) space. The segmented data were modulated and smoothed using a Gaussian kernel of 8 × 8 × 8 mm^3 full-width at half- maximum.

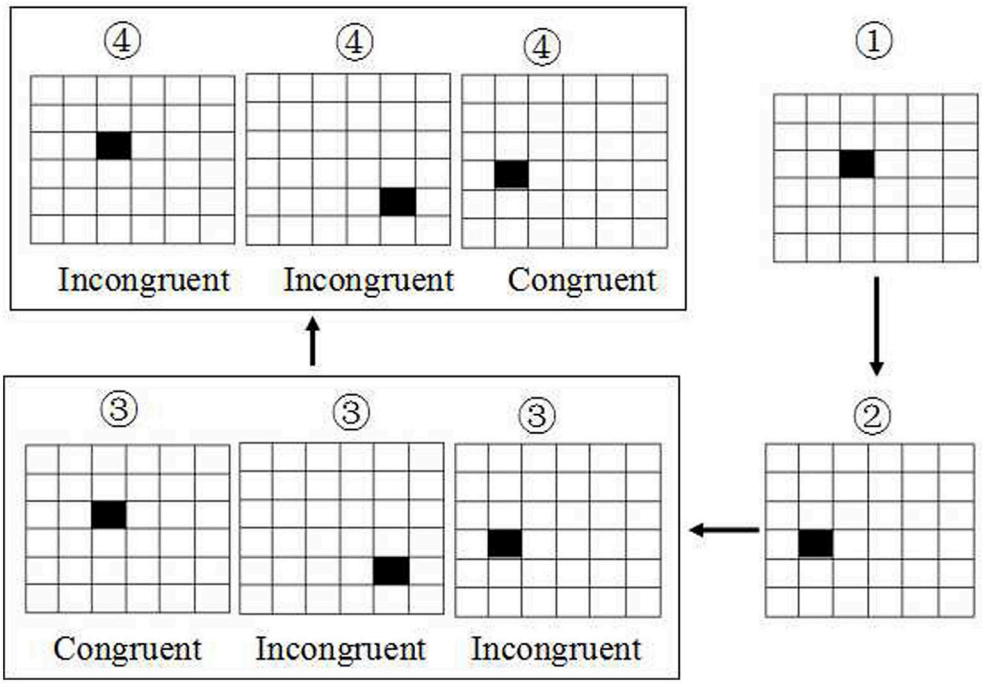

FIGURE 2 | Schematic diagram of spatial working memory. The task was based on visual recognition of a series of 6 × 6 smaller squares with white. The first, second and third small square were filled with black respectively. Then the fourth square will be filled with black immediately once the first black square was recovered to white. At this time, the subjects were asked to make a keypress response to determine whether the location of the fourth black square was the same with the first black square, or subsequent the fifth was in the same location with the second black square, and so on.

Multiple Linear Regression Analysis

Multiple linear regression analysis was performed to evaluate the relationships between the behavioral performance (dependent variable) in the ANT and SWM and the beta value of the main effect brain regions (independent variable) in each group of the 36 h SD study.

Statistics

In the SD study, the behavioral data of the ANT and the SWM were analyzed using one-way repeated measures ANOVA. In the insomnia study, the demographic factors (age, education, and years of education) and the sleep questionnaire data were compared between the patients with insomnia and the GSs using two sample *t*-test. Chi-square (χ^2) test was used for categorical data. The statistical analysis was performed using SPSS version IBM 21.0.

For the VBM data of the SD study, one-way within-subject repeated measures ANOVA was used to analyze the longitudinal data across the six time points during the 36 h process. The different brain regions of the main effect were saved as a mask. For the *post-hoc* analysis between two time points, we either calculated the product between the mask and the T maps or analyzed the difference without applying the mask.

For the VBM data in the insomnia study, unpaired *t*-test was used to investigate the gray matter volume (GMV) difference between the patients with insomnia and the GSs with the age, sex, years of education and total intracranial volume (TIV) as nuisance covariates of no interest.

We analyzed group differences in two ways. First, we used a threshold of $p < 0.05$, corrected for multiple comparisons by family-wise error (FWE) method. Second, we used an uncorrected statistical threshold of $p < 0.001$ with a minimum cluster size (k) of 100 voxels if the correction for multiple comparison failed to detect any difference.

RESULTS

Main Effect in 36 h SD Study

One-way within-subject repeated measures ANOVA with the SD time points as main factor revealed significant GMV differences in the right cerebellum anterior lobe, bilateral striatum (caudate), bilateral thalamus, bilateral insula (BA13), bilateral somatosensory association cortex (paracentral lobule, BA5; precuneus, BA7), bilateral somatosensory cortex (BA2), left superior parietal lobule (BA40), bilateral inferior parietal lobule (BA40), right supplementary motor area (SMA; BA6), bilateral posterior cingulate cortex extending to corpus callosum (BA23), and right cingulate cortex (BA24) [$F_{(5,\ 105)} = 8.637$, $p < 0.05$, $k \geq 100$, corrected by FWE; **Supplemental Table 1**, **Figure 3**].

To account for the intra-individual differences, we then examined the beta values of the main effect areas from the ANOVA in each individual subject. Eighteen out of the 22 subjects (81.82%) exhibited smaller total and mean GMV at 36 h

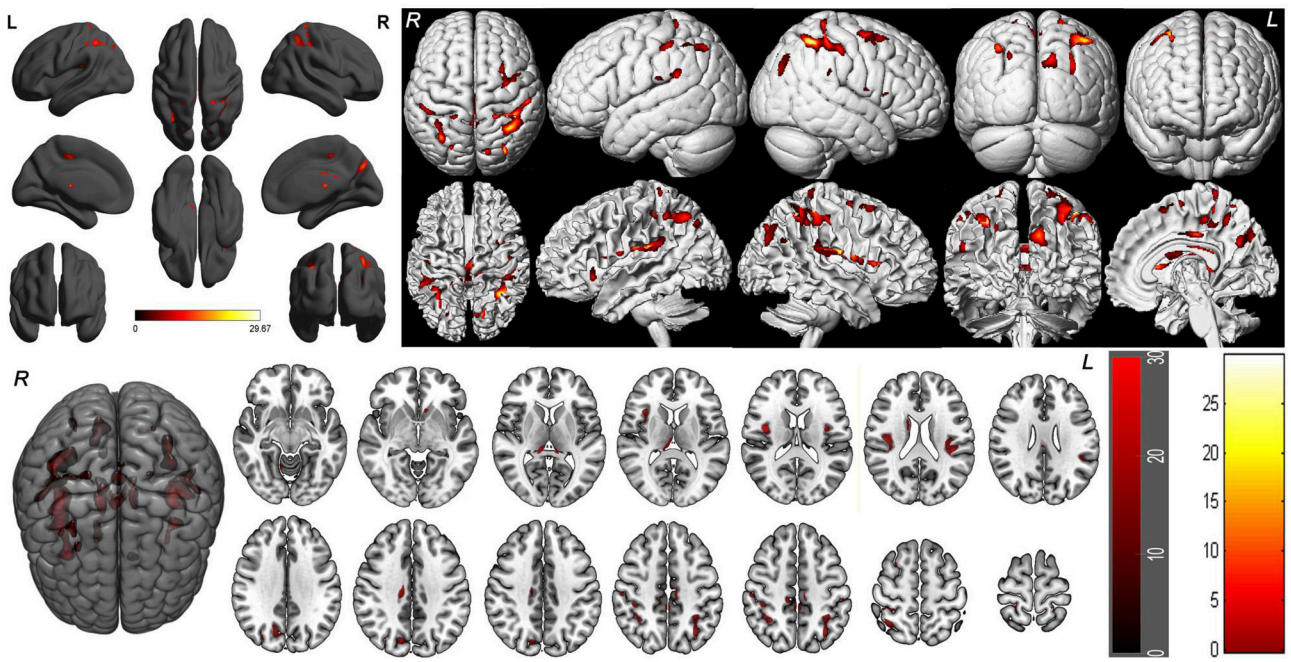

FIGURE 3 | Brain-wide gray matter volume (GMV) differences of the 36 h sleep deprivation (SD) study. Main effect brain areas that passed the statistical criterion using the ANOVA test are marked in red color. Red areas denote positive main effect brain areas in GMV.

SD compared to RW, and the other 4 subjects showed increased GMV (in total 1.02% mean decrease). After one night sleep recovery 20 out of the 22 subjects (90.91%) showed larger GMV and the other two subjects showed decreased GMV (in total 1.75% mean increase) compared to RW. In all subjects, from RW to 36 h SD and from 36 h SD to one night sleep recovery, the total and mean GMV in the main effect brain areas showed a tendency of reduction first and then increase (**Figure 4**).

Post-hoc Tests in 36 h SD Study

To understand how SD at different length of time could contribute to the brain morphometry changes, we applied *post-hoc* tests to assess the GMV differences between various SD time points and the time point of RW using main effect brain regions as mask with an uncorrected statistical threshold ($p < 0.001$, $k \geq 100$, uncorrected; **Supplemental Table 2**, **Figure 5**). A number of brain areas showed increased GMV at 20, 24, 32, and 36 h after the SD started, including the left striatum, right middle cingulate cortex (BA24) and bilateral posterior cingulate cortex extending to corpus callosum (BA23) (**Figures 5A–D**). On the other hand, a number of brain areas began to show decreased GMV at 32 h after the SD started, including the right thalamus, right insula (BA13), bilateral somatosensory association cortex (paracentral lobule, BA5; precuneus, BA7) and right inferior parietal lobule (BA40) (**Figure 5C**). Interestingly, 4 h later at 36 h after the SD started, the number of brain areas with decreased GMV increased, expanding to bilateral somatosensory cortex (BA2, BA3) and right SMA (BA6) (**Figure 5D**). After one night sleep recovery, no areas with decreased GMV were found but the right cerebellum anterior lobe, right striatum (caudate body), bilateral thalamus, bilateral insula (BA13), bilateral somatosensory association cortex (paracentral lobule, BA5; precuneus, BA7), bilateral inferior parietal lobule (BA40), bilateral somatosensory cortex (BA2), left superior parietal lobule (BA40) and right SMA (BA6) showed increased GMV (**Figure 5E**). Many of these brain areas with increased GMV (**Figure 5E**) were in the similar location as the areas showing decreased GMV at the SD time points relative to the time point of RW (**Figures 5C,D**), but they also contained more brain areas.

Additionally we analyzed the GMV differences at each SD time point relative to the time point of RW using a corrected statistical threshold without applying the mask ($p < 0.05$, FWE corrected; **Supplemental Table 3**, **Figure 6**). This allowed to investigate the GMV changes on a broader scale. At 20 h after the SD started, VBM did not reveal any GMV difference relative to the RW. At 24 h after the SD started, bilateral striatum, bilateral cingulate gyrus (BA23), right posterior cingulate cortex (BA30) and right medial prefrontal cortex (BA10) showed increased GMV (**Figure 6A**). No decreased GMV was found. At 32 h after the SD started, only right cingulate gyrus ($t = 5.0707$; $x = 13.5$, $y = -23.5$, $z = 36.5$) showed increased GMV and no decreased GMV was found. At 36 h after the SD started, right cerebellum posterior lobe, left striatum and left somatosensory cortex (BA3) showed increased GMV (**Figure 6B**). The areas that showed decreased GMV included the left cingulate gyrus (BA24) and right temporal pole (BA38) (**Figure 6B**). After one night sleep recovery, bilateral thalamus, left orbitofrontal cortex (BA11), bilateral insula (BA13), right visual association cortex (BA18), bilateral somatosensory association cortex (BA7),

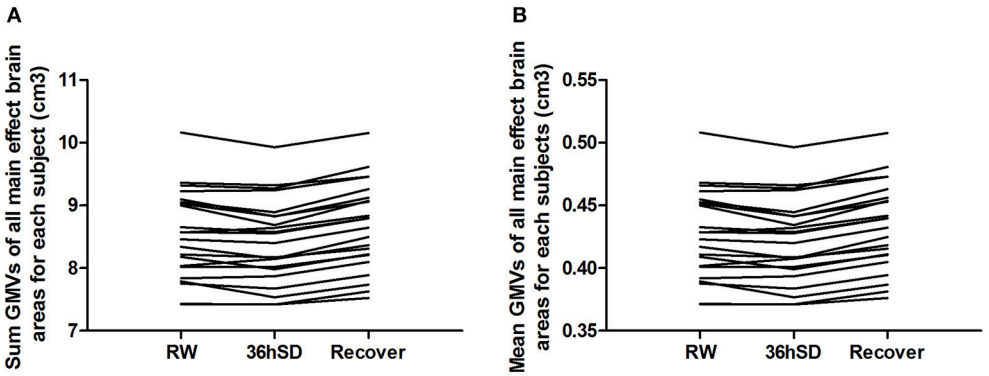

FIGURE 4 | Sum and mean gray matter volume (GMV) of all main effect brain areas for each subject in the 36 h sleep deprivation (SD) study. In all subjects, from rested wakefulness (RW) to 36 h SD and from 36 h SD to one night sleep recovery, the total **(A)** and mean **(B)** GMV in the main effect brain areas showed a tendency of reduction first and then increase.

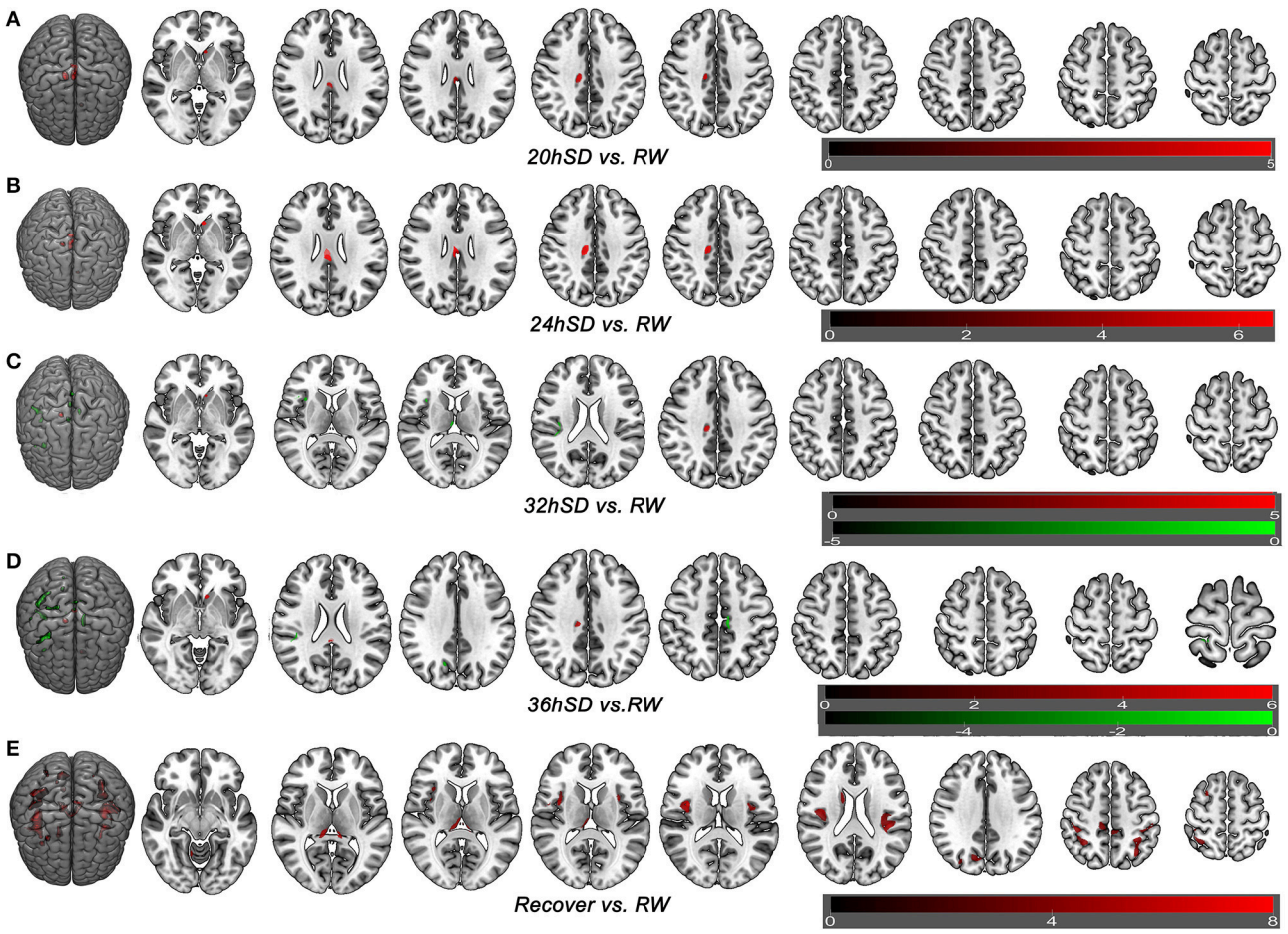

FIGURE 5 | Brain-wide gray matter volume (GMV) differences of *post-hoc* test of each sleep deprivation (SD) time point in the 36 h SD study. The *post-hoc* test of each SD time point against RW was conducted as the product between the GMV differences of each time point and the GMV differences of main effect brain areas. Brain areas that showed GMV differences at each time point during the 36 h SD procedure against RW from the *post-hoc* tests, including the time point of 20 h SD **(A)**, 24 h SD **(B)**, 32 h SD **(C)**, 36 h SD **(D)**, and after one night sleep recovery **(E)**. Red areas denote increased GMV **(A–E)** and green areas denote decreased GMV **(C–D)** in brain areas.

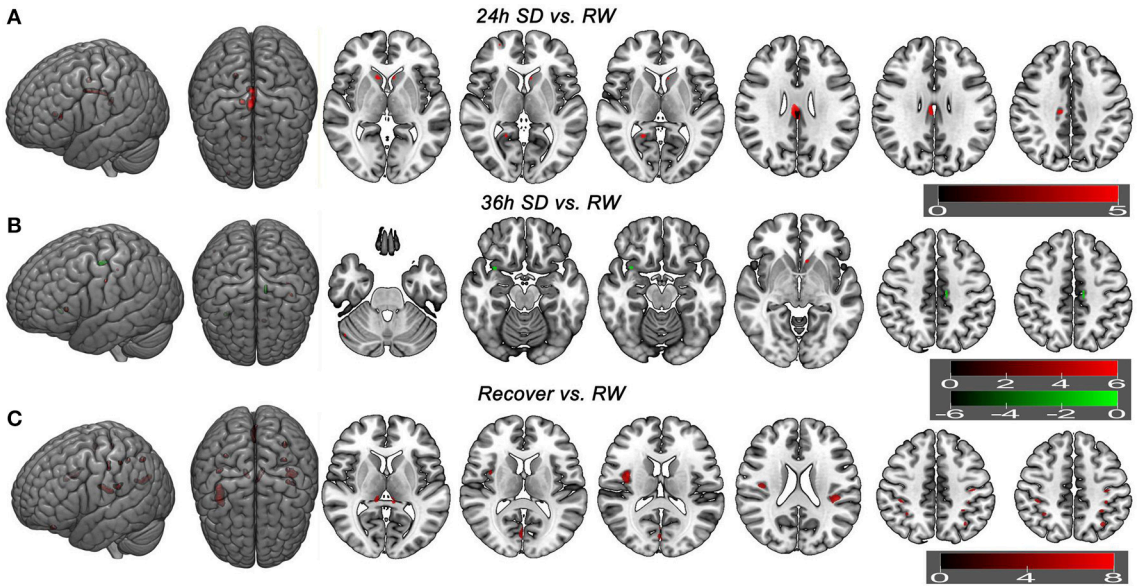

FIGURE 6 | Brain gray matter volume (GMV) differences without applying mask method using *post-hoc t* test. Brain GMV differences were conducted using *post-hoc t*-test without applying the product with the mask of the different brain regions of main effect in 36 h sleep deprivation (SD) study. The statistical threshold was set at family-wise error corrected voxel threshold of $p < 0.05$ of each time in 36h SD study. The right side of the picture indicates the right side of the brain, and the corresponding left side indicates the left side of the brain. Red areas denote increased GMV brain regions **(A–C)** and green areas denote decreased GMV **(B)**. **(A)** Brain GMV differences at 24 h SD relative to rested wakefulness (RW). **(B)** Brain GMV differences at 36 h SD relative to RW. **(C)** Brain GMV differences after one night sleep recovery relative to RW.

bilateral parietal lobe (BA2, BA40) and left primary motor cortex (BA4) showed increased GMV (**Figure 6C**). No decreased GMV was found.

Sample Characteristics of Patients With Insomnia

The demographic characteristics of the patients with insomnia sample are presented in **Table 1**. There were no significant differences in sex distribution ($p = 0.456$), mean age ($p = 0.654$), mean education ($p = 0.694$) and PSQI time in bed ($p = 0.725$). However, compared with GSs, patients with insomnia showed shorter PSQI total sleep time, lower PSQI sleep efficiency, and higher PSQI score, higher SRSS score, higher SAS score, higher SDS score, higher HAMA score, higher HAMD score, higher POMS score, higher score of five negative index in POMS and lower score of two positive index in POMS ($p < 0.001$).

VBM Difference in Patients With Insomnia vs. GSs

There were no significant differences in the TIV, GMV, white matter volume (WMV), CSF volume, GMV/TIV, WMV/TIV, CSF volume (CSFM)/TIV and GMV/WMV between patients with insomnia and GSs ($p > 0.05$) (**Table 2**).

VBM did not reveal any GMV difference between patients with insomnia and GSs using a two sample *t*-test ($p < 0.05$, FWE corrected). When using an uncorrected statistical criterion ($p < 0.001$, $k \geq 100$), we found GMV differences localized in the right hemisphere (**Supplemental Table 3**, **Figure 7**), with increased GMV in the fusiform gyrus (BA 37), cluster of cerebellum anterior lobe and visual association cortex (BA18), cluster of claustrum and insula (BA13), primary auditory area (superior temporal gyrus, BA22, BA42) and SMA (BA 6), and with decreased GMV in the visual association cortex (BA18).

Behavioral Findings of 36 h SD Study

We examined the attention and working memory in the ANT and SWM tests at different time points during the SD Procedure. The accuracy rate, reaction time and lapse rate of the ANT were different across the six SD time points using one-way repeated measures ANOVA [Greenhouse-Geisser correction, accuracy rate: $F_{(1.956,\ 41.072)} = 8.299$, $p = 0.001$, **Figure 8A**; reaction time $F_{(3.268,\ 68.631)} = 11.242$, $p < 0.001$, **Figure 8B**; lapse rate $F_{(1.975,\ 41.473)} = 7.034$, $p = 0.002$, **Figure 8C**]. The accuracy rate showed a tendency of gradual decrease (**Figure 8A**), and the reaction time and lapse rate showed a tendency of gradual increase as the SD hours prolonged (**Figures 8B,C**). The accuracy and reaction time restored after one night sleep recovery, but the accuracy rate and reaction time did not reach the level of RW completely. Interestingly, the subjects showed the lowest accuracy rate, longest reaction time and highest lapse rate at the time point of 24 h after the SD started. Furthermore, we measured the alertness, orienting and executive control from the ANT processes. The reaction time of spatial orientation and executive control were different across the SD time points [orienting: $F_{(5,\ 105)} = 2.683$, $p = 0.025$; executive control: $F_{(5,\ 105)} = 6.003$, $p < 0.001$; **Figure 8D**]. The reaction time of alertness was not different across the six time points [$F_{(5,\ 105)} = 0.277$, $p = 0.925$;

TABLE 1 | Group characteristics of patients with insomnia and good sleepers.

	Patients with insomnia	GSs	*t*-value	*p*-value
DEMOGRAPHICS				
Mean age, year	48.92 ± 11.38	47.87 ± 9.15	0.45	0.654
Sex (male, female)	39 (10, 29)	39 (13, 26)	0.555[#]	0.456[#]
Education, year	6.95 ± 3.87	7.28 ± 3.58	−0.395	0.694
SLEEP QUESTIONNAIRES				
Duration of insomnia, year	6.52 ± 5.65	N/A	N/A	N/A
Pittsburgh Sleep Quality Index (PSQI)	15.05 ± 2.24	2.44 ± 0.88	32.781	<0.001
PSQI total sleep time, hour	3.44 ± 1.24	7.38 ± 0.59	−17.965	<0.001
PSQI time in bed, hour	8.36 ± 1.18	8.43 ± 0.48	−0.354	0.725
PSQI sleep efficiency, %	42.14 ± 17.24	87.34 ± 5.4	−15.622	<0.001
Self Rating Scale Of Sleep (SRSS)	34.64 ± 4.77	15.92 ± 1.48	23.407	<0.001
Insomnia Severity Index (ISI)	18 ± 3.01	N/A	N/A	N/A
Self-rating Anxiety Scale (SAS)	41.14 ± 8.69	27.69 ± 2.7	9.235	<0.001
Self-Rating Depression Scale (SDS)	49.17 ± 9.78	31.26 ± 3.07	10.919	<0.001
Hamilton Anxiety Scale (HAMA)	8.1 ± 3.7	1.85 ± 0.78	10.32	<0.001
Hamilton Depression Scale (HAMD)	9.56 ± 4.89	2.26 ± 1.12	9.094	<0.001
Profile of Mood States (POMS)	119.49 ± 21.22	83.08 ± 5.81	−9.701	<0.001
Five negative index of POMS	31.67 ± 17.28	8.69 ± 3.25	8.16	<0.001
Two positive index of POMS	12.38 ± 7.64	25.62 ± 3.77	10.333	<0.001

[#]*chi-square value; Data are mean ± standard deviation values; GSs, Good sleepers; N/A, Not applicable; Self-rating Anxiety Scale and Self-Rating Depression Scale showed the standard score. The five negative index comprised nervousness, wrath, fatigue, depression and confusion, and the two positive index comprised energy and self-esteem.*

TABLE 2 | Brain volume of patients with insomnia and GSs.

	TIV (cm^3)	GMV (cm^3)	WMV (cm^3)	CSFM Vol (cm^3)	GMV/TIV(%)	WMV/TIV(%)	CSFM Vol/TIV(%)	GMV/WMV
Patients with insomnia	1430.87 ± 123.04	618.33 ± 58.73	512.7 ± 52.37	299.85 ± 34.16	43.21 ± 1.61	35.8 ± 1.44	20.98 ± 1.92	1.21 ± 0.07
GSs	1455.37 ± 108.3	627.02 ± 43.37	517.92 ± 51.17	310.43 ± 46.46	43.16 ± 2.25	35.55 ± 1.65	21.29 ± 2.44	1.22 ± 0.09
t	−0.933	−0.744	−0.445	−1.146	0.121	0.714	−0.612	−0.42
p	0.354	0.459	0.658	0.255	0.904	0.478	0.542	0.676

Data are mean ± standard deviation values; GSs, Good sleepers; TIV, Total intracranial volume; GMV, Gray matter volume; WMV, White matter volume; CSFM, Cerebrospinal fluid matter; Vol, Volume.

Figure 8D]. In the SWM test, the accuracy rate did not show an effect of SD time [$F_{(5, 105)} = 0.935$, $p = 0.461$; **Figure 8E**], however there was a trend of gradual decrease as the SD hours prolonged and then a trend of increase after one night sleep recovery.

The intra-individual coefficient of variability for ANT accuracy rate, ANT reaction time, and SWM accuracy rate showed a tendency of increase as the SD hours prolonged and showed decrease after one night sleep recovery (**Figure 8F**). The accuracy rate of the ANT showed the highest intra-individual coefficient of variability at the time point of 24 h SD compared to other five time points.

Intra-Individual Differences in Behavior for Each Subject

We conducted the intra-individual differences in behavior as the intra-individual GMV differences in brain areas. We calculated the accuracy rate and reaction time for each subject (**Supplemental Figure 1**). In the ANT test, eighteen of the subjects shower lower accuracy rate, and the other four subjects showed higher accuracy rate at the time point of 36 h SD compared to RW (**Supplemental Figure 1A**). Twelve of the subjects demonstrated lower accuracy rate, two subjects showed no differences, and the other eight subjects indicated higher accuracy rate after one night sleep recover compared with RW (**Supplemental Figure 1A**). Seventeen of the subjects demonstrated longer reaction time, and the other five subjects showed shorter reaction time at the time point of 36h SD compared to RW (**Supplemental Figure 1B**). Ten of the subjects showed longer reaction time and the other twelve of the subjects indicated shorter reaction time after one night sleep recover compared with RW (**Supplemental Figure 1B**). In individual subjects, from RW to 36 h SD and from 36 h SD to one night sleep recovery, the accuracy rate in ANT showed a tendency of reduction first (36 h SD vs. RW, 3.94% mean decrease) and

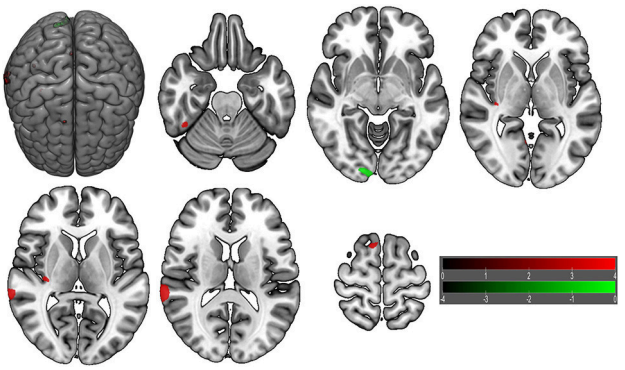

FIGURE 7 | Brain gray matter volume (GMV) differences of patients with insomnia relative to good sleepers. The statistical threshold was set at uncorrected voxel threshold of $p < 0.001$ with a minimum cluster threshold of 100 voxels. The right side of the picture indicates the right side of the brain, and the corresponding left side indicates the left side of the brain. Green areas denote decreased GMV and red areas denote increased GMV.

then increase (recovery vs. RW, 1.39% mean decrease), and the reaction time showed an inverse tendency of increase first (36 h SD vs. RW, 9.00% mean increase) and then decrease (recovery vs. RW, 0.05% mean increase) (**Supplemental Figure 1**).

In the SWM, nine of the subjects demonstrated lower accuracy rate, seven subjects showed no differences, and the other six subjects indicated higher accuracy rate at the time point of 36 h SD compared to RW (36 h SD vs. RW, 2.7% mean decrease) (**Supplemental Figure 1C**). Five of the subjects demonstrated lower accuracy rate, nine subjects showed no differences, and the other eight subjects indicated higher accuracy rate after one night sleep recover compared with RW (recovery vs. RW, 1.46% mean increase) (**Supplemental Figure 1C**). Eleven of the subjects demonstrated longer reaction time, and the other eleven subjects showed shorter reaction time at the time point of 36 h SD compared to RW (36 h SD vs. RW, 0.26% mean decrease) (**Supplemental Figure 1D**). Five of the subjects showed longer reaction time and the other seventeen of the subjects indicated shorter reaction time after one night sleep recover compared with RW (recovery vs. RW, 5.39% mean decrease) (**Supplemental Figure 1D**).

Regression Analysis Between VBM and Behavior

To investigate whether the structural changes during the SD status may have correlations with the behavior, we performed multiple linear regression between the behavioral parameters in the attention and working memory tasks and the beta values of the main effect brain areas at each SD time point (**Table 3**). Across the SD time points, the accuracy rate in the ANT and the SWM tests showed linear correlations with the beta value of many brain areas, including the somatosensory association cortex and insula. At the time points of RW and one night sleep recovery, linear relationships were found in the parietal lobe (somatosensory cortex and inferior parietal lobule).

The alertness in the ANT showed linear relationships with the beta value of the striatum, parietal lobe, insula and thalamus across the SD time points, and the executive control in the ANT showed linear relationships with the beta value of the insula, somatosensory association cortex, parietal lobe and SMA. However, no brain areas showed correlations with the alertness or executive control at the time point of RW and one night sleep recovery. Interestingly, at the time point of 24 h SD, the alertness displayed linear correlation with the beta value of the striatum and the executive control showed linear relationship with the beta value of the SMA, and no correlation was found at other time points.

DISCUSSION

Brain Morphological Changes During the Acute SD

We found in our SD study that insufficient sleep is associated with widespread brain morphological changes. Although molecular basis for the microstructure-level changes requires further investigation, acute SD is associated with altered gene expression involved in macromolecule biosynthesis (34–37) in human studies and altered gene expression involved in cell membrane lipids and myelin in the mouse brain (34, 38, 39). The susceptibility of these cellular substrates to the rapid changes following sleep loss might contribute to the brain microstructure changes as we observed in our VBM analysis. In the animal studies, SD could lead to neuronal marker changes for apoptosis and morphology, and these changes were restored after sleep recovery (63, 64). Consistent with these patterns, our VBM data showed progressive structural atrophy as SD hours prolonged and these changes were restored and replaced by extensive and larger morphologic brain inflation after one night sleep recovery. Previous diffusion tensor imaging study showed that SD is associated with widespread fractional anisotropy decreases in several brain areas and as the waking prolonged the decreases become larger (65), which may associated with the reduced interstitial space volumes and increased resistance to water flux in the brain after waking than during sleep (66) and particularly susceptible of cell membrane lipids and myelin to insufficient sleep (39, 40). In our longitudinal data of 36 h SD procedure, the brain atrophy began to appear at 32 h SD and aggravated at 36 h SD. In agreement with the brain morphology, the accumulative negative effects were found in attention and spatial memory tests, but after one night sleep recovery they were restored incompletely showing a delayed recovery. We hypothesized that the VBM changes observed in the present study are more likely to be related to the changes in tissue hydration or other phenomena.

Circadian Rhythm Influences During SD

A recent study has shown that the brain responses during the day and prolonged wakefulness showed circadian rhythmic patterns (67). Subcortical areas including the striatum and thalamus showed strong correlations with the melatonin levels and these areas showed increased responses when later hours in the day start. We also found increased GMV in the striatum starting at the time point of 20 h SD, and these increased GMV remained into the later stage of the SD. Evidence also indicates that individuals with late chronotype who prefer to go to bed late in

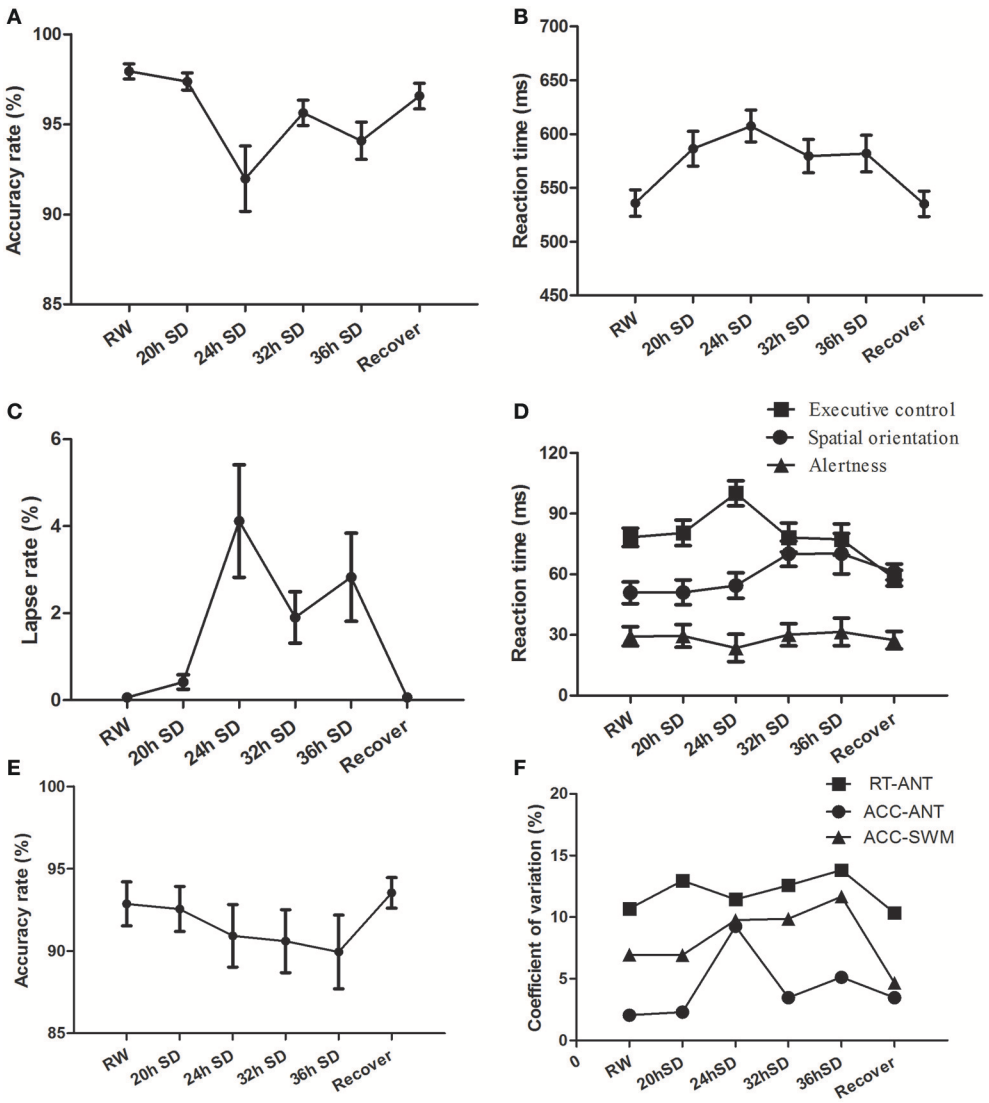

FIGURE 8 | Behavioral findings of attention network test (ANT) and spatial working memory test (SWM). Each behavioral measurement was taken at six time points during the sleep deprivation (SD) session. **(A)** Accuracy rate of the ANT. **(B)** Reaction time of the ANT. **(C)** Lapse rate of the ANT. **(D)** Reaction time for the alertness, spatial orientation and executive control of the ANT. **(E)** Accuracy rate of the SWM. **(F)** Coefficient of variation values of three indexes, including reaction time of the ANT, accuracy rate of the ANT, and accuracy rate of the SWM. Data are presented as mean ± standard values.

the evening had structural differences in the cingulate cortex and corpus callosum (68). In our SD study, we also found increased GMV in the corpus callosum and cingulate cortex. Considering the similar brain areas found in our study and the others, the structural changes in our VBM analysis may reflect the influence of circadian rhythm.

At the time point of 24 h SD, the subjects exhibited the lowest accuracy rate, longest reaction time and highest lapse rate in the ANT compared to the other time points. Accordingly, at this time point a number of increased GMV areas in the bilateral striatum and bilateral cingulate cortex extending to corpus callosum were found, and these areas existed even after the FWE correction. Specifically, we found that at 24 h SD the alertness displayed linear correlation with the beta value of striatum and the executive control showed linear correlation with the beta value of SMA, and these relationships were not found at other SD time points. At this time point of 8:00 a.m. in the morning, the participants usually woke up in their daily schedule in the process of getting out of bed and they showed reduced alertness. The SMA area was implicated in sensory processing, working memory, executive control and spatial-bodily attention (69, 70). Therefore the structural changes we observed in our data may underlie the circadian rhythm and prolonged wakefulness to modulate the attentional performance.

Acute SD vs. Chronic Insomnia

Chronic insomnia is thought to be maintained by excessive negatively toned cognitive activity with autonomic arousal and emotional distress (71). The exaggerated cortical and somatic

TABLE 3 | Multiple linear regression analysis between the beta value of main effect areas and behavioral findings.

Group	Dependent variable	Independent variables	Coefficient (R^2)	β	Standard error	*t*-value	*p*-value
20hSD	Accuracy rate in ANT	Left precuneus	0.368	−0.351	0.103	−3.415	0.003
20hSD	Alertness in ANT	Left postcentral gyrus	0.275	−395.578	143.535	−2.756	0.012
20hSD	Executive control in ANT	Right insula	0.355	413.265	124.528	3.319	0.003
20hSD	Accuracy rate in SWM	Left Insula, Inferior parietal lobule	0.598	0.419	0.141	2.971	0.008
		Left superior parietal lobule, Inferior parietal lobule		0.387	0.170	2.269	0.036
		Left postcentral gyrus		−0.868	0.279	−3.109	0.006
20hSD	Reaction time in SWM	Right precuneus	0.272	−1158.708	423.6	−2.735	0.013
24hSD	Accuracy rate in ANT	Left paracentral lobule	0.304	−0.573	0.194	−2.954	0.008
24hSD	Alertness in ANT	Right caudate body	0.286	353.412	124.862	2.83	0.01
24hSD	Spatial orientation in ANT	Right insula	0.231	−330.661	135.044	−2.449	0.024
24hSD	Executive control in ANT	Right precuneus	0.557	−165.228	57.974	−2.85	0.01
		Right middle frontal gyrus		662.865	135.704	4.885	<0.001
24hSD	Accuracy rate in SWM	Left insula	0.461	−1.191	0.328	−3.625	0.002
		Left Insula, Inferior Parietal Lobule		0.495	0.215	2.308	0.032
24hSD	Reaction time in SWM	Right precuneus	0.303	−1516.186	513.985	−2.95	0.008
32h SD	Alertness in ANT	Left Insula, Inferior parietal lobule	0.208	170.21	74.381	2.288	0.033
32h SD	Spatial orientation in ANT	Left precuneus	0.296	410.993	141.7	2.9	0.009
32h SD	Executive control in ANT	Right insula	0.369	565.979	170.759	3.314	0.004
		Precuneus, Paracentral lobule		−354.971	165.907	−2.140	0.046
32h SD	Accuracy rate in SWM	Left precuneus	0.48	−1.180	0.380	−3.106	0.006
		Right precuneus		0.442	0.155	2.850	0.010
32h SD	Reaction time in SWM	Right precuneus	0.585	−1834.941	360.138	−5.095	<0.001
		Left precuneus		1520.079	508.598	2.989	0.008
36hSD	Accuracy rate in ANT	Right insula	0.426	−0.579	0.213	−2.725	0.013
		Right precuneus		0.340	0.098	3.484	0.002
36hSD	Lapse rate in ANT	Right precuneus	0.265	−25.945	9.656	−2.687	0.014
36hSD	Alertness in ANT	Left thalamus	0.184	−436.246	205.713	−2.121	0.047
36hSD	Accuracy rate in SWM	Right insula	0.42	1.962	0.534	3.676	0.002
		Left insula		−1.350	0.517	−2.612	0.017
36hSD	Reaction time in SWM	Right precuneus	0.246	−975.657	381.748	−2.556	0.019
Recover	Accuracy rate in ANT	Left postcentral gyrus, inferior parietal lobule	0.372	−0.363	0.105	−3.445	0.003
Recover	Reaction time in ANT	Left postcentral gyrus, inferior parietal lobule	0.239	−481.855	192.372	−2.505	0.021
Recover	Spatial orientation in ANT	Left paracentral lobule	0.317	−127.442	41.866	−3.044	0.006
Recover	Reaction time in SWM	Right precuneus	0.3	−966.936	330.269	−2.928	0.008

activation can lead to increased sensory information processing and inability to initiate or maintain sleep (20, 72, 73), and may be a result of increased brain activities. We found that both in the SD study and the insomnia study that the insula and cerebellum showed increased GMV. This demonstrates that acute and chronic sleep loss may also share similar neurobiological representation in brain morphology. In the SD study after one night sleep recovery only brain areas with increased GMV were found. Similarly, patients with insomnia also mainly found morphological differences in brain regions with increased GMV. This demonstrates that the status of subjects who underwent SD process and then received one night sleep recovery may exhibit analogous brain activation characteristics to the status of patients with insomnia who underwent subjective experience of chronically disturbed and non-refreshing sleep.

Although using an uncorrected statistical threshold we found a number of brain areas with GMV changes in patients with insomnia, using a strict criterion we did not observe differences between patients with insomnia and GSs. This probably demonstrates that the patients with insomnia were not prone to the brain microstructure changes already. Under the less stringent method we found altered GMV in the patients with insomnia in the temporal cortex, primary auditory area, insula, SMA and visual association cortex. For the acute SD the main effect areas with GMV changes were showed in the sensory cortex, motor cortex and subcortical thalamus. Therefore the two types of short-term and chronic sleep losses mainly exhibited non-overlapping altered brain areas.

In the insomnia study, the superior temporal cortex with increased GMV contains the primary auditory area (BA42). Previous study has shown that normal activation of the auditory cortex is decreased to help maintain sleep in response to external stimuli (74). Therefore, our observation of increased GMV in the auditory cortex may highlight the reduced capacity to

disengage from external information processing of auditory stimuli, which was consistent with the clinical characteristics of insomnia patients with shallow sleep and increased sensitivity to surrounding environments. Our data therefore support the theory of hyperarousal, which may be a core predisposing or perpetuating factor of ultimately hampering the ability to initiate or maintain sleep.

Previous meta-analytical data demonstrated that the threat or anxiety hypothesis is associate with insula (75), and the craving hypothesis is associated with ventral striatum and cingulated cortex (76). Patients with insomnia underwent prolonged experience of chronically disturbed and non-refreshing sleep, and may display threat or anxiety in response to sleep-related cues. Subjects who underwent acute SD process may mainly display craving to sleep but not threat or anxiety (77). Our previous neuroimaging studies also found that insufficient sleep resulted in abnormal regional brain activity in the threat-related brain areas and craving-related brain areas (8, 20, 21, 78–80). Our observation of increased GMV in the insula or cingulated cortex in the insomnia study and increased GMV in the striatum in the SD study might support the theory of threat and craving hypothesis.

The paracentral lobule is considered to be negatively correlated with vigor activity (81). It has been found that the inferior parietal cortex area is impaired after SD and may represent an most reliable early biological marker of individual resistance to SD (7, 8, 82, 83). The postcentral gyrus is the main receptive region for external stimuli as the location of the primary somatosensory cortex. Recently the postcentral gyrus was shown to be implicated with the default mode network (84), which is a functional brain hub showing coupled slow signal fluctuations in the absence of external stimuli during restful waking and sleep (85). In the SD study, these areas with decreased GMV were found with several correlations with the ANT and SWM. Our observations of decreased GMV in theses somatosensory areas after acute SD in individuals who showed a possible insufficiency to enter into "resting state" status may reflect inhibition in sensory-informational processing and difficulties in cognitive function.

CONCLUSIONS

In summary, acute SD and insomnia showed widespread changes in gray matter microstructure with shared but also distinct neurobiological representation in brain morphology. Acute SD may be associated with inhibition in sensory-informational processing with decreased GMV in the somatosensory areas to compensate for the effects of sleep loss on advanced cognitive function, while the insomnia may be associated with inability to disengage from external information processing of auditory stimuli with increased GMV in the primary auditory area. Prolonged acute SD together with one night sleep recovery exhibit accumulative atrophic effect and recovering plasticity on brain morphology, in line with the behavioral changes on attentional and working memory tasks. Taken together, clarifying the biological underpinnings of these microstructural alterations could advance our understanding of the neurobiological mechanism of waking and sleep. One of the strengths of the present study is the relatively large sample size in the insomnia study and longitudinal data in the SD study; however, there are several limitations that should be noted. First, our findings are limited by the use of the Fitbit Flex tracker to monitor the sleep quality in our experience (20, 86). Although we cannot provide direct evidence to prove whether the FITBIT tracker provides a valid and reliable measure of objective sleep, we compared some patients' data between the FITBIT and the PSG, and found the results were similar. In fact, our sample was screened to exclude individuals with medical or psychiatric disorders that may affect sleep, and the diagnosis of primary insomnia mainly depends on the experience of senior physicians who have been working for more than 20 years. Second, the subjects were not monitored by continuous EEG in the SD procedure, but a simple questionnaire was administered immediately after the MRI scan to ask whether the subjects were awake during the scan. The data of subjects who fell asleep during the scan were excluded.

AUTHOR CONTRIBUTIONS

X-JD and YZ wrote the main manuscript text. X-JD, JJ, LP, HG, GL, and YZ conceived and designed the whole experiment. X-JD, XN, and B-XL collected the data. X-JD, JH, and ZZ analyzed the data.

ACKNOWLEDGMENTS

This work was supported by grants from National Natural Science Foundation of China (grant No 81701678), Science and Technology Support Program of Jiangxi Province (grant No: 20141BBG70026), One Hundred Talents Program of CAS (YZ), Shenzhen city government KQCX2015033117354153 (YZ), Guangdong Innovative and Entrepreneurial Research Team Program No. 2014ZT05S020 (YZ) and Shenzhen Peacock Innovation Team Project KQTD20140630180249366 (YZ).

SUPPLEMENTARY MATERIAL

The Supplementary Material for this article can be found online at: https://www.frontiersin.org/articles/10.3389/fpsyt.2018.00266/full#supplementary-material

Supplemental Figure 1 | Accuracy rate and reaction time in the ANT and spatial working memory (SWM) for each subject in the 36 h sleep deprivation (SD) study. **(A)** Accuracy rate of the ANT for each subject. **(B)** Reaction time of the ANT for each subject. **(C)** Accuracy rate of the SWM for each subject. **(B)** Reaction time of the SWM for each subject. In all subjects, from rested wakefulness (RW) to 36 h SD and from 36 h SD to one night sleep recovery, the accuracy rate showed a tendency of reduction first and then increase, and the reaction time showed a tendency of increase first and then decrease **(A–D)**.

Supplemental Table 1 | The gray matter volume differences of main effect in the 36 h sleep deprivation study. R, right; L, left; BA, Brodmann's area; MNI, montreal neurological institute; N/A, Not applicable. The statistical threshold was set at corrected voxel threshold of $p < 0.05$ with a minimum cluster threshold of 100 voxels, corrected by family-wise error.

Supplemental Table 2 | The *post-hoc* differences of gray matter volume with the product with the mask of the different brain regions of main effect in the 36 h sleep

deprivation (SD) study. RW, Rested wakefulness; R, right; L, left; BA, Brodmann's area; MNI, montreal neurological institute; N/A, Not applicable. The statistical threshold was set at uncorrected voxel threshold of $p < 0.001$ with a minimum cluster threshold of 100 voxels ($t = 3.1697$).

Supplemental Table 3 | The gray matter volume differences without applying mask method in the 36 h sleep deprivation (SD) study and in the chronic insomnia study. RW, Rested wakefulness; R, right; L, left; BA, Brodmann's area; MNI, montreal neurological institute; N/A, Not applicable; GSs, good sleepers. The statistical threshold was set at family-wise error corrected voxel threshold of $p < 0.05$ of each time in the 36 h SD study without product with the mask image of main effect, and at uncorrected voxel threshold of $p < 0.001$ with a minimum cluster threshold of 100 voxels in patients with insomnia.

REFERENCES

1. Davies SK, Ang JE, Revell VL, Holmes B, Mann A, Robertson FP, et al. Effect of sleep deprivation on the human metabolome. *Proc Natl Acad Sci USA* (2014) 111:10761–6. doi: 10.1073/pnas.1402663111
2. Gamble K, Berry R, Frank SJ, Young ME. Circadian clock control of endocrine factors. *Nat Rev Endocrinol.* (2014) 10:466–75. doi: 10.1038/nrendo.2014.78
3. Gomez-Gonzalez B, Dominguez-Salazar E, Hurtado-Alvarado G, Esqueda-Leon E, Santana-Miranda R, Rojas-Zamorano JA, et al. Role of sleep in the regulation of the immune system and the pituitary hormones. *Ann N Y Acad Sci.* (2012) 1261:97–106. doi: 10.1111/j.1749-6632.2012.06616.x
4. Smith K. Neuroscience: off to night school. *Nature* (2013) 497:S4–5. doi: 10.1038/497S4a
5. Gottesmann C. noradrenaline involvement in basic and higher integrated REM sleep processes. *Prog Neurobiol.* (2008) 85:237–72. doi: 10.1016/j.pneurobio.2008.04.002
6. Silva RH, Abilio VC, Takatsu AL, Kameda SR, Grassl C, Chehin AB, Medrano WA, Calzavara MB, et al. Role of hippocampal oxidative stress in memory deficits induced by sleep deprivation in mice. *Neuropharmacology* (2004) 46:895–903. doi: 10.1016/j.neuropharm.2003.11.032
7. Dai XJ, Gong HH, Wang YX, Zhou FQ, Min YJ, Zhao F, et al. Gender differences in brain regional homogeneity of healthy subjects after normal sleep and after sleep deprivation: a resting-state fMRI study. *Sleep Med.* (2012) 13:720–7. doi: 10.1016/j.sleep.2011.09.019
8. Dai XJ, Liu CL, Zhou RL, Gong HH, Wu B, Gao L, et al. Long-term total sleep deprivation decreases the default spontaneous activity and connectivity pattern in healthy male subjects: a resting-state fMRI study. *Neuropsychiatr Dis Treat.* (2015) 11:761–72. doi: 10.2147/NDT.S78335
9. Edwards RR, Quartana PJ, Allen RP, Greenbaum S, Earley CJ, Smith MT. Alterations in pain responses in treated and untreated patients with restless legs syndrome: associations with sleep disruption. *Sleep Med.* (2011) 12:603–9. doi: 10.1016/j.sleep.2010.09.018
10. Ohayon MM, Smolensky MH, Roth T. Consequences of shiftworking on sleep duration, sleepiness, and sleep attacks. *Chronobiol Int.* (2010) 27:575–89. doi: 10.3109/07420521003749956
11. Tsigos C, Chrousos GP. Hypothalamic-pituitary-adrenal axis, neuroendocrine factors and stress. *J Psychosom Res.* (2002) 53:865–71. doi: 10.1016/S0022-3999(02)00429-4
12. Walker MP, Stickgold R. Sleep, memory, and plasticity. *Annu Rev Psychol.* (2006) 57:139–66. doi: 10.1146/annurev.psych.56.091103.070307
13. Naidoo N, Giang W, Galante RJ, Pack AI. Sleep deprivation induces the unfolded protein response in mouse cerebral cortex. *J Neurochem.* (2005) 92:1150–7. doi: 10.1111/j.1471-4159.2004.02952.x
14. Koban M, Swinson KL. Chronic REM-sleep deprivation of rats elevates metabolic rate and increases UCP1 gene expression in brown adipose tissue. *Am J Physiol Endocrinol Metab.* (2005) 289:E68–74. doi: 10.1152/ajpendo.00543.2004
15. Ohayon MM. Epidemiology of insomnia: what we know and what we still need to learn. *Sleep Med Rev.* (2002) 6:97–111. doi: 10.1053/smrv.2002.0186
16. Altena E, Van Der Werf YD, Strijers RL, Van Someren EJ. Sleep loss affects vigilance: effects of chronic insomnia and sleep therapy. *J Sleep Res.* (2008) 17:335–43. doi: 10.1111/j.1365-2869.2008.00671.x
17. Edinger JD, Means MK, Carney CE, Krystal AD. Psychomotor performance deficits and their relation to prior nights' sleep among individuals with primary insomnia. *Sleep* (2008) 31:599–607. doi: 10.1093/sleep/31.5.599
18. Varkevisser M, Kerkhof GA. Chronic insomnia and performance in a 24-h constant routine study. *J Sleep Res.* (2005) 14:49–59. doi: 10.1111/j.1365-2869.2004.00414.x
19. Gao L, Bai L, Zhang Y, Dai XJ, Netra R, Min Y, et al. Frequency-dependent changes of local resting oscillations in sleep-deprived brain. *PLoS ONE* (2015) 10:e0120323. doi: 10.1371/journal.pone.0120323
20. Dai XJ, Nie X, Liu X, Pei L, Jiang J, Peng DC, et al. Gender differences in regional brain activity in patients with chronic primary insomnia: evidence from a resting-state fMRI Study. *J Clin Sleep Med.* (2016) 12:363–74. doi: 10.5664/jcsm.5586
21. Dai XJ, Peng DC, Gong HH, Wan AL, Nie X, Li HJ, et al. Altered intrinsic regional brain spontaneous activity and subjective sleep quality in patients with chronic primary insomnia: a resting-state fMRI study. *Neuropsychiatr Dis Treat.* (2014) 10:2163–75. doi: 10.2147/NDT.S69681
22. Nie X, Shao Y, Liu SY, Li HJ, Wan AL, Nie S et al. Functional connectivity of paired default mode network subregions in primary insomnia. *Neuropsychiatr Dis Treat.* (2015) 11:3085–93. doi: 10.2147/NDT.S95224
23. Altena E, Vrenken H, Van Der Werf YD, van den Heuvel OA, Van Someren EJ. Reduced orbitofrontal and parietal gray matter in chronic insomnia: a voxel-based morphometric study. *Biol Psychiatry* (2010) 67:182–5. doi: 10.1016/j.biopsych.2009.08.003
24. Joo EY, Noh HJ, Kim JS, Koo DL, Kim D, Hwang KJ, et al. Brain gray matter deficits in patients with chronic primary insomnia. *Sleep* (2013) 36:999–1007. doi: 10.5665/sleep.2796
25. Bumb JM, Schilling C, Enning F, Haddad L, Paul F, Lederbogen F, et al. Pineal gland volume in primary insomnia and healthy controls: a magnetic resonance imaging study. *J Sleep Res.* (2014) 23:274–80. doi: 10.1111/jsr.12125
26. Joo EY, Kim H, Suh S, Hong SB. Hippocampal substructural vulnerability to sleep disturbance and cognitive impairment in patients with chronic primary insomnia: magnetic resonance imaging morphometry. *Sleep* (2014) 37:1189–98. doi: 10.5665/sleep.3836
27. Noh HJ, Joo EY, Kim ST, Yoon SM, Koo DL, Kim D, et al. The relationship between hippocampal volume and cognition in patients with chronic primary insomnia. *J Clin Neurol.* (2012) 8:130–8. doi: 10.3988/jcn.2012.8.2.130
28. Riemann D, Voderholzer U, Spiegelhalder K, Hornyak M, Buysse DJ, Nissen C, et al. Chronic insomnia and MRI-measured hippocampal volumes: a pilot study. *Sleep* (2007) 30:955–8. doi: 10.1093/sleep/30.8.955
29. Spiegelhalder K, Regen W, Baglioni C, Kloppel S, Abdulkadir A, Hennig J, et al. Insomnia does not appear to be associated with substantial structural brain changes. *Sleep* (2013) 36:731–7. doi: 10.5665/sleep.2638
30. Winkelman JW, Benson KL, Buxton OM, Lyoo IK, Yoon S, O'Connor S, et al. Lack of hippocampal volume differences in primary insomnia and good sleeper controls: an MRI volumetric study at 3 Tesla. *Sleep Med.* (2010) 11:576–82. doi: 10.1016/j.sleep.2010.03.009
31. Winkelman JW, Plante DT, Schoerning L, Benson K, Buxton OM, O'Connor SP et al. Increased rostral anterior cingulate cortex volume in chronic primary insomnia. *Sleep* (2013) 36:991–8. doi: 10.5665/sleep.2794
32. Alhola P, Polo-Kantola P. Sleep deprivation: impact on cognitive performance. *Neuropsychiatr Dis Treat.* (2007) 3:553–67.
33. Krause AJ, Simon EB, Mander BA, Greer SM, Saletin JM, Goldstein-Piekarski AN, et al. The sleep-deprived human brain. *Nat Rev Neurosci.* (2017) 18:404–18. doi: 10.1038/nrn.2017.55
34. Mongrain V, Hernandez SA, Pradervand S, Dorsaz S, Curie T, Hagiwara G, et al. Separating the contribution of glucocorticoids and wakefulness to the molecular and electrophysiological correlates of sleep homeostasis. *Sleep* (2010) 33:1147–57. doi: 10.1093/sleep/33.9.1147
35. Mackiewicz M, Shockley KR, Romer MA, Galante RJ, Zimmerman JE, Naidoo N, et al. Macromolecule biosynthesis. a key function of sleep. *Physiol Genomics* (2007) 31:441–57. doi: 10.1152/physiolgenomics.00275.2006
36. Cirelli C, LaVaute TM, Tononi G. Sleep and wakefulness modulate gene expression in Drosophila. *J Neurochem.* (2005) 94:1411–9. doi: 10.1111/j.1471-4159.2005.03291.x

37. Mackiewicz M, Zimmerman JE, Shockley KR, Churchill GA, Pack AI. What are microarrays teaching us about sleep? *Trends Mol Med.* (2009) 15:79–87. doi: 10.1016/j.molmed.2008.12.002
38. Cirelli C, Gutierrez CM, Tononi G, Extensive and divergent effects of sleep and wakefulness on brain gene expression. *Neuron* (2004) 41:35–43. doi: 10.1016/S0896-6273(03)00814-6
39. Bellesi M, Pfister-Genskow M, Maret S, Keles S, Tononi G, Cirelli C. Effects of sleep and wake on oligodendrocytes and their precursors. *J Neurosci.* (2013) 33:14288–300. doi: 10.1523/JNEUROSCI.5102-12.2013
40. Hinard V, Mikhail C, Pradervand S, Curie T, Houtkooper RH, Auwerx J, et al. Key electrophysiological, molecular, and metabolic signatures of sleep and wakefulness revealed in primary cortical cultures. *J Neurosci.* (2012) 32:12506–17. doi: 10.1523/JNEUROSCI.2306-12.2012
41. Hofstetter S, Tavor I, Tzur Moryosef S, Assaf Y. Short-term learning induces white matter plasticity in the fornix. *J Neurosci.* (2013) 33:12844–50. doi: 10.1523/JNEUROSCI.4520-12.2013
42. Tost H, Braus DF, Hakimi S, Ruf M, Vollmert C, Hohn F, et al. Acute D2 receptor blockade induces rapid, reversible remodeling in human cortical-striatal circuits. *Nat Neurosci.* (2010) 13:920–2. doi: 10.1038/nn.2572
43. Murugaiah KD, Ukponmwan OE. Functional reactivity of central cholinergic systems following desipramine treatments and sleep deprivation. *Naunyn Schmiedebergs Arch Pharmacol.* (2003) 368:294–300. doi: 10.1007/s00210-003-0784-6
44. Schule C, Di Michele F, Baghai T, Romeo E, Bernardi G, Zwanzger P, et al. Neuroactive steroids in responders and nonresponders to sleep deprivation. *Ann N Y Acad Sci.* (2004) 1032:216–23. doi: 10.1196/annals.1314.024
45. Gally JA, Edelman GM. Neural reapportionment: an hypothesis to account for the function of sleep. *C R Biol.* (2004) 327:721–7. doi: 10.1016/j.crvi.2004.05.009
46. Schoenfeld TJ, McCausland HC, Morris HD, Padmanaban V, Cameron HA. Stress and loss of adult neurogenesis differentially reduce hippocampal volume. *Biol. Psychiatry* (2017). 2:914–23. doi: 10.1016/j.biopsych.2017.05.013
47. Bellesi M, de Vivo L, Chini M, Gilli F, Tononi G, Cirelli C. Sleep loss promotes astrocytic phagocytosis and microglial activation in mouse cerebral cortex. *J Neurosci.* (2017) 37:5263–73. doi: 10.1523/JNEUROSCI.3981-16.2017
48. May A, Gaser C. Magnetic resonance-based morphometry: a window into structural plasticity of the brain. *Curr Opin Neurol.* (2006) 19:407–11. doi: 10.1097/01.wco.0000236622.91495.21
49. Ashburner J, Friston KJ. Unified segmentation. *Neuroimage* (2005) 26:839–51. doi: 10.1016/j.neuroimage.2005.02.018
50. Ashburner J, Friston KJ. Voxel-based morphometry–the methods. *Neuroimage* (2000) 11(6 Pt. 1):805–21. doi: 10.1006/nimg.2000.0582
51. Good CD, Johnsrude IS, Ashburner J, Henson RN, Friston KJ, Frackowiak RS. A voxel-based morphometric study of ageing in 465 normal adult human brains. *Neuroimage* (2001) 14(1 Pt. 1):21–36. doi: 10.1006/nimg.2001.0786
52. American Academy of Sleep Medicine. International classification of sleep disorders- second edition (ICSD-2). In: Hauri PJ, editor, *International Classification of Sleep Disorders Steering Committee*, Chicago, IL (2005).
53. American Psychiatric Association. *Diagnostic Criteria From DSM-IV-TR*. Washington, DC: American Psychiatric Association (2000).
54. Buysse DJ, Reynolds CF 3rd, Monk TH, Berman SR, Kupfer DJ, The pittsburgh sleep quality index: a new instrument for psychiatric practice and research. *Psychiatry Res.* (1989) 28:193–213. doi: 10.1016/0165-1781(89)90047-4
55. Bastien CH, Vallières A, Morin, C. M. Validation of the insomnia severity index as an outcome measure for insomnia research. *Sleep Med.* (2001) 2:297–307. doi: 10.1016/S1389-9457(00)00065-4
56. Zung WK. A self-rating depression scale. *Arch Gen Psychiatry* (1965) 12:63–70.
57. Zung WW. A rating instrument for anxiety disorders. *Psychosomatics* (1971) 12:371–9.
58. Hamilton M. A rating scale for depression. *J Neurol Neurosurg Psychiatry* (1960) 23:56–62.
59. Hamilton M. The assessment of anxiety states by rating. *Br J Med Psychol.* (1959) 32:50–5.
60. McNair DM, Lorr M, Droppleman LF. *Manual for the Profile of Mood States*. San Diego, CA: Educational and Industrial Testing Services (1971).
61. Fan J, McCandliss BD, Fossella J, Flombaum JI, Posner MI. The activation of attentional networks. *Neuroimage* (2005) 26:471–9. doi: 10.1016/j.neuroimage.2005.02.004
62. Fan J, McCandliss BD, Sommer T, Raz A, Posner MI. Testing the efficiency and independence of attentional networks. *J Cogn Neurosci.* (2002) 14:340–7. doi: 10.1162/089892902317361886
63. Biswas S, Mishra P, Mallick BN. Increased apoptosis in rat brain after rapid eye movement sleep loss. *Neuroscience* (2006) 142:315. doi: 10.1016/j.neuroscience.2006.06.026
64. Somarajan BI, Khanday MA, Mallick BN. Rapid eye movement sleep deprivation induces neuronal apoptosis by noradrenaline acting on alpha1 adrenoceptor and by triggering mitochondrial intrinsic pathway. *Front Neurol.* (2016) 7:25. doi: 10.3389/fneur.2016.00025
65. Elvsashagen T, Norbom LB, Pedersen PO, Quraishi SH, Bjornerud A, Malt UF, et al. Widespread changes in white matter microstructure after a day of waking and sleep deprivation. *PLoS ONE* (2015) 10:e0127351. doi: 10.1371/journal.pone.0127351
66. Xie L, Kang H, Xu Q, Chen MJ, Liao Y, Thiyagarajan M, et al. Sleep drives metabolite clearance from the adult brain. *Science* (2013) 342:373–7. doi: 10.1126/science.1241224
67. Muto V, Jaspar M, Meyer C, Kusse C, Chellappa SL, Degueldre C, et al. Local modulation of human brain responses by circadian rhythmicity and sleep debt. *Science* (2016) 353:687–90. doi: 10.1126/science.aad2993
68. Rosenberg J, Maximov, II, Reske M, Grinberg F, Shah NJ. "Early to bed, early to rise": diffusion tensor imaging identifies chronotype-specificity. *Neuroimage* (2014) 84:428–34. doi: 10.1016/j.neuroimage.2013.07.086
69. Chung GH, Han YM, Jeong SH, Jack CR, Jr. Functional heterogeneity of the supplementary motor area. *AJNR Am J Neuroradiol.* (2005) 26:1819–23. Available online at: http://www.ajnr.org/content/26/7/1819.full.pdf
70. Chen AC. Pain perception and its genesis in the human brain. *Acta Physiologica Sinica.* (2008) 60:677–85.
71. Harvey AG, A cognitive model of insomnia. *Behav Res Ther.* (2002) 40:869–93. doi: 10.1016/S0005-7967(01)00061-4
72. O'Byrne JN, Berman Rosa M, Gouin JP, Dang-Vu TT. Neuroimaging findings in primary insomnia. *Pathol Biol.* (2014) 62:262–9. doi: 10.1016/j.patbio.2014.05.013
73. Perlis ML, Merica H, Smith MT, Giles DE. Beta EEG activity and insomnia. *Sleep Med Rev.* (2001) 5:363–374. doi: 10.1053/smrv.2001.0151
74. Czisch M, Wetter TC, Kaufmann C, Pollmacher T, Holsboer F, Auer DP. Altered processing of acoustic stimuli during sleep: reduced auditory activation and visual deactivation detected by a combined fMRI/EEG study. *Neuroimage* (2002) 16:251–8. doi: 10.1006/nimg.2002.1071
75. Etkin A, Wager TD. Functional neuroimaging of anxiety: a meta-analysis of emotional processing in PTSD, social anxiety disorder, and specific phobia. *Am J Psychiatry* (2007) 164:1476–88. doi: 10.1176/appi.ajp.2007.07030504
76. Schacht JP, Anton RF, Myrick H. Functional neuroimaging studies of alcohol cue reactivity: a quantitative meta-analysis and systematic review. *Addict Biol.* (2013) 18:121–33. doi: 10.1111/j.1369-1600.2012.00464.x
77. Dai XJ. Brain response to sleep-related attentional bias in patients with chronic insomnia. *J Thorac Dis.* (2017) 9:1466–68. doi: 10.21037/jtd.2017.05.23
78. Gao L, Zhang M, Gong H, Bai L, Dai XJ, Min Y, Zhou F. Differential activation patterns of FMRI in sleep-deprived brain: restoring effects of acupuncture. *Evid Based Compl. Altern. Med.* (2014) 2014:465760. doi: 10.1155/2014/465760
79. Li HJ, Dai XJ, Gong HH, Nie X, Zhang W, Peng DC. Aberrant spontaneous low-frequency brain activity in male patients with severe obstructive sleep apnea revealed by resting-state functional MRI. *Neuropsychiatr Dis Treat.* (2015) 11:207–14. doi: 10.2147/NDT.S73730.
80. Peng DC, Dai XJ, Gong HH, Li HJ, Nie X, Zhang W. Altered intrinsic regional brain activity in male patients with severe obstructive sleep apnea: a resting-state functional magnetic resonance imaging study. *Neuropsychiatr Dis Treat.* (2014) 10:1819–26. doi: 10.2147/NDT.S67805
81. Kunisato Y, Okamoto Y, Okada G, Aoyama S, Demoto Y, Munakata A, Nomura M, et al. Modulation of default-mode network activity by acute tryptophan depletion is associated with mood change: a resting state functional magnetic resonance imaging study. *Neurosci Res.* (2011) 69:129–34. doi: 10.1016/j.neures.2010.11.005

82. De Havas JA, Parimal S, Soon CS, Chee MW. Sleep deprivation reduces default mode network connectivity and anti-correlation during rest and task performance. *Neuroimage* (2012) 59:1745–51. doi: 10.1016/j.neuroimage.2011.08.026
83. Chee, MWL, Chuah, LYM. Functional neuroimaging insights into how sleep and sleep deprivation affect memory and cognition. *Curr Opin Neurol.* (2008) 21:417–423. doi: 10.1097/WCO.0b013e3283052cf7
84. Tomasi D, Volkow ND. Association between functional connectivity hubs and brain networks. *Cereb Cortex* (2011) 21:2003–2013. doi: 10.1093/cercor/bhq268
85. Fukunaga M, Horovitz SG, van Gelderen P, de Zwart JA, Jansma JM, Ikonomidou VN, et al. Large-amplitude, spatially correlated fluctuations in BOLD fMRI signals during extended rest and early sleep stages. *Magn Reson Imaging* (2006) 24:979–92. doi: 10.1016/j.mri.2006.04.018
86. Liu X, Zheng J, Liu BX, Dai XJ. Altered connection properties of important network hubs may be neural risk factors for individuals with primary insomnia. *Sci Rep.* (2018) 8:5891. doi: 10.1038/s41598-018-23699-3

Conflict of Interest Statement: The authors declare that the research was conducted in the absence of any commercial or financial relationships that could be construed as a potential conflict of interest.

frontiers in Psychiatry

ORIGINAL RESEARCH
published: 17 January 2019
doi: 10.3389/fpsyt.2018.00749

Rested-Baseline Responsivity of the Ventral Striatum Is Associated With Caloric and Macronutrient Intake During One Night of Sleep Deprivation

Brieann C. Satterfield[1], *Adam C. Raikes*[1] *and William D. S. Killgore*[1,2]*

[1] *Social, Cognitive, and Affective Neuroscience Laboratory, Department of Psychiatry, College of Medicine, University of Arizona, Tucson, AZ, United States,* [2] *Department of Psychiatry, McLean Hospital, Harvard Medical School, Belmont, MA, United States*

OPEN ACCESS

Edited by:
Hengyi Rao,
University of Pennsylvania, United States

Reviewed by:
Angel Nunez,
Universidad Autónoma de Madrid, Spain
Qihong Zou,
Peking University, China
Tingyong Feng,
Southwest University, China

***Correspondence:**
William D. S. Killgore
killgore@psychiatry.arizona.edu

Specialty section:
This article was submitted to Sleep and Chronobiology, a section of the journal Frontiers in Psychiatry

Received: *07 August 2018*
Accepted: *19 December 2018*
Published: *17 January 2019*

Citation:
Satterfield BC, Raikes AC and Killgore WDS (2019) Rested-Baseline Responsivity of the Ventral Striatum Is Associated With Caloric and Macronutrient Intake During One Night of Sleep Deprivation. Front. Psychiatry 9:749. doi: 10.3389/fpsyt.2018.00749

Background: Sleep loss contributes to obesity through a variety of mechanisms, including neuroendocrine functioning, increased hunger, and increased food intake. Additionally, sleep loss alters functional activation within brain regions associated with reward and behavioral control. However, it remains unknown whether individual differences in baseline neural functioning can predict eating behaviors during total sleep deprivation (TSD). We used functional magnetic resonance imaging (fMRI) to test the hypothesis that individuals with increased baseline responsiveness within reward regions are more vulnerable to TSD-induced overeating.

Methods: $N = 45$ subjects completed several fMRI scans during a single pre-TSD session that included performance on the Multi-Source Interference Task (MSIT) and the *n*-back task. Subjects returned to the laboratory for an overnight TSD session, during which they were given *ad libitum* access to 10,900 kcal of food. Leftover food and packaging were collected every 6 h (00:00, 06:00, and 12:00) to measure total food consumption. Subjects reported sleepiness every hour and performed a food rating task every 3 h.

Results: Functional activation within the ventral striatum during the MSIT and *n*-back positively correlated with total caloric and carbohydrate intake during the final 6 h (06:00–12:00) of TSD. Activation within the middle and superior temporal gyri during the MSIT also correlated with total carbohydrates consumed. Food consumption did not correlate with subjective sleepiness, hunger, or food desire.

Conclusions: Individual differences in neural activity of reward processing areas (i.e., nucleus accumbens) *prior to* sleep deprivation are associated with an individual's propensity to overeat during subsequent sleep deprivation. This suggests that individual differences within reward processing pathways are potential key factors in sleep loss related overeating. Sleep loss and obesity are tightly linked. Both phenomena have been associated with increased neural activation in regions associated with reward, inhibitory control, and disrupted dopamine signaling. Elevated baseline reward sensitivity

in the ventral striatum appears to be further compounded by sleep deprivation induced dysfunction in the reward neurocircuitry, increasing the likelihood of overeating. Our findings suggest that large individual differences in baseline responsiveness of hedonic reward pathways may modulate the association between sleep loss and obesity.

Keywords: sleep deprivation, ventral striatum, nucleus accumbens, food consumption, reward

INTRODUCTION

The social and economic demands of living in our modern 24/7 society have contributed to two pervasive problems: insufficient sleep and obesity (1). The National Sleep Foundation recommends that adults obtain ≥7 h of sleep per night (2). However, 35% of adults in the United States sleep <7 h per night (3), a nightly duration that has been on the decline for the last several decades. Simultaneously, obesity rates have dramatically increased, with over one third of the adult population being classified as obese (4). Epidemiological evidence suggests a strong association between the declining levels of sleep and increasing rates of obesity (1, 5–7).

Sleep loss contributes to weight gain through several physiological, behavioral, and neural mechanisms. From a physiological perspective, sleep loss disrupts the normal functioning of hormones that regulate appetite (ghrelin) and satiety (leptin). Studies have demonstrated that sleep restriction results in elevated levels of ghrelin and reduced levels of leptin, leading to increased feelings of hunger (8–11). Behavioral studies of sleep restriction and sleep deprivation have also demonstrated how sleep loss impacts eating behaviors. Sleep loss leads to increased energy intake, while energy expenditure does not change (12, 13), contributing to overall weight gain (14). Individuals tend to increase their overall total caloric intake (13–16), especially in the form of carbohydrates (16) and fat (13) during sleep loss. These extra calories come from snacks (17, 18) and increased meal frequency (14).

While studies have focused on how sleep loss disrupts neuroendocrine signaling and modifies eating behavior, few have investigated the brain's neural response to food stimuli. There are several interacting neural networks which drive food intake behavior, including connections between several key cortical [orbital frontal cortex (OFC), prefrontal cortex (PFC), insula, and anterior cingulate cortex (ACC)] and limbic (amygdala, hippocampus, and basal ganglia) regions (19–22). Volkow et al. (22) suggest that obesity may be the result of an imbalance between neural circuits that promote eating behaviors (reward-saliency and motivation-drive circuits) and those that control and inhibit behavioral responses (learning-condition and inhibitory control-emotion regulation circuits) (22). Sleep loss also disrupts communication between cortical regulatory and subcortical reward systems. There is elevated neural activity in regions associated with reward and risky decision-making and attenuated activity in cortical regions associated with inhibitory control (23–25). The parallels in altered signaling patterns in these key systems for both obesity and sleep loss suggest that both conditions result in a loss of top-down inhibitory control over reward-processing regions.

Studies investigating the neural responses to food stimuli associated with daytime sleepiness, sleep restriction, and total sleep deprivation (TSD) have found evidence supporting a disruption of behavioral control and reward systems (21, 26–30). Excessive daytime sleepiness is associated with reduced neural activation in the ventromedial PFC (vmPFC), an area involved in inhibitory control, when viewing images of high calorie foods. Reduced activation in this region also correlates with subjective difficulty restricting food consumption (21). Lack of inhibition from the frontal control system may release a "brake" on subcortical pathways involved in modulating reward-based behaviors, such as eating.

Sleep restriction also impacts neural activity in regions associated with reward, including the nucleus accumbens (NAc), putamen, and vmPFC. Neural activation within these regions tends to increase when viewing food items, further supporting the notion that sleep loss alters normal reward processing and inhibitory control (27, 31). Similarly, viewing images of calorie-rich unhealthy food increases activity in regions associated with hedonic eating (i.e., eating for pleasure), including the frontal, temporal, and parietal cortices, as well as the OFC and insula (30). Activity in the inferior frontal gyrus, a region associated with inhibitory control, has also been found to increase in response to food cues (27). In addition to the regions described above, several avenues of research have found functional activation and connectivity changes in areas of the salience network [i.e., ACC, insula, etc. (32)]. This network is involved in identifying homeostatically relevant stimuli and evaluating and selecting valued options, such as food (26, 33, 34). The ACC also makes efferent and afferent connections with regions involved in reward pathways (33). Benedict et al. (26) were the first to investigate neural responses to food stimuli during TSD, finding that one night of sleep loss resulted in increased neural activation in the ACC (26). Further, one night of TSD enhanced functional connectivity between regions of the salience network, including the dorsal ACC and putamen, in relation to total fat consumption (28). Findings within the ACC suggest that sleep loss may modulate the desire for and rewarding properties of food, thus increasing the likelihood of overconsumption. Greer et al. (29)

Abbreviations: ACC, Anterior Cingulate Cortex; ART, Artifact Detection Tool; BMI, Body Mass Index; DLPFC, Dorsal Lateral Prefrontal Cortex; GLM, General Linear Model; fMRI, Functional Magnetic Resonance Imaging; FWE, Family-Wise Error; kcal, Kilocalories; KSS, Karolinksa Sleepiness Scale; MINI, Mini International Neuropsychiatric Interview; MNI, Montreal Neurological Institute; MSIT, Multi-Source Interference Task; NAc, Nucleus Accumbens; OFC, Orbital Frontal Cortex; PET, Positron Emission Tomography; PFC, Prefrontal Cortex; RDI, Recommended Daily Intake; SPM, Statistical Parametric Mapping; TE, Echo Time; TR, Repetition Time; TSD, Total Sleep Deprivation; vmPFC, Ventromedial Prefrontal Cortex.

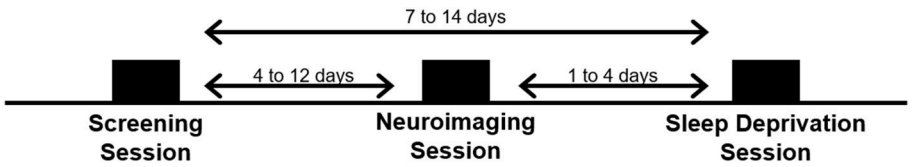

FIGURE 1 | Schematic of the three experimental visits for the study.

found that one night of sleep loss resulted in decreased neural activity in appetite evaluation regions (ACC, PFC, insula) and increased activation in the amygdala, further supporting the notion of reduced inhibitory control and increased reward drive during sleep loss (29).

Strong evidence points to altered functional activation within behavioral control and reward systems as one mechanism underlying the propensity to overeat during sleep loss. However, little work has focused on how individual differences in baseline neural activity within these circuits are associated with food consumption throughout a period of TSD. Individual differences in reward sensitivity are associated with the brain's response to food stimuli under rested conditions (19). Reward drive, as assessed by questionnaire, correlates with increased neural activation in regions of the fronto-striatal-midbrain reward circuitry (19). This hyper-responsivity of the reward network leads to an increased vulnerability to overeat. Here, we used functional magnetic resonance imaging (fMRI) to investigate how differences in pre-TSD functional activation within reward-related neural circuits can predict an individual's propensity to increase caloric and macronutrient intake during sleep loss. Specifically, in light of the well-established deficits in prefrontal inhibitory control during sleep deprivation (24, 35), we hypothesized that baseline hyper-activation in regions related to reward drive (e.g., ventral striatum) would be associated with an increased tendency to overeat during a subsequent period of sleep deprivation.

METHODS

Subjects

Forty-five healthy adults (20–45 y; 22 females) participated in this three-part study conducted in the McLean Hospital Sleep Research Laboratory. Subjects eligible for study participation met the following criteria: free from sleep, psychological, neurological or other medical disorders; right-handed as assessed by the Edinburgh Handedness Inventory (36); primary English speakers; no vision impairment, unless corrected to normal with contact lenses; no drug or alcohol abuse in the past 6 months; no history of smoking or tobacco use in the past year; and no contraindications for neuroimaging, including pregnancy or metal in the body. In order to control for fluctuations in menstrual hormones which could directly impact performance and brain neurochemistry, females underwent the functional neuroimaging scan during the follicular phase of their menstrual cycle or were taking monophasic contraceptives. Female subjects were excluded if they used multiphasic birth control.

All study procedures were approved by the Institutional Review Board (IRB) of McLean Hospital and the United States Army Human Research Protection Office (HRPO). All subjects gave written informed consent in accordance with the Declaration of Helsinki and were financially compensated for their time.

Experimental Design

Subjects visited the laboratory on three separate occasions: a screening session, a neuroimaging session, and a TSD session. See **Figure 1**.

Screening Session

Subjects first visited the lab for a comprehensive screening session. All study procedures were explained and subjects completed a series of questionnaires, including a brief psychiatric evaluation using the Mini International Neuropsychiatric Interview [MINI; (37)] to further confirm eligibility. Subjects were fitted with a wrist activity monitor (Actiwatch-2, Philips Respironics, Bend, OR) to track at-home sleep and wake patterns for at least 1 week (10.8 ± 3.3 days) prior to the third visit (i.e., the TSD session). Subjects also completed a daily online sleep diary during this time.

Neuroimaging Session (Pre-TSD)

Subjects returned to the lab ∼1 week (8.4 ± 3.2 days) following the initial screening session for a second visit. A 2 h afternoon neuroimaging session was conducted to collect structural and functional images while subjects performed a series of neurobehavioral tasks, including the Multi-Source Interference Task (MSIT) and the *n*-back task, which are described in detail below. Subjects were asked to refrain from alcohol consumption 48 h prior to the second visit and were not allowed to take any over-the-counter medications on the day of the neuroimaging scan. Additionally, subjects were asked to maintain their habitual caffeine usage on the day of the scan to minimize withdrawal effects on brain vasculature.

Total Sleep Deprivation (TSD) Session

Subjects returned to the lab for their final visit, which was scheduled 1–4 days following the neuroimaging session (2.4 ± 1.5 days). On the two nights prior to the TSD session, subjects were instructed to go to bed between 22:00 and 23:00 and remain in bed for at least 8 h. Subjects were required to wake no later than 08:00 and received a wake-up call at 07:30 from the research staff on the morning of the TSD session. Compliance was verified by wrist actigraphy. The TSD session began when subjects woke

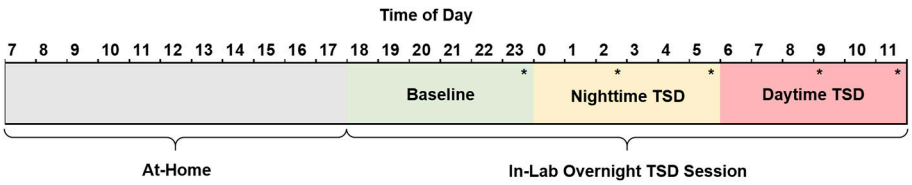

FIGURE 2 | Schematic of the 29 h TSD session. Subjects woke by 08:00, arrived at the sleep laboratory by 18:30, and remained awake until 12:00 the following day at which time they were discharged and allowed to leave the lab. Consumed food was calculated for three periods of the TSD session: baseline (18:00–23:59, green), nighttime TSD (00:00–05:59, yellow), and daytime TSD (06:00–12:00, red). Subjects performed a food rating task (*) five times throughout the night. Subjects completed the KSS (not shown) hourly beginning at 19:15. TSD, total sleep deprivation; KSS, Karolinska Sleepiness Scale.

on the day of the visit, and ended at 12:00 the following day, after ∼29 h of continuous wakefulness. After awakening on the morning of the TSD session, naps were prohibited until the end of the study. Subjects were also not allowed to consume caffeine for 24 h prior to arriving at the lab. Subjects were also asked to fast, from 13:00 until arrival at the lab later that afternoon (∼5.5 h of fasting before arrival).

Subjects arrived at the lab by 18:30 and remained awake until they were released at 12:00 the following day (**Figure 2**). Upon arrival, height and weight measurements were collected and used to calculate body mass index (BMI) following the standard formula [(weight (lbs.)/height (in.)^2) x 703]. Subjects were allowed to read, play games, and watch TV or DVDs during their free time. Additionally, subjects could access the internet to read news, watch videos, or play games. However, contact with individuals outside of the lab via personal cellphones, social media, chatting, or email was prohibited. Subjects participated in the TSD session in pairs in our controlled laboratory environment, which included a common room and individual testing rooms used for cognitive performance assessments. Light levels were kept at a fixed level and the ambient temperature remained constant for the duration of the study. Further, subjects did not have exposure to natural sunlight while in the lab. A trained research assistant was on staff at all times to administer study procedures and observe behavior throughout the overnight session. Subjects were also monitored with a closed-circuit camera for the duration of the session.

Neurobehavioral Tasks

Subjects performed a series of computerized neurobehavioral tasks during the baseline neuroimaging session and throughout the overnight TSD session. Here, we will focus on two pre-TSD (i.e., neuroimaging session) fMRI tasks (MSIT and *n*-back task), and one TSD task (Food Rating task). Subjects performed practice sessions of both the MSIT and *n*-back before entering the fMRI scanner.

Multi-Source Interference Task

The MSIT (38) was the first of three neurobehavioral tasks performed in the MRI scanner at ∼14:20 (± 55 min), following scanner calibration and structural imaging. The MSIT commonly activates the cingulo-frontal parietal network, which is important for attention and monitoring cognitive interference (39). During the task, subjects were shown a series of three numbers (0, 1, 2, or 3). One number (target) was always different from the other two numbers (distractors). Numbers were presented during either control or interference trials. In the control trials, subjects pressed the button that corresponded to the *spatial location* of the target number (i.e., 100, 020, 003), where 0s served as distractors. In the interference trials, subjects pressed the button that corresponded to the *identity* of the target (i.e., different) number (i.e., 221, 233, 322), where identical numbers served as distractors. The MSIT is described in more detail elsewhere (40). Brain activation contrast maps were created for the Interference > Control condition for each individual.

n-back Task

The *n*-back task was the second of three neurobehavioral tasks performed in the MRI scanner, immediately following the MSIT at ∼14:30 (± 55 min). The *n*-back task activates the dorsal lateral prefrontal cortex (DLPFC) and parts of the parietal cortex important for working memory (41). During the task, subjects were presented with a series of letters. Subjects pressed a button to indicate whether or not the current letter on the screen was the pre-specified target letter, the same as the letter displayed one letter earlier in the series (1-back), or the same as the letter displayed two letters back (2-back), depending on the cognitive load of the trial. The *n*-back is described in more detail elsewhere (42). Brain activation contrast maps were created for the 2-back > 0-back condition for each individual.

Food Rating Task

During the overnight TSD session, subjects performed a food rating task once every 3 h, beginning at 23:35. During the task, subjects were first asked to rate their current level of hunger on a 7-point Likert scale from 1 ("not at all hungry") to 7 ("extremely hungry"). Subjects were then shown a total of 70 food and non-food images in a randomized order. Images were either of neutral objects (e.g., flowers, trees, rocks), high-calorie foods (e.g., cheeseburgers, French fries, milkshakes), or low-calorie foods (e.g., fruits, vegetables, whole-grains). Subjects were asked to rate how much they would like to eat each item at that moment on a 7-point Likert scale from 1 ("do not want to eat it") to 7 ("strongly desire to eat it"). Similar versions of this task have been reported and described elsewhere (20, 43, 44).

Karolinska Sleepiness Scale (KSS)

The KSS is a 9-point Likert scale used to measure subjective sleepiness (45). Subjects rated their current level of sleepiness

from 1 ("extremely alert") to 9 ("very sleepy, great effort to keep awake, fighting sleep"). The KSS was administered hourly beginning at 19:15 as part of a larger standardized test battery that is outside the scope of this paper.

Food

Prior to the start of the TSD session, a trained research assistant prepared identical food baskets for each subject, labeled with the corresponding subject number. For a full list of food items, see the Supplemental Material (**Table S1**). Subjects recorded all food and drink items they consumed the morning of the TSD session and were required to fast from 13:00 to 18:30 (∼5.5 h) prior to entering the laboratory. Following study arrival and intake procedures at 18:30, subjects had *ad libitum* access to 10,900 kcal of food throughout the entire TSD period (see **Table 2** for nutritional breakdown). Subjects discarded food packaging and unwanted leftovers in individualized trash bins labeled with their corresponding subject number. Trained research assistants also observed and recorded food intake throughout the TSD session. Discarded packaging and leftover food items were collected at 6 h intervals (00:00, 06:00, and 12:00). Total calories, calories from fat, grams of fat, grams of carbohydrates, grams of protein, and grams of sugar were documented according to the per serving nutritional values on the food packaging. For items that did not have packaging (apples, bananas) nutritional information was obtained from the U.S. Department of Agriculture Food Composition Database (https://ndb.nal.usda.gov/ndb/). For items partially consumed, values were recorded to the nearest fraction (i.e., $^1/_4$, $^1/_3$, $^1/_2$, $^2/_3$) of the full nutritional value listed. For analytic purposes, food consumption was broken down into three 6 h periods (Baseline: 18:00–23:59; Nighttime TSD: 00:00–05:59; Daytime TSD: 06:00–12:00) see **Figure 2**.

Neuroimaging Methods

Subjects underwent an fMRI scan at the end of the second visit. Neuroimaging scans were collected on a 3.0 Tesla Siemens Tim Trio Scanner (Siemens, Erlangen, Germany) with a 32-channel head coil. First, structural T1-weighted 3D images were collected with a magnetization-prepared rapid gradient-echo (MPRAGE) sequence (repetition time [TR] = 2.1 s; echo time [TE] = 2.3 ms; flip angle (FA) = 12°) over 176 sagittal slices (256 × 256 matrix) with a slice thickness of 1.0 mm (voxel size = 1.0 × 1.0 × 1.0 mm). T2*-weighted functional scans were collected over 34 transverse slices (3.5 mm thickness, no gap) using an interleaved sequence (TR = 2.0 s; TE = 30 ms; FA = 90°) with 198 images and 239 images collected per slice for the MSIT and *n*-back, respectively. Data were collected with a 22.4 cm field of view, 64 × 64 acquisition matrix, and a voxel size of 3.5 × 3.5 × 3.5 mm^3.

Image Processing

Functional neuroimaging scans were analyzed and processed using Statistical Parametric Mapping software (SPM12; Welcome Department of Cognitive Neurology, London, UK; http://www.fil.ion.ucl.ac.uk/spm/). The raw functional images were first realigned and unwarped. Realigned images were co-registered to each individual's T1-weighted structural image. Subject images were then normalized from the original native space to the 3D space of the Montreal Neurological Institute (MNI) using forward deformation fields. The images were then spatially smoothed with a 6 mm full-width half maximum isotropic Gaussian kernel and resliced to 2 × 2 × 2 mm^3 voxels using 4th degree B-spline interpolations. Low frequency confounds were removed using a high-pass filter with a 128 s cutoff period. The standard canonical hemodynamic response function for SPM12 was employed, and serial correlation was corrected using a first-order autoregressive model (AR1). The Artifact Detection Tool (ART; http://www.nitrc.org/projects/artifact_detect/) for SPM12 was used to remove motion and spiking artifacts. Scans exceeding 3 standard deviations in mean global intensity, scan-to-scan motion that exceeded 1 mm, and the first scan of each run were regressed out of each 1st level analysis.

Statistical Analyses

First level analyses were conducted in SPM12 using a general linear model (GLM) to create subject-specific brain activation maps by contrasting the Interference and Control conditions (Interference > Control) on the MSIT and the 2-back and 0-back conditions (2-back > 0-back) on the *n*-back. Contrast images were then entered into separate second level multiple regression models to assess the relationship between well-rested functional activation during the MSIT and *n*-back tasks and caloric and macronutrient consumption during the three periods of the TSD session. Gender, BMI, and caloric/macronutrient intake during baseline (18:00–00:00) were included as covariates for nighttime TSD and daytime TSD analyses.

Whole brain-analyses were initially height thresholded at $p < 0.001$ (uncorrected). Cluster-level statistics were corrected for family-wise error (FWE) at $p < 0.05$. For *post-hoc* analyses, the first eigenvariates for the significant clusters were extracted from SPM12 for regression and plotting purposes in SAS (v9.4). Additionally, Pearson's partial correlations, controlling for BMI and gender, were used to compare caloric and macronutrient intake to baseline and TSD subjective sleepiness levels. Simple linear regression models were used to individually assess the relationship between individual caloric intake and macronutrient intake and subjective hunger food desire ratings and KSS score as a function of time awake. Additionally, linear regression was used to assess the relationship between BMI and caloric/macronutrient and gender and caloric/macronutrient intake during each TSD period.

RESULTS

Subject Characteristics

Subject characteristics are summarized in **Table 1**.

Caloric and Macronutrient Intake

During the at-home portion of the study on the first day of sleep deprivation (∼11 h total), subjects consumed an average of 1135.2 ± 414.9 total calories and 379.9 ± 232.1 calories from fat prior to entering the laboratory. They consumed 158.2 ± 169.8 g of carbohydrates, 52.2 ± 27.0 g of sugar, 117.1 ± 1.0 g of fat, and 45.6 ± 23.3 g of protein. Throughout the in-laboratory portion

of the TSD session (17 h total), subjects consumed an average of 2,503.4 ± 754.0 total calories of the 10,900 calories available. On average, they consumed 769.4 ± 302.6 calories from fat, 380.7 ± 124.6 g of carbohydrates, 187.9 ±75.5 g of sugar, 85.5 ± 33.6 g of fat, and 61.2 ± 18.9 g of protein. Total caloric and macronutrient intake for the overnight session exceeded the recommended daily intake (RDI) values for an entire day based on a 2,000-calorie diet (**Table 2**).

Body mass index (BMI) did not predict total caloric intake during any of the three TSD periods (baseline: $[F_{(1,43)} = 2.80, p = 0.10, R^2 = 0.06]$; nighttime TSD: $[F_{(1,43)} = 2.56, p = 0.12, R^2 = 0.06]$; daytime TSD: $[F_{(1,43)} = 1.96, p = 0.17, R^2 = 0.04]$). Likewise, BMI did not predict total calories from fat, grams of fat, or grams of carbohydrates for any of the TSD periods $[F_{(1,43)} < 3.48, p > 0.07]$. However, higher BMI was significantly associated with more grams of sugar consumed during baseline $[F_{(1,43)} = 5.66, p = 0.02]$, but not during nighttime or daytime TSD. Higher BMI was also significantly associated with more grams of protein consumed during nighttime TSD $[F_{(1,43)} = 4.63, p = 0.04]$, but not during baseline or daytime TSD. Gender was not a significant predictor of total caloric intake during any of the three TSD periods (baseline: $[F_{(1,43)} = 1.69, p = 0.20]$; nighttime TSD: $[F_{(1,43)} = 0.0, p = 0.97]$; daytime TSD: $[F_{(1,43)} = 0.09, p = 0.76]$). Gender did not predict total calories from fat, grams of fat, grams of carbohydrates, or grams of protein consumed during any of the TSD periods $[F_{(1,43)} < 3.13, p > 0.08]$. However, males consumed significantly more sugar during baseline $[F_{(1,43} = 4.81, p = 0.03]$ compared to females. These differences were not apparent during nighttime or daytime TSD. Full statistical results can be found in the Supplemental Material (**Table S2**).

TABLE 1 | Subject characteristic.

Characteristic	Mean (± *SD*)
Age (y)	25.4 ± 5.6
Height (m)	1.7 ± 0.1
Weight (kg)	72.7 ± 12.9
BMI (kg/m^2)[a]	23.9 ± 3.7
Normal weight ($n = 30$)	21.8 ± 1.9
Overweight ($n = 12$)	27.3 ± 1.3
Obese ($n = 3$)	31.8 ± 1.6
Time in bed (min)[b]	501.7 ± 77.4
Sleep duration (min)[b]	448.7 ± 72.7
Bedtime (hh:mm ± min)[b]	22 : 56 ± 68.7
Wake time (hh:mm ± min)[b]	07 : 17 ± 61.4

[a] *BMI categories are defined as follows: Normal: 18.5–24.9 kg/m^2; Overweight: 25.0–29.9 kg/m^2; Obese: >30.0 kg/m^2.*
[b] *Time in bed, sleep duration, and bed and wake times were derived from wrist actigraphy for the one night prior to the TSD period.*

Neural Correlates of Caloric and Macronutrient Intake

Figure 3 shows the clusters (FWE corrected) with significant correlations between MSIT (Interference > Control) performance and total caloric (blue) or carbohydrate (green) intake. While no regions of the brain were associated with calorie consumption during the baseline and overnight periods, we observed a significant correlation between activation within the ventral striatum and calories consumed ($p = 0.024$) in the next-day period between 06:00 and 12:00 during TSD (**Figure 3A**). This pattern was accounted for primarily by a significant correlation in the ventral striatum for grams of carbohydrates consumed ($p = 0.016$) during the same timeframe (**Figure 3A**). In addition, we observed significant correlations in the right middle temporal gyrus ($p < 0.001$) and the left superior temporal gyrus ($p = 0.038$) for grams of carbohydrates consumed (**Figure 3B**). Activation in the reward circuitry, specifically the NAc, while performing the MSIT under well-rested conditions predicted both total calories consumed and total carbohydrates consumed during hours 23–29 of continuous wakefulness (i.e., the last 6 h of the TSD session; **Figure 3A**). Similarly, activation in areas associated with viewing unhealthy food (30) (middle and superior temporal gyri) predicted increased carbohydrate consumption (**Figure 3B**). Higher activation in each region was associated with increased caloric and carbohydrate consumption (**Figure 4**). However, activation in these regions did not predict consumption of total calories from fat, grams of sugar, grams of

TABLE 2 | Caloric and macronutrient intake across the in-laboratory sleep deprivation session.

		At-Home[b] 08:00–13:00		Baseline 18:00–23:59		Nighttime TSD 00:00–05:59		Daytime TSD 06:00–11:59		Total TSD		
	Available[a]	Mean	*SD*	Mean	*SD*	Mean	*SD*	Mean	*SD*	Mean	*SD*	% RDI[c]
Total calories (kcal)	10,900	1135.2	414.9	1175.2	468.1	780.9	419.0	547.4	226.9	2503.4	754.0	125.2
Calories from fat (kcal)	2,700	379.9	232.1	414.8	207.1	246.1	162.9	108.6	91.9	769.4	302.6	109.9
Carbohydrates (g)	1,400	158.2	69.6	163.5	77.2	117.1	64.7	100.1	40.0	380.7	124.6	138.4
Sugar (g)	600	52.2	27.0	75.5	44.5	55.0	36.9	57.4	24.4	187.9	75.5	375.7
Fat (g)	300	117.1	169.8	46.2	23.1	27.3	18.1	12.0	10.2	85.5	33.6	109.6
Protein (g)	200	45.6	23.3	29.2	11.7	19.2	12.2	12.8	8.5	61.2	18.9	122.4

[a] *Values are rounded to the nearest 100. Available values refer to in-lab portion only.*
[b] *Self-reported food diaries were used to calculate nutritional information. Subjects were required to fast from 13:00–18:30 prior to arriving at the lab.*
[c] *Recommended Daily Intake (RDI) as set by the United States Food and Drug Administration.*

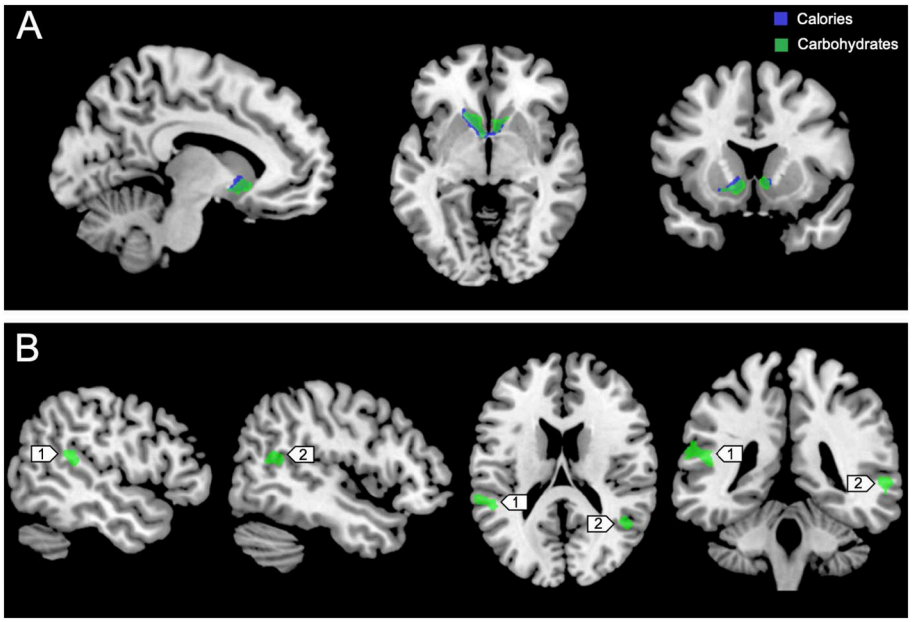

FIGURE 3 | Whole-brain analyses ($p < 0.001$, cluster corrected; $p < 0.05$, FWE) of MSIT activation during the Interference > Control condition. **(A)** Sagittal, axial, and coronal views of significant activation in the nucleus accumbens (MNI: −10, 10, −8) as it correlates with total calories (blue) and total carbohydrates (green) consumed during the last 6 h of sleep deprivation (i.e., 06:00–12:00). **(B)** Significant activation in the left superior temporal gyrus (1; MNI:−64, −36, 18) and right middle temporal gyrus (2; MNI: 64, −46, 4) as it correlates with total carbohydrates (green) consumed during the last 6 h of sleep deprivation. FWE, Family-wise error; MSIT, Multi-Source Interference Task; MNI, Montreal Neurological Institute.

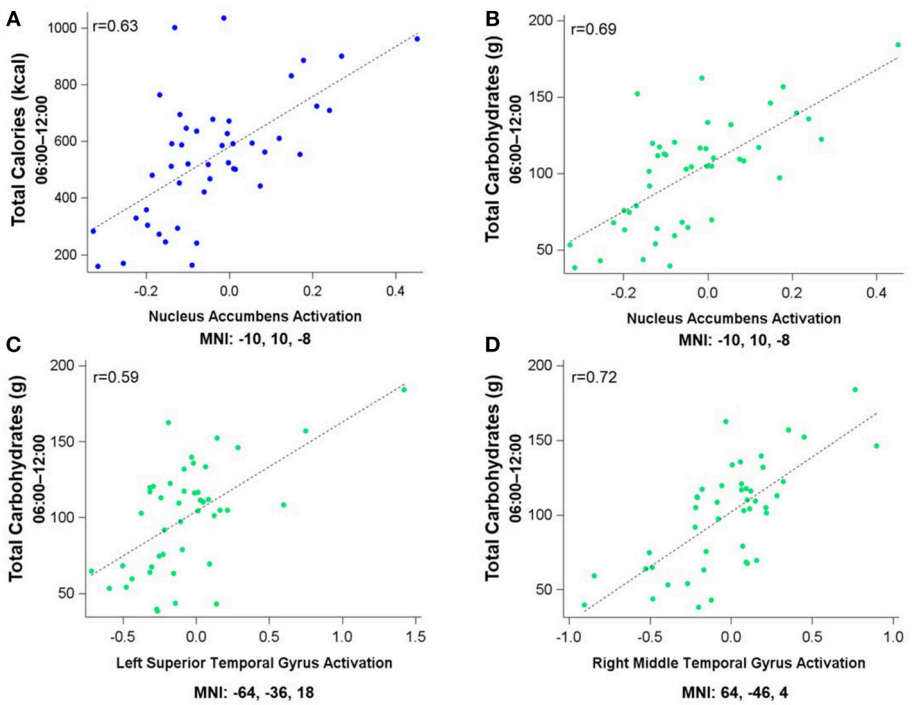

FIGURE 4 | Residualized eigenvariates for the neural activation in the left nucleus accumbens during the MSIT Interference > Control condition as it relates to **(A)** total calories and **(B)** total carbohydrates consumed during the last 6 h of sleep deprivation and **(C,D)** activation in the temporal gyri as it relates to total carbohydrates consumed during the last 6 h of sleep deprivation.

TABLE 3 | Cluster maxima for whole-brain multiple regression analyses of the MSIT Interference > Control condition and *n*-back 2-back > 0-back condition as it pertains to caloric and carbohydrate consumption.

	Anatomical region	Hemisphere	Cluster size	T_{40}	Cluster p^a	x	y	z
MSIT								
Calories	Nucleus accumbens	L	181	5.15	0.024	−10	10	−8
Carbohydrates	Nucleus accumbens	L	196	5.97	0.016	−10	10	−8
	Middle temporal gyrus	R	423	6.39	<0.001	64	−46	4
	Superior temporal gyrus	L	158	4.47	0.038	−64	−36	18
***n*-back**								
Calories	Nucleus accumbens	L	226	4.41	0.026	−4	18	2
Carbohydrates	Nucleus accumbens	L	266	4.46	0.013	−4	18	2

[a] *Cluster level analyses were family-wise error corrected at $p < 0.05$, with whole-brain analyses thresholded at $p < 0.001$. MSIT, Multi-Source Interference Task.*

fat, or grams of protein. Neuroimaging results are summarized in **Table 3**.

Figure 5 shows the clusters (FWE corrected) with significant correlations between *n*-back performance (2-back > 0-back) and total caloric (blue) and carbohydrate (green) intake. Critically, there was no association between brain activation and calorie consumption at baseline or during the night. However, similar to the previous findings for the MSIT, we observed a significant correlation between activation of the ventral striatum during the *n*-back and subsequent calories consumed ($p = 0.026$) during the morning between 06:00 and 12:00 during TSD (**Figure 5**). Likewise, we observed a significant correlation in the ventral striatum for grams of carbohydrates consumed ($p = 0.013$) in the same timeframe (**Figure 5**). Similar to the MSIT, activation in the NAc while performing the *n*-back under well-rested conditions predicted both total caloric intake and grams of carbohydrates consumed during the last 6 h of TSD. Higher activation in this region was associated with higher caloric and carbohydrate intake (**Figure 6**). However, like the MSIT, activation did not predict consumption of total calories from fat, grams of sugar, grams of fat, or grams of protein. Neuroimaging results are summarized in **Table 3**.

Subjective Sleepiness (KSS) Ratings

Subjective ratings of sleepiness were low during the baseline period (3.73 ± 0.73) and steadily increased across the nighttime (5.78 ± 2.01) and daytime TSD hours (6.41 ± 2.00) as expected with extended wakefulness. KSS scores during the baseline, nighttime, and daytime TSD periods were not significantly correlated with total caloric ($r < 0.10$, $p > 0.53$) or carbohydrate ($r < 0.16$, $p > 0.30$) intake (**Figure S1**). Full statistical results are reported in the Supplemental Material (**Table S3**).

Subjective Hunger and Food Desire Ratings

Average subjective hunger ratings were low during both the nighttime (2.34 ± 0.89) and daytime TSD (2.26 ± 1.17) periods. **Figure 7** shows subjective hunger ratings and desire ratings for high- and low-calorie foods across the TSD period in relation to total caloric intake. Regression analyses indicated that average hunger ratings did not change across the sleep deprivation session [$F_{(1,223)} = 0.12$, $p = 0.73$, $R^2 < 0.001$]. Likewise, there was no change in desire for high-calorie [$F_{(1,223)} = 2.32$, $p = 0.13$, $R^2 = 0.01$] or low-calorie [$F_{(1,223)} = 3.03$, $p = 0.08$, $R^2 = 0.01$] foods across time. However, total caloric and carbohydrate intake did change across the sleep deprivation period (calories: [$F_{(1,133)} = 59.49$, $p < 0.001$, $R^2 = 0.31$]; carbohydrates: [$F_{(1,133)} = 23.11$, $p < 0.001$, $R^2 = 0.15$]), generally declining with longer time awake. Hunger ratings were stable for the duration of the overnight session.

DISCUSSION

This study investigated whether pre-TSD neural activation in reward-related brain regions was associated with total caloric and macronutrient intake during one night of sleep deprivation. On average, subjects consumed 2,500 kcal throughout the 17 h in-lab portion of the TSD session, exceeding the recommended total daily value of 2,000 kcal (46). The observed caloric intake during extended wakefulness was similar to other sleep restriction (18) and sleep deprivation studies (28). Moreover, we found that functional activation in the bilateral NAc (most prominently on the left) during two independent cognitively demanding tasks (i.e., MSIT and *n*-back) pre-TSD (**Figures 3A**, **5**) was significantly associated with total caloric (**Figures 4A**, **6A**) and carbohydrate (**Figures 4B**, **6B**) intake during the last 6 h of TSD (06:00–12:00). In addition, while not predicted, we found that activation within the middle and superior temporal gyri (**Figure 3B**) also correlated with total carbohydrate consumption during the same timeframe (**Figures 4C,D**). Baseline activation was not associated with calories from fat, grams of fat, grams of protein, or grams of sugar consumed during any portion of the overnight TSD session. To our knowledge, this is the first study to demonstrate that individual differences in baseline activation of the ventral striatum are potentially *predictive* of eating behaviors several days later during one night of TSD.

Our findings suggest that individuals with greater baseline responsiveness within the reward system (i.e., NAc) when well-rested may be most vulnerable to overeating during subsequent

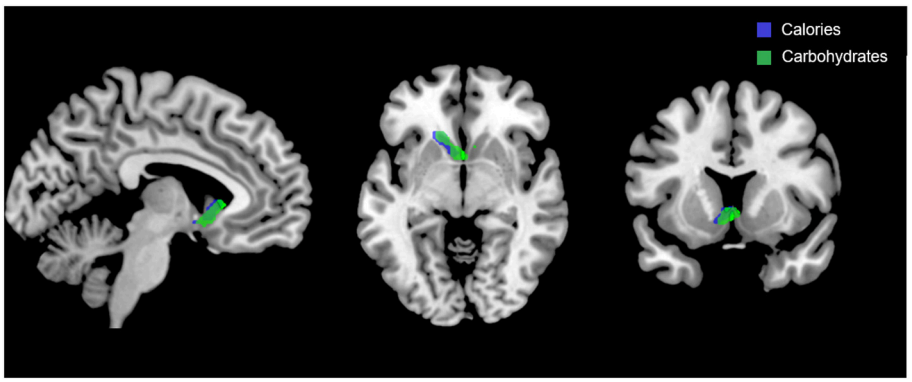

FIGURE 5 | Whole-brain analyses ($p < 0.001$, cluster corrected; $p < 0.05$, FWE) of *n*-back activation during the 2-back > 0-back condition. Sagittal, axial, and coronal views of significant activation in the nucleus accumbens (MNI:−4, 18, 2) as it correlates with total calories (blue) and total carbohydrates (green) consumed during the last 6 h of sleep deprivation (i.e., 06:00–12:00). FWE, Family-wise error; MNI, Montreal Neurological Institute.

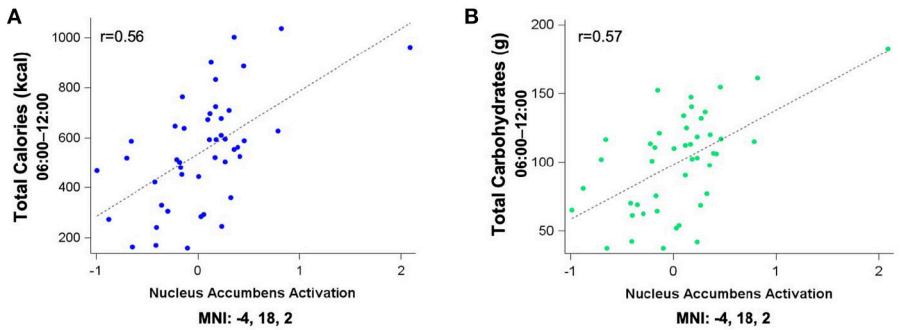

FIGURE 6 | Residualized eigenvariates for the neural activation in **(A)** the left nucleus accumbens during the *n*-back 2-back > 0-back condition as it relates to total calories (blue) and **(B)** total carbohydrates (green) consumed during the last 6 h of sleep deprivation.

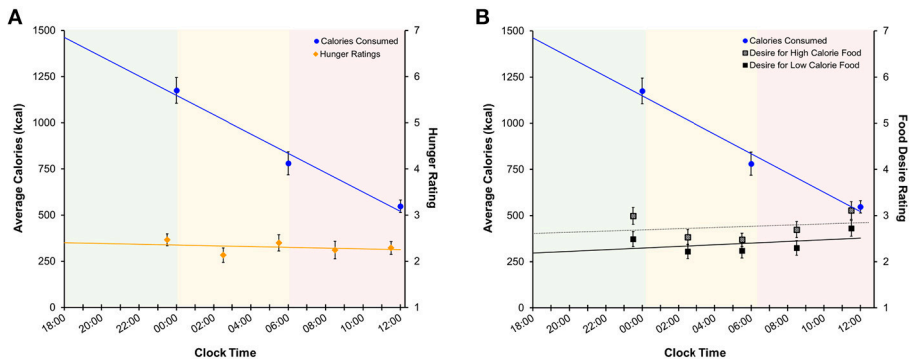

FIGURE 7 | Regression models of mean (±SE) **(A)** calories consumed (left axis) and subjective hunger ratings (right axis) and **(B)** calories consumed and food desire ratings across the sleep deprivation period. Shaded areas represent the three TSD periods. Green: baseline; yellow: nighttime TSD; red: daytime TSD. TSD, total sleep deprivation.

sleep deprivation. As outlined in greater detail in the sections that follow, we suggest that when considered in light of the well-known decreases in prefrontal inhibitory control that occur during sleep deprivation, those individuals with the greatest sustained NAc reward responses may be most prone to overconsuming calories when lacking sleep. Excess reward responsiveness in conjunction with sleep loss-induced deficits in prefrontal inhibitory control is likely to represent a problematic

combination when one encounters attractive high-calorie foods.

Our findings complement evidence from previous studies assessing the neural responses to food cues and subsequent food intake (47) or weight gain (48) during rested conditions and studies assessing neural responses to food stimuli during sleep restriction or TSD (26, 27, 29, 31). Studies using fMRI have shown increased neural reactivity in reward-related brain regions, specifically in the NAc, in response to food images during both rested (47, 48) and sleep-restricted conditions (27, 31). St. Onge et al. (31) found that when sleep was restricted to 4 h per night for six nights, subjects showed increased neural activity in reward-related regions, including the NAc and the superior temporal gyri, when viewing images of food vs. images of non-food items (31). In a follow-up study, they found that viewing unhealthy foods during sleep restriction increased neural activation in several cortical regions, including the middle and superior temporal gyri (30). Further, the temporal gyri have been implicated in the perception and cognitive processing of emotional stimuli (49), including increased neural responses to food stimuli during a satiated state (50). Individuals diagnosed with anorexia nervosa, compared to controls, do not show such elevated responses, suggesting that altered activation patterns in these regions may be related to increased responsiveness to the pleasurable characteristics of food, and therefore may contribute to the control of food intake (50). We found that high pre-TSD activation in these cortical areas is strongly associated with carbohydrate consumption during TSD. Additionally, a recent study by Demos et al. (27) found that when sleep was restricted to 6 h per night for four nights, neural activity increased in the left and right NAc when viewing images of food (27). In addition to findings in studies of sleep restriction, studies in well-rested individuals have shown that increased reactivity of the NAc to food stimuli is associated with both weight gain (48) and increased snacking behavior (47). Taken together, these studies demonstrate that individual differences in responsivity of the fronto-striatal-midbrain reward circuitry contribute to increased hedonic food consumption during sleep loss. While we did not measure fMRI activation *during* sleep deprivation, prior evidence suggests that sleep loss does in fact alter activation patterns of the reward system in response to food stimuli (26, 27, 29, 31). Therefore, it is plausible that individuals with increased striatal activity prior to sleep loss, as shown here, may be more susceptible to TSD-induced perturbations to the underlying neurocircuitry associated with reward-driven behaviors, thus contributing to the tendency to overeat.

Imaging studies in obese individuals suggest that there is a discrepancy between the enhanced sensitivity of an expected reward (i.e., seeing food) and a decreased sensitivity to the gratifying effects of the reward (i.e., eating food). That is, there is an increased propensity to overeat because the reward expectation is never met (22). We propose that a similar phenomenon may be occurring during TSD, especially among those individuals with elevated baseline reward sensitivity. The data here suggest that individuals with higher baseline neural responsiveness within the NAc have a "reward anticipation reserve," meaning that they are more likely to expect a reward from their actions (25), but the reward expectations may not be fully met.

While not directly assessed in the present study, we speculate dopamine[1] may play a mechanistic role in the present findings. Dopamine is a key neurotransmitter in reward circuits and underlies the pleasurable properties of food. Overweight and obese individuals show signs of disrupted reward processing within the striatum, including altered neural activity and dopamine release, as well as decreased dopamine D_2 receptor availability (22, 52). Interestingly, sleep loss impairs dopamine signaling in a similar manner, such that dopamine D_2 receptors are downregulated, (53, 54) and neural activation in the ventral striatum is increased, (27, 29–31) both of which are similar to findings in overweight and obese individuals. Due to the downregulation of D_2 receptors in the striatum, it is probable that dopamine is unable to bind effectively to the limited number of D_2 receptors that are available. Therefore, dopamine signals that indicate a reward expectation have been met are potentially disrupted. The effect that sleep loss has on dopamine function within the striatum may be amplified in individuals with elevated baseline reward sensitivity, making these individuals more vulnerable to overeating during sleep loss. Alternatively, the reduction of dopamine D_2 receptor availability may push the system into a D_1 receptor dominated state, thereby promoting reward-driven behavior, such as eating (55).

Dopamine signaling within the striatum is also linked to the receptor activity of a well-characterized neural substrate, adenosine. Adenosine accumulates with extended wakefulness and has been implicated in homeostatic sleep regulation, as it inhibits neural activity in wake-promoting regions of the brain (56). Within the striatum, dopamine D_2 receptors are co-localized with adenosine A_{2A} receptors and functionally interact in an antagonistic manner (57). That is, the binding of adenosine to the A_{2A} receptors inhibits the actions of the dopamine D_2 receptors, thus impairing downstream dopamine-related neurotransmission. The inhibition of D_2 receptor activity by adenosine, in combination with the downregulation of D_2 receptors during sleep loss, may also contribute to overeating by further disrupting normal reward signaling pathways.

In addition to increased reward sensitivity and disrupted dopamine signaling in the basal ganglia, there is evidence from positron emission topography (PET) imaging that one night of TSD reduces glucose metabolism within the PFC, including the vmPFC (24). The vmPFC is considered an inhibitory emotional control region, and dysfunction may contribute to a loss of inhibitory control over subcortical reward regions, such as the NAc. Loss of inhibitory control over emotional responses can lead to increased risky behavior and impulsivity, potentially increasing the tendency to overeat

[1]Dopamine exerts its effects on reward circuits by binding to either D_1 or D_2 receptor subtypes located throughout the brain, including the fronto-striatal reward pathways. It should be noted that these subtypes have different functional implications that are beyond the scope of this paper (51).

(58–61). Risky decisions during sleep loss are associated with increased NAc activation, (25) similar to how the brain responds when viewing images of food when sleep restricted (27, 31). This increase in neural activation during risky decision making presumably results in an elevated expectation of reward (25). Simultaneously, neural activation within the OFC is reduced, suggesting an attenuated ability to learn from any negative consequences from the risky behavior, (25) such as weight gain associated with increased caloric intake. Additionally, reduced PFC glucose metabolism is correlated with reduced D_2 receptor availability in obese individuals, further implicating impaired inhibitory control in overeating (52). Taken together, these earlier studies suggest that in combination with individual differences in baseline NAc activation, sleep loss may amplify the inability to inhibit impulsive eating behavior and increase the expectation of reward from eating, ultimately leading to over consumption of high calorie foods and carbohydrates.

Similar to findings in previous studies (27, 29, 47) we found no association between hunger ratings and food consumption during TSD (**Figure 7A** and **Figure S2A**), as hunger ratings remained stable throughout each period of the TSD session. Desire for high- and low-calorie foods also remained stable across the night (**Figure 7B** and **Figure S2B**). While both hunger and food desire ratings remained stable, it should be noted that overall caloric (**Figure 7**) and carbohydrate (**Figure S2**) intake decreased as a function of time awake. However, subjects consumed roughly 60% of the recommended RDI within the first 6 h of the study (**Table 2**), suggesting that the decline in consumption is a result of satiation. It is important to note that subjects still consumed a significant number of calories during the nighttime and daytime TSD periods, and the findings for the final morning period were statistically controlled for calorie consumption in the prior periods. Further, we did not find evidence that subjective sleepiness is correlated with increased caloric and carbohydrate intake (**Figure S1**). Taken together, our results suggest that: (1) hunger or desire for food was not the primary driving force for the excessive food consumption demonstrated here; and (2) subjects were not overeating due to increased sleepiness or as a means to stay awake. These findings offer further support of the mechanistic theory that impaired functioning within the reward circuitry contributes to heightened hedonic motivations for food during TSD.

The present study demonstrates a strong association between pre-TSD reward sensitivity and the tendency to overeat during sleep loss. However, several limitations should be addressed. First, neuroimaging scans were not collected during the TSD session, which limits our ability to understand the dynamic changes in brain activation patterns as they relate to caloric and macronutrient intake, hunger, desire for food, and sleepiness. Further, it remains unknown whether or not the findings presented are unique to TSD, or whether the neural activation and food consumption patterns are also observed under well-rested control conditions. However, it is important to note that we only found a significant relationship between pre-TSD activation and food consumption during hours 23–29 of wakefulness, and not during the first 12 h of the in-lab TSD session, suggesting that the effects are only present following a sufficient amount of sleep loss. Future studies should assess the relationship between brain activation patterns and food consumption in well-rested and TSD groups. Second, although subjects provided a self-report log of foods consumed prior to arriving at the laboratory, it is impossible to completely verify compliance with the 5 h fasting period before the in-lab portion of the study. Third, it should be noted that our study population consisted of young, healthy adults, and we do not know how our findings are generalizable to other populations. Additionally, increased caloric and macronutrient intake during sleep loss, and its relation to obesity, is a multifaceted problem. Eating behaviors may be modified by a number of physiological and environmental factors including changes in appetite and satiety hormones, meal timing, gender, BMI, genetics, and lifestyle (6, 62). Our BMI range was not restricted, and included individuals classified as either normal, overweight, or obese (**Table 1**). While we showed no association between BMI and caloric/carbohydrate consumption, this factor should not be overlooked in future studies as some evidence suggests that brain responses to food images differs among lean and obese individuals (63, 64). In addition, we showed no gender differences in total caloric or carbohydrate intake, only differences in baseline sugar consumption. Due to the limited scope of the paper, we did not assess lifestyle, hormones, or genetic markers as possible additional factors that may modulate some of the hedonic pathways discussed here.

Overall, we demonstrated that pre-TSD activation within the ventral striatum, as well as the middle and superior temporal gyri, is associated with eating behaviors during a single night of sleep loss. Individuals with elevated neural activity in these regions consumed significantly more calories and carbohydrates after a night of sleep deprivation. These findings suggest that there are large individual differences in baseline functioning within hedonic reward pathways and sleep loss further disrupts functioning in these pathways. Elevated reward sensitivity appears to impact eating behaviors during sleep loss and may be a major contributor to the etiology of sleep loss related obesity.

AUTHOR CONTRIBUTIONS

BS conducted the MRI data processing and statistical analyses, and drafted the initial manuscript. AR assisted with manuscript revisions. WK designed the study, secured funding, collected the data, assisted with data interpretation, and critique, as well as contributed to manuscript review and revisions.

FUNDING

This work was supported by the Defense Advanced Research Projects Agency (DARPA) by the DARPA Young Faculty Award (D12AP00241) granted to WK. Opinions, interpretations,

conclusions, and recommendations are those of the authors and are not necessarily endorsed by DARPA or the U.S. Department of Defense.

ACKNOWLEDGMENTS

We gratefully acknowledge the contributions of Mareen Weber, Elisabeth Olson, Christian Webb, Maia Kipman, Sophie DelDonno, Zack Schwab, Lily (Preer) Sonis, Hanna Gogel, Olga Tkachenko, and David Penetar to data collection.

SUPPLEMENTARY MATERIAL

The Supplementary Material for this article can be found online at: https://www.frontiersin.org/articles/10.3389/fpsyt.2018.00749/full#supplementary-material

REFERENCES

1. Bayon V, Leger D, Gomez-Merino D, Vecchierini M-F, Chennaoui M. Sleep debt and obesity. *Ann Med.* (2014) 46:264–72. doi: 10.3109/07853890.2014.931103
2. Hirshkowitz M, Whiton K, Albert SM, Alessi C, Bruni O, DonCarlos L, et al. National Sleep Foundation's sleep time duration recommendations: methodology and results summary. *Sleep Heal.* (2015) 1:40–3. doi: 10.1016/j.sleh.2014.12.010
3. Liu Y, Wheaton A, Chapman D, Cunningham T, Lu H, Croft J. Prevalence of healthy sleep duration among adults - United States, 2014. *Morb Mortal Wkly Rep.* (2016) 65:137–41. doi: 10.15585/mmwr.mm6608a2
4. Segal LM, Rayburn J, Beck SE. *The State of Obesity: Better Policies for a Healthier America*. Trust for America's Health and Robert Wood Johnson Foundation (2017).
5. Cappuccio FP, Taggart FM, Kandala N-B, Currie A, Peile E, Stranges S, et al. Meta-analysis of short sleep duration and obesity in children and adults. *Sleep* (2008) 31:619–26. doi: 10.1093/sleep/31.5.619
6. Dashti HS, Scheer F, Jacques PF, Lamon-Fava S, Ordovás JM. Short sleep duration and dietary intake: epidemiologic evidence, mechanisms, and health implications. *Adv Nutr.* (2015) 6:648–59. doi: 10.3945/an.115.008623.648
7. St-Onge M-P. Sleep-obesity relation: underlying mechanisms and consequences for treatment. *Obes Rev.* (2017) 18:34–9. doi: 10.1111/obr.12499
8. Schmid SM,Hallschmid M, Jauch-Chara K, Born J, Schultes B. A single night of sleep deprivation increases ghrelin levels and feelings of hunger in normal-weight healthy men. *J. Sleep Res.* (2008) 17:331–4. doi: 10.1111/j.1365-2869.2008.00662.x
9. Spiegel K, Leproult R, L'Hermite-Balériaux M, Copinschi G, Penev PD, Van Cauter E. Leptin levels are dependent on sleep duration: relationships with sympathovagal balance, carbohydrate regulation, cortisol, and thyrotropin. *J. Clin. Endocrinol. Metab.* (2004) 89:5762–71. doi: 10.1210/jc.2004-1003
10. Spiegel K, Tasali E, Penev P, Van Cauter E. Sleep curtailment in healthy young men is associated with decreased leptin levels, elevated ghrelin levels, and increased hunger and appetite. *Am Coll Physicians* (2004) 141:846–50. doi: 10.7326/0003-4819-141-11-200412070-00008
11. Taheri S, Lin L, Austin D, Young T, Mignot E. Short sleep duration is associated with reduced leptin, elevated ghrelin, and increased body mass index. *PLoS Med.* (2004) 1:e62. doi: 10.1371/journal.pmed.0010062
12. Al Khatib HK, Harding SV, Darzi J, Pot GK. The effects of partial sleep deprivation on energy balance: a systematic review and meta-analysis. *Eur J Clin Nutr.* (2016) 71:614–24. doi: 10.1038/ejcn.2016.201
13. St-Onge M, Roberts A, Chen J, Kelleman M, O'Keeffe M, Roychoudhury A, et al. Short sleep duration increases energy intakes but does not change energy expenditure in normal-weight individuals. *Am J Clin Nutr.* (2011) 94:410–6. doi: 10.3945/ajcn.111.013904.introduction
14. Spaeth AM, Dinges DF, Goel N. Effects of experimental sleep restriction on weight gain, caloric intake, and meal timing in healthy adults. *Sleep* (2013) 36:981–90. doi: 10.5665/sleep.2792
15. Calvin AD, Carter RE, Adachi T, MacEdo PG, Albuquerque FN, Van Der Walt C, et al. Effects of experimental sleep restriction on caloric intake and activity energy expenditure. *Chest* (2013) 144:79–86. doi: 10.1378/chest.12-2829
16. Markwald RR, Melanson EL, Smith MR, Higgins J, Perreault L, Eckel RH, et al. Impact of insufficient sleep on total daily energy expenditure, food intake, and weight gain. *Proc Natl Acad Sci. USA.* (2013) 110:5695–700. doi: 10.1073/pnas.1216951110
17. Heath G, Roach GD, Dorrian J, Ferguson SA, Darwent D, Sargent C. The effect of sleep restriction on snacking behaviour during a week of simulated shiftwork. *Accid. Anal. Prev.* (2012) 45S:62–7. doi: 10.1016/j.aap.2011.09.028
18. Nedeltcheva AV, Kilkus JM, Imperial J, Kasza K, Schoeller DA, Penev PD. Sleep curtailment is accompanied by increased intake of calories from snacks. *Am J Clin Nutr.* (2009) 89:126–33. doi: 10.3945/ajcn.2008.26574
19. Beaver JD, Lawrence AD, van Ditzhuijzen J, Davis MH, Woods A, Calder AJ. Individual differences in reward drive predict neural responses to images of food. *J Neurosci.* (2006) 26:5160–6. doi: 10.1523/JNEUROSCI.0350-06.2006
20. Killgore WDS, Young AD, Femia LA, Bogorodzki P, Rogowska J, Yurgelun-Todd DA. Cortical and limbic activation during viewing of high- versus low-calorie foods. *Neuroimage* (2003) 19:1381–94. doi: 10.1016/S1053-8119(03)00191-5
21. Killgore WDS, Schwab ZJ, Weber M, Kipman M, Deldonno SR, Weiner MR, et al. Daytime sleepiness affects prefrontal regulation of food intake. *Neuroimage* (2013) 71:216–23. doi: 10.1016/j.neuroimage.2013.01.018
22. Volkow ND, Wang G-J, Baler RD. Reward, dopamine and the control of food intake: implications for obesity. *Trends Cogn Sci.* (2011) 15:37–46. doi: 10.1016/j.tics.2010.11.001
23. Gujar N, Yoo S-S, Hu P, Walker MP. Sleep deprivation amplifies reactivity of brain reward networks, biasing the appraisal of postive emotional experiences. *J Neurosci.* (2011) 31:4466–74. doi: 10.1523/jneurosciI.3220-10.2011.Sleep
24. Thomas ML, Sing HC, Belenky G, Holcomb HH, Mayberg HS, Dannals RF, et al. Neural basis of alertness and cognitive performance impairments during sleepiness I. Effects of 48 and 72 h of sleep deprivation on waking human regional brain activity. *J. Sleep Res.* (2000) 9:335–52. doi: 10.1016/S1472-9288(03)00020-7
25. Venkatraman V, Chuah YML, Huettel SA, Chee MWL. *Sleep* deprivation elevates expectation of gains and attenuates response to losses following risky decisions. *Sleep* (2007) 30:603–9. doi: 10.1093/sleep/30.5.603
26. Benedict C, Brooks SJ, O'Daly OG, Almè MS, Morell A, Åberg K, et al. Acute sleep deprivation enhances the brain's response to hedonic food stimuli: an fMRI study. *J Clin Endocrinol Metab.* (2012) 97:E443–7. doi: 10.1210/jc.2011-2759
27. Demos KE, Sweet LH, Hart CN, McCaffery JM, Williams SE, Mailloux KA, et al. The effects of experimental manipulation of sleep duration on neural response to food cues. *Sleep* (2017) 40:1–9. doi: 10.1093/sleep/zsx125
28. Fang Z, Spaeth AM, Ma N, Zhu S, Hu S, Goel N, et al. Altered salience network connectivity predicts macronutrient intake after sleep deprivation. *Sci Rep.* (2015) 5:8215. doi: 10.1038/srep08215
29. Greer SM, Goldstein AN, Walker MP. The impact of sleep deprivation on food desire in the human brain. *Nat Commun.* (2013) 4:2259. doi: 10.1038/ncomms3259
30. St-Onge M-P, Wolfe S, Sy M, Shechter A, Hirsch J. Sleep restriction increases the neuronal response to unhealthy food in normal-weight individuals. *Int J Obes.* (2014) 38:411–6. doi: 10.1038/ijo.2013.114
31. St-Onge M-P, McReynolds A, Trivedi ZB, Roberts AL, Sy M, Hirsch J. Sleep restriction leads to increased activation of brain regions sensitive to food stimuli. *Am J Clin Nutr.* (2012) 95:818–24. doi: 10.3945/ajcn.111.027383
32. Uddin LQ. Anatomy of the salience network. In: Farr A, editors. *Salience Network of the Human Brain.* London: Academic Press (2017). p. 5–10. doi: 10.1016/B978-0-12-804593-0.00002-3
33. Haber SN, Knutson B. The reward circuit: linking primate anatomy and human imaging. *Neuropsychopharmacology* (2010) 35:4–26. doi: 10.1038/npp.2009.129

34. Uddin LQ. Functions of the salience network. In: *Salience Network of the Human Brain*. London: Academic Press (2017). p. 11–16. doi: 10.1016/B978-0-12-804593-0.00003-5
35. Drummond SPA, Paulus MP, Tapert SF. Effects of two nights sleep deprivation and two nights recovery sleep on response inhibition. *J Sleep Res.* (2006) 15:261–5. doi: 10.1111/j.1365-2869.2006.00535.x
36. Oldfield RC. The assessment and analysis of handedness: the Edinburgh inventory. *Neuropsychologia* (1971) 9:97–113. doi: 10.1016/0028-3932(71)90067-4
37. Sheehan DV, Lecrubier Y, Sheehan KH, Amorim P, Janavs J, Weiller E, et al. The mini-international neuropsychiatric interview (M.I.N.I): the development and validation of a structured diagnostic psychiatric interview for DSM-IV and ICD-10. *J Clin Psychiatry* (1998) 20:22–33.
38. Bush G, Shin LM, Holmes J, Rosen BR, Vogt BA. The multi-source interference task: validation study with fMRI in individual subjects. *Mol Psychiatry* (2003) 8:60–70. doi: 10.1038/sj.mp.4001217
39. Bush G, Shin LM. The multi-source interference task: an fMRI task that reliably actiates the cingulo-frontal-parietal cognitive/attention network. *Nat Protoc.* (2006) 1:308–13. doi: 10.1038/nprot.2006.48
40. Gruber SA, Dahlgren MK, Sagar KA, Gönenc A, Killgore WDS. Age of onset of marijuana use impacts inhibitory processing. *Neurosci Lett.* (2012) 511:89–94. doi: 10.1016/j.neulet.2012.01.039
41. Drobyshevsky A, Baumann SB, Schneider W. A rapid fMRI task battery for mapping of visual, motor, cognitive, and emotional function. *Neuroimage* (2006) 31:732–44. doi: 10.1016/j.neuroimage.2005.12.016
42. Alkozei A, Smith R, Pisner DA, Vanuk JR, Markowski SM, Fridman A, et al. Exposure to blue light increases subsequent functional activation of the prefrontal cortex during performance of a working memory task. *Sleep* (2016) 3:1671–80. doi: 10.5665/sleep.6090
43. Killgore WDS, Weber M, Schwab ZJ, Kipman M, DelDonno SR, Webb CA, et al. Cortico-limbic responsiveness to high-calorie food images predicts weight status among women. *Int J Obes.* (2013) 37:1435–42. doi: 10.1038/ijo.2013.26
44. Killgore WDS, Yurgelun-Todd DA. Body mass predicts orbitofrontal activity during visual presentations of high-calorie foods. *Neuroreport* (2005) 16:859–63. doi: 10.1097/00001756-200505310-00016
45. Åkerstedt T, Anund A, Axelsson J, Kecklund G. Subjective sleepiness is a sensitive indicator of insufficient sleep and impaired waking function. *J Sleep Res.* (2014) 23:240–52. doi: 10.1111/jsr.12158
46. US Department of Health and Human Services and US Department of Agriculture. *2015 – 2020 Dietary Guidelines for Americans* (2015). doi: 10.1097/NT.0b013e31826c50af
47. Lawrence NS, Hinton EC, Parkinson JA, Lawrence AD. Nucleus accumbens response to food cues predicts subsequent snack consumption in women and increased body mass index in those with reduced self-control. *Neuroimage* (2012) 63:415–22. doi: 10.1016/j.neuroimage.2012.06.070
48. Demos KE, Heatherton TF, Kelley WM. Individual differences in nucleus accumbens activity to food and sexual images predicts weight gain and sexual behavior. *J Neurosci.* (2012) 32:5549–52. doi: 10.1523/jneurosci.5958-11.2012
49. Mourão-Miranda J, Volchan E, Moll J, De Oliveira-Souza R, Oliveira L, Bramati I, et al. Contributions of stimulus valence and arousal to visual activation during emotional perception. *NeuroImage* (2003) 20:1955–63. doi: 10.1016/j.neuroimage.2003.08.011
50. Santel S, Baving L, Krauel K, Münte TF, Rotte M. Hunger and satiety in anorexia nervosa: fMRI during cognitive processing of food pictures. *Brain Res*. (2006) 1114:138–48. doi: 10.1016/j.brainres.2006.07.045
51. Keeler JF, Pretsell DO, Robbins TW. Functional implications of dopamine D1 vs. D2 receptors: a "prepare and select" model of the striatal direct vs. indirect pathways. *Neuroscience* (2014) 282:156–75. doi: 10.1016/j.neuroscience.2014.07.021
52. Volkow ND, Wang G-J, Fowler JS, Telang F. Overlapping neuronal circuits in addiction and obesity: evidence of systems pathology. *Philos Trans R Soc B Biol Sci.* (2008) 363:3191–200. doi: 10.1098/rstb.2008.0107
53. Volkow ND, Wang G-J, Telang F, Fowler FS, Logan J, Wong C, et al. Sleep deprivation decreases binding of [11C] raclopride's to dopamine D2/D3 receptors in the human brain. *J Neurosci.* (2008) 28:8454–61. doi: 10.1523/jneurosci.1443-08.2008
54. Volkow ND, Tomasi D, Wang G-J, Telang F, Fowler JS, Logan J, et al. Evidence that sleep deprivation downregulates dopamine D2R in ventral striatum in the human brain. *J Neurosci.* (2012) 32:6711–7. doi: 10.1523/jneurosci.0045-12.2012
55. Krause AJ, Simon EB, Mander BA, Greer SM, Saletin JM, Goldstein-Piekarski AN, et al. The sleep-deprived human brain. *Nat Rev.* (2017) 18:404–18. doi: 10.1038/nrn.2017.55
56. Basheer R, Strecker RE, Thakkar MM, McCarley RW. Adenosine and sleep-wake regulation. *Prog Neurobiol.* (2004) 73:379–96. doi: 10.1016/j.pneurobio.2004.06.004
57. Hillion J, Canals M, Torvinen M, Casadó V, Scott R, Terasmaa A, et al. Coaggregation, cointernalization, and codesensitization of adenosine A2A receptors and dopamine D2 receptors. *J Biol Chem.* (2002) 20:18091–7. doi: 10.1074/jbc.M107731200
58. Killgore WDS. Sleep deprivation and behavioral risk-taking. In: Watson RR, editor. *Modulation of Sleep by Obesity, Diabetes, Age, and Diet*. London: Academic Press (2015). p. 279–87. doi: 10.1016/B978-0-12-420168-2.00030-2
59. Killgore WDS, Balkin TJ, Wesensten NJ. Impaired decision making following 49 hours of sleep deprivation. *J Sleep Res.* (2006) 15:7–13. doi: 10.1111/j.1365-2869.2006.00487.x
60. Killgore WDS, Grugle NL, Balkin TJ. Gambling when sleep deprived: don't bet on stimulants. *Chronobiol Int.* (2012) 29:43–54. doi: 10.3109/07420528.2011.635230
61. Mckenna BS, Dickinson DL, Orff HJ, Drummond SPA. The effects of one night of sleep deprivation on known-risk and ambiguous-risk decisions. *J Sleep Res.* (2007) 16:245–52. doi: 10.1111/j.1365-2869.2007.00591.x
62. Smeets PAM, Charbonnier L, van Meer F, van der Laan LN, Spetter MS. Food-induced brain responses and eating behaviour. *Proc Nutr Soc.* (2012) 71:511–20. doi: 10.1017/S0029665112000808
63. Gautier J-F, Chen K, Salbe AD, Bandy D, Pratley RE, Heiman M, et al. Differential brain responses to satiation in obese and lean men. *Diabetes* (2000) 49:838–46. doi: 10.2337/diabetes.49.5.838
64. Gautier J-F, Del Parigi A, Chen K, Salbe AD, Bandy D, Pratley RE, et al. Effect of satiation on brain activity in obese and lean women. *Obes Res.* (2001) 9:676–84. doi: 10.1038/oby.2001.92

Conflict of Interest Statement: The authors declare that the research was conducted in the absence of any commercial or financial relationships that could be construed as a potential conflict of interest.

frontiers in Neurology

ORIGINAL RESEARCH
published: 02 August 2018
doi: 10.3389/fneur.2018.00588

Altered Regional Cortical Brain Activity in Healthy Subjects After Sleep Deprivation: A Functional Magnetic Resonance Imaging Study

Lingling Chen[1], *Xueliang Qi*[1] *and Jiyong Zheng*[2]*

[1] *Department of Pediatric Internal Medicine, Linyi Central Hospital, Yishui, China,* [2] *Department of Medical Imaging, The Affiliated Huaian No. 1 People's Hospital of Nanjing Medical University, Huaian, China*

OPEN ACCESS

Edited by:
Xi-jian Dai,
Jinling Hospital and Medical School of Nanjing University, China

Reviewed by:
Angel Nunez,
Universidad Autonoma de Madrid, Spain
Weiguang Li,
Beijing Normal University, China

***Correspondence:**
Jiyong Zheng
jyzhengdoctor@126.com

Specialty section:
This article was submitted to Sleep and Chronobiology, a section of the journal Frontiers in Neurology

Received: *18 April 2018*
Accepted: *29 June 2018*
Published: *02 August 2018*

Citation:
Chen L, Qi X and Zheng J (2018) Altered Regional Cortical Brain Activity in Healthy Subjects After Sleep Deprivation: A Functional Magnetic Resonance Imaging Study. Front. Neurol. 9:588. doi: 10.3389/fneur.2018.00588

Objective: To investigate acute sleep deprivation (SD)-related regional brain activity changes and their relationships with behavioral performances.

Methods: Twenty-two female subjects underwent an MRI scan and an attention network test at rested wakefulness (RW) status and after 24 h SD. The amplitude of low-frequency fluctuations (ALFF) was used to investigate SD-related regional brain activity changes. We used the receiver operating characteristic (ROC) curve to evaluate the ability of the ALFF differences in regional brain areas to distinguish the SD status from the RW status. We used Pearson correlations to evaluate the relationships between the ALFF differences in brain areas and the behavioral performances during the SD status.

Results: Subjects at the SD status exhibited a lower accuracy rate and a longer reaction time relative to the RW status. Compared with RW, SD showed significant lower ALFF values in the right cerebellum anterior lobe, and higher ALFF areas in the bilateral inferior occipital gyrus, left thalamus, left insula, and bilateral postcentral gyrus. The area under the curve values of the specific ALFF differences in brain areas were (mean ± std, 0.851 ± 0.045; 0.805–0.93). Further, the ROC curve analysis demonstrated that the ALFF differences in those regional brain areas alone discriminated the SD status from the RW status with high degrees of sensitivities (82.16 ± 7.61%; 75–93.8%) and specificities (81.23 ± 11.39%; 62.5–93.7%). The accuracy rate showed negative correlations with the left inferior occipital gyrus, left thalamus, and left postcentral gyrus, and showed a positive correlation with the right cerebellum.

Conclusions: The ALFF analysis is a potential indicator for detecting the excitation–inhibition imbalance of regional cortical activations disturbed by acute SD with high performances.

Keywords: sleep deprivation, receiver operating characteristic, area under the curve, amplitude of low frequency fluctuations, functional magnetic resonance imaging

INTRODUCTION

Sleep is a necessary physical need for normal life, and we spend nearly one-third of our life sleeping. Sleep deprivation (SD), widespread in the current society, is caused by environmental factors or personal reasons and generally has deleterious effects on emotional regulation, memory, attention, and executive control function (1–5). Long-term SD can lead to multiorgan and multisystem dysfunction and has been shown to have negative impacts on metabolic, physiological, psychological, and/or behavioral reactivity with a greater risk of being a serious disease (6–10). However, their mechanisms are still unclear.

Resting state functional MRI (rfMRI) does not need the use of radioactive tracers and can combine functional and structural images, making the imaging method suitable for exploring the mechanisms of and obtaining insights into the pathophysiology of diseases (3); furthermore, rfMRI can be used to find the location of altered neuronal spontaneous brain activity. Recently, numerous scholars have focused their attentions on whether short-term SD has detrimental effects on regional neuronal spontaneous brain activity and cognitive function. RfMRI studies have consistently found altered cognitive domains, and altered regional spontaneous brain activity and functional connectivity patterns in the sleep-deprived brain (3, 6, 11–19), suggesting that the internal brain activity and intra-/inter- connectivity patterns for the internal processing of information are disturbed by SD. Furthermore, recent studies have found that SD has accumulative negative effects on brain morphology and advanced cognitive function (attention and working memory), showing that as SD hours prolonged, more areas show reduced gray matter volume, and after one night's sleep the brain atrophy is restored and replaced by increased gray matter volume (10). However, few studies have considered the gender factor in the neuroimaging studies of sleep disorders, and both female and male subjects were combined in these studies. Thus, the neurological mechanism of the location of altered neuronal spontaneous brain activity based on gender has not been fully studied.

Amplitude of low-frequency fluctuations (ALFF) measurement has the ability to locate where (in which brain region) regional spontaneous brain activity was disturbed with less computation complexity and high test–retest reliability characterization (20–24). Theses characterizations may make the ALFF analysis a useful tool and potential indicator for rs-fMRI data to explore the various potential neurobiological mechanisms by locating the altered regional spontaneous brain activity and functional connectivity patterns (3). Recently, ALFF analysis has been successfully applied to the exploration of neural mechanism of primary insomnia (24), wakefulness and light sleep (25), and obstructive sleep apnea (22). In this framework, in the present study we hypothesized that the ALFF measurement has the ability to locate acute SD-induced regional brain activity with high sensitivity and specificity. To test this hypothesis, we used the ALFF analysis as a potential indicator to locate the underlying altered regional functional brain activity during the SD status relative to the rested wakefulness (RW) status, and further explored the potential neurobiological mechanisms of SD in female subjects with respect to the location of altered neuronal spontaneous brain activity. Specifically, the receiver operating characteristic (ROC) curve was used to investigate the abilities of the ALFF analysis in distinguishing the SD status from the RW status. Pearson correlations were used to evaluate the relationships between the ALFF differences in brain areas and the behavioral performances during the SD status.

MATERIALS AND METHODS

Subjects

The present study was approved by the Medical Research Ethical Committee. The Affiliated Huaian No.1 People's Hospital of Nanjing Medical University. Twenty-two healthy female subjects (age, 26.91 $\pm$ 6.05 years; education, 15.77 $\pm$ 1.15 years; mean $\pm$ std) were recruited. All subjects met the following criteria as in previous studies (3, 6): (1) right-handed; (2) good sleep habit without any symptoms of sleep disorders such as difficulties in initiating and/or maintaining sleep, with Pittsburgh sleep quality index score < 5; (3) never taken alcohol, stimulants, cigarette, hypnotic or psychoactive medications, diet pills, and caffeine for $\geq$3 months during and prior to the current study; (4) regular dietary habit with moderate weight and body shape; (5) without foreign implants, and inborn and acquired diseases.

Each of the subjects underwent the MRI scan twice, once during RW status and the other after 24 h acute SD. The acute SD session started from 19:00 p.m. on the first day and lasted until 7:00 p.m. on the second day. Before the MRI scan, all volunteers underwent an attention network test (26, 27). Food and water were provided during the SD procedure. The temperature of the room was maintained between 23 and 27°C. The staff of our team used video monitors and worked in turns to make sure that the participants did not fall asleep. If the participants showed signs of falling asleep, they were immediately awakened using an alarm clock by staff. A simple questionnaire was used to evaluate whether the subjects were asleep during the MRI scan. All subjects provided their written informed consent voluntarily.

MRI

The MRI examination was performed using an acquired clinical 3.0-Tesla MRI scanner (SIEMENS Trio Tim, Siemens Healthcare, Erlangen, Germany) with a standard eight-channel head coil. First, we acquired a high-resolution 3D anatomical image with 176 T1-weighted images in a sagittal orientation: repetition time = 1,950 ms, gap = 0 mm, echo time = 2.3 ms, thickness = 1 mm, acquisition matrix = 248 × 256, flip angle = 9°, field of view = 244 × 252 mm. Second, we also acquired 240 functional images using a single-shot gradient-recalled echo-planar imaging pulse sequence (repetition time = 3,000 ms, gap = 0.5 mm, echo time = 25 ms, thickness = 5.0 mm, flip angle = 90°, acquisition matrix = 32 × 32, field of view = 210 × 210 mm).

Data Analysis

The first 10 time points of the functional images were discarded because of the possible instability of the initial MRI signal and to allow the participants to adapt to the scanning environment. Data preprocessing of the remaining resting-state images was

performed using the Data Processing & Analysis for Brain Imaging (DPABI 2.1, http://rfmri.org/DPABI) toolbox, adopting the Digital Imaging and Communications in Medicine (DICOM) standard for form transformation, slice timing, head motion correction, spatial normalization, and spatial smoothing using a Gaussian kernel of $8 \times 8 \times 8$ mm^3 full-width at half-maximum. Participants with more than 1.5 mm maximum translation in x, y, or z directions and 1.5° of motion rotation were removed. After the head motion correction, the rest of the functional images were spatially normalized and resampled to Montreal Neurological Institute (MNI) space at a resolution of $3 \times 3 \times 3$ mm^3. Linear regression was applied to remove several sources of possible spurious covariates, including 24 head motion parameters obtained in the realigning step, signal from a region in the cerebrospinal fluid or/and centered in the white matter, and global signal averaged over the whole brain. After preprocessing, the time series were further linearly detrended and temporally band-pass filtered (0.01–0.1 Hz). The details of the ALFF calculation have been reported in previous studies (3, 28). To reduce the global effects of variability across the participants, the mean ALFF value of each voxel was divided by the global mean ALFF value for each participant.

Statistical Analysis

Data are presented as mean ± standard deviation (mean ± std). Pair *t*-tests were used for demographic factors (age, years of education, and clinical factors), and a chi-squared (χ^2) test was used for categorical data (gender). $p < 0.05$ was considered to be a significant difference.

A pair *t*-test was used to investigate the ALFF differences in regional brain areas of the subjects during the acute SD status relative to the RW status with the gender, age, and years of education as nuisance covariates of no interest. AlphaSim correction (threshold of individual voxel of $p < 0.01$ and cluster level of $p < 0.05$ with contiguous voxel size ≥20) was used to determine the statistical differences.

We used the ROC curve to evaluate the ability of the ALFF differences in regional brain areas to distinguish the SD status from the RW status, and we used Pearson correlations to evaluate the relationships between the ALFF differences in brain areas and the behavioral performances during the SD status. The statistical threshold was set at $p < 0.05$.

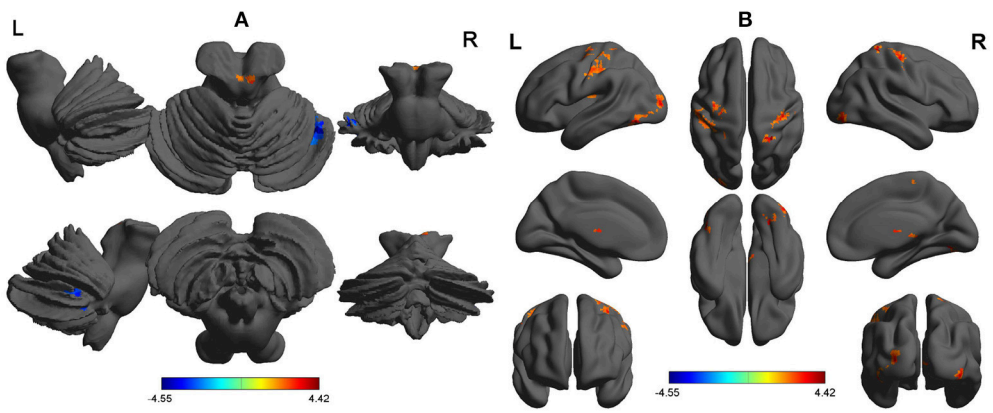

FIGURE 1 | ALFF differences between SD group and RW group. The differences covered cerebellum with lower ALFF **(A)**, and inferior occipital gyrus, thalamus, insula, and postcentral gyrus with higher ALFF **(B)**. The color in the map represents the differences. The red color signifies increase in ALFF areas, and the blue signifies decrease in ALFF areas. ALFF, Amplitude of low-frequency fluctuations; SD, Sleep deprivation; RW, Rested wakefulness; R, right; L, left.

TABLE 1 | ALFF differences in brain areas between SD and RW.

Brain regions of peak coordinates	R/L	BA	Voxel size	*t*-score of peak voxel	Peak MNI coordinates
					X, Y, Z
Cerebellum Anterior Lobe	R	N/A	33	−4.5537	39, −54, −33
Inferior Occipital Gyrus	L	18, 19	142	4.4223	−48, −84, −6
Inferior Occipital Gyrus	R	18, 19	74	3.5394	39, −84, −9
Thalamus	L	N/A	89	4.1044	−6, −24, 18
Insula	L	13	43	3.9142	−36, −18, 21
Postcentral Gyrus	L	3, 6	235	3.9225	−36, −27, 42
Postcentral Gyrus	R	3	230	4.2278	27, −45, 66

The statistical threshold was set at corrected significance level of individual voxel $p < 0.01$ using an AlphaSim-corrected threshold of cluster $p < 0.05$.
ALFF, Amplitude of low-frequency fluctuation; SD, Sleep deprivation; RW, Rested wakefulness; R, right; L, left; BA, Brodmann's area; MNI, Montreal neurological institute; N/A, Not applicable.

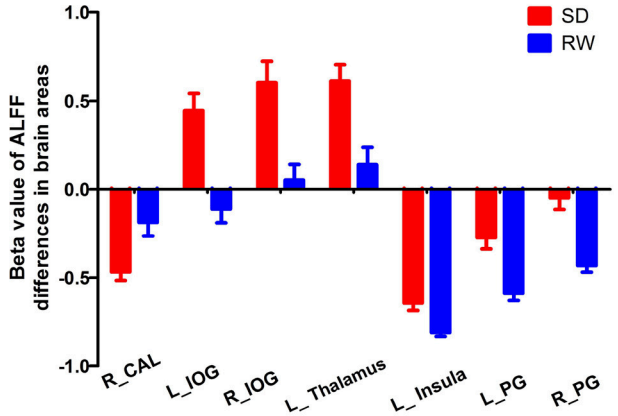

FIGURE 2 | Mean beta values of ALFF differences in regional brain areas. Significant differences were found for beta value of all ALFF brain areas between SD and RW ($p < 0.001$). ALFF, Amplitude of low-frequency fluctuations; SD, Sleep deprivation; RW, Rested wakefulness; R, right; L, left; CAL, Cerebellum anterior lobe; IOG, Inferior occipital gyrus; PG, Precentral gyrus.

TABLE 2 | ROC curve for the ALFF differences in brain areas between SD and RW.

Brain area	AUC	Sensitivity (%)	Specificity (%)	Cut off point*
R_Cerebellum Anterior Lobe	0.805	75	81.2	−0.351
L_ Inferior Occipital Gyrus	0.875	75	87.5	0.206
R_Inferior Occipital Gyrus	0.809	81.3	75	0.2065
L_Thalamus	0.867	87.5	75	0.1155
L_Insula	0.82	93.8	62.5	−0.8015
L_ Postcentral Gyrus	0.848	75	93.7	−0.405
R_ Postcentral Gyrus	0.93	87.5	93.7	−0.3095

**Cut off point of mean ALFF signal value.*
ROC, Receiver operating characteristic; ALFF, Amplitude of low-frequency fluctuation; SD, Sleep deprivation; RW, Rested wakefulness; AUC, Area under the curve; R, Right; L, Left.

RESULTS

Behavioral Characteristics

Compared with the RW status, the acute SD status had a lower response in accuracy rate (mean ± std, 24 h SD = 96.07 ± 3.2%, RW = 97.85 ± 1.69%; $t = -2.125$, $p = 0.046$) and a longer response in reaction time (24 h SD = 633.99 ± 79.05 ms; RW = 537.97 ± 46.49 ms; $t = 5.554$, $p < 0.001$).

ALFF Differences Between Groups

Compared with RW, SD had significant lower ALFF areas in the right cerebellum anterior lobe (**Figure 1A**), and higher ALFF areas in the bilateral inferior occipital gyrus (Brodmann's area, BA 18, 19), left thalamus, left insula (BA 13), and bilateral postcentral gyrus (BA 3, 6) (**Table 1**, **Figure 1B**).

ROC Curve

The mean beta value of ALFF differences in the altered areas were extracted (**Figure 2**). These different ALFF differences in brain areas were further used for the ROC curve to evaluate their abilities to distinguish the acute SD status from the RW status. The area under the curve (AUC) values of those specific ALFF differences in brain areas were (0.851 ± 0.045; 0.805–0.93).

Further, the ROC curve demonstrated that the ALFF differences in those regional brain areas alone discriminated the acute SD status from the RW status with high degrees of sensitivities (82.16 ± 7.61%; 75–93.8%) and specificities (81.23 ± 11.39%; 62.5–93.7%) with cut-off points of −0.351, 0.206, 0.2065, 0.1155, −0.8015, −0.405, and −0.3095 (mean beta signal value), respectively (**Table 2**, **Figure 3**).

Pearson Correlation Analysis

The accuracy rate demonstrated a positive correlation with the ALFF value in the right cerebellum anterior lobe ($r = 0.496$, $p = 0.019$; **Figure 4A**), and negative correlations with the ALFF values in the left inferior occipital gyrus ($r = -0.602$, $p = 0.003$; **Figure 4B**), left thalamus ($r = -0.522$, $p = 0.013$; **Figure 4C**) and left postcentral gyrus ($r = 0.656$, $p = 0.001$; **Figure 4D**) during the acute SD status, respectively. None of the other correlations between the ALFF values in those different areas and the behavioral performances during the acute SD status were found ($p > 0.05$).

DISCUSSION

In the present study, we used ALFF analysis to demonstrate the differences in regional brain areas associated with acute SD, and their correlations with the clinical performances. Specifically, we found that SD was associated with widespread regional brain activities with lower ALFF values in the right cerebellum anterior lobe, and with higher ALFF values in the bilateral inferior occipital gyrus (BA 18, 19), left thalamus, left insula (BA 13), and bilateral postcentral gyrus. Furthermore, during the SD status, the accuracy rate showed correlations with the beta value of ALFF differences in those brain areas. Recently, the ROC curve is widely used to evaluate the reliability of a neuroimaging technique in distinguishing one group from another group (3, 22, 24). In general, the AUC value is considered as excellent between 0.9 and 1, considered as good between 0.8 and 0.9, considered as fair between 0.7 and 0.8, considered as poor between 0.6 and 0.7, and considered as failed between 0.5 and 0.6. In the present study, the ROC curve revealed that the ALFF differences in those brain areas had good discriminating abilities with a high AUC value (> 0.8). Further diagnostic analysis showed that these areas discriminated the SD status from the RW status with high degrees of sensitivities (mean, 82.16 ± 7.61%; 75–93.8%) and specificities (mean, 81.23 ± 11.39%; 62.5–93.7%).

In a previous study, a total of 16 healthy subjects (8 females, 8 males) were recruited, and SD was found to be associated with several ALFF differences in brain areas (29); however, the study did not take the gender differences into account. Previous studies have shown that there are wide gender differences in brain

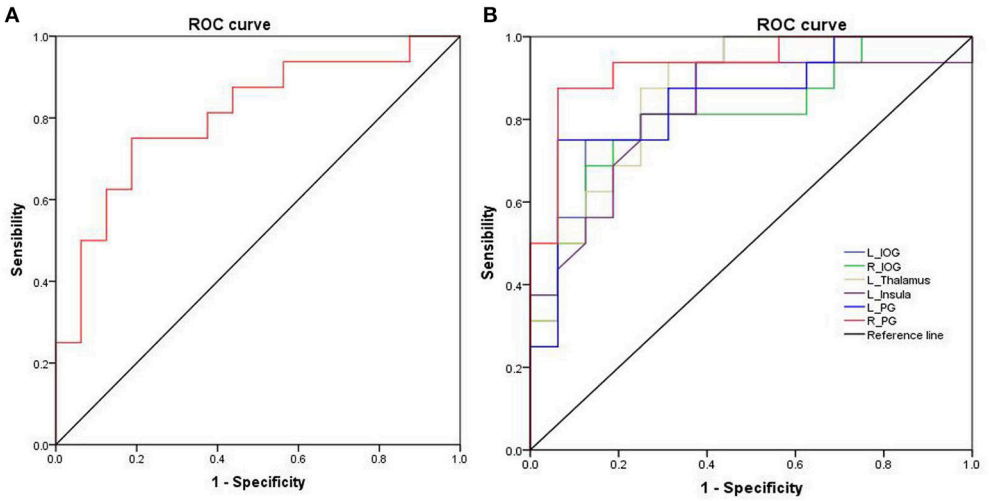

FIGURE 3 | ROC curve analysis of ALFF differences in regional brain areas. ROC curve of cerebellum **(A)** and other areas **(B)**. ROC, Receiver operating characteristic; ALFF, Amplitude of low-frequency fluctuation; R, right; L, left; IOG, Inferior occipital gyrus; PG, Precentral gyrus.

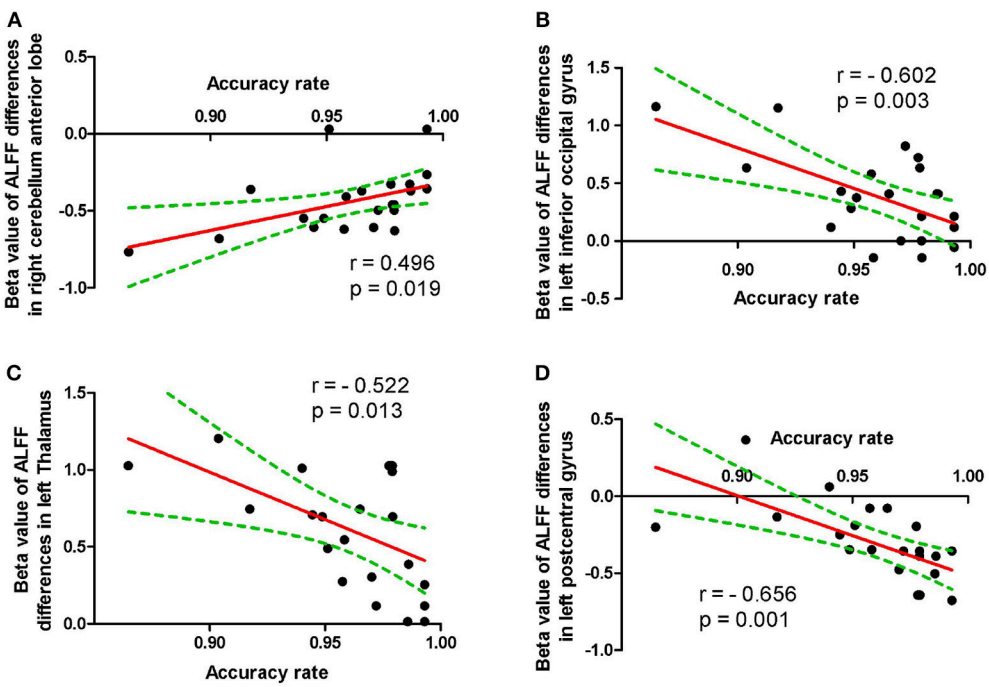

FIGURE 4 | Pearson correlation between behavioral performances and beta values of ALFF differences in brain areas. Pearson correlation between accuracy rate and cerebellum **(A)**, left inferior occipital gyrus **(B)**, left thalamus **(C)** and left postcentral gyrus **(D)**. ALFF, Amplitude of low-frequency fluctuation.

activity in healthy subjects both at the SD status and the RW status, and in patients with chronic insomnia relative to good sleepers in sleep neuroimaging studies (6, 24). In this framework, the present study only recruited healthy female subjects to exclude the effect of the gender factor. Specifically, we found that SD was associated with widespread regional brain activities with lower ALFF values and higher ALFF values, and this finding is different from that of the previous study. Therefore, our findings support the standpoint that the gender factor should be taken into account in the neuroimaging studies of sleep disorders (6, 24).

The hyperarousal and increased glucose utilization in patients with chronic primary insomnia were found in neurocognitive, neuroimaging, and physiological studies (30–32). Hyperarousal

refers to magniloquent cognitive, somatic, and/or cortical activation, further leading to increased sensory information processing (33, 34), which is a core predisposing factor of chronic primary insomnia (35). Previous neuroimaging studies also found hyperarousal reactivation in several brain areas in individuals after SD and patients with chronic primary insomnia (6, 24). The present study found that SD is associated with increased ALFF areas in widespread regional brain areas, and these increased ALFF areas show negative correlations with the accuracy rate. There are two prevalent speculations for the increased regional brain activities (36). One explanation of the hyperarousal model could be that this is a brain compensation mechanism. Previous diffusion tensor imaging study showed that 23 h SD is associated with widespread fractional anisotropy decreases in several brain areas and as the waking prolonged the decreases become larger (37). Another explanation of the increased ALFF areas in widespread regional brain areas may be that the hyperactivation in these widespread regional brain areas may be interpreted as an enhanced neural effort to offset these decreased brain structures associated with SD. A previous task study found that the parietal lobe was not activated after normal sleep but was activated after SD (38). The occipital lobe and postcentral gyrus were found with higher regional homogeneity and ALFF values (6, 17); the thalamus was also found with higher ALFF value after acute SD (17), and the thalamus and insula were activated by acupuncture after acute SD (39). These findings were consistent with our study, and may reflect dynamic, compensatory changes in cerebral activation after SD.

The lower ALFF values in brain areas may indicate a consistent decrease of regional neuronal activity with poor synchronization and without in order (6). Poor regulation of behaviors and emotions are core features of SD. The cerebellum is involved in coordinating movement, and emotional and cognitive functions (6, 24), and associated with the aberrant regional brain activity in sleep disorders, such as patients with primary insomnia (24, 40) and obstructive sleep apnoea (41). In the present study, SD compared with RW had a significant lower ALFF value in the right cerebellum anterior lobe, and the mean ALFF value in this area had a positive correlation with accuracy rate ($r = 0.496$, $p = 0.019$). The decreased regional brain activity in the right cerebellum anterior lobe may reflect that the sleep-deprived brain needs to attempt to recruit more specific brain areas with advanced cognitive functions to accomplish the cognitive performance because of a continuing decline in the cerebellum activity. Interestingly, Wang et al. showed different findings of altered SD-related regional brain activities in several areas (29). Since the gender factor may influence the results in the neuroimaging studies of sleep disorders (6, 24), we therefore speculated that the differences between our study and Wang et al.'s study may be associated with the gender factor.

CONCLUSIONS

In summary, the ALFF analysis is a useful index to locate the underlying altered regional brain activities in individuals during the SD status relative to the RW status with high degrees of sensitivities and specificities. SD is associated with the model of excitation–inhibition imbalance of cortical activations. These findings expand our knowledge and may help in deeper understanding of the neurobiological mechanisms underlying acute SD. Furthermore, the gender factor should be taken into account in the neuroimaging studies of sleep disorders. However, there are several potential limitations that should be noted. First, our study has a relatively small sample size and future studies on a larger number of sample sizes are necessary to corroborate our findings. Second, in our study the design of replication is not addressed. Third, the electronystagmogram has been used to dynamically monitor the sleep.

AUTHOR CONTRIBUTIONS

LC wrote the main manuscript text. JZ conceived and designed the whole experiment. LC and XQ collected the data. JZ analyzed the data.

REFERENCES

1. Drummond SPA, Brown GG. The effects of total sleep deprivation on cerebral responses to cognitive performance. *Neuropsychopharmacology* (2001) 25:68–73. doi: 10.1016/S0893-133X(01)00325-6
2. Jackson ML, Hughes ME, Croft RJ, Howard ME, Crewther D, Kennedy GA. The effect of sleep deprivation on BOLD activity elicited by a divided attention task. *Brain Imaging Behav.* (2011) 5:97–108. doi: 10.1007/s11682-011-9115-6
3. Dai XJ, Liu CL, Zhou RL, Gong HH, Wu B, Gao L. Long-term sleep deprivation decreases the default spontaneous activity and connectivity pattern in healthy male subjects: a resting-state fMRI study. *Neuropsychiatr Dis Treat.* (2015) 11:761–72. doi: 10.2147/NDT.S78335
4. Luber B, Stanford AD, Bulow P, Nguyen T, Rakitin BC, Habeck C. Remediation of sleep-deprivation-induced working memory impairment with fMRI-guided transcranial magnetic stimulation. *Cereb Cortex* (2008) 18:2077–85. doi: 10.1093/cercor/bhm231
5. Nilsson JP, Söderström M, Karlsson AU, Lekander M, Akerstedt T, Lindroth NE. Less effective executive functioning after one night's sleep deprivation. *J Sleep Res.* (2005) 14:1–6. doi: 10.1111/j.1365-2869.2005.00442.x
6. Dai XJ, Gong HH, Wang YX, Zhou FQ, Min YJ, Zhao F. Gender differences in brain regional homogeneity of healthy subjects after normal sleep and after sleep deprivation: a resting-state fMRI study. *Sleep Med.* (2012) 13:720–7. doi: 10.1016/j.sleep.2011.09.019
7. Ohayon MM, Smolensky MH, Roth T. Consequences of shiftworking on sleep duration, sleepiness, and sleep attacks. *Chronobiol Int.* (2010) 27:575–89. doi: 10.3109/07420521003749956
8. Walker MP, Stickgold R. Sleep, memory and plasticity. *Annu Rev Psychol.* (2006) 57:139–66. doi: 10.1146/annurev.psych.56.091103.070307
9. Tsigos C, Chrousos GP. Hypothalamic-pituitary-adrenal axis, neuroendocrine factors and stress. *J Psychosom Res.* (2002) 53:865–71. doi: 10.1016/S0022-3999(02)00429-4
10. Dai XJ, Jiang J, Zhang Z. Plasticity and susceptibility of brain morphometry alterations to insufficient sleep. *Front. Psychiatry* (2018) 8:9. doi: 10.3389/fpsyt.2018.00266
11. De Havas JA, Parimal S, Soon CS, Chee MW. Sleep deprivation reduces default mode network connectivity and anti-correlation during rest and task performance. *Neuroimage* (2012) 59:1745–51. doi: 10.1016/j.neuroimage.2011.08.026

12. Bosch OG, Rihm JS, Scheidegger M, Landolt HP, Stämpfli P, Brakowski J. et al. Sleep deprivation increases dorsal nexus connectivity to the dorsolateral prefrontal cortex in humans. *Proc Natl Acad Sci USA*. (2013) 110:19597–602. doi: 10.1073/pnas.1317010110
13. Shao Y, Wang L, Ye E, Jin X, Ni W, Yang Y. Decreased thalamocortical functional connectivity after 36 hours of total sleep deprivation: evidence from resting state FMRI. *PLoS ONE* (2013) 8:e78830. doi: 10.1371/journal.pone.0078830
14. Piantoni G, Cheung BL, Van Veen BD, Romeijn N, Riedner BA, Tononi G. Disrupted directed connectivity along the cingulate cortex determines vigilance after sleep deprivation. *Neuroimage* (2013) 79:213–22. doi: 10.1016/j.neuroimage.2013.04.103
15. Yoo SS, Gujar N, Hu P, Jolesz FA, Walker MP. The human emotional brain without sleep-a prefrontal amygdala disconnect. *Curr Biol*. (2007) 17:R877–8. doi: 10.1016/j.cub.2007.08.007
16. Picchioni D, Duyn JH, HorovitzSG. Sleep and the functional connectome. *Neuroimage* 80:387–96. doi: 10.1016/j.neuroimage.2013.05.067
17. Gao L, Bai L, Zhang Y, Dai XJ, Netra R, Min Y. Frequency-dependent changes of local resting oscillations in sleep-deprived brain. *PLoS ONE* (2015) 10:e0120323. doi: 10.1371/journal.pone.0120323
18. Basner M, Rao H, Goel N, Dinges DF. Sleep deprivation and neurobehavioral dynamics. *Curr Opin Neurobiol.* (2013) 23:854–63. doi: 10.1016/j.conb.2013.02.008
19. Goel N, Rao H, Durmer JS, Dinges DF. Neurocognitive consequences of sleep deprivation. *Semin Neurol.* (2009) 29:320–39. doi: 10.1055/s-0029-1237117
20. Simpson JR, Snyder AZ, Gusnard DA, Raichle ME. Emotion-induced changes in human medial prefrontal cortex: I. During cognitive task performance. *Proc Natl Acad Sci USA*. (2001) 98:683–87. doi: 10.1073/pnas.98.2.683
21. Mason MF, Norton MI, Van Horn JD, Wegner DM, Grafton ST, Macrae CN. Wandering minds:the default network and stimulus-independent thought. *Science* (2007) 315:393–5. doi: 10.1126/science.1131295
22. Li HJ, Dai XJ, Gong HH, Nie X, Zhang W, Peng DC. Aberrant spontaneous low-frequency brain activity in male patients with severe obstructive sleep apnea revealed by resting-state functional MRI. *Neuropsychiatr Dis Treat*. (2015) 11:207–14. doi: 10.2147/NDT.S73730
23. Yan H, Zhang Y, Chen H, Wang Y, Liu Y. Altered effective connectivity of the default mode network in resting-state amnestic type mild cognitive impairment. *J Int Neuropsychol Soc.* (2013) 19:400–9. doi: 10.1017/S1355617712001580
24. Dai XJ, Nie X, Liu X, Pei L, Jiang J, Peng DC. Gender differences in regional brain activity in patients with chronic primary insomnia: evidence from a resting-state fMRI study. *J Clin Sleep Med.* (2016) 12:363–74. doi: 10.5664/jcsm.5586
25. Horovitz SG, Fukunaga M, de Zwart JA, van Gelderen P, Fulton SC, Balkin TJ. Low frequency BOLD fluctuations during resting wakefulness and light sleep: a simultaneous EEG-fMRI study. *Hum Brain Mapp.* (2008) 29: 671–82. doi: 10.1002/hbm.20428
26. Fan J, McCandliss BD, Sommer T, Raz A, Posner MI. Testing the efficiency and independence of attentional networks. *J Cogn Neurosci.* (2002) 14:340–7. doi: 10.1162/089892902317361886
27. Fan J, McCandliss BD, Fossella J, Flombaum JI, Posner MI. The activation of attentional networks. *Neuroimage* (2005) 26:471–9. doi: 10.1016/j.neuroimage.2005.02.004
28. Huang X, Zhong YL, Zeng XJ, Zhou F, Liu XH, Hu PH. Disturbed spontaneous brain activity pattern in patients with primary angle-closure glaucoma using amplitude of low-frequency fluctuation: a fMRI study. *Neuropsychiatr Dis Treat*. (2015) 11:1877–83. doi: 10.2147/NDT.S87596
29. Wang L, Chen Y, Yao Y. Sleep deprivation disturbed regional brain activity in healthy subjects: evidence from a functional magnetic resonance-imaging study. *Neuropsychiatr Dis Treat*. (2016) 12:801–7. doi: 10.2147/NDT.S99644
30. Nofzinger EA, Buysse DJ, Germain A, Price JC, Miewald JM, Kupfer DJ. Functional neuroimaging evidence for hyperarousal in insomnia. *Am J Psychiatry* (2004) 161:2126–8. doi: 10.1176/appi.ajp.161.11.2126
31. Harvey AG. A cognitive model of insomnia. *Behav Res Ther.* (2002) 40:869–93. doi: 10.1016/S0005-7967(01)00061-4
32. Merica H, Blois R, Gaillard JM. Spectral characteristics of sleep EEG in chronic insomnia. *Eur J Neurosci.* (1998) 10:1826–34. doi: 10.1046/j.1460-9568.1998.00189.x
33. Perlis ML, Merica H, Smith MT, Giles DE. Beta EEG activity and insomnia. *Sleep Med Rev.* (2001) 5:363–74. doi: 10.1053/smrv.2001.0151
34. O'Byrne JN, Berman Rosa M, Gouin JP, Dang-Vu TT. Neuroimaging findings in primary insomnia. *Pathol Biol.* (2014) 62:262–9. doi: 10.1016/j.patbio.2014.05.013
35. Perlis ML, Smith MT, Pigeon WR. Etiology and pathophysiology of insomnia. In: Kryger MH, Roth T, Dement WC, editors. *Principles and Practice of Sleep Medicine*, 4th ed. Philadelphia, PA: Elsevier Inc (2005). p. 714–25.
36. Luo X, Guo L, Dai XJ, Wang Q, Zhu W, Miao X. Abnormal intrinsic functional hubs in alcohol dependence: evidence from a voxelwise degree centrality analysis. *Neuropsychiatr Dis Treat*. (2017) 13:2011–20. doi: 10.2147/NDT.S142742
37. Elvsåshagen T, Norbom LB, Pedersen PØ, Quraishi SH, Bjørnerud A, Malt UF. Widespread changes in white matter microstructure after a day of waking and sleep deprivation. *PLoS ONE* (2015) 10:e0127351. doi: 10.1371/journal.pone.0127351
38. Drummond SP, Brown GG, Gillin JC, Stricker JL, Wong EC, Buxton RB. Altered brain response to verbal learning following sleep deprivation. *Nature* (2000) 403:655–7. doi: 10.1038/35001068
39. Gao L, Zhang M, Gong H, Bai L, Dai XJ, Min Y. Differential activation patterns of FMRI in sleep-deprived brain: restoring effects of acupuncture. *Evid Based Complement Alternat Med.* (2014) 2014:465760. doi: 10.1155/2014/465760
40. Dai XJ, Peng DC, Gong HH, Wan AL, Nie X, Li HJ. Altered intrinsic regional brain spontaneous activity and subjective sleep quality in patients with chronic primary insomnia:a resting-state fMRI study. *Neuropsychiatr Dis Treat* (2014) 10:2163–75. doi: 10.2147/NDT.S69681
41. Peng DC, Dai XJ, Gong HH, Li HJ, Nie X, Zhang W. Altered intrinsic regional brain activity in male patients with severe obstructive sleep apnoea: a resting-state fMRI study. *Neuropsychiatr Dis Treat.* (2014) 10:1819–26 doi: 10.2147/NDT.S67805

Conflict of Interest Statement: The authors declare that the research was conducted in the absence of any commercial or financial relationships that could be construed as a potential conflict of interest.

frontiers in Neurology

ORIGINAL RESEARCH
published: 16 July 2018
doi: 10.3389/fneur.2018.00546

Altered Long- and Short-Range Functional Connectivity Density in Healthy Subjects After Sleep Deprivations

Dan Kong[1], Run Liu[2], Lixiao Song[3], Jiyong Zheng[1]*, Jiandong Zhang[1] and Wei Chen[4]*

[1] Department of Medical Imaging, The Affiliated Huai'an No. 1 People's Hospital of Nanjing Medical University, Huai'an, China, [2] Department of Radiology, The Affiliated Xi'an Central Hospital of Xi'an Jiaotong University, Xi'an, China, [3] Department of Hematology, The Affiliated Huai'an No. 1 People's Hospital of Nanjing Medical University, Huai'an, China, [4] Department of Interventional Radiology, The Affiliated Huai'an No. 1 People's Hospital of Nanjing Medical University, Huai'an, China

OPEN ACCESS

Edited by:
Xi-jian Dai,
Jinling Hospital and Medical School of Nanjing University, China

Reviewed by:
Xuming Liu,
Wenzhou City People's Hospital, China
Alexander Nikolaevich Savostyanov, State Scientific-Research Institute of Physiology & Basic Medicine, Russia

***Correspondence:**
Dan Kong
156017532@qq.com
Jiyong Zheng
jyzhengdoctor@126.com

Specialty section:
This article was submitted to Sleep and Chronobiology, a section of the journal Frontiers in Neurology

Received: *22 May 2018*
Accepted: *19 June 2018*
Published: *16 July 2018*

Citation:
Kong D, Liu R, Song L, Zheng J, Zhang J and Chen W (2018) Altered Long- and Short-Range Functional Connectivity Density in Healthy Subjects After Sleep Deprivations. Front. Neurol. 9:546. doi: 10.3389/fneur.2018.00546

Objective: To investigate the brain functional organization induced by sleep deprivation (SD) using functional connectivity density (FCD) analysis.

Methods: Twenty healthy subjects (12 female, 8 male; mean age, 20.6 ± 1.9 years) participated a 24 h sleep deprivation (SD) design. All subjects underwent the MRI scan and attention network test twice, once during rested wakefulness (RW) status, and the other was after 24 h acute SD. FCD was divided into the shortFCD and longFCD. Receiver operating characteristic (ROC) curve was used to evaluate the discriminating ability of those FCD differences in brain areas during the SD status from the RW status, while Pearson correlations was used to evaluate the relationships between those differences and behavioral performances.

Results: Subjects at SD status exhibited lower accuracy rate and longer reaction time relative to RW status. Compared with RW, SD had a significant decreased shortFCD in the left cerebellum posterior lobe, right cerebellum anterior lobe, and right orbitofrontal cortex, and increased shortFCD in the left occipital gyrus, bilateral thalamus, right paracentral lobule, bilateral precentral gyrus, and bilateral postcentral gyrus. Compared with RW, SD had a significant increased longFCD in the right precentral gyrus, bilateral postcentral gyrus, and right visuospatial network, and decreased longFCD in the default mode network. The area under the curve values of those specific FCD differences in brain areas were (mean ± std, 0.933 ± 0.035; 0.863∼0.977). Further ROC curve analysis demonstrated that the FCD differences in those brain areas alone discriminated the SD status from the RW status with high degree of sensitivities (89.19 ± 6%; 81.3∼100%) and specificities (89.15 ± 6.87%; 75∼100%). Reaction time showed a negative correlation with the right orbitofrontal cortex ($r = -0.48$, $p = 0.032$), and accuracy rate demonstrated a positive correlation with the right default mode network ($r = 0.573$, $p = 0.008$).

Conclusions: The longFCD and shortFCD analysis might be potential indicator biomarkers to locate the underlying altered intrinsic brain functional organization disturbed by SD. SD sustains the cognitive performance by the decreased high-order cognition related areas and the arousal and sensorimotor related areas.

Keywords: sleep deprivation, functional connectivity density, receiver operating characteristic, sensorimotor, short-range, long-range

INTRODUCTION

Sleep deprivation, widespread in current society, can be caused by environmental factors or personal reasons. It generally has a deleterious effect on emotional regulation, memory, attention, and executive control function (1–5), and even metabolic, physiological, psychological, and/or behavioral reactivity with a greater risk of being multiorgan and multisystem dysfunction (6–9). Recently, several studies have demonstrated structural and functional changes in the frontal cortex, parietal cortex, and temporal cortex in individuals after acute SD (1, 6, 10–21); however, the neurologic mechanism of acute SD has not been fully studied.

Resting-state functional MRI (rfMRI) can combine the functional images and structural images without exposure to radioactive tracers, which makes the rfMRI suitable for mechanism and pathophysiology exploration in several diseases (1). The advance of rfMRI can help us non-invasively explore the functional organization in the human brain thus better characterize the changes of regional neuronal spontaneous brain activity and intrinsic connectivity patterns to understand the underlying neural basis of neuropsychiatric disorders.

Seed-based functional connectivity studies have revealed abnormal connectivity patterns in individuals with insufficient sleep in brain regions related to emotion and cognition (13, 18, 21–26); however, the seed-based functional connectivity analysis provides limited information about the relationships between the time series of a given seed point area and the time series of other areas in a whole brain network (27, 28). Voxel-based functional connectivity density (FCD) was used to identify the distribution of hubs in the human brain (29). In contrast to the seed-based functional connectivity analysis, the FCD analysis, similar to the degree centrality analysis, provides an opportunity for unbiased searches abnormalities within the whole brain without the need for a prior definition of regions of interest (27). The FCD can be divided into the short-range FCD and long-range FCD on the basis of the neighboring relationships between brain voxels (30). Recently, the FCD analysis has been widely applied to the exploration of the neurophysiological basis of several diseases (31–34), and reveals extra information which cannot be provided by the seed-based functional connectivity analysis. In this framework, in the present study we utilized the potential indicators of shortFCD and longFCD approaches to characterize the changes of intrinsic functional connectivity strength after acute SD status relative to rested wakefulness (RW) status, and further explore the potential neurobiological mechanisms of SD.

MATERIALS AND METHODS

Subjects

Twenty healthy subjects (12 female, 8 male; mean age, 20.6 ± 1.9 years; mean education, 14.5 ± 1.19 years) participated in a 24 h SD design experiment. All subjects met the following criteria, as in previous studies (1, 6):

- Right-handed
- Good sleep habits without any symptoms of sleep disorders [such as difficulties in sleep onset (> 30 min) and/or maintaining sleep]
- Pittsburgh sleep quality index score < 5
- No consumption of any nicotine, hypnotic, or psychoactive medications, diet pills, alcohol, and caffeine for ≥ 3 months prior and during to the current study
- Regular dietary habit with moderate weight and body shape
- No foreign implants, inborn, and acquired diseases

Each of the subjects underwent the MRI scan twice; once during RW status, and the other after 24 h' acute SD. The acute SD process started at 19:00 on the first day and lasted until 07:00 in the second day. The food and water were provided during the SD procedure. The temperature of the room was maintained between 23°C and 27°C. The team took turns to monitor and make sure that the participants did not fall asleep using video monitors. This study was approved by the Medical Research Ethical Committee of The Affiliated Huai'an No. 1 People's Hospital of Nanjing Medical University in accordance with the Declaration of Helsinki. All volunteers participated voluntarily and were informed of the purposes, methods, and potential risks of this study, and signed an informed consent form.

MRI

The MRI examination was performed, via acquisition, on a clinical 3T MRI scanner (SIEMENS Trio, Erlangen, Siemens, Germany) with a standard eight-channel head coil using a 12-channel array coil. First, we acquired a high-resolution 3D anatomical images with 176 T1-weighted images in a sagittal orientation: repetition time = 1950 ms, gap = 0 mm, echo time = 2.3 ms, thickness = 1 mm, acquisition matrix = 248 × 256, flip angle = 9°, field of view = 244 × 252 mm. Second, we also acquired 240 functional images using a single-shot Gradient-Recalled Echo-Planar Imaging pulse sequence (repetition time = 3000 ms, gap = 0.5 mm, echo time = 25 ms, thickness = 5.0 mm, flip angle = 90°, acquisition matrix = 32 × 32, field of view = 210 × 210 mm).

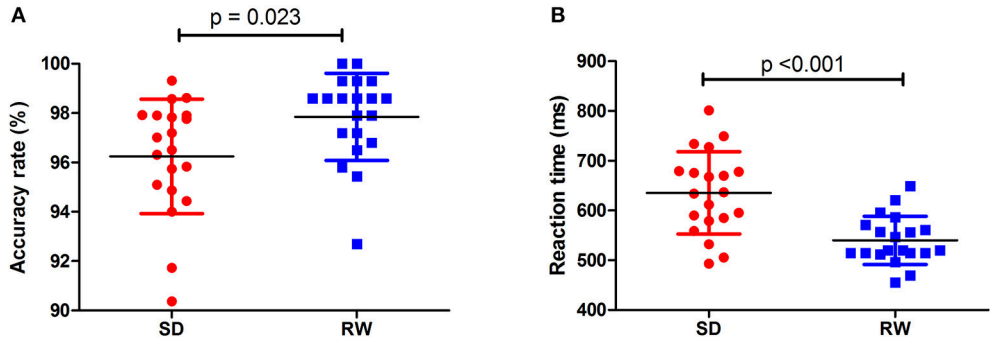

FIGURE 1 | Behavioral findings of ANT. The accuracy rate and reaction time of RW group **(A)** and SD group **(B)**, respectively. Data is presented as mean ± standard error. ANT, Attention network test; SD, Sleep deprivation; RW, Rested wakefulness.

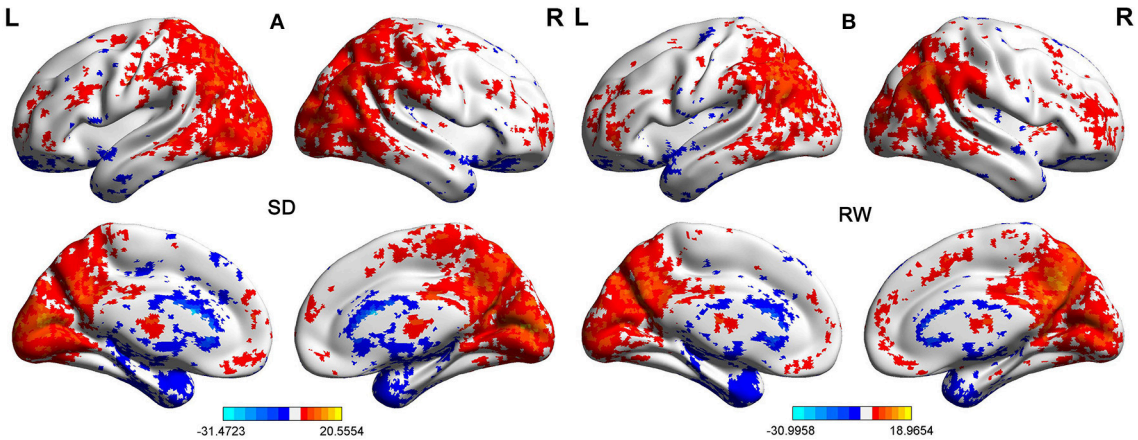

FIGURE 2 | One sample *t*-test differences of SD and RW in Binarized shortFCD. The Binarized shortFCD maps in the SD group **(A)** and the RW group **(B)**, respectively. These maps are the results of the within-groups using one-sample *t*-tests, corrected by FDR. L, left; R, right; SD, sleep deprivation; RW, rested wakefulness; shortFCD, short-range functional connectivity density; FDR, false discovery rate.

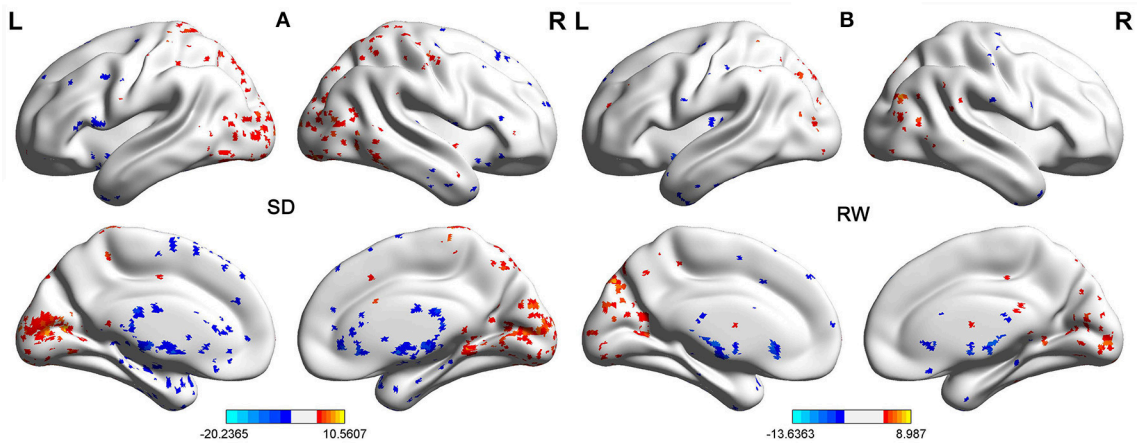

FIGURE 3 | One sample *t*-test differences of SD and RW in Binarized longFCD. The Binarized longFCD maps in the SD group **(A)** and the RW group **(B)**, respectively. These maps are the results of the within-groups using one-sample *t*-tests, corrected by FDR. L, left; R, right; SD, sleep deprivation; RW, rested wakefulness; longFCD, long-range functional connectivity density; FDR, false discovery rate.

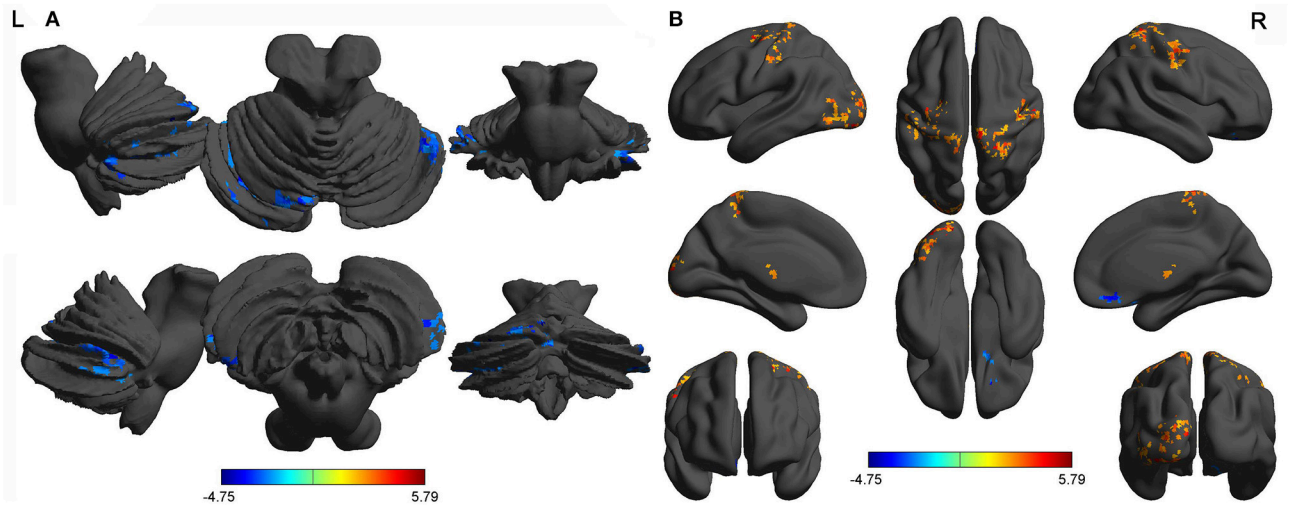

FIGURE 4 | Binarized shortFCD differences between SD and RW. The color in the map represents the differences. The blue signifies decreased binarized shortFCD in brain areas **(A)**, and the red color signifies increased binarized shortFCD in brain areas **(B)**. shortFCD, short-range functional connectivity density; SD, Sleep deprivation; RW, Rested wakefulness; L, left; R, right.

TABLE 1 | The binarized shortFCD differences between SD and RW.

Brain regions of peak coordinates	R/L	BA	Voxel size	*t*-score of peak voxel	MNI coordinates
					X, Y, Z
Cerebellum Posterior Lobe	L	N/A	75	−4.7451	−30 −69 −27
Cerebellum Anterior Lobe	R	N/A	62	−3.8821	51 −48 −36
Cerebellum Posterior Lobe	L	N/A	54	−4.7238	−3 −75 −18
Inferior Frontal Gyrus	R	11	87	−4.0611	18 24 −15
Lingual Gyrus, Middle Occipital Gyrus	L	18, 19	216	5.3825	−15 −93 −12
Thalamus	L, R	N/A	82	5.7899	9 −18 9
Precentral Gyrus, Postcentral Gyrus	R	3, 4, 6	157	4.6467	54 −12 57
Postcentral Gyrus	L	2, 3	72	3.5485	−30 −36 45
Postcentral Gyrus, Paracentral Lobule	R	3, 4	200	4.5221	9 −33 75
Precentral Gyrus	L	6	93	4.2005	−24 −6 63
Postcentral Gyrus	L	3, 5	68	4.7094	−18 −42 57

Between-group differences in binarized shortFCD thresholded at r = 0.3. The statistical threshold was set at corrected significance level of individual two-tailed voxel-wise p < 0.05 using an AlphaSim corrected threshold of cluster p < 0.05.
shortFCD, short-range functional connectivity density; SD, sleep deprivation; RW, rested wakefulness; R, right; L, left; BA, Brodmann's area; MNI, Montreal Neurological Institute; N/A, Not applicable.

TABLE 2 | The binarized longFCD differences between SD and RW.

Brain regions of peak coordinates	R/L	BA	Voxel size	t-score of peak voxel	MNI coordinates
					X, Y, Z
Postcentral Gyrus, Precentral Gyrus	R	3, 4	108	5.1923	51 −24 51
Superior Parietal Lobule	R	7, 40	52	3.8173	33 −42 42
Postcentral Gyrus	L	3, 4	40	4.0239	−42 −27 63
Supramarginal Gyrus	R	39	42	−3.6057	51 −66 27

Between-group differences in binarized shortFCD thresholded at r = 0.3. The statistical threshold was set at corrected significance level of individual two-tailed voxel-wise p < 0.05 using an AlphaSim corrected threshold of cluster p < 0.05.
longFCD, long-range functional connectivity density; R, right; L, left; BA, Brodmann's area; MNI, Montreal Neurological Institute; N/A, Not applicable.

Attention Network Test (ANT)

Before the MRI scan, all volunteers underwent an attention network test (ANT) (1, 12, 35, 36). The ANT contained three cue conditions (no cue, center cue, spatial cue) and two target conditions (congruent and incongruent). The visual stimuli consisted of a row of five horizontal black arrows pointing leftward or rightward with the target arrow in the center. The participants responded to the direction of the central arrow by pressing the left or right buttons of the computer mouse. The task measured alerting, orienting, and conflict effects by calculating the difference between the response time and the presentation time under three different cue conditions. The accuracy rate using corrected recognition, reaction time using only trials with correct responses, and lapse rate using missing recognition, were calculated.

Data Analysis

First, the first 10 time points of the functional images were deleted, due to the possible instability of the initial MRI signal.

The remaining data was analyzed by Data Processing & Analysis for Brain Imaging (DPABI 2.1, http://rfmri.org/DPABI) toolbox based on MATLAB2010a (Mathworks, Natick, MA, USA). The data preprocessing contained the following steps: including the format transformation, slice timing, head motion correction spatial normalization to the Montreal Neurological Institute (MNI) space, and smooth. The data of participants with > 1.5 mm maximum translation in x, y, or z directions and >1.5° degree of motion rotation were removed. Based on the recent work showing that higher-order models benefit from the removal of head motion effects (37, 38), after the head motion correction, The functional images were re-sampled at a resolution of 3 × 3 × 3 mm^3 during the spatial normalization. Linear regression was applied to remove the effects of spurious covariates, including the Friston 24 head motion parameters, global mean signal, white matter and cerebrospinal fluid signal. Next, the functional images were entered into temporally bandpass filtered (0.01–0.1 Hz) and linearly detrended.

Calculation of Long FCD and ShortFCD Calculation Maps

The local and global FCD maps for each individual were calculated in a gray matter (GM) mask. The number of functional connections of a given voxel was considered as a degree of a node in a binary graph. First, we defined the functional connectivity between a given voxel with each of other voxels in the whole brain with a correlation threshold of $r > 0.25$ (39). In the present study, we adopted the threshold of $r = 0.3$ to calculate the FCD maps. Second, the longFCD and shortFCD were defined based on the neighborhood strategy. We defined the voxels with a correlation threshold of $r > 0.25$ inside their neighborhood (radius sphere ≤6 mm) as shortFCD, and defined the voxels with a correlation threshold of $r > 0.25$ outside their neighborhood (radius sphere > 6 mm) as long FCD. Next, the shortFCD and longFCD maps of each subject were divided by the mean value so as to convert to Z scores to improve the normality. Finally, the shortFCD and longFCD maps underwent spatial smoothing with a Gaussian kernel of 6 × 6 × 6 mm^3 full-width at half-maximum using SPM8. The detailed procedure of the shortFCD and longFCD is given in a previous study (29).

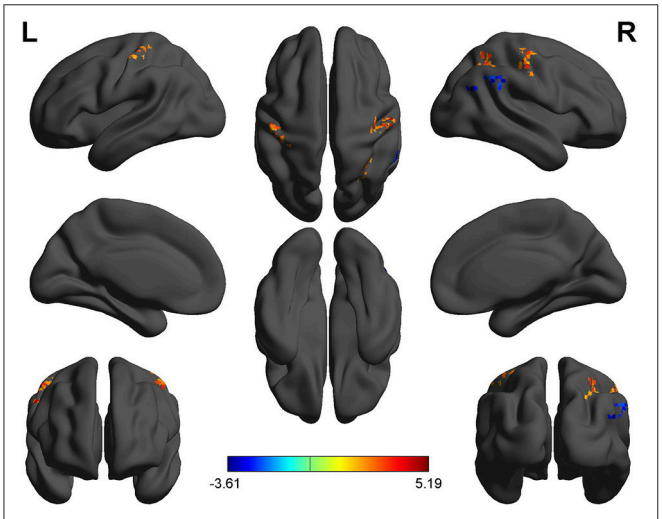

FIGURE 5 | Binarized longFCD differences between SD and RW. The color in the map represents the differences. The red color signifies increased binarized longFCD in brain areas, and the blue signifies decreased binarized longFCD in brain areas. longFCD, long-range functional connectivity density; SD, Sleep deprivation; RW, Rested wakefulness; L, left; R, right.

Statistical Analysis

Data was presented as mean ± standard deviation (mean ± std). Pair *t*-tests were used for demographic factors (age, years of education, and ANT findings). $p < 0.05$ was considered as significant.

Pair *t*-tests were used to investigate the FCD differences in regional brain areas of the subjects during the acute SD status relative to the RW status. AlphaSim correction (threshold of individual voxel of $p < 0.05$ and cluster level of $p < 0.05$) was used to determine the statistical differences.

We used the receiver operating characteristic (ROC) curve to investigate the ability of those binarized FCD differences in regional brain areas to distinguish the SD status from the RW status, and we used Pearson correlations to evaluate the relationships between those binarized FCD differences in brain areas and ANT during the SD status. The statistical threshold was set at $P < 0.05$.

RESULTS

Ant Findings

Individuals at acute SD status showed a lower accuracy rate (acute SD = 96.25 ± 2.32%, RW = 97.85 ± 1.77%; $t = -2.482$, $p = 0.023$; **Figure 1A**) and a longer reaction time (acute SD = 635.27 ms ± 82.68 ms; RW = 540.01 ± 48.37 ms; $t = 5.013$, $p < 0.001$; **Figure 1B**) during the ANT relative to the individuals at RW status.

FCD Differences Between-Groups

First, we performed one-sample *t*-test to explore the FCD differences at within-group level for each group. **Figure 2** shows the shortFCD maps in the SD group (**Figure 2A**) and RW group (**Figure 2B**), respectively. **Figure 3** shows the longFCD maps in the SD group (**Figure 3A**) and RW group (**Figure 3B**), respectively. The covered differences in brain areas both in binarized shortFCD and in binarized longFCD were larger in the SD group than that of RW group.

Second, we performed pair t-tests to explore the FCD differences between-groups. Compared with RW, acute SD had significant decreased binarized shortFCD areas in the left cerebellum posterior lobe, right cerebellum anterior lobe (**Figure 4A**) and right inferior frontal gyrus (orbitofrontal cortex), and increased binarized shortFCD areas in the left occipital gyrus, bilateral thalamus, right paracentral lobule, bilateral precentral gyrus, and bilateral postcentral gyrus (**Table 1**, **Figure 4B**). Compared with RW, acute SD had significant increased binarized longFCD areas in the right precentral gyrus, bilateral postcentral gyrus, and right superior

TABLE 3 | ROC curve for the binarized shortFCD differences in brain areas between SD and RW.

Brain area	AUC	Sensitivity (%)	Specificity (%)	Cut off Point*
L _Cerebellum Posterior Lobe	0.906	81.3	93.7	0.242
R_Cerebellum Anterior Lobe	0.922	87.5	87.5	−0.0365
L_Cerebellum Posterior Lobe	0.863	87.5	81.2	0.5555
R_Inferior Frontal Gyrus	0.977	87.5	100	−0.2065
L_Lingual Gyrus, Middle Occipital Gyrus	0.91	93.8	81.2	0.3715
L, R_Thalamus	0.922	81.3	93.7	0.5005
R_Precentral Gyrus, Postcentral Gyrus	0.922	87.5	87.5	0.16
L_Postcentral Gyrus	0.887	87.5	87.5	0.006
R_Postcentral Gyrus, Paracentral Lobule	0.977	100	87.5	0.2995
L_Precentral Gyrus	0.961	87.5	93.7	−0.166
L_Postcentral Gyrus	0.914	93.8	75	0.1635

Cut off point of mean shortFCD signal value.

ROC, Receiver operating characteristic; shortFCD, short-range functional connectivity density; SD, Sleep deprivation; RW, Rested wakefulness; AUC, Area under the curve; R, Right; L, Left.

TABLE 4 | ROC curve for the binarized longFCD differences in brain areas between SD and RW.

Brain area	AUC	Sensitivity (%)	Specificity (%)	Cut off Point*
R_Postcentral Gyrus, Precentral Gyrus	0.965	81.3	100	0.2845
R_Superior Parietal Lobule	0.973	100	87.5	0.0165
L_Postcentral Gyrus	0.949	93.8	87.5	0.1275
R_Supramarginal Gyrus	0.949	87.5	93.7	−0.048

Cut off point of mean longFCD signal value.

ROC, Receiver operating characteristic; longFCD, long-range functional connectivity density; SD, Sleep deprivation; RW, Rested wakefulness; AUC, Area under the curve; R, Right; L, Left.

parietal lobule in the visuospatial network, and decreased binarized longFCD areas in the right supramarginal gyrus in the default mode network (**Table 2**, **Figure 5**).

ROC Curve

The mean beta value of binarized shortFCD (**Figure 6A**) and binarized longFCD (**Figure 6B**) differences in those altered brain areas were extracted. These different binarized FCD differences in brain areas were further used for the ROC curve to evaluate their ability to distinguish the acute SD status from the RW status. The area under the curve (AUC) values of those specific binarized FCD differences in brain areas were (mean ± std, 0.933 ± 0.035; 0.863∼0.977). Further ROC curve demonstrated that the binarized FCD differences in those regional brain areas alone discriminated the acute SD status from the RW status with high degree of sensitivities (mean ± std, 89.19 ± 6%; 81.3∼100%) and specificities (mean ± std, 89.15 ± 6.87%; 75∼100%) (**Tables 3–4**, **Figure 7**).

Pearson Correlation Analysis

The reaction time showed negative correlation with the mean beta value of binarized shortFCD in the right inferior frontal gyrus ($r = -0.48$, $p = 0.032$; **Figure 8A**), and the accuracy rate demonstrated a positive correlation with the mean beta value of binarized longFCD in the right supramarginal gyrus ($r = 0.573$, $p = 0.008$; **Figure 8B**). None of the other correlations between the mean beta value of binarized FCD in other different areas and the ANT during the acute SD status were found ($p > 0.05$).

DISCUSSION

In the present study, we utilized shortFCD and longFCD analysis to characterize the differences of intrinsic functional connectivity induced by acute SD, and their correlations with the ANT. Specifically, we found that acute SD was associated with binarized shortFCD alterations in more regional brain areas than that of binarized longFCD. Acute SD was associated with a significant decrease in binarized shortFCD areas in the cerebellum posterior/anterior lobe and orbitofrontal cortex, and significant increase in the occipital gyrus, thalamus, paracentral lobule, and precentral/postcentral gyrus. Using the binarized longFCD method, only the supramarginal gyrus in the default mode network with decreased binarized longFCD were observed after acute SD relative to RW, and significantly increased binarized longFCD in the precentral/postcentral gyrus and visuospatial network were found. Furthermore, the ANT showed correlations with the beta value of FCD differences in those brain areas during the SD status. Recently, the ROC curve was widely used to applied into the exploration of the reliability of one neuroimaging approach as a potential indicator in distinguishing one group from the other group (1, 40, 41). In general, an AUC value between 0.9 and 1 is considered as excellent, while a value between 0.8 and 0.9 is considered as good. In the present study, the ROC curve demonstrated that the AUC values of the binarized FCD differences in those brain areas showed good discriminating abilities with extremely high AUC values (0.933 ± 0.035; 0.863∼0.977). Further diagnostic analysis revealed that the binarized FCD differences in those regional brain areas alone discriminated the acute SD status from the RW status with extremely high degree of sensitivity (89.19 ± 6%; 81.3∼100%) and specificities (89.15 ± 6.87%; 75∼100%).

The default-mode network is thought to be associated with self-referential mental activity (42), extraction of episodic memory (43), sleep and daydreaming (1, 44), and social cognitive processes related to decision making and self-regulation (45, 46). The orbitofrontal cortex, connected with prefrontal, and deep structures known to mediate sensorimotor processing,

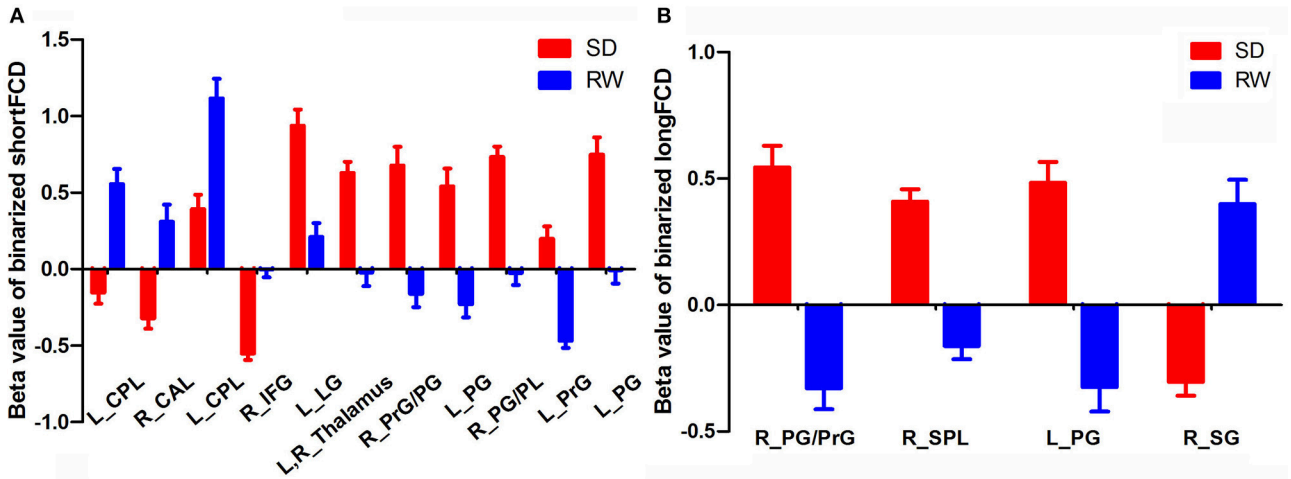

FIGURE 6 | Binarized shortFCD value **(A)** and longFCD value **(B)** of between-group differences in brain areas. Data are mean ± standard error values. L, left; R, right; shortFCD, short-range functional connectivity density; longFCD, long-range functional connectivity density; CPL, Cerebellum posterior lobe; CAL, Cerebellum anterior lobe; IFG, Inferior frontal gyrus; LG, Lingual gyrus; PrG, precentral gyrus; PG, Postcentral gyrus; PL, Paracentral lobule; SPL, Superior parietal lobule; SG, Supramarginal gyrus; SD, Sleep deprivation; RW, Rested wakefulness.

motivation, and self-evaluation, is thought to be responsible for mediating the interactions between emotional processes and cognitive functions (47, 48), and play a significant role in fatigue, executive functions, attention, and motivation (49–51). This area is particularly vulnerable to subjects with sleep loss (40, 41, 52, 53). The decreased gray matter volume in the orbitofrontal cortex has previously been reported in patients with daytime sleepiness and chronic insomnia (54, 55). In the present study, we found that acute SD was associated with a significant decreased binarized longFCD within the default mode network node and decreased binarized shortFCD in the right orbitofrontal cortex, which showed an extremely high degree of sensitivity and specificity in distinguishing the acute SD status from the RW status. In addition, the accuracy rate of the ANT demonstrated a positive correlation with the mean beta value of binarized longFCD in the default mode network node, and the reaction time of the ANT showed negative correlation with the mean beta value of binarized shortFCD in the orbitofrontal cortex. We speculated that the decreased long-/shortFCD in the default mode network and orbitofrontal cortex implicated the brain's exertion of voluntary control to remain awake and perform, which might be sensitive biomarkers for advanced cognitive function.

Higher level visual brain areas are divided into two distinct visual pathways: the object properties processing pathway and the spatial properties processing pathway (56–58). The spatial properties processing pathway runs from the occipital lobe up to the posterior parietal lobe and has been called the dorsal system. This system processes object localization and spatial attributes, and is also essential for guiding movements. Damage to the dorsal pathway disrupts the ability to visualize locations or perceive space. The postcentral gyrus is the main receptive region for external stimuli as the location of the primary somatosensory cortex. Recently the postcentral gyrus was implicated with the default mode network (59), which are functional brain hubs showing coupled slow signal fluctuations in the absence of external stimuli during restful waking and sleep (60). The thalamus is a vital region in integrating neural activity from widespread neocortical inputs and outputs, and is thought to play an important role in regulating state of sleep and wakefulness. Previous PET studies have revealed that SD could increase the metabolic rate of glucose in the visual cortex, somatosensory cortex, and fusiform gyrus, which were much higher after 48 h and 72 h than after 24 h SD (61, 62). Previous neuroimaging studies observed disturbed regional spontaneous neural activities in brain areas of the two visual pathways in insomnia patients and individuals after SD (6, 15, 25, 40, 63). In the present study we observed acute SD was associated with altered FCD areas in the thalamus and dorsal system, including significant increased binarized shortFCD areas in the occipital gyrus, thalamus and postcentral gyrus, and increased binarized longFCD areas in the postcentral gyrus and visuospatial network. The increased FCD in these regions in the visual pathway could be considered a compensatory effect to sustain the cognitive performance despite a continuing decline of activity in the higher cognition related areas. This may generate an excessive hyperarousal status, which leads to increased sensory information processing (64).

There are extensive round-trip nerve interactive fibers between the cerebellum posterior lobe(s) and the cerebral cortex. The cerebellum posterior lobe(s) has been widely used for adjusting nerve function, adjusting the start, and planning and coordinating movement. It also works together with the cerebrum to complete functions; such as cognition, language, and emotion; and to initiate, plan, and coordinate movement (65–67). In light of mounting evidence for cerebellar involvement in various neurologic and psychiatric conditions, including obstructive sleep apnea (53), depression (68), primary insomnia (40, 63), mood

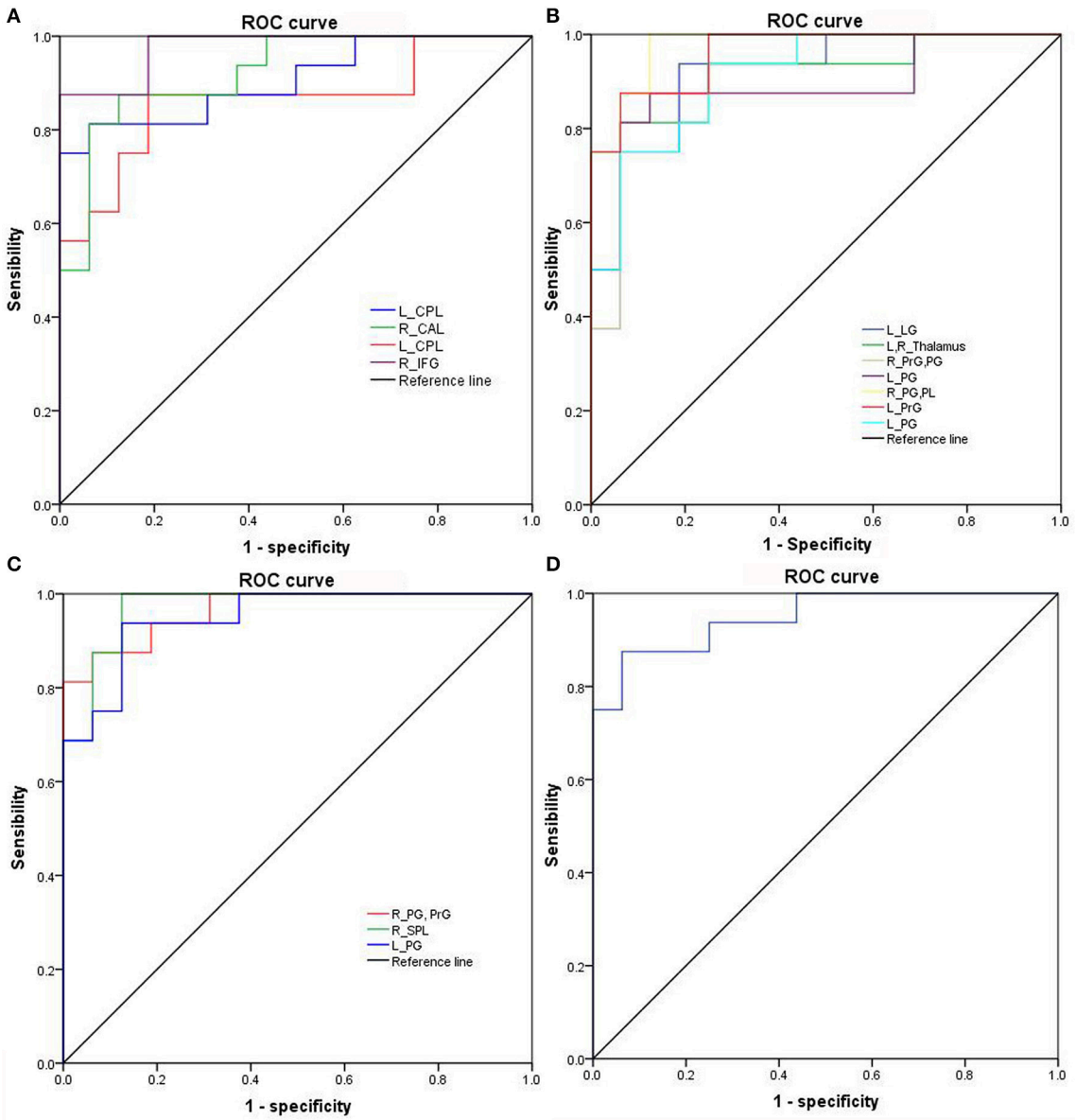

FIGURE 7 | ROC curve of binarized FCD differences in regional brain areas. ROC curve of regional brain areas with decreased binarized shortFCD **(A)**, increased binarized shortFCD **(B)**, increased binarized longFCD **(C)**, and decreased binarized longFCD **(D)**. ROC, Receiver operating characteristic; R, right; L, left; CPL, Cerebellum posterior lobe; CAL, Cerebellum anterior lobe; IFG, Inferior frontal gyrus; LG, Lingual gyrus; PrG, precentral gyrus; PG, Postcentral gyrus; PL, Paracentral lobule; SPL, Superior parietal lobule; SG, Supramarginal gyrus; SD, Sleep deprivation; RW, Rested wakefulness; shortFCD, short-range functional connectivity density; longFCD, long-range functional connectivity density.

disorders (69) and sleep deprivation (6); this is crucial. In the present study we found acute SD showed decreased shortFCD in the cerebellum, which may indicate functional deficits associated with decreased ability in adjusting coordinate movement.

CONCLUSIONS

In summary, the longFCD and shortFCD analysis might be sensitive biomarkers to locate the underlying altered intrinsic brain functional organization in individuals during SD status relative to RW status with high degree of sensitivities and specificities. Specifically, the shortFCD analysis is more sensitive to locating the functional organization with more alterations in regional brain areas than that of longFCD. In the present study, we found that the longFCD and short FCDs in the high-order cognition related areas decreased while the arousal and sensorimotor related areas increased to sustain the cognitive performance. These findings expand our

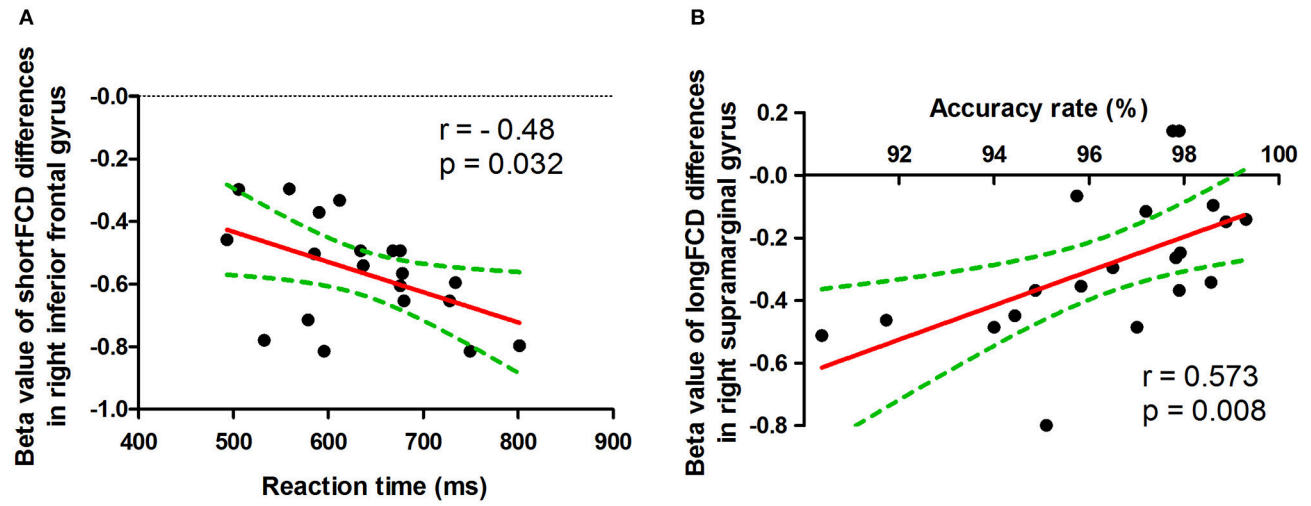

FIGURE 8 | Pearson correlation between beta value of FCD differences in brain areas and ANT. ShortFCD, short-range functional connectivity density; longFCD, long-range functional connectivity density.

knowledge and may help give us insight into a deeper understanding of the neurobiological mechanisms of how the functional organization was altered in the sleep-deprived brain.

There are several limitations that should be noted. First, our study has a relatively small sample size and future studies with a larger sample size is necessary to corroborate our findings. Second, the electronystagmogram has not been used to dynamically monitor the sleep in the SD procedure.

AUTHOR CONTRIBUTIONS

DK wrote the main manuscript text, DK, RL, JiyZ, and WC conceived and designed the whole experiment, DK, LS, and JiaZ collected the data, DK, RL, and JiyZ analyzed the data.

ACKNOWLEDGMENTS

This work was supported by Key Research and Development Projects in Shaanxi province in the field of social development (2017SF-081).

REFERENCES

1. Dai XJ, Liu CL, Zhou RL, Gong HH, Wu B, Gao L, et al. Long-term total sleep deprivation decreases the default spontaneous activity and connectivity pattern in healthy male subjects: a resting-state fMRI study. *Neuropsychiatr Dis Treat* (2015) 11:761–72. doi: 10.2147/NDT.S78335
2. Drummond SP, Brown GG. The effects of total sleep deprivation on cerebral responses to cognitive performance. *Neuropsychopharmacology* (2001) 25:S68–73. doi: 10.1016/S0893-133X(01)00325-6
3. Jackson ML, Hughes ME, Croft RJ, Howard ME, Crewther D, Kennedy GA, et al. The effect of sleep deprivation on BOLD activity elicited by a divided attention task. *Brain Imaging Behav.* (2011) 5:97–108. doi: 10.1007/s11682-011-9115-6
4. Luber B, Stanford AD, Bulow P, Nguyen T, Rakitin BC, Habeck C, et al. Remediation of sleep-deprivation-induced working memory impairment with fMRI-guided transcranial magnetic stimulation. *Cereb Cortex* (2008) 18:2077–85. doi: 10.1093/cercor/bhm231
5. Nilsson JP, Soderstrom M, Karlsson AU, Lekander M, Akerstedt T, Lindroth NE, et al. Less effective executive functioning after one night's sleep deprivation. *J Sleep Res.* (2005) 14:1–6. doi: 10.1111/j.1365-2869.2005.00442.x
6. Dai XJ, Gong HH, Wang YX, Zhou FQ, Min YJ, Zhao F, et al. Gender differences in brain regional homogeneity of healthy subjects after normal sleep and after sleep deprivation: a resting-state fMRI study. *Sleep Med.* (2012) 13:720–7. doi: 10.1016/j.sleep.2011.09.019
7. Ohayon MM, Smolensky MH, Roth T. Consequences of shiftworking on sleep duration, sleepiness, and sleep attacks. *Chronobiol Int.* (2010) 27:575–89. doi: 10.3109/07420521003749956
8. Tsigos C, Chrousos GP. Hypothalamic-pituitary-adrenal axis, neuroendocrine factors and stress. *J Psychosom Res.* (2002) 53:865–71. doi: 10.1016/S0022-3999(02)00429-4
9. Walker MP, Stickgold R. Sleep, memory, and plasticity. *Annu Rev Psychol.* (2006) 57:139–66. doi: 10.1146/annurev.psych.56.091103.070307
10. Bosch OG, Rihm JS, Scheidegger M, Landolt HP, Stampfli P, Brakowski J, et al. Sleep deprivation increases dorsal nexus connectivity to the dorsolateral prefrontal cortex in humans. *Proc Natl Acad Sci USA.* (2013) 110:19597–602. doi: 10.1073/pnas.1317010110
11. Cui J, Tkachenko O, Gogel H, Kipman M, Preer LA, Weber M, et al. Microstructure of frontoparietal connections predicts individual resistance to sleep deprivation. *Neuroimage* (2015) 106:123–33. doi: 10.1016/j.neuroimage.2014.11.035
12. Dai XJ, Jiang J, Zhang Z, Nie X, Liu BX, Pei L, et al. Plasticity and susceptibility of brain morphometry alterations to insufficient sleep. *Front Psychiatry* (2018) 8:266. doi: 10.3389/fpsyt.2018.00266
13. De Havas JA, Parimal S, Soon CS, Chee MW. Sleep deprivation reduces default mode network connectivity and anti-correlation during rest and task performance. *Neuroimage* (2012) 59:1745–51. doi: 10.1016/j.neuroimage.2011.08.026
14. Elvsashagen T, Norbom LB, Pedersen PO, Quraishi SH, Bjornerud A, Malt UF, et al. Widespread changes in white matter microstructure after

a day of waking and sleep deprivation. *PLoS ONE* (2015) 10:e0127351. doi: 10.1371/journal.pone.0127351
15. Gao L, Bai L, Zhang Y, Dai XJ, Netra R, Min Y, et al. Frequency-dependent changes of local resting oscillations in sleep-deprived brain. *PLoS ONE* (2015) 10:e0120323. doi: 10.1371/journal.pone.0120323
16. Gao L, Zhang M, Gong H, Bai L, Dai XJ, Min Y, et al. Differential activation patterns of FMRI in sleep-deprived brain: restoring effects of acupuncture. *Evid Based Complement Alternat Med.* (2014) 2014:465760. doi: 10.1155/2014/465760
17. Rocklage M, Williams V, Pacheco J, Schnyer DM. White matter differences predict cognitive vulnerability to sleep deprivation. *Sleep* (2009) 32:1100–3. doi: 10.1093/sleep/32.8.1100
18. Shao Y, Wang L, Ye E, Jin X, Ni W, Yang Y, et al. Decreased thalamocortical functional connectivity after 36 hours of total sleep deprivation: evidence from resting state FMRI. *PLoS ONE* (2013) 8:e78830. doi: 10.1371/journal.pone.0078830
19. Verweij IM, Romeijn N, Smit DJ, Piantoni G, Van Someren EJ, van der Werf YD. Sleep deprivation leads to a loss of functional connectivity in frontal brain regions. *BMC Neurosci.* (2014) 15:88. doi: 10.1186/1471-2202-15-88
20. Wang L, Chen Y, Yao Y, Pan Y, Sun Y. Sleep deprivation disturbed regional brain activity in healthy subjects: evidence from a functional magnetic resonance-imaging study. *Neuropsychiatr Dis Treat* (2016) 12:801–7. doi: 10.2147/NDT.S99644
21. Yeo BT, Tandi J, Chee MW. Functional connectivity during rested wakefulness predicts vulnerability to sleep deprivation. *Neuroimage* (2015) 111:147–58. doi: 10.1016/j.neuroimage.2015.02.018
22. Killgore WD, Schwab ZJ, Kipman M, Deldonno SR, Weber M. Insomnia-related complaints correlate with functional connectivity between sensory-motor regions. *Neuroreport* (2013) 24:233–40. doi: 10.1097/WNR.0b013e32835edbdd
23. Li Y, Wang E, Zhang H, Dou S, Liu L, Tong L, et al. Functional connectivity changes between parietal and prefrontal cortices in primary insomnia patients: evidence from resting-state fMRI. *Eur J Med Res.* (2014) 19:32. doi: 10.1186/2047-783X-19-32
24. Liu X, Yan Z, Wang T, Yang X, Feng F, Fan L, et al. Connectivity pattern differences bilaterally in the cerebellum posterior lobe in healthy subjects after normal sleep and sleep deprivation: a resting-state functional MRI study. *Neuropsychiatr Dis Treat* (2015) 11:1279–89. doi: 10.2147/NDT.S84204
25. Nie X, Shao Y, Liu SY, Li HJ, Wan AL, Nie S, et al. Functional connectivity of paired default mode network subregions in primary insomnia. *Neuropsychiatr Dis Treat* (2015) 11:3085–93. doi: 10.2147/NDT.S95224
26. Shao Y, Lei Y, Wang L, Zhai T, Jin X, Ni W, et al. Altered resting-state amygdala functional connectivity after 36 hours of total sleep deprivation. *PLoS ONE* (2014) 9:e112222. doi: 10.1371/journal.pone.0112222
27. Liu X, Zheng J, Liu BX, Dai XJ. Altered connection properties of important network hubs may be neural risk factors for individuals with primary insomnia. *Sci Rep.* (2018) 8:5891. doi: 10.1038/s41598-018-23699-3
28. Luo X, Guo L, Dai XJ, Wang Q, Zhu W, Miao X, et al. Abnormal intrinsic functional hubs in alcohol dependence: evidence from a voxelwise degree centrality analysis. *Neuropsychiatr Dis Treat* (2017) 13:2011–20. doi: 10.2147/NDT.S142742
29. Tomasi D, Volkow ND. Functional connectivity density mapping. *Proc Natl Acad Sci USA.* (2010) 107:9885–90. doi: 10.1073/pnas.1001414107
30. Tomasi D, Volkow ND. Aging and functional brain networks. *Mol Psychiatry* (2012) 471:549–58. doi: 10.1038/mp.2011.81
31. Tomasi D, Volkow ND. Gender differences in brain functional connectivity density. *Hum Brain Mapp.* (2012) 33:849–60. doi: 10.1002/hbm.21252
32. Wang J, Wei Q, Yuan X, Jiang X, Xu J, Zhou X, et al. Local functional connectivity density is closely associated with the response of electroconvulsive therapy in major depressive disorder. *J Affect Disord.* (2018) 225:658–64. doi: 10.1016/j.jad.2017.09.001
33. Zhang Y, Xie B, Chen H, Li M, Liu F, Chen H. Abnormal functional connectivity density in post-traumatic stress disorder. *Brain Topogr.* (2016) 29:405–11. doi: 10.1007/s10548-016-0472-8
34. Tomasi D, Volkow ND. Resting functional connectivity of language networks: characterization and reproducibility. *Mol Psychiatry* (2012) 17:841–54. doi: 10.1038/mp.2011.177
35. Fan J, McCandliss BD, Fossella J, Flombaum JI, Posner MI. The activation of attentional networks. *Neuroimage* (2005) 26:471–9. doi: 10.1016/j.neuroimage.2005.02.004
36. Fan J, McCandliss BD, Sommer T, Raz A, Posner MI. Testing the efficiency and independence of attentional networks. *J Cogn Neurosci.* (2002) 14:340–7. doi: 10.1162/089892902317361886
37. Satterthwaite TD, Elliott MA, Gerraty RT, Ruparel K, Loughead J, Calkins ME, et al. An improved framework for confound regression and filtering for control of motion artifact in the preprocessing of resting-state functional connectivity data. *Neuroimage* (2013) 64:240–56. doi: 10.1016/j.neuroimage.2012.08.052
38. Yan CG, Cheung B, Kelly C, Colcombe S, Craddock RC, Di Martino A, et al. A comprehensive assessment of regional variation in the impact of head micromovements on functional connectomics. *Neuroimage* (2013) 76:183–201. doi: 10.1016/j.neuroimage.2013.03.004
39. Buckner RL, Sepulcre J, Talukdar T, Krienen FM, Liu H, Hedden T, et al. Cortical hubs revealed by intrinsic functional connectivity: mapping, assessment of stability, and relation to Alzheimer's disease. *J Neurosci.* (2009) 29:1860–73. doi: 10.1523/JNEUROSCI.5062-08.2009
40. Dai XJ, Nie X, Liu X, Pei L, Jiang J, Peng DC, et al. Gender differences in regional brain activity in patients with chronic primary insomnia: evidence from a resting-state fMRI study. *J Clin Sleep Med.* (2016) 12:363–74. doi: 10.5664/jcsm.5586
41. Li HJ, Dai XJ, Gong HH, Nie X, Zhang W, Peng DC. Aberrant spontaneous low-frequency brain activity in male patients with severe obstructive sleep apnea revealed by resting-state functional MRI. *Neuropsychiatr Dis Treat* (2015) 11:207–14. doi: 10.2147/NDT.S73730
42. Gusnard DA, Akbudak E, Shulman GL, Raichle ME. Medial prefrontal cortex and self-referential mental activity: relation to a default mode of brain function. *Proc Natl Acad Sci USA* (2001) 98:4259–64. doi: 10.1073/pnas.071043098
43. Cabeza R, Dolcos F, Graham R, Nyberg L. Similarities and differences in the neural correlates of episodic memory retrieval and working memory. *Neuroimage* (2002) 16:317–30. doi: 10.1006/nimg.2002.1063
44. Mason MF, Norton MI, Van Horn JD, Wegner DM, Grafton ST, Macrae CN. Wandering minds: the default network and stimulus-independent thought. *Science* (2007) 315:393–5. doi: 10.1126/science.1131295
45. Bechara A, Damasio H, Damasio AR. Emotion, decision making and the orbitofrontal cortex. *Cereb Cortex* (2000) 10:295–307. doi: 10.1093/cercor/10.3.295
46. Beer JS, Lombardo MV, Bhanji JP. Roles of medial prefrontal cortex and orbitofrontal cortex in self-evaluation. *J Cogn Neurosci.* (2010) 22:2108–19. doi: 10.1162/jocn.2009.21359
47. Etkin A, Egner T, Kalisch R. Emotional processing in anterior cingulate and medial prefrontal cortex. *Trends Cogn Sci.* (2011) 15:85–93. doi: 10.1016/j.tics.2010.11.004
48. Libedinsky C, Smith DV, Teng CS, Namburi P, Chen VW, Huettel SA, et al. Sleep deprivation alters valuation signals in the ventromedial prefrontal cortex. *Front Behav Neurosci.* (2011) 5:70. doi: 10.3389/fnbeh.2011.00070
49. Hamilton DA, Brigman JL. Behavioral flexibility in rats and mice: contributions of distinct frontocortical regions. *Genes Brain Behav.* (2015) 14:4–21. doi: 10.1111/gbb.12191
50. Hong SB, Kim JW, Choi EJ, Kim HH, Suh JE, Kim CD, et al. Reduced orbitofrontal cortical thickness in male adolescents with internet addiction. *Behav Brain Funct.* (2013) 9:11. doi: 10.1186/1744-9081-9-11
51. Pardini M, Bonzano L, Roccatagliata L, Mancardi GL, Bove M. The fatigue-motor performance paradox in multiple sclerosis. *Sci Rep.* (2013) 3:2001. doi: 10.1038/srep02001
52. Goel N, Rao H, Durmer JS, Dinges DF. Neurocognitive consequences of sleep deprivation. *Semin Neurol.* (2009) 29:320–39. doi: 10.1055/s-0029-1237117
53. Peng DC, Dai XJ, Gong HH, Li HJ, Nie X, Zhang W. Altered intrinsic regional brain activity in male patients with severe obstructive sleep apnea: a resting-state functional magnetic resonance imaging study. *Neuropsychiatr Dis Treat* (2014) 10:1819–26. doi: 10.2147/NDT.S67805
54. Altena E, Vrenken H, Van Der Werf YD, van den Heuvel OA, Van Someren EJ. Reduced orbitofrontal and parietal gray matter in chronic

insomnia: a voxel-based morphometric study. *Biol Psychiatry* (2010) 67:182–5. doi: 10.1016/j.biopsych.2009.08.003
55. Killgore WD, Schwab ZJ, Kipman M, DelDonno SR, Weber M. Voxel-based morphometric gray matter correlates of daytime sleepiness. *Neurosci Lett.* (2012) 518:10–3. doi: 10.1016/j.neulet.2012.04.029
56. Blazhenkova O, Kozhevnikov M. The new object-spatial-verbal cognitive style model: Theory and measurement. *Appl Cogn Psychol.* (2008) 23:638–63. doi: 10.1002/acp.1473
57. Kosslyn SM, Ganis G, Thompson WL. Neural foundations of imagery. *Nat Rev Neurosci.* (2001) 2:635–42. doi: 10.1038/35090055
58. Kozhevnikov M, Kosslyn S, Shephard J. Spatial versus object visualizers: a new characterization of visual cognitive style. *Mem Cogn.* (2005) 33:710–26. doi: 10.3758/BF03195337
59. Tomasi D, Volkow ND. Association between functional connectivity hubs and brain networks. *Cerebral Cortex* (2011) 21:2003–13. doi: 10.1093/cercor/bhq268
60. Fukunaga M, Horovitz SG, van Gelderen P, de Zwart JA, Jansma JM, Ikonomidou VN, et al. Large-amplitude, spatially correlated fluctuations in BOLD fMRI signals during extended rest and early sleep stages. *Magn Reson Imaging* (2006) 24:979–92. doi: 10.1016/j.mri.2006.04.018
61. Thomas M, Sing H, Belenky G, Holcomb H, Mayberg H, Dannals R, et al. Neural basis of alertness and cognitive performance impairments during sleepiness. I. Effects of 24 h of sleep deprivation on waking human regional brain activity. *J Sleep Res.* (2000) 9:335–52. doi: 10.1046/j.1365-2869.2000.00225.x
62. Wu JC, Gillin JC, Buchsbaum MS, Hershey T, Hazlett E, Sicotte N, et al. The effect of sleep deprivation on cerebral glucose metabolic rate in normal humans assessed with positron emission tomography. *Sleep* (1991) 14:155–62.
63. Dai XJ, Peng DC, Gong HH, Wan AL, Nie X, Li HJ, et al. Altered intrinsic regional brain spontaneous activity and subjective sleep quality in patients with chronic primary insomnia: a resting-state fMRI study. *Neuropsychiatr Dis Treat.* (2014) 10:2163–75. doi: 10.2147/NDT.S69681
64. Perlis ML, Merica H, Smith MT, Giles DE. Beta EEG activity and insomnia. *Sleep Med Rev.* (2001) 5:363–74. doi: 10.1053/smrv.2001.0151
65. Desmond J, Marvel C. Cognition: cerebellum role. *Encyclopedia Neurosci.* (2009) 2:1079–85. doi: 10.1016/B978-008045046-9.00411-3
66. Parvizi J, Anderson SW, Martin CO, Damasio H, Damasio AR. Pathological laughter and crying: a link to the cerebellum. *Brain* (2001) 124:1708–19. doi: 10.1093/brain/124.9.1708
67. Yoo SS, Teh EK, Blinder RA, Jolesz FA. Modulation of cerebellar activities by acupuncture stimulation: evidence from fMRI study. *Neuroimage* (2004) 22:932–40. doi: 10.1016/j.neuroimage.2004.02.017
68. Liu ZF, Xu C, Xu Y, Wang YF, Zhao B, Lv YT, et al. Decreased regional homogeneity in insula and cerebellum: A resting-state fMRI study in patients with major depression and subjects at high risk for major depression. *Psychiat Res-Neuroim* (2010) 182:211–5. doi: 10.1016/j.pscychresns.2010.03.004
69. Soares JC, Mann JJ. The anatomy of mood disorders - Review of structural neuroimaging studies. *Biol Psychiat.* (1997) 41:86–106. doi: 10.1016/S0006-3223(96)00006-6

Conflict of Interest Statement: The authors declare that the research was conducted in the absence of any commercial or financial relationships that could be construed as a potential conflict of interest.

frontiers in Neurology

ORIGINAL RESEARCH
published: 13 June 2018
doi: 10.3389/fneur.2018.00363

Topological Reorganization of the Default Mode Network in Severe Male Obstructive Sleep Apnea

Liting Chen[1†], Xiaole Fan[2†], Haijun Li[1], Chenglong Ye[1], Honghui Yu[1], Honghan Gong[1], Xianjun Zeng[1], Dechang Peng[1] and Liping Yan[3]**

[1] Department of Radiology, The First Affiliated Hospital of Nanchang University, Nanchang, Jiangxi, China, [2] Department of General Surgery, The First Affiliated Hospital of Nanchang University, Nanchang, Jiangxi, China, [3] Department of Cardiology, People's Hospital of Jiangxi Province, Nanchang, Jiangxi, China

OPEN ACCESS

Edited by:
Xi-jian Dai,
Medical School of Nanjing University, China

Reviewed by:
Feng Liu,
Tianjin Medical University General Hospital, China
Federico Giove,
Centro Fermi – Museo storico della fisica e Centro studi e ricerche Enrico Fermi, Italy

***Correspondence:**
Dechang Peng
pengdcdoctor@163.com;
Liping Yan
824852148@qq.com

†These authors have contributed equally to this work.

Specialty section:
This article was submitted to Sleep and Chronobiology, a section of the journal Frontiers in Neurology

Received: 10 December 2017
Accepted: 04 May 2018
Published: 13 June 2018

Citation:
Chen L, Fan X, Li H, Ye C, Yu H, Gong H, Zeng X, Peng D and Yan L (2018) Topological Reorganization of the Default Mode Network in Severe Male Obstructive Sleep Apnea. Front. Neurol. 9:363. doi: 10.3389/fneur.2018.00363

Impaired spontaneous regional activity and altered topology of the brain network have been observed in obstructive sleep apnea (OSA). However, the mechanisms of disrupted functional connectivity (FC) and topological reorganization of the default mode network (DMN) in patients with OSA remain largely unknown. We explored whether the FC is altered within the DMN and examined topological changes occur in the DMN in patients with OSA using a graph theory analysis of resting-state functional magnetic resonance imaging data and evaluated the relationship between neuroimaging measures and clinical variables. Resting-state data were obtained from 46 male patients with untreated severe OSA and 46 male good sleepers (GSs). We specifically selected 20 DMN subregions to construct the DMN architecture. The disrupted FC and topological properties of the DMN in patients with OSA were characterized using graph theory. The OSA group showed significantly decreased FC of the anterior–posterior DMN and within the posterior DMN, and also showed increased FC within the DMN. The DMN exhibited small-world topology in both OSA and GS groups. Compared to GSs, patients with OSA showed a decreased clustering coefficient (C_p) and local efficiency, and decreased nodal centralities in the left posterior cingulate cortex and dorsal medial prefrontal cortex, and increased nodal centralities in the ventral medial prefrontal cortex and the right parahippocampal cortex. Finally, the abnormal DMN FC was significantly related to C_p, path length, global efficiency, and Montreal cognitive assessment score. OSA showed disrupted FC within the DMN, which may have contributed to the observed topological reorganization. These findings may provide further evidence of cognitive deficits in patients with OSA.

Keywords: obstructive sleep apnea, default mode network, cognitive function, resting-state functional magnetic resonance imaging, graph theory

INTRODUCTION

Obstructive sleep apnea (OSA) is a common sleep-disordered breathing condition characterized by repetitive cessations of breathing and/or reduced airflow due to frequent episodes of complete (apnea) or partial (hypopneas) obstruction of the upper airway during sleep. These respiratory events lead to sleep fragmentation (1), chronic intermittent hypoxemia (2), repetitive arousals, oxygen desaturation, and hypercapnic hypoxia. Moderate to severe OSA is estimated to occur in 12% of women and

up to 30% of men aged between 30 and 70 years, and these estimated prevalence rates are increasing as the population ages and due to the ongoing obesity epidemic (3). OSA is associated with an increased risk of both traffic and occupational accidents (4), decreased quality of life, and long-term health problems resulting from a number of concomitant diseases, including hypertension, cardiovascular impairment, stroke, chronic kidney disease (5), depression (6), anxiety, metabolic syndrome, insomnia, cognitive dysfunction, and even Alzheimer's disease (7). OSA is also associated with cognitive dysfunction, which is an important independent predictor of mortality, even in the absence of dementia manifestations. Cognitive deficits, including deficits in attention, memory, psychomotor function, executive functions, visuospatial function, and language ability, have been observed in patients with OSA (8, 9). Unfortunately, the neurological basis of neurocognitive dysfunction in patients with OSA has not been examined in detail.

Neuroimaging studies have been widely applied to explain these cognitive deficits and have revealed that patients with OSA show alterations in multiple brain regions, which are responsible for cognitive, affective, autonomic, and sensorimotor control (10–13). According to recent resting-state functional magnetic resonance imaging (rs-fMRI) studies, patients with OSA exhibited significant global and regional connectivity deficits, particularly in the default mode network (DMN) (14), salience network (SN), central executive network (CEN) (15).

The DMN is critical for maintaining brain function in the resting-state and experiences progressive deactivation as the brain engages in goal-directed activity. The DMN is a large-scale network that includes a set of highly interconnected brain regions, such as the posterior cingulate cortex (PCC), precuneus, medial prefrontal cortex, and the medial, lateral and inferior parietal regions, which contribute to internal mentation, attention, and adaptive functions (16). In previous studies, patients with OSA showed significant regional deficits in spontaneous activity in DMN subregions (17–19). In addition, Zhang found patients with OSA exhibited structural and functional deficits in the anterior DMN and functional compensation in the posterior DMN (20) using independent component analysis (ICA). Moreover, Li et al. observed altered functional connectivity (FC) between eight pairs of DMN subregions, which was associated with cognitive impairment (21). Patients with OSA show abnormal deactivation in the DMN during working memory tasks. The deactivation of DMN regions is significantly associated with behavioral performance and episodic memory impairments, plays a role in cognitive impairment in patients with OSA (14). However, these previous studies were limited to the spontaneous abnormalities in local brain regions and did not directly assess important topological changes in the DMN of patients with OSA.

Accumulating evidence implicates aberrant activity in the DMN in cognitive impairments and symptoms associated with neuropsychiatric disorders, such as mild cognitive impairment (22), social anxiety disorder (23), primary insomnia (24), and depression (25). Functional alterations in the DMN have been proposed as a quantitative MRI assessment that may facilitate the clinical prognosis and diagnosis (26). Previous study that utilized graph theory approaches revealed alterations in the topological properties of the gray matter volume (GMV) structural network (27) and the brain functional network (28) in individuals with OSA. However, whether the FC is altered within the subregions of the DMN and the topological changes that occur in the DMN in patients with OSA remain unclear.

Here, we hypothesized that the cognitive impairment observed in patients with OSA might be attributed to disrupted FC and the topological configuration of the DMN, and the topological reorganization may probably related to abnormal DMN FC. To test our hypothesis, we applied graph theory approaches to analyze FC and the topological organization of the DMN in male patients with untreated severe OSA and examined the relationships between neuroimaging measures and clinical index.

MATERIALS AND METHODS

Participants

Fifty male patients with newly diagnosed untreated severe OSA and 46 male education- and age-matched good sleepers (GSs) were recruited from the Sleep Monitoring Room of the Respiratory Department at the First Affiliated Hospital of Nanchang University, China, from June 2015 to February 2017. Sex differences, depression, obesity, and anxiety may affect spontaneous brain activity, and female OSA patients exhibited a lower apnea–hypopnea index (AHI), which was frequently accompanied by depression and anxiety (29–32). To improve the credibility of our study, we only recruited untreated male patients with severe OSA to rule out potential confounders of sex differences, severity of OSA, depression, and anxiety. The inclusion criteria for patients with OSA and GSs were (1) OSA: an AHI greater than or equal to 30; GSs: an AHI less than 5; (2) male sex; (3) right-handedness; and (4) aged older than 20 years but less than 60 years. The exclusion criteria for all participants were (1) a history of other sleep disorders, such as insomnia or sleep-related eating disorder; (2) identifiable focal or diffuse abnormalities in structural MR images; (3) a history of neurological or mental illnesses (e.g., head injury, depression, psychosis, neurodegenerative diseases, hypothyroidism, and epilepsy); (4) a history of addiction; (5) a history of cerebrovascular disease; and (6) MRI contraindications, such as claustrophobia, metallic implants, or devices in the body. The study protocol was approved by the Medical Research Ethics Committee and the Institutional Review Board of the First Affiliated Hospital of Nanchang University. The current study was conducted according to the principles of the Declaration of Helsinki and the approved guidelines. Written informed consent was obtained from all participants.

Overnight Polysomnography (PSG)

Prior to collecting MRI brain scans, overnight PSG was performed on all participants using the Respironics LE-Series Physiological Monitoring System (Alice5 LE, FL, USA) to confirm the OSA/GS diagnosis and to exclude other sleep disorders. On the day prior to overnight PSG, all participants were required to refrain from using hypnotics and consuming alcoholic beverages or

coffee. Overnight PSG was recorded from 10:00 p.m. to 6 a.m. A standard electroencephalogram (EEG, F4/M1, C4/M1, O2/M1, F3/M2, C3/M2, and O1/M2), chin electromyogram, electrocardiogram, electrooculogram, thoracic and abdominal respiratory movements, oral and nasal airflow, oxygen saturation (SaO2), body posture, and snoring were recorded. Studies were scored by a PSG technician and reviewed by a qualified sleep medicine physician according to the American Academy of Sleep Medicine (AASM) guidelines (33). Obstructive apnea was defined as any 10 s or longer decrease in airflow ≥90% with evidence of persistent respiratory effort. Hypopnea was defined as a reduction in airflow ≥30% lasting for more than 10 s, accompanied by 4% or greater oxygen desaturation and/or EEG arousal (33). The AHI was computed as the mean number of apnea and hypopnea events per hour during sleep. The arousal index (AI) was calculated as the average number of EEG arousals per hour of sleep.

Neuropsychological Assessments

Each participant was evaluated with the Epworth sleepiness scale (ESS) (Chinese version) for excessive daytime sleepiness, which requires the participant to rate his/her probability of falling asleep in eight different situations on a scale of increasing probability from 0 to 3. The aggregate score of the ESS is 24, with a score greater than 6 indicating sleepiness, a score greater than 11 indicating excessive sleepiness, and a score greater than 16 suggesting risky sleepiness. In addition, we used the Montreal Cognitive Assessment (MoCA, Chinese version) (34) as a rapid screening tool to assess cognitive function in all participants, including executive function, calculation, memory, attention, abstraction, language, and orientation. The total MoCA score is 30, with a score less than or equal to 26 indicating the presence of a mild cognitive impairment.

MRI Data Acquisition

All MRI data were collected on a 3.0-T MRI system (Siemens, Erlangen, Germany) by implementing an 8-channel phased-array head coil at the First Affiliated Hospital of Nanchang University, China. Comfortable fixed foam pads were used to reduce head movements and ear plugs were used to minimize scanner noise. First, each participant underwent conventional T1 and T2-weighted imaging to exclude the presence of massive brain lesions. Then, both an 8-min rs-fMRI scan with an echo planar imaging sequence [repetition time (TR) = 2,000 ms, echo time (TE) = 30 ms, field of view (FOV) = 230 mm × 230 mm, thickness = 4.0 mm, gap = 1.2 mm, flip angle = 90°, matrix = 64 × 64, slices = 30] and high-resolution three-dimensional T1-weighted structural MR images using a magnetization-prepared rapidly acquired gradient echo sequence with generalized autocalibrating partially parallel acquisition (GRAPPA) for K space fill (TR = 1,900 ms, TE = 2.26 ms, FOV = 250 mm × 250 mm, thickness = 1.0 mm, gap = 0.5 mm, flip angle = 9°, resolution matrix = 256 × 256, slices = 176) were collected. During the rs-fMRI scan, all subjects were asked to remain motionless, relax, keep their eyes closed, and avoid thinking systematically or falling asleep. After the MRI scan, the participants were asked whether they fell asleep and/or avoided thinking systematically during the entire scan.

Functional Magnetic Resonance Imaging Data Preprocessing

Image preprocessing was performed using the Data Processing & Analysis Assistant for Resting-State Brain Imaging (DPABI, Chinese Academy of Sciences, Beijing, China[1]) (35) and Statistical Parametric Mapping (SPM8),[2] which is run on the MATLAB R2012a (MathWorks, Natick, MA, USA) platform. Preprocessing included the following steps: (1) the first 10 volumes of each functional time series were discarded; (2) slice timing correction was performed for the remaining 230 volumes; (3) three-dimensional head motion correction was conducted for small head movements; (4) high-resolution T1-weighted structural images were co-registered to the mean realigned functional images for each individual, and the transformed T1 structural images were segmented into gray matter, white matter, and cerebrospinal fluid using a new segment algorithm with the diffeomorphic anatomical registration through exponentiated lie algebra (DARTEL) tool (36), the realigned functional volumes were spatially normalized to the Montreal Neurological Institute (MNI) space using the normalization parameters estimated in DARTEL, and then each voxel was re-sampled to 3 mm × 3 mm × 3 mm; (5) the images were spatially smoothed with a 6-mm full-width at half-maximum Gaussian kernel; (6) the time series were further linearly detrended, and temporal bandpass filtering (0.01–0.08 Hz) was performed to reduce the effect of physiological high-frequency noise and low-frequency drifts; and (7) to further reduce possible sources of artifacts, the nuisance signal (white matter, cerebrospinal fluid, and global signal) and the Friston 24-parameter model (37) were regressed from the time series of all voxels using multiple regression analyses. The participants were excluded if the maximum head motion of maximum rotation was more than 2.0°, the maximum orthogonal direction displacement was more than 2.0 mm, or the mean relative root mean square was greater than 0.2 mm, according to the criteria (38, 39). Four patients with OSA were excluded. Finally, 46 male patients with untreated severe OSA and 46 male age- and education-matched GSs were included in the current study.

DMN Construction and Graph Analyses

Definition of DMN Subregions

According to a previous study, we focused on the DMN and chose a specific set of 20 regions of interest (ROI) with substantial agreement with the functional and anatomic partitions of the DMN (**Table 1**) (16).

DMN Functional Connectivity and Graph Analyses

A network is composed of a set of nodes and edges between different nodes. The mean time series for each voxel within the ROI of the DMN was extracted using spherical seeds (6 mm in radius) based on the MNI coordinate system. Next, the Pearson correlation coefficients were computed between each pair of DMN subregions in each participant to generate a 20 × 20 correlation matrix of the DMN. Then, we used the graph theoretical network

[1] http://www.restfmri.net (Accessed: 2008).

[2] http://www.fil.ion.ucl.ac.uk (Accessed: 1994).

TABLE 1 | Regions of interest within the default mode network (DMN).

Regions	Abbreviation	Brodmann areas	Montreal Neurological Institute (MNI)		
			x	*y*	*z*
Anterior medial prefrontal cortex	aMPFC.L	10, 32	−6	52	−2
	aMPFC.R		6	52	−2
Posterior cingulate cortex	PCC.L	23, 31	−8	−56	26
	PCC.R		8	−56	26
Dorsal medial prefrontal cortex	dMPFC	9, 32	0	52	26
Temporal parietal junction	TPJ.L	40, 39	−54	−54	28
	TPJ.R		54	−54	28
Lateral temporal cortex	LTC.L	21, 22	−60	−24	−18
	LTC.R		60	−24	−18
Temporal pole	TempP.L	21	−50	14	−40
	TempP.R		50	14	−40
Ventral medial prefrontal cortex	Vmpfc	11, 24, 25, 32	0	26	−18
Posterior inferior parietal lobule	pIPL.L	39	−44	−74	32
	pIPL.R		44	−74	32
Retrosplenial cortex	Rsp.L	29, 30, 19	−14	−52	8
	Rsp.R		14	−52	8
Parahippocampal cortex	PHC.L	20, 36, 19	−28	−40	−12
	PHC.R		28	−40	−12
Hippocampal formation	HF.L	20, 36	−22	−20	−26
	HF.R		22	−20	−26

Coordinates are based on the MNI coordinate system, and each region of the DMN was acquired by spherical seeds with a radius of 6 mm.

analysis (GRETNA)[3] toolbox (40) to evaluate the topological organization of the DMN.

Threshold Selection

In this study, the DMN was modeled based on an undirected, binarized method. The establishment of a sparsity threshold (Sp), which is defined as the fraction of the number of existing edges divided by the maximum possible number of edges in a network, ensured that the resulting networks had the same number of edges and minimized the influence of potential confounders on the overall correlation strength between groups (41). In the present study, we computed the network properties of the DMN over a wide range of sparsity levels (from 0.05 to 0.50 using an interval of 0.01), in which the number of spurious edges was minimized and the small-world parameters could be properly estimated (42).

Network Metrics

In this study, we used the graph theory approach to calculate the global and nodal network properties of the DMN in patients with OSA and GSs. The area under the curve (AUC) of each network metric was calculated for statistical comparison, which was extracted by thresholding across a range of sparsity values to depict changes in the topological characterization of brain networks, and which is susceptible to detecting topological alterations of brain disorders (41, 43).

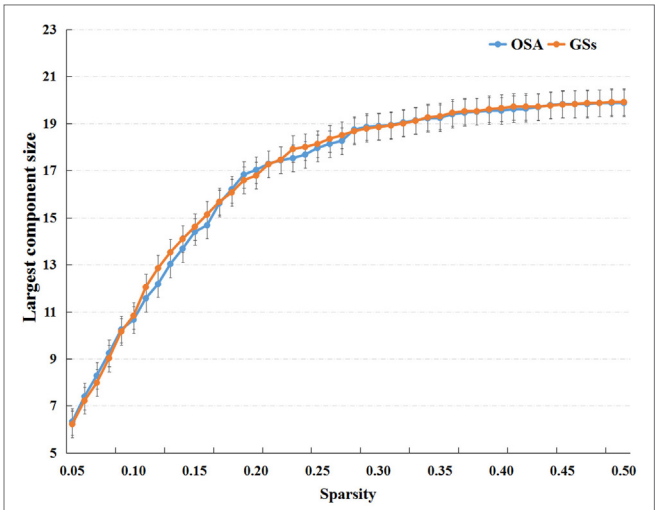

FIGURE 1 | The largest component sizes of individual networks both of the patients with obstructive sleep apnea (OSA) and good sleepers (GSs) over the sparsity range of 0.05–0.50.

Global Network Metrics

Small-World Parameters

Small-world parameters (1) small-worldness, σ, is a fascinating model for the description of complex brain networks that not only support both specialized and integrated information processing but also facilitates an energy-efficient balance between network segregation and integration. Mathematically, a real brain network is considered a small-world network if it displays a much higher clustering coefficient (C_p) and a similar characteristic path length (L_p) (compared with 1,000 matched random networks in our study) and meets the following criteria: normalized clustering coefficients $\gamma = C_{P_{real}} / C_{P_{rand}} > 1$ and normalized characteristic path length $\lambda = L_{P_{real}} / L_{P_{rand}} \approx 1$. The small-worldness, $\sigma = \gamma/\lambda$, is typically >1 for small-world networks (44, 45); (2) The clustering coefficient of node *i* (*Ci*) is defined as the percentage of the number of existing connections among the node's nearest neighbors and the maximum possible number of connections. The clustering coefficient of network C_p is the average of *Ci* across nodes, which is a measure of network segregation (44); (3) The characteristic path length, L_p, is quantified as the average of the shortest path length that links all pairs of nodes in the network, which is the most commonly used measure of network information integration (45). The characteristic path length was calculated as the "harmonic mean" distance between all possible pairs of regions to deal with the possible disconnected graphs dilemma in the present study (46). The largest component sizes of individual networks over the sparsity range of 0.05–0.50 with an interval of 0.01, see in **Figure 1**.

Network Efficiency

Network efficiency, including global efficiency, E_{glob}, which represents the capacity of parallel information transmission over

[3]http://www.nitrc.org/projects/gretna/ (Accessed: December 12, 2012).

the network, and local efficiency, E_{loc}, represents the capacity of a network to transmit information at the local level and measures the fault tolerance of the network (42).

Regional Network Metrics

The degree for a brain region is defined as the number of edges of a node that connect with the remaining nodes in the network, thus measuring how interactive a particular node is in the network. The nodal betweenness is designated as the fraction of shortest paths between two nodes passing through the area in the network and measures the influence of a region on network communication. Nodal efficiency is defined as the inverse of the harmonic mean of the shortest path length in the network, quantifying the importance of the nodes for communication within the network (42).

Statistical Analysis

Demographic and clinical characteristics of the OSA and GS groups were compared using independent two-sample *t*-tests with IBM Statistical Package for the Social Sciences 20.0 software (IBM SPSS Inc., Chicago, IL, USA). Independent two-sample *t*-tests were performed to compare group differences in the AUC of global network metrics and ROI-ROI FC of the DMN. We also compared nodal properties between patients with OSA and GSs and Bonferroni correction was performed for multiple comparison. The effects of age, body mass index (BMI), and educational level were diminished by a regression analysis. Abnormal DMN FC was calculated as the average of the correlation coefficients of the DMN in patients with OSA that showed significant between-group differences. The relationships between abnormal DMN FC and topological metrics of the DMN, and the relationships between network metrics with significant between-group differences and clinical indices in the OSA group were investigated using a Pearson correlation analysis. $p < 0.05$ was considered statistically significant.

RESULTS

Demographic and Clinical Data

As shown in **Table 2**, significant inter-group differences were observed in BMI, AHI, total sleep time, Stage 1, rapid eye movement (REM), AI, $SaO_2 < 90\%$, average SaO2, oxygen desaturation index, nadir SaO2, MoCA score, visuospatial/executive, delayed memory, attention, abstraction, orientation and ESS score ($p < 0.05$). No inter-group differences in Stage 2 or Stages 3 + 4 were observed ($p > 0.05$).

TABLE 2 | Comparison of the demographic and clinical data from the patients with OSA and GSs.

Characteristics	Patients with OSA (*N* = 46)	GSs (*N* = 46)	*t*-Value	*p*-Value
BMI, kg/m^2	27.52 ± 3.30	23.09 ± 1.96	7.827	<0.001*
AHI/h	58.26 ± 20.37	2.51 ± 1.21	18.529	<0.001*
Total sleep time, min	372.26 ± 83.88	398.30 ± 18.94	−2.054	0.043*
Stage 1, %	31.28 ± 17.38	10.22 ± 3.72	8.037	<0.001*
Stage 2, %	39.12 ± 14.78	40.74 ± 7.05	−0.672	0.504
Stages 3 + 4, %	22.49 ± 18.21	21.15 ± 4.54	0.483	0.630
REM, %	7.29 ± 7.96	21.89 ± 7.48	−9.070	<0.001*
Arousal index/h	40.36 ± 23.63	11.93 ± 2.79	8.102	<0.001*
$SaO_2 < 90$, %	31.15 ± 21.34	0.27 ± 0.17	9.813	<0.001*
Average SaO_2, %	90.69 ± 4.46	95.59 ± 2.41	−6.547	<0.001*
Oxygen desaturation index	54.42 ± 25.51	2.84 ± 1.4	14.897	<0.001*
Nadir SaO_2, %	66.26 ± 12.46	90.33 ± 2.88	−12.765	<0.001*
MoCA score	25.17 ± 2.11	27.74 ± 1.39	−6.883	<0.001*
Visuospatial/ executive	4.07 ± 0.83	4.67 ± 0.63	−3.960	<0.001*
Delayed memory	3.20 ± 1.17	4.85 ± 0.36	−9.172	<0.001*
Attention	5.33 ± 0.99	5.83 ± 0.38	−3.194	0.002*
Language	2.04 ± 0.56	2.83 ± 0.38	−7.860	<0.001*
Abstraction	1.50 ± 0.51	1.85 ± 0.36	−3.790	<0.001*
Orientation	5.72 ± 0.66	5.93 ± 0.25	−2.102	0.038*
ESS score	12.11 ± 3.84	3.39 ± 2.18	13.405	<0.001*

Data are presented as the mean ± SD.
OSA, obstructive sleep apnea; GSs, good sleepers; BMI, body mass index; AHI, apnea–hypopnea index; REM, rapid eye movement; $SaO_2 < 90\%$, percentage of total sleep time spent at an oxygen saturation less than 90%; MoCA, Montreal cognitive assessment; ESS, Epworth sleepiness scale; N, number.
**p < 0.05, which was considered statistically significant.*

Changes in FC Within the DMN Between Patients With OSA and GSs

Compared to GSs, patients with OSA exhibited significantly decreased FC between the bilateral PCC and the bilateral hippocampal formation (HF) and left retrosplenial cortex (Rsp), between the left temporal pole (TempP) and the dorsal medial prefrontal cortex (dMPFC) and left temporal parietal junction (TPJ), between the left Rsp and the bilateral anterior medial prefrontal cortex (aMPFC) and the left posterior inferior parietal lobule (pIPL), between the bilateral HF and the bilateral Rsp, and between the right HF and the right TPJ and the right pIPL. Patients with OSA displayed significantly increased FC in the DMN between the right TempP and the right parahippocampal cortex (PHC) and between the right and left HF, compared to GSs (**Figure 2**; **Table 3**). The abnormal DMN FC was positively correlated with C_p ($r = 0.384$, $p = 0.008$) and L_p ($r = 0.338$, $p = 0.022$), and negatively correlated with E_{glob} ($r = -0.565$, $p < 0.001$) in patients with OSA (see **Figure 3**).

Differences in Global Network Measures of the DMN

In the defined wide range of thresholds (here from 0.05 to 0.50), both the patients with OSA and GSs exhibited σ value larger than 1, γ value obviously larger than 1, and λ value of approximately equal to 1 (see **Figure 4**), suggesting that both patients with OSA and GSs have typical small-world topology. However, compared to GSs, patients with OSA showed a significantly decreased C_p ($t = -2.200$, $p = 0.030$) and a decreased E_{loc} ($t = -1.942$, $p = 0.054$), which have a trend for difference. There was no significant difference in σ ($t = 0.412$, $p = 0.483$), L_p ($t = -0.004$, $p = 0.997$) or E_{glob} ($t = -0.035$, $p = 0.972$). Global network measures are illustrated in **Figure 5**.

Group Differences in Regional Network Measures of the DMN

Patients with OSA showed abnormal nodal centrality, which showed significant between-group differences in at least one

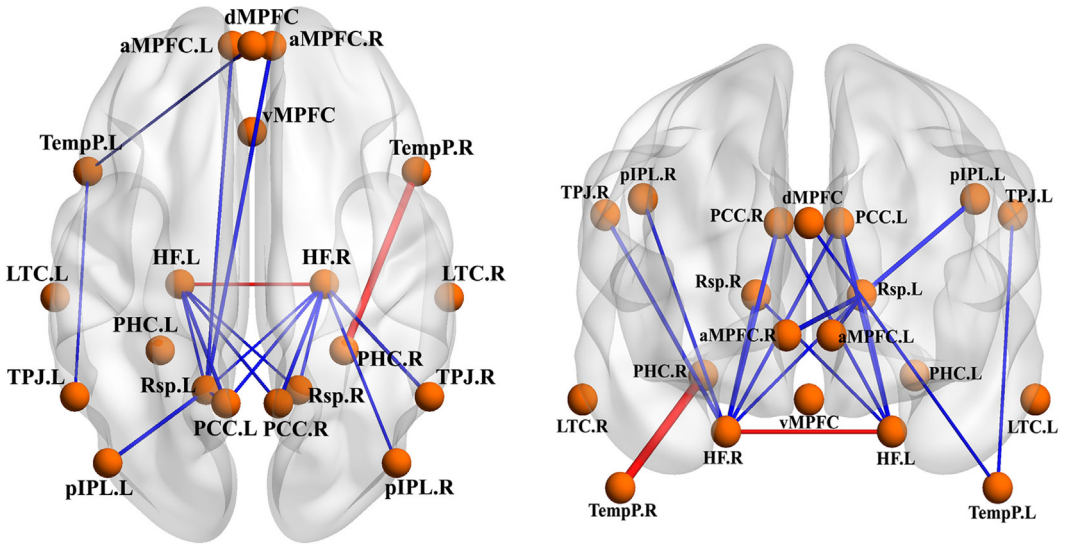

FIGURE 2 | Abnormal functional connectivity (FC) within the default mode network (DMN) between patients with obstructive sleep apnea (OSA) and good sleepers (GSs). The blue edges represent decreased FC in patients with OSA compared to GSs and the red edges represent increased FC within the DMN. Undirected edges correspond to *t*-values, with a larger *t*-value corresponding to a thicker edge ($p < 0.05$, uncorrected).

TABLE 3 | Abnormal functional connectivity (FC) within the default mode network (DMN) between patients with obstructive sleep apnea (OSA) and good sleepers (GSs).

Brain region 1	Brain region 2	*t*-Value	*p*-Value
PCC.L	Rsp.L	−2.490	0.015
PCC.L	HF.L	−2.948	0.004
PCC.L	HF.R	−2.479	0.015
PCC.R	HF.L	−2.412	0.018
PCC.R	HF.R	−2.940	0.004
TempP.L	dMPFC	−2.146	0.035
TempP.L	TPJ.L	−2.137	0.035
TempP.R	PHC.R	2.100	0.039
Rsp.L	aMPFC.L	−2.555	0.012
Rsp.L	aMPFC.R	−3.086	0.003
Rsp.L	pIPL.L	−3.045	0.003
HF.L	Rsp.L	−2.257	0.026
HF.L	Rsp.R	−2.050	0.043
HF.L	HF.R	2.557	0.012
HF.R	TPJ.R	−2.791	0.006
HF.R	pIPL.R	−2.417	0.018
HF.R	Rsp.L	−2.096	0.039
HF.R	Rsp.R	−2.555	0.012

Abnormal FC within the DMN between patients with OSA and GSs ($p < 0.05$, uncorrected).
L, left; R, right; PCC, posterior cingulate cortex; Rsp, retrosplenial cortex; HF, hippocampal formation; TempP, temporal pole; dMPFC, dorsal medial prefrontal cortex; TPJ, temporal parietal junction; PHC, parahippocampal cortex; aMPFC, anterior medial prefrontal cortex; pIPL, posterior inferior parietal lobule.

nodal metric, including nodal betweenness, nodal efficiency, and nodal degree. Compared with the GSs, patients with OSA showed decreased nodal centralities in the left PCC and dMPFC, and increased nodal centralities in the vMPFC and the right PHC ($p < 0.05$, uncorrected). Regional network measures are illustrated in **Table 4**.

Correlations Between Network Measures With Group Differences and Clinical Variables

Within the OSA group, the abnormal DMN FC was negatively correlated with the MoCA score ($r = -0.366$, $p = 0.012$). C_p was negatively correlated with the MoCA score ($r = -0.332$, $p = 0.024$) and delayed memory ($r = -0.306$, $p = 0.039$). The nodal degree of the left PCC was positively correlated with the nadir SaO_2 ($r = 0.317$, $p = 0.032$), and nodal betweenness of the right PHC was positively correlated with the MoCA score ($r = 0.309$, $p = 0.037$). The nodal betweenness ($r = 0.297$, $p = 0.045$), degree ($r = 0.358$, $p = 0.015$), and efficiency ($r = 0.334$, $p = 0.023$) of the right PHC were positively correlated with delayed memory (see **Figure 6**).

DISCUSSION

The present study applied graph theory approaches to provide evidence that the cognitive impairments observed in patients with OSA might be attributed to the topological configuration of the DMN, which probably resulted from the abnormal DMN FC. Although the DMN of patients with OSA exhibited small-world properties, patients with OSA showed decreased C_p and E_{loc}, abnormal nodal centralities in the DMN, and abnormal FC within the DMN, implying a disturbance in the functional differentiation of the DMN. In addition, the abnormal DMN FC was related to C_p, L_p, E_{glob}, and the MoCA score. The disrupted topological properties of the DMN significantly influenced cognitive function, including delayed memory and memory extraction in patients with OSA.

Abnormal FC Within the DMN in Patients With OSA

The current study revealed significantly decreased FC in the anterior–posterior DMN involving the prefrontal, parietal and

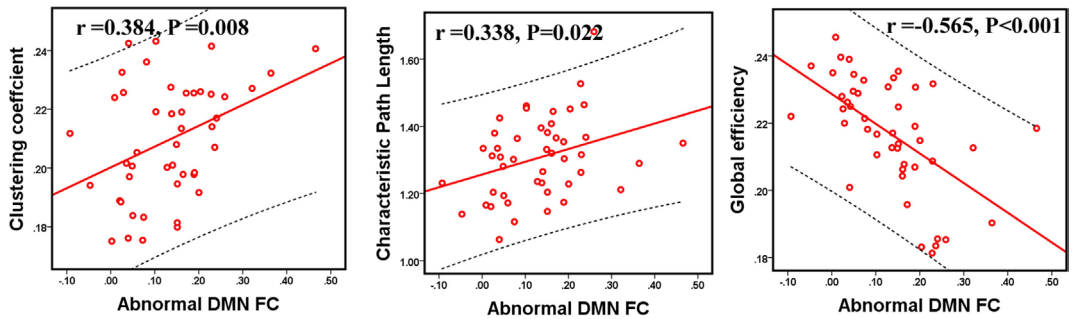

FIGURE 3 | The relationship between abnormal functional connectivity (FC) and topological metrics of the default mode network (DMN) in patients with obstructive sleep apnea (OSA). The abnormal DMN FC value was significantly correlated with C_p, L_p, and E_{glob} in patients with OSA. $p < 0.05$, which was considered statistically significant.

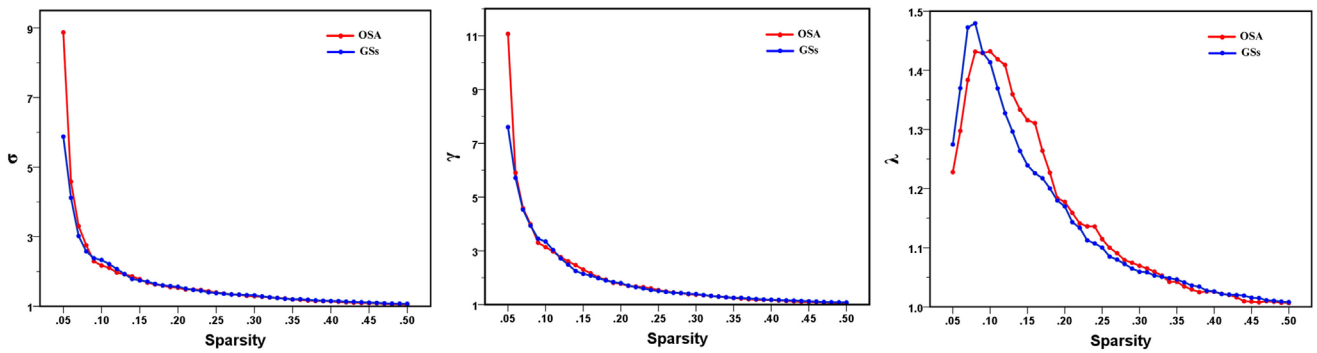

FIGURE 4 | Small-world parameters of default mode network in patients with obstructive sleep apnea (OSA) and good sleepers (GSs). Graphs show that in the defined wide range of thresholds, both the patients with OSA and GSs exhibited normalized clustering coefficient (γ) obviously larger than 1, normalized path lengths (λ) approximately equal to 1, and small-worldness (σ) larger than 1, suggesting that both OSA patients and GSs show typical small-world topology.

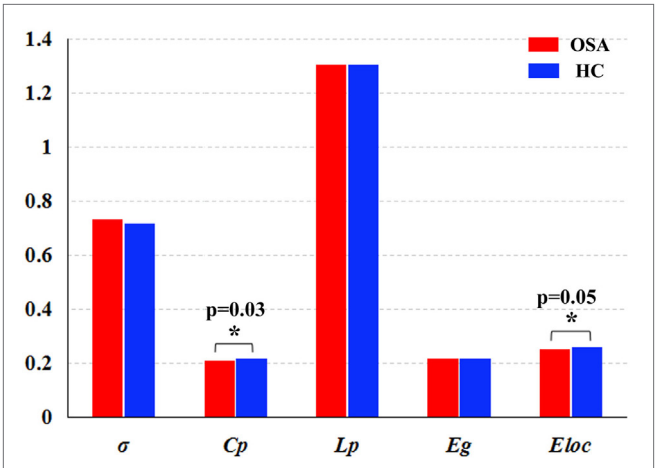

FIGURE 5 | Graphs showing the small-world parameters and network efficiency of the default mode network in patients with obstructive sleep apnea (OSA) and good sleepers (GSs). Although OSA and GSs have typical small-world topology, compared to GSs, patients with OSA showed a significantly decreased C_p ($t = -2.200$, $p = 0.030$) ($p < 0.05$, uncorrected), and a decreased E_{loc} ($t = -1.943$, $p = 0.054$), which have a trend for difference.

TABLE 4 | Between-group differences in regional network measures of the default mode network (DMN) in patients with obstructive sleep apnea (OSA) and good sleepers.

DMN region	Nodal betweenness		Nodal degree		Nodal efficiency	
	t-Value	*p*-Value	*t*-Value	*p*-Value	*t*-Value	*p*-Value
PCC.L	−4.427	**<0.001***	−2.883	**0.005#**	−3.552	**0.001***
dMPFC	−1.989	**0.049#**	−1.375	0.172	−1.324	0.189
vMPFC	2.475	**0.015#**	1.172	0.244	0.403	0.688
PHC.R	2.017	**0.047#**	2.833	**0.006#**	2.074	**0.041#**

Patients with OSA showed abnormal nodal centrality in PCC.L, dMPFC, vMPFC, and PHC.R, which showed significant between-group differences in at least one of the three nodal metrics.

#p < 0.05, uncorrected.

**Bonferroni correction p = 0.05.*

PCC.L, left posterior cingulate cortex; dMPFC, dorsal medial prefrontal cortex; vMPFC, ventral medial prefrontal cortex; PHC.R, right parahippocampal cortex.

temporal regions in patients with OSA. Zhang et al. (20) found that patients with OSA exhibited decreased FC in the anterior DMN and a compensatory increased FC in the posterior DMN. Decreased FC in the anterior–posterior DMN indicated that the

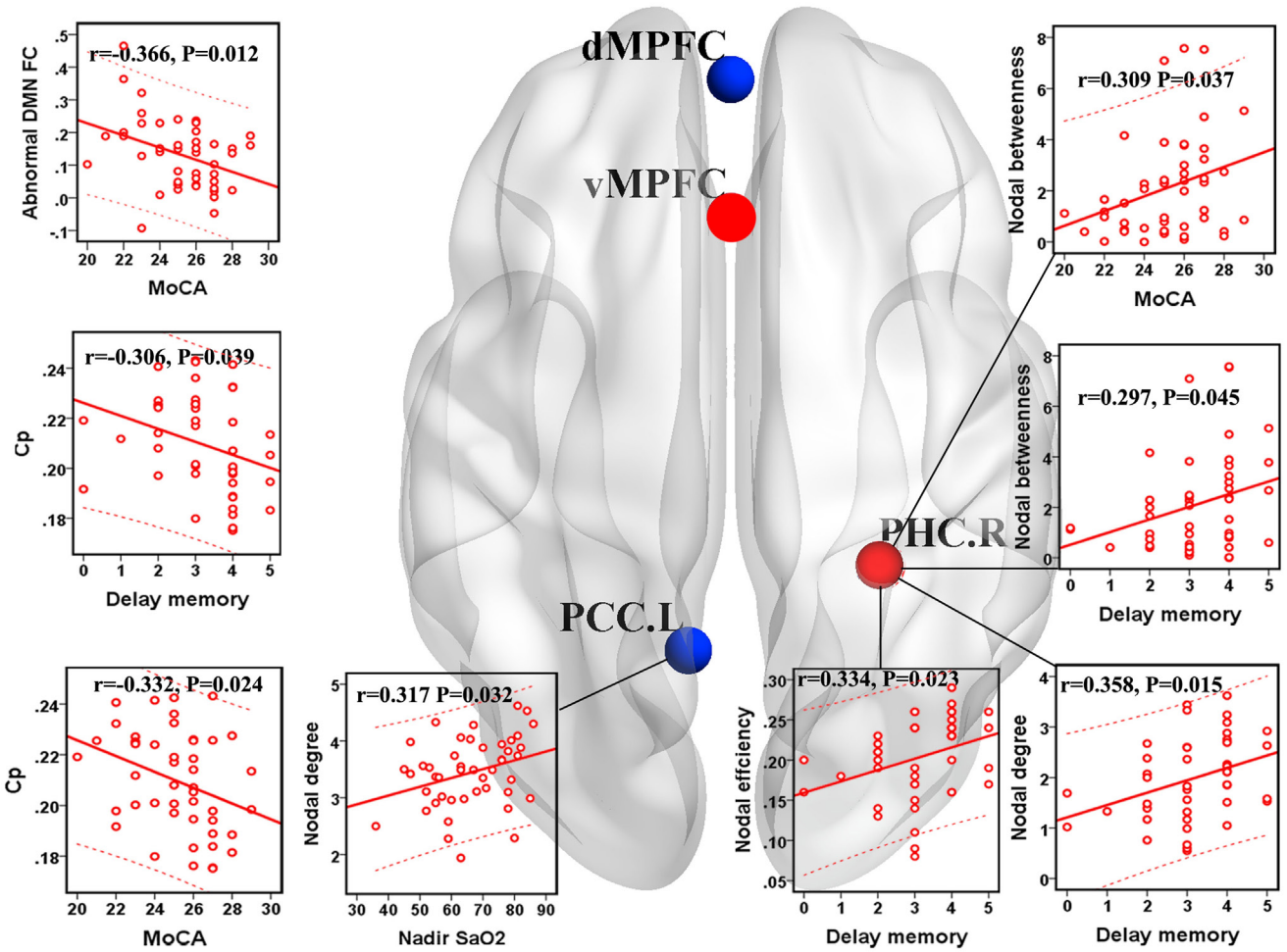

FIGURE 6 | Correlations between network measures with group differences and clinical variables in patients with obstructive sleep apnea (OSA). Scatter plot showed the relationship between the aberrant network attribute parameters and clinical index in patients with OSA. The red ball represents the increased nodal centrality and the blue ball represents the decreased nodal centrality. E_{loc}, local efficiency; C_p, clustering coefficient; PCC.L, left posterior cingulate cortex; PHC.R, right parahippocampal cortex.

transmission of information and integration of long-distance connectivity between different regions may be damaged in patients with OSA.

We also observed significantly decreased FC in the posterior DMN, which includes the PCC, HF, temporal, and parietal lobes and the limbic system. E_{loc} predominantly reflects short-distance connections between neighboring regions (45). Decreased short-distance connections that are primarily located in the posterior DMN may lead to decreased C_p and decreased E_{loc} of the DMN in patients with OSA. The PCC and HF are connected anatomically and functionally, and these functional interactions are presumed to underlie normal episodic memory capacity (47). Patients with OSA showed decreased FC between the right HF and the PCC, which is related to delayed memory (21). Based on the results, the OSA group showed decreased FC between the bilateral PCC and the bilateral HF, consistent with previous studies (21). Decreased FC in the anterior–posterior DMN and posterior DMN may further indicate cognitive impairments in patients with OSA (48).

Park observed abnormal FC in various brain regions, and altered FC subsequently resulted in disrupted topological properties in patients with OSA, particularly in the integrative aspects of brain network organization (49). Given the significant association between abnormal DMN FC and C_p, L_p, and E_{glob} of the DMN in the current study, we believe that disrupted FC within the DMN may contribute to the topological reconfiguration of the DMN in patients with OSA. Furthermore, abnormal DMN FC was associated with the MoCA score. Therefore, the abnormal DMN FC may partially explain the impaired cognitive function and topological reconfiguration in patients with OSA.

Global Network Measures of the DMN

Patients with OSA have recently been shown to display an abnormal small-world organization in both functional (28, 49) and structural (27) brain networks. In the present study, both patients with OSA and GSs showed efficient economic small-world organization in the DMN. Although the DMN has

small-world properties, our results identified decreased C_p and E_{loc} of the DMN in patients with OSA. Thus, individuals with OSA likely have sparse connectivity and disconnections between adjacent brain regions in the DMN, resulting in decreased C_p and E_{loc}. C_p is a metric that quantifies the strength of network segregation (50). The present results indicate a decline in functional differentiation in the DMN, suggesting that highly local specialization and the integrity of the DMN may be impaired in patients with OSA. E_{loc} essentially reflects the fault tolerance of the network and the capacity for transmitting information over local networks (45). Our finding of a decreased E_{loc} suggests disrupted DMN architecture in patients with OSA that is characterized by higher vulnerability and a decreased capacity for regional information processing. Moreover, C_p was negatively correlated with the MoCA score and delayed memory, further illustrating that disrupted global topology of the DMN influence cognitive impairments in patients with OSA, including delayed memory and memory extraction.

Regional Network Measures

Nodal betweenness centrality, nodal efficiency, and nodal degree were combined to compare the regional topological organization between patients with OSA and GSs in our study. Deceased nodal centrality was identified in the PCC and dMPFC. The PCC has strong reciprocal connections with other structures involved in cognitive function (51), the collection and evaluation of information, attention processing, personal significance, and evoked emotion (16). Previous structural neuroimaging studies have observed decreased GMV (52) and white matter integrity (53) in the PCC in patients with OSA. Furthermore, patients with OSA show decreased brain activation, decreased degree centrality, and FC alterations in the PCC (17, 18, 20, 21, 54). DMN dysfunction is associated with impairments in cognitive performance (55, 56). Intermittent hypoxia is a major factor in DMN dysfunction in patients with OSA (14, 21). We also observed a positive correlation between the nodal degree of the left PCC and nadir SaO2, suggesting that the functional damage of the PCC was related to intermittent hypoxia, which may be a major factor involved in DMN dysfunction and may further explain cognitive dysfunction in patients with OSA.

The dMPFC subsystem includes the dMPFC, temporal parietal junction, lateral temporal cortex, and TempP, which are involved in social cognition, metacognition, and mental state inference (16). Patients with OSA displayed decreased FC and reduced GMV in the MPFC of the anterior DMN, indicating structural and functional deficits (20). The OSA group showed decreased nodal centrality of the dMPFC, but a compensatory increase in nodal centrality of the ventral medial prefrontal cortex in the present study, which may also confirm the deficiency in the dMPFC subsystem of the DMN in patients with OSA.

The PHC plays an important role in episodic memory, autobiographical memory and episodic simulation, spatial memory, scene perception, and spatial navigation (47). Previous voxel-based morphometry studies revealed that atrophy (57) and regional cerebral blood flow were significantly reduced in the bilateral PHC (58), which may be related to cognitive impairments in patients with OSA. Nevertheless, we found a compensatory increase in nodal centrality in the right PHC, which was positively correlated with delayed memory, may partially explain the deficits in memory, spatial learning, memory extraction and attention in patients with OSA.

Limitations

Several limitations in this study should be addressed. First, we only revealed the small-world properties of the DMN, but patients with OSA exhibited disruptions in the DMN, as well as the SN and CEN (15). Therefore, further investigations of other specific brain networks are necessary. Second, we only specifically selected 20 nodes of the DMN (16) and characterized the DMN using an unbiased seed-based FC approach. More nodes of the DMN should be used to construct the DMN and the present findings should be validated by ICA. Third, the global network measures, nodal centrality, and ROI-ROI FC results were not corrected by multiple comparisons, meaning that this study should be considered an exploratory analysis. In addition, a more detailed neuropsychological assessment questionnaire must be used to obtain more interesting data.

CONCLUSION

In the current GRAPPA study, patients with OSA showed disrupted FC and topological reorganization of the DMN. Abnormal DMN FC may contribute to the topological configuration of the DMN and cognitive impairment in patients with OSA. These results provide important insights into the neurobiological mechanisms of both disrupted FC and disrupted network properties of the DMN, which may partially account for the impaired cognitive function in patients with OSA.

ETHICS STATEMENT

The study protocol was approved by the Medical Research Ethics Committee and the Institutional Review Board of the First Affiliated Hospital of Nanchang University. The current study was conducted according to the principles of the Declaration of Helsinki and the approved guidelines. Written informed consent was obtained from all participants.

AUTHOR CONTRIBUTIONS

All authors listed have made a substantial, direct, and intellectual contribution to the work and approved it for publication.

FUNDING

This work was supported by grants from the Natural Science Foundation of China (Grant No. 81560285), the Graduate Innovation Foundation of Jiangxi, China (Grant No. YC2016-S100), the Natural Science Foundation of Jiangxi, China (Grant No. 20171BAB205070, 20132BAB205100), the Education Department Foundation of Jiangxi, China (Grant No. 700544006), the Science and Technology Support Program of Jiangxi, China (Grant No. 20132BBG70061, 20141BBG70026) and the Doctoral Project Startup Fund (Grant No. 700544005).

REFERENCES

1. Ferri R, Drago V, Aricò D, Bruni O, Remington RW, Stamatakis K, et al. The effects of experimental sleep fragmentation on cognitive processing. *Sleep Med* (2010) 11:378–85. doi:10.1016/j.sleep.2010.01.006
2. Lim DC, Pack AI. Obstructive sleep apnea and cognitive impairment: addressing the blood-brain barrier. *Sleep Med Rev* (2014) 18:35–48. doi:10.1016/j.smrv.2012.12.003
3. Peppard PE, Young T, Barnet JH, Palta M, Hagen EW, Hla KM. Increased prevalence of sleep-disordered breathing in adults. *Am J Epidemiol* (2013) 177:1006. doi:10.1093/aje/kws342
4. Strohl KP, Brown DB, Collop N, George C, Grunstein R, Han F, et al. An official American Thoracic Society clinical practice guideline: sleep apnea, sleepiness, and driving risk in noncommercial drivers. An update of a 1994 statement. *Am J Respir Crit Care Med* (2013) 187:1259. doi:10.1164/rccm.201304-0726ST
5. Yayan J, Rasche K, Vlachou A. Obstructive sleep apnea and chronic kidney disease. *Adv Exp Med Biol* (2017) 1022:11–8. doi:10.1007/5584_2017_35
6. Kerner NA, Roose SP. Obstructive sleep apnea is linked to depression and cognitive impairment: evidence and potential mechanisms. *Am J Geriatr Psychiatry* (2016) 24:496–508. doi:10.1016/j.jagp.2016.01.134
7. Daulatzai MA. Evidence of neurodegeneration in obstructive sleep apnea: relationship between obstructive sleep apnea and cognitive dysfunction in the elderly. *J Neurosci Res* (2015) 93:1778–94. doi:10.1002/jnr.23634
8. Bucks RS, Olaithe M, Eastwood P. Neurocognitive function in obstructive sleep apnoea: a meta-review. *Respirology* (2013) 18:61–70. doi:10.1111/j.1440-1843.2012.02255.x
9. Olaithe M, Bucks RS, Hillman DR, Eastwood PR. Cognitive deficits in obstructive sleep apnea: insights from a meta-review and comparison with deficits observed in COPD, insomnia, and sleep deprivation. *Sleep Med Rev* (2017) 38:39–49. doi:10.1016/j.smrv.2017.03.005
10. Morrell MJ, Jackson ML, Twigg GL, Ghiassi R, Mcrobbie DW, Quest RA, et al. Changes in brain morphology in patients with obstructive sleep apnoea. *Thorax* (2010) 65:908–14. doi:10.1136/thx.2009.126730
11. Torelli F, Moscufo N, Garreffa G, Placidi F, Romigi A, Zannino S, et al. Cognitive profile and brain morphological changes in obstructive sleep apnea. *Neuroimage* (2011) 54:787–93. doi:10.1016/j.neuroimage.2010.09.065
12. Kumar R, Chavez AS, Macey PM, Woo MA, Yango FL, Harper RM. Altered global and regional brain mean diffusivity in patients with obstructive sleep apnea. *J Neurosci Res* (2012) 90:2043. doi:10.1002/jnr.23083
13. Nie S, Peng D, Gong H, Li H, Chen L, Ye C. Resting cerebral blood flow alteration in severe obstructive sleep apnoea: an arterial spin labelling perfusion fMRI study. *Sleep Breath* (2017) 21:487–95. doi:10.1007/s11325-017-1474-9
14. Prilipko O, Huynh N, Schwartz S, Tantrakul V, Kim JH, Peralta AR, et al. Task positive and default mode networks during a parametric working memory task in obstructive sleep apnea patients and healthy controls. *Sleep* (2011) 34:293A–301A. doi:10.1093/sleep/34.3.293
15. Khazaie H, Veronese M, Noori K, Emamian F, Zarei M, Ashkan K, et al. Functional reorganization in obstructive sleep apnoea and insomnia: a systematic review of the resting-state fMRI. *Neurosci Biobehav Rev* (2017) 77:219–31. doi:10.1016/j.neubiorev.2017.03.013
16. Andrews-Hanna JR, Reidler JS, Sepulcre J, Poulin R, Buckner RL. Functional-anatomic fractionation of the brain's default network. *Neuron* (2010) 65:550–62. doi:10.1016/j.neuron.2010.02.005
17. Santarnecchi E, Sicilia I, Richiardi J, Vatti G, Polizzotto NR, Marino D, et al. Altered cortical and subcortical local coherence in obstructive sleep apnea: a functional magnetic resonance imaging study. *J Sleep Res* (2013) 22:337–47. doi:10.1111/jsr.12006
18. Peng D, Dai X, Gong H, Li H, Nie X, Zhang W. Altered intrinsic regional brain activity in male patients with severe obstructive sleep apnea: a resting-state functional magnetic resonance imaging study. *Neuropsychiatr Dis Treat* (2014) 10:1819. doi:10.2147/NDT.S67805
19. Li HJ, Dai XJ, Gong HH, Nie X, Zhang W, Peng DC. Aberrant spontaneous low-frequency brain activity in male patients with severe obstructive sleep apnea revealed by resting-state functional MRI. *Neuropsychiatr Dis Treat* (2015) 11:207–14. doi:10.2147/NDT.S73730
20. Zhang Q, Wang D, Qin W, Li Q, Chen B, Zhang Y, et al. Altered resting-state brain activity in obstructive sleep apnea. *Sleep* (2013) 36:651. doi:10.5665/sleep.2620
21. Li HJ, Nie X, Gong HH, Zhang W, Nie S, Peng DC. Abnormal resting-state functional connectivity within the default mode network subregions in male patients with obstructive sleep apnea. *Neuropsychiatr Dis Treat* (2016) 12:203–12. doi:10.2147/NDT.S97449
22. Wang L, Li H, Liang Y, Zhang J, Li X, Shu N, et al. Amnestic mild cognitive impairment: topological reorganization of the default-mode network. *Radiology* (2013) 268:501–14. doi:10.1148/radiol.13121573
23. Liu F, Guo W, Fouche JP, Wang Y, Wang W, Ding J, et al. Multivariate classification of social anxiety disorder using whole brain functional connectivity. *Brain Struct Funct* (2015) 220:101–15. doi:10.1007/s00429-013-0641-4
24. Liu X, Zheng J, Liu B, Dai X. Altered connection properties of important network hubs may be neural risk factors for individuals with primary insomnia. *Sci Rep* (2018) 8:5891. doi:10.1038/s41598-018-23699-3
25. Yin Y, Wang Z, Zhang Z, Yuan Y. Aberrant topographical organization of the default mode network underlying the cognitive impairment of remitted late-onset depression. *Neurosci Lett* (2016) 629:26–32. doi:10.1016/j.neulet.2016.06.048
26. Ewers M, Sperling RA, Klunk WE, Weiner MW, Hampel H. Neuroimaging markers for the prediction and early diagnosis of Alzheimer's disease dementia. *Trends Neurosci* (2011) 34:430. doi:10.1016/j.tins.2011.05.005
27. Luo Y, Wang D, Liu K, Weng J, Guan Y, Chan KCC, et al. Brain structure network analysis in patients with obstructive sleep apnea. *PLoS One* (2015) 10:e0139055. doi:10.1371/journal.pone.0139055
28. Chen L, Fan X, Li H, Nie S, Gong H, Zhang W, et al. Disrupted small-world brain functional network topology in male patients with severe obstructive sleep apnea revealed by resting-state fMRI. *Neuropsychiatr Dis Treat* (2017) 13:1471–82. doi:10.2147/NDT.S135426
29. Macey PM, Woo MA, Kumar R, Cross RL, Harper RM. Relationship between obstructive sleep apnea severity and sleep, depression and anxiety symptoms in newly-diagnosed patients. *PLoS One* (2010) 5:e10211. doi:10.1371/journal.pone.0010211
30. Dai XJ, Gong HH, Wang YX, Zhou FQ, Min YJ, Zhao F, et al. Gender differences in brain regional homogeneity of healthy subjects after normal sleep and after sleep deprivation: a resting-state fMRI study. *Sleep Med* (2012) 13:720–7. doi:10.1016/j.sleep.2011.09.019
31. Oathes DJ, Patenaude B, Schatzberg AF, Etkin A. Neurobiological signatures of anxiety and depression in resting-state fMRI. *Biol Psychiatry* (2015) 77:385–93. doi:10.1016/j.biopsych.2014.08.006
32. Dai X, Nie X, Liu X, Pei L, Jiang J, Peng D, et al. Gender differences in regional brain activity in patients with chronic primary insomnia: evidence from a resting-state fMRI study. *J Clin Sleep Med* (2016) 12:363–74. doi:10.5664/jcsm.5586
33. Berry RB, Budhiraja R, Gottlieb DJ, Gozal D, Iber C, Kapur VK, et al. Rules for scoring respiratory events in sleep: update of the 2007 AASM manual for the scoring of sleep and associated events. Deliberations of the sleep apnea definitions task force of the American Academy of Sleep Medicine. *J Clin Sleep Med* (2012) 8:597–619. doi:10.5664/jcsm.2172
34. Chen KL, Xu Y, Chu AQ, Ding D, Liang XN, Nasreddine ZS, et al. Validation of the Chinese version of Montreal cognitive assessment basic for screening mild cognitive impairment. *J Am Geriatr Soc* (2016) 64:285–90. doi:10.1111/jgs.14530
35. Yan C, Wang X, Zuo X, Zang Y. DPABI: data processing & analysis for (resting-state) brain imaging. *Neuroinformatics* (2016) 14:339–51. doi:10.1007/s12021-016-9299-4
36. Goto M, Abe O, Aoki S, Hayashi N, Miyati T, Takao H, et al. Diffeomorphic anatomical registration through exponentiated lie algebra provides reduced effect of scanner for cortex volumetry with atlas-based method in healthy subjects. *Neuroradiology* (2013) 55:869. doi:10.1007/s00234-013-1193-2
37. Friston KJ, Williams S, Howard R, Frackowiak RS, Turner R. Movement-related effects in fMRI time-series. *Magn Reson Med* (1996) 35:346. doi:10.1002/mrm.1910350312
38. Van Dijk KR, Sabuncu MR, Buckner RL. The influence of head motion on intrinsic functional connectivity MRI. *Neuroimage* (2012) 59:431–8. doi:10.1016/j.neuroimage.2011.07.044

39. Yan CG, Craddock RC, Zuo XN, Zang YF, Milham MP. Standardizing the intrinsic brain: towards robust measurement of inter-individual variation in 1000 functional connectomes. *Neuroimage* (2013) 80:246–62. doi:10.1016/j.neuroimage.2013.04.081
40. Wang J, Wang X, Xia M, Liao X, Evans A, He Y. GRETNA: a graph theoretical network analysis toolbox for imaging connectomics. *Front Hum Neurosci* (2015) 9:386. doi:10.3389/fnhum.2015.00386
41. Zhang J, Wang J, Wu Q, Kuang W, Huang X, He Y, et al. Disrupted brain connectivity networks in drug-naive, first-episode major depressive disorder. *Biol Psychiatry* (2011) 70:334–42. doi:10.1016/j.biopsych.2011.05.018
42. Achard S, Bullmore E. Efficiency and cost of economical brain functional networks. *PLoS Comput Biol* (2007) 3:e17. doi:10.1371/journal.pcbi.0030017
43. Liu F, Zhuo C, Yu C. Altered cerebral blood flow covariance network in schizophrenia. *Front Neurosci* (2016) 10:308. doi:10.3389/fnins.2016.00308
44. Watts DJ, Strogatz SH. Collective dynamics of 'small-world' networks. *Nature* (1998) 393:440–2. doi:10.1038/30918
45. Rubinov M, Sporns O. Complex network measures of brain connectivity: uses and interpretations. *Neuroimage* (2010) 52:1059–69. doi:10.1016/j.neuroimage.2009.10.003
46. Newman MEJ. Mixing patterns in networks. *Phys Rev E Stat Nonlin Soft Matter Phys* (2003) 67:026126. doi:10.1103/PhysRevE.67.026126
47. Ranganath C, Ritchey M. Two cortical systems for memory-guided behaviour. *Nat Rev Neurosci* (2012) 13:713. doi:10.1038/nrn3338
48. Zhang Q, Qin W, He X, Li Q, Chen B, Zhang Y, et al. Functional disconnection of the right anterior insula in obstructive sleep apnea. *Sleep Med* (2015) 16:1062–70. doi:10.1016/j.sleep.2015.04.018
49. Park B, Palomares JA, Woo MA, Kang DW, Macey PM, Yan-Go FL, et al. Disrupted functional brain network organization in patients with obstructive sleep apnea. *Brain Behav* (2016) 6:e00441. doi:10.1002/brb3.441
50. Bullmore E, Sporns O. Complex brain networks: graph theoretical analysis of structural and functional systems. *Nat Rev Neurosci* (2009) 10:186–98. doi:10.1038/nrn2575
51. Torta DM, Cauda F. Different functions in the cingulate cortex, a meta-analytic connectivity modeling study. *Neuroimage* (2011) 56:2157–72. doi:10.1016/j.neuroimage.2011.03.066
52. Joo EY, Tae WS, Min JL, Kang JW, Park HS, Lee JY, et al. Reduced brain gray matter concentration in patients with obstructive sleep apnea syndrome. *Sleep* (2010) 33:235. doi:10.1093/sleep/33.2.235
53. Macey PM, Kumar R, Woo MA, Valladares EM, Yan-Go FL, Harper RM. Brain structural changes in obstructive sleep apnea. *Sleep* (2008) 31:967–77.
54. Li H, Li L, Shao Y, Gong H, Zhang W, Zeng X, et al. Abnormal intrinsic functional hubs in severe male obstructive sleep apnea: evidence from a voxel-wise degree centrality analysis. *PLoS One* (2016) 11:e0164031. doi:10.1371/journal.pone.0164031
55. Fox MD, Snyder AZ, Vincent JL, Corbetta M, Van Essen DC, Raichle ME. From the cover: the human brain is intrinsically organized into dynamic, anticorrelated functional networks. *Proc Natl Acad Sci U S A* (2005) 102:9673–8. doi:10.1073/pnas.0504136102
56. Lucas-Jiménez O, Ojeda N, Peña J, Díez-Cirarda M, Cabrera-Zubizarreta A, Gómez-Esteban JC, et al. Altered functional connectivity in the default mode network is associated with cognitive impairment and brain anatomical changes in Parkinson's disease. *Parkinsonism Relat Disord* (2016) 33:58–64. doi:10.1016/j.parkreldis.2016.09.012
57. Weng H, Tsai Y, Chen C, Lin Y, Yang C, Tsai Y, et al. Mapping gray matter reductions in obstructive sleep apnea: an activation likelihood estimation meta-analysis. *Sleep* (2014) 37:167–75. doi:10.5665/sleep.3330
58. Joo EY, Tae WS, Sun JH, Cho JW, Hong SB. Reduced cerebral blood flow during wakefulness in obstructive sleep apnea-hypopnea syndrome. *Sleep* (2007) 30:1515–20. doi:10.1093/sleep/30.11.1515

Conflict of Interest Statement: The authors declare that the research was conducted in the absence of any commercial or financial relationships that could be construed as a potential conflict of interest.

frontiers in Neurology

ORIGINAL RESEARCH
published: 02 November 2018
doi: 10.3389/fneur.2018.00936

Recursive Partitioning Analysis of Fractional Low-Frequency Fluctuations in Narcolepsy With Cataplexy

Xiao Fulong[1], Lu Chao[2], Zhao Dianjiang[3], Zou Qihong[4], Zhang Wei[5], Zhang Jun[5] and Han Fang[1]**

[1] Department of Respiratory and Critical Care Medicine, Sleep Medicine Center, Peking University People's Hospital, Beijing, China, [2] Department of Radiology, Peking University International Hospital, Beijing, China, [3] Center for MRI Research, Academy for Advanced Interdisciplinary Studies, Peking University, Beijing, China, [4] PKU-Upenn Sleep Center, Peking University International Hospital, Beijing, China, [5] Department of Neurology, Peking University People's Hospital, Beijing, China

OPEN ACCESS

Edited by:
Hengyi Rao,
University of Pennsylvania,
United States

Reviewed by:
Hiroshi Kadotani,
Shiga University of Medical Science,
Japan
Axel Steiger,
Max-Planck-Institut für Psychiatrie,
Germany
Benito de Celis Alonso,
Benemérita Universidad Autónoma
de Puebla, Mexico

***Correspondence:**
Zhang Jun
who626@163.com
Han Fang
hanfang1@hotmail.com

Specialty section:
This article was submitted to Sleep and Chronobiology, a section of the journal Frontiers in Neurology

Received: *11 August 2018*
Accepted: *16 October 2018*
Published: *02 November 2018*

Citation:
Fulong X, Chao L, Dianjiang Z, Qihong Z, Wei Z, Jun Z and Fang H (2018) Recursive Partitioning Analysis of Fractional Low-Frequency Fluctuations in Narcolepsy With Cataplexy. Front. Neurol. 9:936. doi: 10.3389/fneur.2018.00936

Objective: To identify narcolepsy related regional brain activity alterations compared with matched healthy controls. To determine whether these changes can be used to distinguish narcolepsy from healthy controls by recursive partitioning analysis (RPA) and receiver operating characteristic (ROC) curve analysis.

Method: Fifty-one narcolepsy with cataplexy patients (26 adults and 25 juveniles) and sixty matched heathy controls (30 adults and 30 juveniles) were recruited. All subjects underwent a resting-state functional magnetic resonance imaging scan. Fractional low-frequency fluctuations (fALFF) was used to investigate narcolepsy induced regional brain activity alterations among adult and juveniles, respectively. Recursive partitioning analysis and Receiver operating curve analysis was used to seek the ability of fALFF values within brain regions in distinguishing narcolepsy from healthy controls.

Results: Compared with healthy controls, both adult and juvenile narcolepsy had lower fALFF values in bilateral medial superior frontal gyrus, bilateral inferior parietal lobule and supra-marginal gyrus. Compared with healthy controls, both adult and juvenile narcolepsy had higher fALFF values in bilateral sensorimotor cortex and middle temporal gyrus. Also juvenile narcolepsy had higher fALFF in right putamen and right thalamus compared with healthy controls. Based on RPA and ROC curve analysis, in adult participants, fALFF differences in right medial superior frontal gyrus can discriminate narcolepsy from healthy controls with high degree of sensitivity (100%) and specificity (88.9%). In juvenile participants, fALFF differences in left superior frontal gyrus can discriminate narcolepsy from healthy controls with moderate degree of sensitivity (57.1%) and specificity (88.9%).

Conclusion: Compared with healthy controls, both the adult and juvenile narcolepsy showed overlap brain regions in fALFF differences after case-control comparison. Furthermore, we propose that fALFF value can be a helpful imaging biomarker in distinguishing narcolepsy from healthy controls among both adults and juveniles.

Keywords: narcolepsy, functional magnetic resonance imaging, fractional low-frequency fluctuations, recursive partitioning analysis, receiver operating characteristic curve analysis

INTRODUCTION

Narcolepsy is a chronic sleep disorder, characterized by excessive daytime sleepiness, cataplexy, sleep paralysis, hypnagogic, and hypnopompic hallucination and disturbed nocturnal sleep. A deficient endogenous orexin system due to neuronal degeneration in the hypothalamus is the main pathophysiology of the narcolepsy in the human (1). It is indicated that loss of hypocretin is thought to be an underlying cause to the sleep-related changes and cataplexy, also deficiency in hypocretin system can result in the abnormal cognition and emotion observed in narcolepsy patients (2).

In the past decades, neuroimaging techniques have played an important role in the understanding of physiology and pathology in human sleep medicine (3, 4). Changes in brain structure and function have been investigated in hypersomnia and narcolepsy (5–8). These studies include the measurement of brain structure, such as voxel-based morphometry, diffusion tensor imaging, and metabolic studies using spectroscopy, as well as functional view, such as positron emission tomography (PET), single photon emission computed tomography (SPECT), and functional magnetic resonance imaging (fMRI). Detection of local dysfunction is crucial to the clinical research and clinical practice. Results from previous neuroimaging studies suggested that reduction of hypocretin can lead to attenuation in both resting state glucose metabolism and perfusion within cortex (9). Abnormal perfusion and glucose metabolism in the hypothalamus and prefrontal cortex has been detected among narcolepsy using PET and SPECT (5, 10). A very recent PET research in a large group of junior narcolepsy patients observed that abnormality in many frontal and subcortical brain areas, exhibited significantly correlation with neuro-cognition performance (7).

Resting state fMRI can provide information about spontaneous brain activity by assessment of blood oxygen level dependent (BOLD) signal fluctuations. The resting BOLD signal fluctuations are thought to represent spontaneous and functional process, although on a slower time response. Brain regions involved in specific task or stimuli display coherent low BOLD signal fluctuations in the resting state. Amplitude of low-frequency fluctuations (ALFF), in which the square root of power spectrum was integrated in a low-frequency range, was developed for detecting the local intensity of BOLD signal fluctuations (11). ALFF has already been applied to fMRI studies about attention deficit hyperactivity disorder and Alzheimer's disease, also in the exploration of neural mechanism of sleep disorders, such as insomnia, sleep deprivation and sleep apnea (11–14). Although ALFF was considered to be a useful tool in detecting the regional neural activity, physiological noise, such as the repetition times in MRI scan and so on, are not critically considered in the ALFF calculation. Therefore, a modified calculation called fractional amplitude of low-frequency fluctuation (fALFF), which means the ratio of the power spectrum of low frequency (0.01–0.08 Hz) to that of the entire frequency range, has been proven to suppress non-specific noise components and improve the effectiveness in exploring local BOLD signals (15). Considering the robustness and stability of ALFF and fALFF calculation, both the ALFF and fALFF can be indicated as potential biomarkers in neuroimaging studies (16).

Recursive partitioning analysis (RPA) could provide a simple, straightforward and intuitive method to classify subjects or to identify synergistic interaction among numerous factors (17, 18). RPA is considered to be a machine learning method and usually requires a large sample to establish a classification model from a training data and verify this model by another test sample. RPA can be realized through computer and many medical care studies have used RPA to detect prognostic and risk factors (19, 20), as well as diagnosis in imaging study (21). Classification and regression tree (CRT) analysis is a kind of tree-building technique from RPA to the generation of clinical decision rules (22). It is a non-parametric method for multi-model numerical data and categorical predictors, also suitable for managing the interactions between predictors which are crucial in determining the outcome. The CRT is a relatively data-driven machine learning calculation, which produces decision tree model easy to interpret (22).

In the present study, we hypothesized that fALFF has the ability to indicate narcolepsy induced neurobiological mechanism with the location of altered neural brain activity, and further distinguish narcolepsy from healthy controls with excellent sensitivity and specificity. Specifically, classification and regression tree form recursive portioning analysis (RPA) and receiver operating characteristic (ROC) curve analysis were used to investigate and validate the ability of fALFF values in distinguishing narcolepsy from healthy controls.

MATERIALS AND METHODS

Participants

Twenty six adult narcolepsy patients and another 25 juvenile patients were recruited as newly diagnosed narcolepsy with cataplexy according to the International Classification of Sleep Disorders (ICSD)-3 (23) from the Sleep Medicine Center of the Respiratory Department at Peking University People's Hospital between November 2016 and February 2018. Another 60 gender- and age- matched healthy volunteers (30 juveniles and 30 adults) were recruited from the hospital and community (**Table 1**). None of healthy controls had any consistent psychiatric or neurologic condition producing excessive daytime sleepiness. All narcolepsy cases were the first-time visitors and previously had never taken psychiatric stimulant medications. The clinical diagnosis of narcolepsy was made by a sleep specialist based on both excessive daytime sleepiness lasting more than 3 months and defined history of cataplexy, according to the International Classification of Sleep Disorders criteria for narcolepsy. The final diagnosis of narcolepsy was confirmed by a polysomnogram followed by a next day multiple sleep latency test (MSLT). Detailed information, including the presentation of excessive

Abbreviations: fMRI, Functional magnetic resonance imaging; PET, Positron emission tomography; SPECT, Single photon emission computed tomography; BOLD, Blood oxygen level dependent; ROC, Receiver operating characteristic; MSLT, Multiple sleep latency test; RPA, Recursive partitioning analysis; AUC, Area under the curve

TABLE 1 | Demography for narcolepsy patients and healthy controls.

	Demography	Narcolepsy patients	Healthy controls	*P*-value
Adult	Gender (female/male)	8/18	12/18	0.58
	Age (year)	25.77 ± 6.64	25.37 ± 4.31	0.786
	Education (year)	10.35 ± 2.3	10.95 ± 3.1	0.488
	Duration of EDS (year)	7 (2.3,12)	-	-
	Duration of cataplexy (year)	6.3 (2.2,10.3)	-	-
Juvenile	Gender (female/male)	5/20	6/24	0.63
	Age (year)	14 ± 2.7	13.3 ± 2.3	0.459
	Education (year)	8 ± 2.7	7.6 ± 2.7	0.688
	Duration of EDS (year)	5.4 (2.9,6.8)	-	-
	Duration of cataplexy (year)	3.8 (1.7, 6.8)	-	-

The P value for gender distribution in the two groups was obtained by the Chi-square test. The P values for differences in age and years of education in the two groups were obtained by the two-sample t test. Values are expressed as the mean±SD or median (25%quartile, 75%quartile). EDS, excessive daytime sleepiness.

daytime sleepiness and cataplexy, hypnagogic hallucinations, and sleep paralysis, were obtained from patients.

The exclusion criteria for both narcolepsy and normal subjects were as follows: (1) other sleep disorders, such as obstructive sleep apnea, insomnia; (2) diabetes, and chronic obstructive pulmonary disease and heart disease; (3) neurological diseases and structural lesion based on brain MRI findings; (4) psychosis disorder; (5) alcohol, drug, and substance abuse; (6) inborn or congenital diseases; (7) MRI contraindications, such as claustrophobia or foreign implants in the body.

This research was performed in accordance with the ethical guidelines of the Declaration of Helsinki (version 2002) and was approved by the Medical Ethics Committee of Peking University People's University. All participants provided written informed consent.

Imaging Data Acquisition

MRI examination was performed exactly following the daytime MSLT. MRI data were obtained on 3T (3 Tesla) scanner (Siemens, Skyra, Germany) using an 8-channel brain phased-array coil. Foam pads were used to minimize subject head motion, and headphones were used to reduce scanner noise. Resting BOLD MRI scans were obtained with gradient-echo planar imaging (TR = 2030 ms, TE = 30ms, slice = 33, FA = 90°, FOV = 224 × 224 mm, matrix = 64 × 64, voxel size=3.5 × 3.5 × 3.5), after the BOLD MRI scan, a high-resolution T1-weighted structural image was acquired with the following parameters: TR = 1900 ms, TE = 2.55 ms, FA = 9°, FOV = 240 × 240 mm, thickness = 1 mm. A total 240 brain functional volumes were acquired in the resting BOLD MRI scans. All participants, including patients and controls were asked to resist sleeping in order to remain fully awake (5, 24), not to move and keep eye open during the whole MRI scan, supervised clinically and by video both a physician and a technician during the whole process. In addition, we controlled for the absence of emotional triggering factors during the entire process to avoid cataplexy-related events.

Functional Imaging Data Analysis

Functional MRI data preprocessing was performed using the Data Processing & Analysis for Resting State Brain Imaging V2.1 [DPABI V2.1 (25)], which works with Statistical Parametric Mapping (SPM8) implemented in the MATLAB (The Math Works, Inc., Natick, MA, USA) platform. The first 5 functional volume images of each subject's dataset were discarded, then the remaining fMRI data were corrected for slice timing and realigned for motion correction. Participants with head motion exceeding 3 mm in translation and 3° in rotation were rejected. Anatomical and functional images were manually reoriented to the anterior commissure, and structural images were co-registered to the functional images for each subject using a linear transformation. Also the transformed structural images were segmented into gray matter, white matter, and cerebrospinal fluid by the new segmentation in SPM8. For adult participants, the functional images were normalized to the standard Montreal Neurological Institute (MNI) space template with a resampling voxel size of 3 × 3 × 3 mm. For juvenile participants, the functional images were normalized to the CCHMC pediatric brain template (irc.cchmc.org, The imaging research center, Cincinnati Children's Hospital Medical Center) (26) with a resampling voxel size of 3 × 3 × 3 mm. The normalized functional images were smoothed using a Gaussian filter 4 mm FWHM. Linear trends were removed within each time series. The covariates were regressed out from the time series of every voxel, including the white matter signal, cerebrospinal fluid signal, Friston 24 motion parameters (27, 28) and the global signal. The calculation of the fALFF have been reported in previous studies (15). After fALFF calculation, the time series were filtered using typical temporal bandpass (0.01–0.1Hz) to reduce low-frequency drift, physiological high-frequency respiratory and cardiac noise. To reduce the global effects of variability across the participants, the individual fALFF map was transformed to Z score (minus the global mean value and then divided by the standard deviation) other than simply being divided by the global mean (15).

STATISTICAL ANALYSIS

Demographic Data

The demographic data differences between narcolepsy and healthy controls were computed by independent two sample *t*-test with the IBM Statistical Package for the Social Sciences 23.0 software (IBM SPSS Inc., Chicago, IL, USA). We set the significance level at $P < 0.05$. Values are expressed as the *mean* ± *SD* or *median (25%quartile, 75%quartile)*.

Between Group Differences in FALFF

A two-sample *t*-test was performed between narcolepsy and controls using age, gender, and years of education as nuisance covariates to assess case-control comparison in fALFF among adults and juveniles, respectively, corrected for false discovery rate (FDR, $P < 0.05$).

Recursive Partitioning Analysis (RPA)

Narcolepsy cases and healthy controls were randomly split into testing data and validation data in the proportion of 7:3, respectively. Testing data was used to develop decision tree model by recursive partitioning analysis (70%) and validation data was used to test the developed model (30%). In the analysis of between group fALFF differences, the brain regions showing statistically significant in adults or juveniles were selected as ROI seeds, respectively, then the mean fALFF value in the region of interesting (ROI) regions were extracted. Recursive partitioning analysis was performed using mean fALFF values within ROI regions showing group differences in adults or juveniles, respectively. We chose the Classification and Regression Trees (CRT) technique in the process of RPA to define narcolepsy or control. The criteria for splitting node including the following: child nodes derived from a parent node should be as homogeneous as possible with the dependent variables, corresponding cut-off points should result in the minimal *P* value, provides the minimal *P* value was ≤ 0.0001 (29). Terminal nodes were identified to a class when the significant level of comparison between 2 terminal nodes was >0.05 (29). As for the validation data, sensitivity, specificity, false positive rate (FPR), false negative rate (FNR), positive predictive value (PPV), negative predictive value (NPV), and accuracy were calculated according to the fALFF value cut-off obtained on the basis of developed decision tree model. ROC analysis was applied to measure the discrimination of the decision tree model. RPA process and ROC curve statistical analysis was performed with R (http://www.R-project.org) and Empower-Stats software (www.empowerstats.com, X&Y solutions, Inc., Boston, MA, USA).

RESULTS

Demographic Data

As shown in **Table 1**, there were no significant differences between narcolepsy and healthy controls in age, gender, years of education.

Differences in FALFF Between Narcolepsy and Healthy Controls

In adult participants, compared with healthy controls, narcolepsy had lower fALFF values in bilateral medial superior frontal gyrus (SFGmed), bilateral inferior parietal lobule (IPL) and left supra-marginal gyrus (SMG). Compared with healthy controls, narcolepsy had higher fALFF values in bilateral sensorimotor cortex (SMC) and bilateral middle temporal gyrus (MTG) (**Figures 1A**, **2A** and **Table S1**). In juvenile participants, compared with healthy controls, narcolepsy had lower fALFF values in bilateral medial superior frontal gyrus, bilateral inferior parietal lobule, left superior frontal gyrus (SFG), and right supra-marginal gyrus. Compared with healthy controls, narcolepsy had higher fALFF values in bilateral sensorimotor cortex, right middle temporal gyrus, right putamen and right thalamus (**Figures 1B**, **2B** and **Table S1**).

Recursive Partitioning Analysis (RPA) of FALFF Values

In adult participants, 18 narcolepsy cases (18/26, 69%) and 21 healthy controls (21/30, 70%) were used as testing data in the recursive partitioning analysis and the developed decision tree model was shown in **Figure 3A**. In juvenile participants, 18 narcolepsy cases (18/25, 72%) and 21 healthy controls (21/30, 70%) were used as testing data in the recursive partitioning analysis and the developed decision tree model was shown in **Figure 3B**. The cut-off fALFF values of these nodes were also shown in the decision tree model (**Figure 3**). In adult participants, 8 narcolepsy cases (8/26, 31%) and 9 healthy controls (9/30, 30%) were used as validation data in the ROC analysis of developed decision tree model (**Figure 4A**). When decision tree model applied to the validation data, it revealed the sensitivity was 100%, and the specificity 88.9%. The FPR was 11.1% and the FNR was 0. Meanwhile the model showed the PPV of 88.9%, the NPV of 100%, and the accuracy of 94.1% (**Table 2**). In juvenile participants, 7 narcolepsy cases (7/25, 28%) and 9 healthy controls (9/30, 30%) were used as validation data in the ROC analysis of developed decision tree model (**Figure 4B**). When decision tree model applied to the validation data, it revealed the sensitivity was 57.1%, and the specificity 88.9%. The FPR was 11.1% and the FNR was 42.9%. Meanwhile the model showed the PPV of 80%, the NPV of 72.7% and the accuracy of 75% (**Table 2**).

DISCUSSION

This study compared fALFF differences in both adult and juvenile narcolepsy patients with those in a group of matched healthy controls. Specially, compared with healthy controls, we identified some overlap brain regions showing significantly different fALFF values in both adult and juvenile narcolepsy patients, including bilateral medial superior frontal gyrus, bilateral sensorimotor cortex, supra-marginal gyrus, middle temporal gyrus, and bilateral inferior parietal lobule. It has been revealed that utility of ROC curve analysis in neuroimaging can distinguish one group of participants from another group of participants (13, 14). Furthermore, by using recursive partitioning analysis and ROC curve analysis, we speculated that the fALFF values in some brain regions were excellent in discriminating narcolepsy subjects from healthy controls in both adults and juvenile with high AUC value.

Low-frequency fluctuation measures are widely used for the assessment of group differences in many previous resting-state studies focusing on clinical case-control comparison (16). Furthermore, standardization has been identified effective in eliminating the dependency of fALFF values on subjective motion (16), so Z score of fALFF (i.e., standardization of fALFF) was used in the between group comparison. In both the adult and juvenile participants, narcolepsy patients showed decreased fALFF in bilateral SFGmed, bilateral supra-marginal gyrus and bilateral IPL compared with healthy controls, while narcolepsy patients showed increased fALFF in bilateral SMC and bilateral middle temporal gyrus compared with healthy controls. Both the

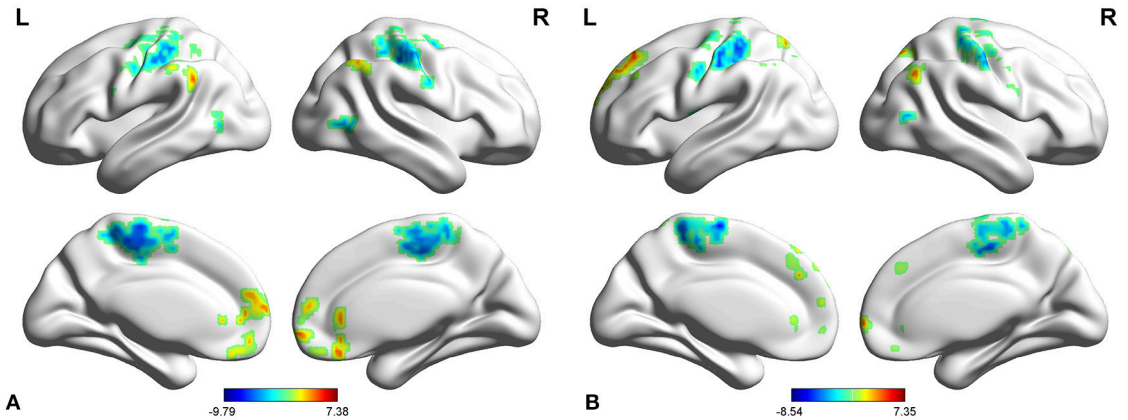

FIGURE 1 | Two-sample *t*-test results for fALFF between narcolepsy and healthy controls among adults **(A)** and juveniles **(B)**.

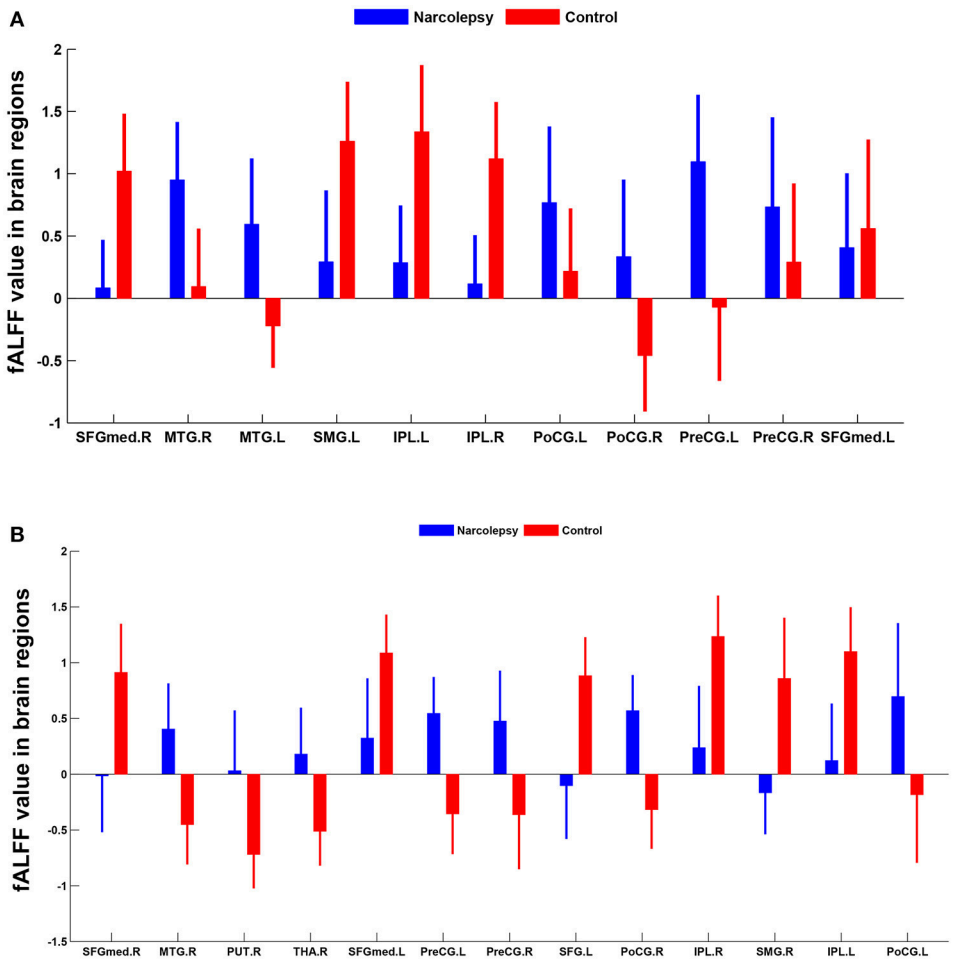

FIGURE 2 | Mean fALFF values differences in regional brain areas between narcolepsy and healthy controls among adults **(A)** and juveniles **(B)**. SFGmed, medial superior frontal gyrus; MTG, middle temporal gyrus; SMG, supra-marginal gyrus; IPL, inferior parietal lobule; PoCG, postcentral gyrus; PreCG, precentral gyrus; PUT, putamen; THA, thalamus; SFG, superior frontal gyrus. L, left; R, right.

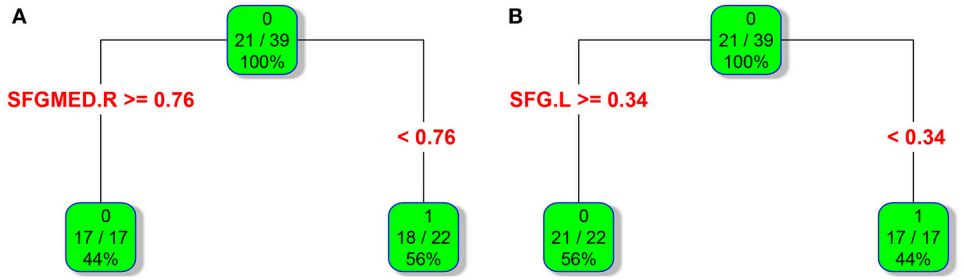

FIGURE 3 | RPA process results of classification and regression tree about fALFF values within two brain regions between narcolepsy and healthy controls among adults **(A)** and juveniles **(B)**. As for each box, the binary value in the top represents group (0, healthy controls; 1, narcolepsy); as for the ratio in the middle, numerator means the size of patients or controls in the box and it is reflected by the top binary value, denominator means sample size in the box; the percentage in the bottom means the percentage of each box sample size in the tree. As for a brain region (or a splitting node), the cut-off fALFF value was also shown. SFGmed, medial superior frontal gyrus; SFG, superior frontal gyrus. L, left; R, right.

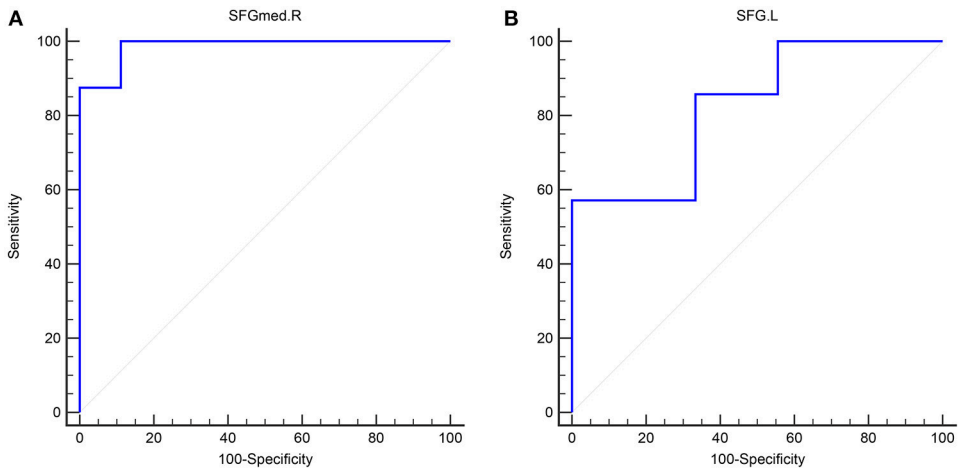

FIGURE 4 | The validation ROC curve of each brain region based on results from RPA analysis for distinguishing narcolepsy from healthy controls among adults **(A)** and juveniles **(B)**. SFGmed, medial superior frontal gyrus; SFG, superior frontal gyrus. L, left; R, right.

medial frontal cortex, supra-marginal gyrus, and parietal lobe are abundant in hypocretin projection (30, 31), which can explain the reduced fALFF value in these regions among narcolepsy due to hypocretin deficiency, consistent with two previous positron emission tomography studies (7, 8). Increased fALFF in bilateral SMC, extending to bilateral paracentral lobule (**Figure 1**), may be a compensation of hypocretin deficiency in motor cortex among narcolepsy, although a contradictory result has been reported hypo-activity in sensorimotor cortex in narcolepsy by transcranial magnetic stimulation (TMS) in a previous study (32). Increased glucose metabolism in temporal lobe has been indicated in previous studies (7, 24), which was consistent with increased fALFF value in middle temporal gyrus in the present study result. Such increased fALFF value or hyper-metabolism in temporal lobe may be related to transient activation of this region, compensation for the hypocretin deficiency.

Meanwhile, especially in juvenile narcolepsy, higher fALFF value in right putamen and right thalamus can be detected compared with healthy controls. Putamen is a component of the salience network (24). The salience network is responsible for integration of sensory and attention information, initiation of responses to significant stimuli as a function of top-down attention and cognitive control process (33, 34). The salience network is also thought to maintain the tonic of alertness, correlated with sympathetic regions (35, 36). Also thalamus is a core brain region responsible for sympathetic regulation, arousal, and wakefulness (35, 36). In our resting-state fMRI study, for drug-free narcolepsy patients, it requires a specific order to resist

TABLE 2 | Validation for Decision tree model about fALFF differences in brain regions between narcolepsy and healthy control.

Group	Brain regions	Sn %	Sp %	FPR %	FNR %	PPV %	NPV %	Accuracy %	AUC
Adult	SFGmed.R	100	88.9	11.1	0	88.9	100	94.1	0.986
Juvenile	SFG.L	57.1	88.9	11.1	42.9	80	72.7	75	0.825

Sn, sensitivity; Sp, specificity; FPR, false positive rate; FNR, false negative rate; PPV, positive predictive value; NPV, negative predictive value; AUC, area under the curve; SFGmed.R, right medial superior frontal gyrus; SFG.L, left superior frontal gyrus.

sleepiness during the MRI scan. The increased fALFF in putamen and thalamus among juvenile narcoleptic patients reinforced its major role in the reservation of the awaking status and the activated sympathetic nervous system. The relatively increased fALFF may reflect the patients' subjective effort to maintain vigilance, consistent with already reported in obstructive sleep apnea (37), in Kleine-Levin syndrome (38) and in PET narcolepsy study (24).

Interestingly, based on the results of classification and regression tree from recursive partitioning analysis, validated ROC curve analysis indicates that in adult participants the fALFF value in right SFGmed alone could discriminate narcolepsy from healthy controls with high degree of sensitivity, specificity, and accuracy (**Figure 4A**). Also in juvenile participants, the validated ROC curve indicated that the fALFF value in left SFG alone could also discriminate narcolepsy from healthy controls with moderate degree of sensitivity, specificity and accuracy (**Figure 4B**). Although there were many brain regions showing fALFF value differences between groups, just one brain region was necessary to discriminate narcolepsy from healthy controls in adults and juveniles, respectively.

The present study has some limitations. Small sample size and single setting should be the first consideration in limitations, especially in the validation data, small sample size may lead to some bias and confounding. Also participants in this study all come from China, which may potentially be not applicable to other ethnic groups. While being fully awake during the whole examination as controlled clinically and by video, but the vigilance state was not monitored through synchronous EEG recording during the MRI scan. Our design cannot directly confirm the absence of short fluctuations in alertness and even short sleep events during the MRI process. Further simultaneous EEG-fMRI studies based on large samples are necessary to confirm our preliminary results on fALFF value differences between narcolepsy and healthy controls, also to compare narcolepsy patients with other hypersomnia and sleep deprivation in resting wakefulness.

To conclude, compared with healthy controls, both the adult and juvenile narcolepsy showed overlap brain regions in fALFF differences after case-control comparison. Furthermore, we propose that fALFF value can be a helpful imaging biomarker in distinguishing narcolepsy from healthy controls among both adults and juveniles.

ETHICS STATEMENT

This study was approved by the Ethical Committee of the Peking University People's Hospital.

AUTHOR CONTRIBUTIONS

ZJ and HF designed the study. XF, LC, ZD, ZQ, and ZW carried out the study. XF performed data analysis and wrote the manuscript.

FUNDING

This work was supported by the National Natural Science Foundation of China (81700088), National Natural Science Foundation of China (81671765), Key International (Regional) Cooperation Program of National Natural Science Foundation of China (81420108002), National Program on Key Basic Research Project of China (973 Program, 2015CB856405), and Beijing Municipal Natural Science Foundation (7172121).

ACKNOWLEDGMENTS

We thank all the patients and healthy volunteers for their collaboration.

SUPPLEMENTARY MATERIAL

The Supplementary Material for this article can be found online at: https://www.frontiersin.org/articles/10.3389/fneur.2018.00936/full#supplementary-material

Table S1 | Significant differences in fALFF value between narcolepsy patients and healthy controls.

Table S2 | Original data for testing RPA and validated ROC analysis.

REFERENCES

1. Nishino S, Okuro M, Kotorii N, Anegawa E, Ishimaru Y, Matsumura M, et al. Hypocretin/orexin and narcolepsy: new basic and clinical insights. *Acta Physiol.* (2010) 198:209–22. doi: 10.1111/j.1748-1716.2009.02012.x
2. Bayard S, Croisier Langenier M, Cochen De Cock V, Scholz S, Dauvilliers Y. Executive control of attention in narcolepsy. *PLoS ONE* (2012) 7:e33525. doi: 10.1371/journal.pone.0033525
3. Desseilles M, Dang-Vu T, Schabus M, Sterpenich V, Maquet P, Schwartz S. Neuroimaging insights into the pathophysiology of sleep disorders. *Sleep* (2008) 31:777–94. doi: 10.1093/sleep/31.6.777
4. Engstrom M, Hallbook T, Szakacs A, Karlsson T, Landtblom AM. Functional magnetic resonance imaging in narcolepsy and the kleine-levin syndrome. *Front Neurol.* (2014) 5:105. doi: 10.3389/fneur.2014.00105
5. Dauvilliers Y, Comte F, Bayard S, Carlander B, Zanca M, Touchon J. A brain PET study in patients with narcolepsy-cataplexy. *J Neuro Neurosurg Psychiatry* (2010) 81:344–8. doi: 10.1136/jnnp.2009.175786
6. Joo EY, Hong SB, Tae WS, Kim JH, Han SJ, Cho YW, et al. Cerebral perfusion abnormality in narcolepsy with cataplexy. *NeuroImage* (2005) 28:410–6. doi: 10.1016/j.neuroimage.2005.06.019
7. Huang YS, Liu FY, Lin CY, Hsiao IT, Guilleminault C. Brain imaging and cognition in young narcoleptic patients. *Sleep Med.* (2016) 24:137–44. doi: 10.1016/j.sleep.2015.11.023
8. Joo EY, Tae WS, Kim JH, Kim BT, Hong SB. Glucose hypometabolism of hypothalamus and thalamus in narcolepsy. *Ann Neurol.* (2004) 56:437–40. doi: 10.1002/ana.20212
9. Drissi NM, Szakacs A, Witt ST, Wretman A, Ulander M, Stahlbrandt H, et al. Altered brain microstate dynamics in adolescents with narcolepsy. *Front Hum Neurosci.* (2016) 10:369. doi: 10.3389/fnhum.2016.00369
10. Hong SB, Tae WS, Joo EY. Cerebral perfusion changes during cataplexy in narcolepsy patients. *Neurology* (2006) 66:1747–9. doi: 10.1212/01.wnl.0000218205.72668.ab
11. Zang YF, He Y, Zhu CZ, Cao QJ, Sui MQ, Liang M, et al. Altered baseline brain activity in children with ADHD revealed by resting-state functional MRI. *Brain Dev.* (2007) 29:83–91. doi: 10.1016/j.braindev.2006.07.002

12. He Y, Wang L, Zang Y, Tian L, Zhang X, Li K, et al. Regional coherence changes in the early stages of Alzheimer's disease: a combined structural and resting-state functional MRI study. *NeuroImage* (2007) 35:488–500. doi: 10.1016/j.neuroimage.2006.11.042
13. Li HJ, Dai XJ, Gong HH, Nie X, Zhang W, Peng DC. Aberrant spontaneous low-frequency brain activity in male patients with severe obstructive sleep apnea revealed by resting-state functional MRI. *Neuropsychiatr Dis Treat.* (2015) 11:207–14. doi: 10.2147/NDT.S73730
14. Dai XJ, Nie X, Liu X, Pei L, Jiang J, Peng DC, et al. Gender differences in regional brain activity in patients with chronic primary insomnia: evidence from a resting-state fMRI study. *J Clin Sleep Med.* (2016) 12:363–74. doi: 10.5664/jcsm.5586
15. Zou QH, Zhu CZ, Yang Y, Zuo XN, Long XY, Cao QJ, et al. An improved approach to detection of amplitude of low-frequency fluctuation (ALFF) for resting-state fMRI: fractional ALFF. *J Neurosci Methods* (2008) 172:137–41. doi: 10.1016/j.jneumeth.2008.04.012
16. Kublbock M, Woletz M, Hoflich A, Sladky R, Kranz GS, Hoffmann A, et al. Stability of low-frequency fluctuation amplitudes in prolonged resting-state fMRI. *NeuroImage* (2014) 103:249–257. doi: 10.1016/j.neuroimage.2014.09.038
17. Cook EF, Goldman L. Empiric comparison of multivariate analytic techniques: advantages and disadvantages of recursive partitioning analysis. *J Chron Dis.* (1984) 37:721–31. doi: 10.1016/0021-9681(84)90041-9
18. Kang S, Kim HS, Kim S, Kim W, Han I. Post-metastasis survival in extremity soft tissue sarcoma: a recursive partitioning analysis of prognostic factors. *Eur J Cancer* (2014) 50:1649–56. doi: 10.1016/j.ejca.2014.03.003
19. Niwinska A, Murawska M. New breast cancer recursive partitioning analysis prognostic index in patients with newly diagnosed brain metastases. *Int J Radiat Oncol Biol Phys.* (2012) 82:2065–71. doi: 10.1016/j.ijrobp.2010.10.077
20. Suzuki H, Asami K, Hirashima T, Okamoto N, Yamadori T, Tamiya M, et al. Stratification of malignant pleural mesothelioma prognosis using recursive partitioning analysis. *Lung* (2014) 192:191–5. doi: 10.1007/s00408-013-9516-y
21. Onuma K, Ishikawa E, Matsuda M, Hirata K, Osuka S, Yamamoto T, et al. Clinical characteristics and neuroimaging findings in 12 cases of recurrent glioblastoma with communicating hydrocephalus. *Neurologia Medico-Chirurgica* (2013) 53:474–81. doi: 10.2176/nmc.53.474
22. Fei Y, Gao K, Hu J, Tu J, Li WQ, Wang W, et al. Predicting the incidence of portosplenomesenteric vein thrombosis in patients with acute pancreatitis using classification and regression tree algorithm. *J Crit Care* (2017) 39:124–130. doi: 10.1016/j.jcrc.2017.02.019
23. AAo Medicine S. *The International Classification of Sleep Disorders. 3rd edn*, Westchester, (2014).
24. Dauvilliers Y, Evangelista E, de Verbizier D, Barateau L, Peigneux P. 18F.fludeoxyglucose-positron emission tomography evidence for cerebral hypermetabolism in the awake state in narcolepsy and idiopathic hypersomnia. *Front Neurol.* (2017) 8:350. doi: 10.3389/fneur.2017.00350
25. Yan CG, Wang XD, Zuo XN, Zang YF. DPABI: Data processing & analysis for (Resting-State) brain imaging. *Neuroinformatics* (2016) 14:339–51. doi: 10.1007/s12021-016-9299-4
26. Wilke M, Schmithorst VJ, Holland SK. Assessment of spatial normalization of whole-brain magnetic resonance images in children. *Hum Brain Mapp.* (2002) 17:48–60. doi: 10.1002/hbm.10053
27. Friston KJ, Williams S, Howard R, Frackowiak RS, Turner R. Movement-related effects in fMRI time-series. *Magn Reson Med.* (1996) 35:346–55. doi: 10.1002/mrm.1910350312
28. Yan CG, Craddock RC, He Y, Milham MP. Addressing head motion dependencies for small-world topologies in functional connectomics. *Front Hum Neurosci.* (2013) 7:910. doi: 10.3389/fnhum.2013.00910
29. Chang YJ, Chung KP, Chen LJ, Chang YJ. Recursive partitioning analysis of lymph node ratio in breast cancer patients. *Medicine* (2015) 94:e208. doi: 10.1097/MD.0000000000000208
30. Taheri S, Zeitzer JM, Mignot E. The role of hypocretins (orexins) in sleep regulation and narcolepsy. *Ann Rev Neurosci.* (2002) 25:283–313. doi: 10.1146/annurev.neuro.25.112701.142826
31. Del Cid-Pellitero E, Garzon M. Hypocretin1/orexinA-immunoreactive axons form few synaptic contacts on rat ventral tegmental area neurons that project to the medial prefrontal cortex. *BMC Neurosci.* (2014) 15:105. doi: 10.1186/1471-2202-15-105
32. Oliviero A, Della Marca G, Tonali PA, Pilato F, Saturno E, Dileone M, et al. Functional involvement of cerebral cortex in human narcolepsy. *J Neurol.* (2005) 252:56–61. doi: 10.1007/s00415-005-0598-1
33. Uddin LQ. Salience processing and insular cortical function and dysfunction. *Nat Rev.* (2015) 16:55–61. doi: 10.1038/nrn3857
34. Spetsieris PG, Ko JH, Tang CC, Nazem A, Sako W, Peng S, et al. Metabolic resting-state brain networks in health and disease. *Proc Natl Acad Sci USA.* (2015) 112:2563–8. doi: 10.1073/pnas.1411011112
35. Sadaghiani S, Scheeringa R, Lehongre K, Morillon B, Giraud AL, Kleinschmidt A. Intrinsic connectivity networks, alpha oscillations, and tonic alertness: a simultaneous electroencephalography/functional magnetic resonance imaging study. *J Neurosci.* (2010) 30:10243–50. doi: 10.1523/JNEUROSCI.1004-10.2010
36. Beissner F, Meissner K, Bar KJ, Napadow V. The autonomic brain: an activation likelihood estimation meta-analysis for central processing of autonomic function. *J Neurosci.* (2013) 33:10503–11. doi: 10.1523/JNEUROSCI.1103-13.2013
37. Ayalon L, Ancoli-Israel S, Klemfuss Z, Shalauta MD, Drummond SP. Increased brain activation during verbal learning in obstructive sleep apnea. *NeuroImage* (2006) 31:1817–25. doi: 10.1016/j.neuroimage.2006.02.042
38. Dauvilliers Y, Bayard S, Lopez R, Comte F, Zanca M, Peigneux P. Widespread hypermetabolism in symptomatic and asymptomatic episodes in Kleine-Levin syndrome. *PLoS One* (2014) 9:e93813. doi: 10.1371/journal.pone.0093813

Conflict of Interest Statement: The authors declare that the research was conducted in the absence of any commercial or financial relationships that could be construed as a potential conflict of interest.

frontiers in Neurology

ORIGINAL RESEARCH
published: 18 May 2018
doi: 10.3389/fneur.2018.00355

Lack of Association Between Shape and Volume of Subcortical Brain Structures and Restless Legs Syndrome

Marco Hermesdorf[1], Benedikt Sundermann[2], Rajesh Rawal[1], András Szentkirályi[1], Udo Dannlowski[3] and Klaus Berger[1]*

[1] Institute of Epidemiology and Social Medicine, University of Münster, Münster, Germany, [2] Department of Clinical Radiology, University Hospital Münster, Münster, Germany, [3] Department of Psychiatry, University of Münster, Münster, Germany

Objective: Previous studies on patients with restless legs syndrome (RLS) yielded inconclusive results in the magnetic resonance imaging (MRI)-based analyses of alterations of subcortical structures in the brain. The aim of this study was to compare volumes as well as shapes of subcortical structures and the hippocampus between RLS cases and controls. Additionally, the associations between the genetic risks for RLS and subcortical volumes were investigated.

Methods: We compared volumetric as well as shape differences assessed by 3 T MRI in the caudate nucleus, hippocampus, globus pallidus, putamen, and thalamus in 39 RLS cases versus 117 controls, nested within a population-based sample. In a subsample, we explored associations between known genetic risk markers for RLS and the volumes of the subcortical structures and the hippocampus.

Results: No significant differences between RLS cases and controls in subcortical and hippocampal shapes and volumes were observed. Furthermore, the genetic risk for RLS was unrelated to any alterations of subcortical and hippocampal gray matter volume.

Interpretation: We conclude that neither RLS nor the genetic risk for the disease give rise to changes in hippocampal and subcortical shapes and gray matter volumes.

Keywords: restless legs syndrome, gray matter volume, subcortical brain structures, genetic risk, risk alleles

OPEN ACCESS

Edited by:
Kai Spiegelhalder, Universitätsklinikum Freiburg, Germany

Reviewed by:
Martin Gorges, Universität Ulm, Germany
Katja Menzler, Philipps-Universität Marburg, Germany

****Correspondence:***
Marco Hermesdorf
hermesdorf@uni-muenster.de

Specialty section:
This article was submitted to Applied Neuroimaging, a section of the journal Frontiers in Neurology

Received: *22 December 2017*
Accepted: *01 May 2018*
Published: *18 May 2018*

Citation:
Hermesdorf M, Sundermann B, Rawal R, Szentkirályi A, Dannlowski U and Berger K (2018) Lack of Association Between Shape and Volume of Subcortical Brain Structures and Restless Legs Syndrome. Front. Neurol. 9:355. doi: 10.3389/fneur.2018.00355

INTRODUCTION

Restless legs syndrome (RLS) is a sensorimotor disorder affecting 2.5–10% of the general population (1). RLS is characterized by unpleasant sensations in the legs or other extremities combined with an urge to move in order to reduce the discomforting sensations. These symptoms typically worsen during periods of rest, thus having a negative impact on sleep and quality of life (2, 3). Genetic factors play an important role in RLS as it has been revealed that several single nucleotide polymorphisms (SNPs) contribute to the development of the disease (4, 5). Furthermore, RLS is believed to be a result of iron insufficiency in the brain, presumably caused by improper iron transportation across the blood–brain barrier leading to dysregulated dopaminergic neurotransmission (6).

Due to the specific role of subcortical structures in dopaminergic neurotransmission (7) and their role in iron deposition and motor function (8), these structures are of particular interest in

the search for neurobiological correlates of RLS. Previous studies employing magnetic resonance imaging (MRI) of the brain provided conflicting results regarding volumetric changes of subcortical gray matter in RLS cases. In particular, a reduction in gray matter volume has been observed in the left hippocampus (9), while others found a significant increase in left hippocampal gray matter associated with RLS (10). Increased gray matter volume in the pulvinar nuclei located inside the thalamus has also been reported (11). In contrast, several studies found no significant associations between RLS and alterations of subcortical gray matter volume (12–15). Most of these studies applied voxel-based morphometry for the detection of local changes in gray matter volume across the brain (9–14). However, specific methods have been developed to detect localized shape differences in subcortical regions and the hippocampus, considering the specific signal characteristics of these brain structures (16). Only a single study investigated such localized shape differences of the thalamus, but did not detect significant shape differences in patients with RLS versus controls (15). Localized shape differences in subcortical regions other than the thalamus have not been investigated in patients with RLS.

The present study aimed to contrast potential differences in localized shape and overall volume of several subcortical gray matter structures (caudate nucleus, globus pallidus, putamen, and thalamus) as well as the hippocampus between RLS cases and controls, all participants in the BiDirect Study. Additionally, we investigated associations between known genetic risks for RLS and potential alterations of subcortical gray matter volume, since MRI-detectable changes in these subcortical structures might be a mediator in the pathway between genotype and RLS.

MATERIALS AND METHODS

Participants

The ongoing BiDirect study is conducted to investigate associations between subclinical arteriosclerosis and depression. For this purpose, the BiDirect study integrates two patient cohorts, one including patients with depression, the other patients with cardiovascular disease, and one general population cohort into one project. Details on methods and design of the BiDirect Study are provided elsewhere (17, 18). Participants in the general population cohort were randomly sampled from the population register of the city of Münster, resulting in 911 individuals included in this cohort. All participants had to be in the age range from 35 to 65 years at recruitment. Informed consent was signed by all study participants in the BiDirect project, which was approved by the ethics committee of the University of Münster and the Westphalian Chamber of Physicians. Within the general population cohort, we performed a nested case-control analysis. Participants from the two patient cohorts of the BiDirect Study were thus not considered in the present analysis. Participants who did not undergo T1-weighted MRI were excluded and RLS-status was assessed in face-to-face interviews by a set of questions that were based on the criteria established by the International RLS Study Group (19). This question set has previously been validated against a standardized neurological examination and both were in good agreement (20). In addition, a physician diagnosis of RLS in the past was assessed. Study participants who positively answered questions on all minimum criteria or reported a physician diagnosis of RLS were classified as RLS cases. In total, 11 participants had a prior physician-based diagnosis of RLS and 28 participants were screened positive by the question set. Participants without a physician diagnosis of RLS and a negative screening were classified as controls. Controls with a previously diagnosed kidney disease and/or diabetes were excluded from the analysis. Based on the group of RLS cases, controls were frequency-matched one to three by the variables age and sex. This resulted in 39 RLS cases and 117 controls for the nested case-control analysis as depicted in **Figure 1**. Furthermore, we conducted a sensitivity power analysis using G*Power (21), revealing that we can detect substantial effects ($f = 0.29$) with a power of 95% in the shape analysis.

Image Acquisition

Magnetic resonance imaging of the brain was performed in all BiDirect participants without contraindications. Structural 3D T1-weighted turbo field echo imaging was performed on a 3 T scanner (Intera, Philips, Best, Netherlands) to obtain 160 sagittal slices with a thickness of 2 mm (reconstructed to 1 mm), resulting in a voxel-size of 1 × 1 × 1 mm (TR = 7.26 ms, TE = 3.56 ms, 9° flip angle, matrix dimension 256 × 256, FOV = 256 × 256 mm).

Image Preprocessing

Magnetic resonance imaging data were preprocessed using FSL (22) version 5.06. Images were linearly registered to the MNI152 template using FLIRT (23). If necessary, images were cropped or bias-field corrected with fsl_anat[1] to ensure optimal registration. The inverse transformation matrix was then applied to the predefined subcortical shape models provided by FSL. With these predefined shape models in native space, subcortical structures of interest (caudate nucleus, hippocampus, globus pallidus, putamen, and thalamus) were segmented from the participants' native space images using a Bayesian appearance model in FIRST (16) and modeled as surface meshes. In a last step, the subcortical surfaces were aligned to a sample-specific mean shape of the respective surface structures applying a 6 degree of freedom transformation whereby differences in rotation and translation were removed.

For the purpose of a volume-based analysis, subcortical structures were boundary corrected and the respective volumes of interest were extracted. In order to adjust for the overall brain volume in the course of analyses, brain volume (i.e., gray and white matter) was estimated by partial volume estimation in FAST (24).

Genotyping

Genotyping was conducted using the Illumina PsychChip array (Illumina, San Diego, CA, USA). Several SNPs in *MEIS1*, *BTBD9*, *MAP2K5*, *PTPRD*, and *TOX3/BC034767* (4, 25–27) have previously been associated with RLS and were selected for the study at hand. Imputation was performed using IMPUTE version 2.3.2 (28). SNPs being in linkage disequilibrium ($R^2 \geq 0.8$) or with a

[1]http://fsl.fmrib.ox.ac.uk/fsl/fslwiki/fsl_anat (Accessed: 2017).

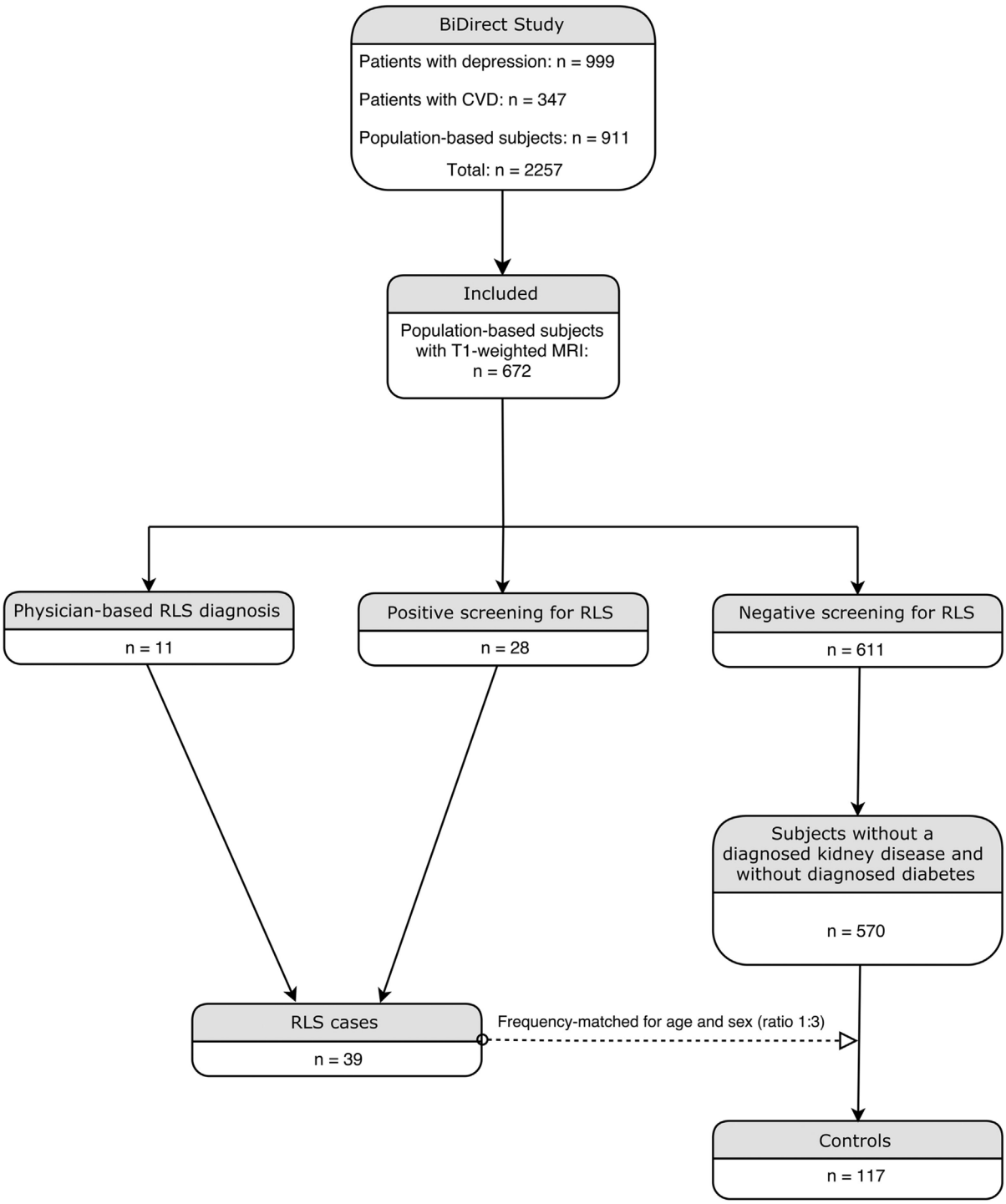

FIGURE 1 | Flowchart illustrating the inclusion procedure.

minor allele frequency below 5% were excluded from the analysis. Statistics regarding linkage disequilibrium were derived from the database of the Broad Institute.[2]

[2]https://archive.broadinstitute.org/mpg/snap (Accessed: 2017).

Comorbidities

We assessed comorbidities using data from face-to-face interviews as well as laboratory data. Previous physician-based diagnoses of stroke, myocardial infarction, and cancer were collected by self-report. Participants were classified as hypertensive

if the mean of the second and third blood pressure readings for systolic blood pressure was ≥140 mm Hg or the diastolic blood pressure exceeded 89 mm Hg. Furthermore, participants with a self-reported physician-based diagnosis of hypertension in combination with use of antihypertensive medication according to the Anatomical Therapeutic Chemical (ATC) Classification System (ATC C02A, C02D, C02L, C03, C07, C08, C09) were also defined as having hypertension. Depression was assessed as a previous physician-based diagnosis *via* self-report or if participants scored ≥16 points on the Center for Epidemiologic Studies Depression Scale (29). Body size and weight were assessed and participants with a body mass index larger than 30 $\frac{kg}{m^2}$ were classified as obese. The presence of thyroid disease was assessed by self-report of a physician-based diagnosis or intake of relevant medication (ATC H03). Thyroid-stimulating hormone (TSH) and free thyroxine (fT_4) levels were used to estimate hypothyroidism (TSH > 4.8 $\frac{\mu IU}{mL}$ and $fT_4 < 13$ $\frac{pmol}{L}$) as well as hyperthyroidism (TSH < 0.3 $\frac{\mu IU}{mL}$ and $fT_4 > 23$ $\frac{pmol}{L}$) and participants in either category were also defined as having thyroid disease. Migraine was assessed as physician-based diagnosis *via* self-report or current use of relevant medication (ATC N02CA, N02CC). A comorbidity index was calculated by summing up the presence of the previously described conditions (stroke, myocardial infarction, cancer, hypertension, depression, obesity, thyroid disease, and migraine). A similar index of cumulative disease burden has been used previously in the context of RLS (30).

Statistical Analysis

Participants with RLS and controls were compared on orthogonal displacements at each vertex regarding the sample-specific mean surfaces of the subcortical structures of interest. These analyses were conducted with a cluster-based *F*-test implemented in FSL randomize (31) with 5,000 permutations. Statistical threshold for significance was set to $p < 0.05$. Extracted volumes of the subcortical structures were compared across groups by several analyses of covariance (ANCOVAs) while adjusting for overall brain volume. The obtained *p*-values were corrected for false discovery rate (FDR) following the Benjamini–Hochberg procedure (32).

Genotyping data were available for 137 participants. For each participant, the number of risk alleles per SNP was noted. For each respective SNP, a logistic regression was conducted with RLS as dependent variable and risk allele frequency as predictor along with age and sex as covariates of no interest. A weighted genetic risk score (GRS) was calculated for each SNP by multiplying the risk allele frequency of the respective SNP with the odds ratio obtained by the logistic regression. Each respective GRS was used as a predictor in multiple regression analyses with the subcortical brain volumes as dependent variables while adjusting for age, sex, and overall brain volume. The analyses of extracted subcortical volumes and genotyping data were conducted in SPSS version 22 (IBM, Armonk, NY, USA).

RESULTS

Subject Demographics

A comparison of group characteristics is summarized in **Table 1**. Participants with RLS and controls did not differ in terms of age and sex. Distributions of comorbidity load were significantly different across groups and the median comorbidity load was higher in RLS cases. Genotyping data were available for 137 (87.8%) participants. The remaining 19 participants were thus not considered for the analyses of genotyping data.

Shape Analyses

The comparisons of the shapes in the caudate nucleus, hippocampus, globus pallidus, putamen, and thalamus across groups did not yield significant differences in either hemisphere. The subcortical and hippocampal shapes of the sample are shown in **Figure 2**. The analyses of extracted volumetric data did not reveal significant group differences after FDR correction (**Table 2**).

TABLE 1 | Comparison of demographic characteristics across groups.

Variable	Participants with RLS *n* = 39	Controls *n* = 117	*p*
Age: mean (SD)	51.21 (8.51)	51.29 (8.33)	0.957
Women: *n* (%)	26 (66.7%)	78 (66.7%)	1
Comorbidity index[a]: median (IQR)	2 (1–2)	1 (0–2)	<0.01
Genotyping data available: *n* (%)	35 (89.7%)	102 (87.2%)	
Duration of disease in years[a]: median (IQR)	5 (2.5–10)		
Frequency of symptoms: *n* (%)			
Less than once in per month	5 (12.8%)		
1–3 times per month	11 (28.2%)		
1–2 times per week	6 (15.4%)		
3–6 times per week	6 (15.4%)		
Daily	8 (20.5%)		
Undetermined	3 (7.7%)		

RLS, restless legs syndrome; IQR, interquartile range.
[a]One participant had incomplete comorbidity data and two participants had missing data on disease duration.
Age was compared with a t-test. Distribution of sex was compared with a χ^2 test and comorbidity load with a Mann–Whitney U-test.

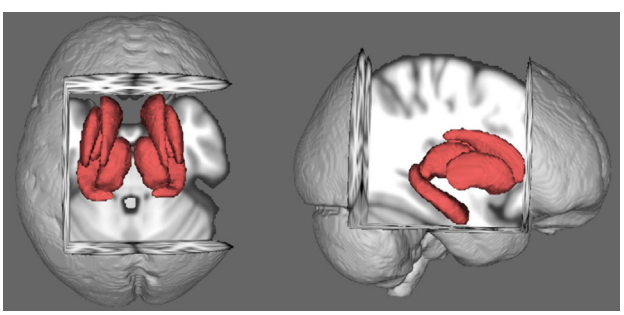

FIGURE 2 | Average shapes of the rigidly aligned subcortical structures in the sample.

Associations Between Risk allele Frequency and RLS

The logistic regressions yielded significant associations between RLS and the risk allele (G) frequency in rs11635424, located in *MAP2K5*. Due to the small sample size, no significant associations were found for the remaining eight SNPs. However, the magnitude of the odds ratios indicated a higher risk for RLS concerning the majority of the SNPs (**Table 3**), in line with prior reports (4, 25, 27, 33).

TABLE 2 | Comparison of subcortical volumes (mm^3 and SE) across groups.[a]

Region	RLS cases $n = 39$	Controls $n = 117$	p	FDR-sig
Left nucleus caudate	3,280.88 (58.56)	3,214.5 (33.8)	0.328	n.s.
Left hippocampus	3,881.74 (56.85)	4,012.67 (32.82)	0.048	n.s.
Left globus pallidus	1,538.77 (44.81)	1,629.51 (25.86)	0.082	n.s.
Left putamen	4,786.91 (81.31)	4,854.70 (46.93)	0.471	n.s.
Left thalamus	7,481.04 (78.46)	7,542.56 (45.29)	0.498	n.s.
Right nucleus caudate	3,381.60 (56.37)	3,308.45 (32.54)	0.263	n.s.
Right hippocampus	4,012.95 (61.09)	4,075.04 (35.26)	0.380	n.s.
Right globus pallidus	1,629.77 (39.02)	1,688.05 (22.52)	0.198	n.s.
Right putamen	4,811.87 (70.33)	4,886.11 (40.59)	0.362	n.s.
Right thalamus	7,252.85 (76.20)	7,270.17 (40.59)	0.844	n.s.

RLS, restless legs syndrome; FDR-sig, false discovery rate corrected significance at $q < 0.05$; n.s., not significant.

[a]*The group comparison is adjusted for overall brain volume.*

TABLE 3 | Associations between allele frequency and RLS.[a]

Single nucleotide polymorphisms (risk allele)	Odds ratio	p
rs12469063 (G)	1.403	0.252
rs6710341 (G)	1.029	0.940
rs3923809 (A)	1.031	0.917
rs4714156 (C)	1.395	0.366
rs9394492 (C)	0.945	0.848
rs4626664 (A)	1.339	0.455
rs11635424 (G)	2.149	0.032
rs6747972 (G)	1.049	0.852
rs3104767 (G)	1.472	0.197

RLS, restless legs syndrome.

[a]*The logistic regressions are adjusted for age and sex.*

Genetic Risk for RLS and Subcortical Volumes

No significant associations between the odds ratio weighted GRS derived from the respective SNPs and subcortical as well as hippocampal volumes were found. The regression coefficients are presented in **Table 4**.

DISCUSSION

In this nested case-control study, we examined potential alterations in shape and volume of subcortical structures and the hippocampus in cases with RLS versus controls. While potential volumetric alterations of subcortical structures and the hippocampus have been investigated previously using VBM (9–15), shape differences in the caudate nucleus, hippocampus, globus pallidus, and putamen have not been compared before between cases with RLS and controls. Analyzing shape differences, however, is important in order to determine the exact locations where potential anatomical changes in subcortical structures occur. Knowledge of localized shape differences may also aid the interpretation of the relationship with other anatomical findings, e.g., when localized changes in thalamic shape are associated with adjacent reductions of white matter volume (34). Our analyses revealed no group differences in either shape or volume of the caudate nucleus, hippocampus, globus pallidus, putamen, and thalamus. The lack of volume differences supports previous findings (12–15), suggesting that RLS is not accompanied by any changes of subcortical gray matter. Instead, it seems more likely that alterations of the dopaminergic system (6), possibly induced by genes involved in neurodevelopment [*MEIS1* (35, 36) and *TOX3* (37)], protection of dopaminergic neurons [*MAP2K5* (38)], sleep disturbances [*BTBD9* (39)], modulation of dopaminergic neurotransmission [*PTPRD* (40)], and iron regulation within the brain [*BTBD9* (41)], may lead to changes in functional brain networks. In particular, increased functional connectivity has been reported in sensory-thalamic, basal ganglia-thalamic, and other cortical and subcortical networks in patients with RLS, whereas symptom severity correlated with increased network connectivity (42). Hence, in the absence of gray matter alterations, RLS is more likely to be characterized by inefficient network performance.

TABLE 4 | Regression coefficients for the GRS per subcortical region.

	GRS rs12469063	GRS rs6710341	GRS rs3923809	GRS rs4714156	GRS rs9394492	GRS rs4626664	GRS rs11635424	GRS rs6747972	GRS rs3104767
Left caudate nucleus	22.17	59.96	18.86	−21.91	4.56	82.02	−3.489	−21.52	3.802
Left hippocampus	29.36	9.56	80.71	49.67	37.60	46.21	−33.49	11.85	14.77
Left globus pallidus	31.40	2.24	−20.92	−29.71	9.74	34.41	11.43	−17.63	−7.20
Left putamen	3.02	65.17	−62.88	−78.58	−52.31	41.77	35.82	−4.80	−20.85
Left thalamus	−14.97	20.83	−29.97	−62.61	−48.98	−10.72	−37.39	−25.45	74.51
Right caudate nucleus	−6.84	38.38	55.30	3.12	−20.29	63.33	−0.13	−13.95	−11.49
Right hippocampus	−9.53	48.50	−14.32	−15.16	48.69	22.36	−28.04	−65.148	28.52
Right globus pallidus	34.81	34.24	−17.79	−14	26.33	44.08	−2.37	4.56	−13.61
Right putamen	−14.59	64.07	17.27	−32.39	−52.04	40.80	−20.83	−8.14	−0.66
Right thalamus	1.60	28.61	−20.06	−67.19	−17.31	37.72	−40.70	−14.14	72.87

GRS, genetic risk score.

The regression analyses were adjusted for age, sex, and overall brain volume.

Although RLS has previously been associated with several SNPs within regions of the above-mentioned genes (4), the exact mechanisms how these SNPs contribute to the development of RLS are still unknown. Hence, we also explored potential associations between known genetic risk markers for RLS and alterations of subcortical volumes to evaluate if these are a potential mediator of the genotype-disease association. Only SNP rs11635424 was significantly associated with RLS. While most of the remaining RLS-related SNPs indicated risks, i.e., odds ratios larger than 1 for the risk alleles, these associations did not reach statistical significance given the small sample size in our study. The magnitude of effect sizes is largely in line with previous studies (4, 25, 27, 33), suggesting that larger samples are advantageous to detect effects of allele frequency in the context of RLS. With regards to the volume of the subcortical structures and the hippocampus, we did not find a significant association with SNP rs11635424 or any of the other eight SNPs, suggesting that RLS-related variations in the genome do not play an important part in the volumetric appearance of subcortical structures and the hippocampus.

The present study is limited by its sample size which is rather small regarding the search for genetic factors contributing to the development of RLS. However, the primary aim was to compare subcortical as well as hippocampal shapes and volumes between RLS cases and controls and to analyze the influence of the odds ratio weighted genetic risk for RLS on subcortical and hippocampal volumes. Within the field of 3 T MRI-literature, the present study is the largest investigating potential volumetric alterations in RLS cases versus controls.

We conclude that RLS is unrelated to changes in shape and volume of the caudate nucleus, hippocampus, globus pallidus, putamen, and thalamus. The SNP rs11635424 was significantly associated with RLS in our sample. The odds ratio weighted GRS from each of the nine SNPs as well as a summed GRS do not account for any volume alterations of subcortical gray matter.

ETHICS STATEMENT

This study was carried out in accordance with the recommendations of the ethics committee of the University of Münster and the Westphalian Chamber of Physicians with written informed consent from all subjects. All subjects gave written informed consent in accordance with the Declaration of Helsinki. The protocol was approved by the University of Münster and the Westphalian Chamber of Physicians.

AUTHOR CONTRIBUTIONS

Design and concept of the BiDirect Study: KB. Preprocessing and data analyses: MH, RR, and AS. Drafting the manuscript and figures: MH. Technical assistance and commenting on the preprocessing of imaging data: BS and UD.

ACKNOWLEDGMENTS

The present work was supported by a grant to KB from the German Federal Ministry of Education and Research (BMBF; grant FKZ-01ER0816 and FKZ-01ER1506). UD was funded by the German Research Foundation (DFG, grant FOR2107 DA1151/5-1; SFB-TRR58, Project C09) and the Interdisciplinary Center for Clinical Research (IZKF) of the medical faculty of Münster (grant Dan3/012/17).

REFERENCES

1. Garcia-Borreguero D, Egatz R, Winkelmann J, Berger K. Epidemiology of restless legs syndrome: the current status. *Sleep Med Rev* (2006) 10:153–67. doi:10.1016/j.smrv.2006.01.001
2. Cuellar NG, Strumpf NE, Ratcliffe SJ. Symptoms of restless legs syndrome in older adults: outcomes on sleep quality, sleepiness, fatigue, depression, and quality of life. *J Am Geriatr Soc* (2007) 55:1387–92. doi:10.1111/j.1532-5415.2007.01294.x
3. Phillips B, Hening W, Britz P, Mannino D. Prevalence and correlates of restless legs syndrome. *Chest* (2006) 129:76–80. doi:10.1378/chest.129.1.76
4. Winkelmann J, Schormair B, Lichtner P, Ripke S, Xiong L, Jalilzadeh S, et al. Genome-wide association study of restless legs syndrome identifies common variants in three genomic regions. *Nat Genet* (2007) 39:1000–6. doi:10.1038/ng2099
5. Stefansson H, Rye DB, Hicks A, Petursson H, Ingason A, Thorgeirsson TE, et al. A genetic risk factor for periodic limb movements in sleep. *N Engl J Med* (2007) 357:639–47. doi:10.1056/NEJMoa072743
6. Earley CJ, Connor J, Garcia-Borreguero D, Jenner P, Winkelman J, Zee PC, et al. Altered brain iron homeostasis and dopaminergic function in restless legs syndrome (Willis-Ekbom disease). *Sleep Med* (2014) 15:1288–301. doi:10.1016/j.sleep.2014.05.009
7. Haber SN. The place of dopamine in the cortico-basal ganglia circuit. *Neuroscience* (2014) 282:248–57. doi:10.1016/j.neuroscience.2014.10.008
8. Sullivan EV, Adalsteinsson E, Rohlfing T, Pfefferbaum A. Relevance of iron deposition in deep gray matter brain structures to cognitive and motor performance in healthy elderly men and women: exploratory findings. *Brain Imaging Behav* (2009) 3:167–75. doi:10.1007/s11682-008-9059-7
9. Chang Y, Chang HW, Song H, Ku J, Earley CJ, Allen RP, et al. Gray matter alteration in patients with restless legs syndrome: a voxel-based morphometry study. *Clin Imaging* (2015) 39:20–5. doi:10.1016/j.clinimag.2014.07.010
10. Hornyak M, Ahrendts JC, Spiegelhalder K, Riemann D, Voderholzer U, Feige B, et al. Voxel-based morphometry in unmedicated patients with restless legs syndrome. *Sleep Med* (2007) 9:22–6. doi:10.1016/j.sleep.2006.09.010
11. Etgen T, Draganski B, Ilg C, Schröder M, Geisler P, Hajak G, et al. Bilateral thalamic gray matter changes in patients with restless legs syndrome. *Neuroimage* (2005) 24:1242–7. doi:10.1016/j.neuroimage.2004.10.021
12. Margariti PN, Astrakas LG, Tsouli SG, Hadjigeorgiou GM, Konitsiotis S, Argyropoulou MI. Investigation of unmedicated early onset restless legs syndrome by voxel-based morphometry, T2 relaxometry, and functional MR imaging during the night-time hours. *Am J Neuroradiol* (2012) 33:667–72. doi:10.3174/ajnr.A2829
13. Celle S, Roche F, Peyron R, Faillenot I, Laurent B, Pichot V, et al. Lack of specific gray matter alterations in restless legs syndrome in elderly subjects. *J Neurol* (2010) 257:344–8. doi:10.1007/s00415-009-5320-2
14. Belke M, Heverhagen JT, Keil B, Rosenow F, Oertel WH, Stiasny-Kolster K, et al. DTI and VBM reveal white matter changes without associated gray matter changes in patients with idiopathic restless legs syndrome. *Brain Behav* (2015) 5(9):e00327. doi:10.1002/brb3.327
15. Rizzo G, Tonon C, Testa C, Manners D, Vetrugno R, Pizza F, et al. Abnormal medial thalamic metabolism in patients with idiopathic restless legs syndrome. *Brain* (2012) 135:3712–20. doi:10.1093/brain/aws266
16. Patenaude B, Smith SM, Kennedy DN, Jenkinson MA. Bayesian model of shape and appearance for subcortical brain segmentation. *Neuroimage* (2011) 56:907–22. doi:10.1016/j.neuroimage.2011.02.046
17. Teismann H, Wersching H, Nagel M, Arolt V, Heindel W, Baune BT, et al. Establishing the bidirectional relationship between depression and subclinical

arteriosclerosis – rationale, design, and characteristics of the BiDirect Study. *BMC Psychiatry* (2014) 14:174. doi:10.1186/1471-244X-14-174
18. Teuber A, Sundermann B, Kugel H, Schwindt W, Heindel W, Minnerup J, et al. MR imaging of the brain in large cohort studies: feasibility report of the population- and patient-based BiDirect study. *Eur Radiol* (2016) 27(1):231–8. doi:10.1007/s00330-016-4303-9
19. Allen RP, Picchietti D, Hening WA, Trenkwalder C, Walters AS, Montplaisi J, et al. Restless legs syndrome: diagnostic criteria, special considerations, and epidemiology. A report from the restless legs syndrome diagnosis and epidemiology workshop at the National Institutes of Health. *Sleep Med* (2003) 4:101–19. doi:10.1016/S1389-9457(03)00010-8
20. Berger K, Von Eckardstein A, Trenkwalder C, Rothdach A, Junker R, Weiland SK. Iron metabolism and the risk of restless legs syndrome in an elderly general population – the MEMO-study. *J Neurol* (2002) 249:1195–9. doi:10.1007/s00415-002-0805-2
21. Faul F, Erdfelder E, Lang A-G, Buchner A. G*Power 3: a flexible statistical power analysis program for the social, behavioral, and biomedical sciences. *Behav Res Methods* (2007) 39:175–91. doi:10.3758/BF03193146
22. Jenkinson M, Beckmann CF, Behrens TEJ, Woolrich MW, Smith SM. FSL. *Neuroimage* (2012) 62:782–90. doi:10.1016/j.neuroimage.2011.09.015
23. Jenkinson M, Bannister P, Brady M, Smith S. Improved optimization for the robust and accurate linear registration and motion correction of brain images. *Neuroimage* (2002) 17:825–41. doi:10.1006/nimg.2002.1132
24. Zhang Y, Brady M, Smith S. Segmentation of brain MR images through a hidden Markov random field model and the expectation-maximization algorithm. *IEEE Trans Med Imaging* (2001) 20:45–57. doi:10.1109/42.906424
25. Schormair B, Kemlink D, Roeske D, Eckstein G, Xiong L, Lichtner P, et al. PTPRD (protein tyrosine phosphatase receptor type delta) is associated with restless legs syndrome. *Nat Genet* (2008) 40:946–8. doi:10.1038/ng.190
26. Spieler D, Kaffe M, Knauf F, Bessa J, Tena JJ, Giesert F, et al. Restless legs syndrome-associated intronic common variant in Meis1 alters enhancer function in the developing telencephalon. *Genome Res* (2014) 24:592–603. doi:10.1101/gr.166751.113
27. Winkelmann J, Czamara D, Schormair B, Knauf F, Schulte EC, Trenkwalder C, et al. Genome-wide association study identifies novel restless legs syndrome susceptibility Loci on 2p14 and 16q12.1. *PLoS Genet* (2011) 7:e1002171. doi:10.1371/journal.pgen.1002171
28. Howie B, Fuchsberger C, Stephens M, Marchini J, Abecasis GR. Fast and accurate genotype imputation in genome-wide association studies through pre-phasing. *Nat Genet* (2012) 44:955–9. doi:10.1038/ng.2354
29. Radloff LS. The CES-D scale: a self-report depression scale for research in the general population. *Appl Psychol Meas* (1977) 1:385–401. doi:10.1177/014662167700100306
30. Szentkiralyi A, Volzke H, Hoffmann W, Trenkwalder C, Berger K. Multimorbidity and the risk of restless legs syndrome in 2 prospective cohort studies. *Neurology* (2014) 82:2026–33. doi:10.1212/WNL.0000000000000470
31. Winkler AM, Ridgway GR, Webster MA, Smith SM, Nichols TE. Permutation inference for the general linear model. *Neuroimage* (2014) 92:381–97. doi:10.1016/j.neuroimage.2014.01.060
32. Benjamini Y, Hochberg Y. Controlling the false discovery rate: a practical and powerful approach to multiple testing. *J R Stat Soc Ser B* (1995) 57:289–300.
33. Schormair B, Plag J, Kaffe M, Gross N, Czamara D, Samtleben W, et al. MEIS1 and BTBD9: genetic association with restless leg syndrome in end stage renal disease. *J Med Genet* (2011) 48:462–6. doi:10.1136/jmg.2010.087858
34. Xia S, Li X, Kimball AE, Kelly MS, Lesser I, Branch C. Thalamic shape and connectivity abnormalities in children with attention-deficit/hyperactivity disorder. *Psychiatry Res* (2012) 204:161–7. doi:10.1016/j.pscychresns.2012.04.011
35. Waskiewicz AJ, Rikhof HA, Hernandez RE, Moens CB. Zebrafish Meis functions to stabilize Pbx proteins and regulate hindbrain patterning. *Development* (2001) 128:4139–51.
36. Erickson T, French CR, Waskiewicz AJ. Meis1 specifies positional information in the retina and tectum to organize the zebrafish visual system. *Neural Dev* (2010) 5:22. doi:10.1186/1749-8104-5-22
37. Sahu SK, Fritz A, Tiwari N, Kovacs Z, Pouya A, Wüllner V, et al. TOX3 regulates neural progenitor identity. *Biochim Biophys Acta* (2016) 1859:833–40. doi:10.1016/j.bbagrm.2016.04.005
38. Cavanaugh JE, Jaumotte JD, Lakoski JM, Zigmond MJ. Neuroprotective role of ERK1/2 and ERK5 in a dopaminergic cell line under basal conditions and in response to oxidative stress. *J Neurosci Res* (2006) 84:1367–75. doi:10.1002/jnr.21024
39. DeAndrade MP, Johnson RL, Unger EL, Zhang L, van Groen T, Gamble KL, et al. Motor restlessness, sleep disturbances, thermal sensory alterations and elevated serum iron levels in Btbd9 mutant mice. *Hum Mol Genet* (2012) 21:3984–92. doi:10.1093/hmg/dds221
40. Earley CJ, Uhl GR, Clemens S, Ferré S. Connectome and molecular pharmacological differences in the dopaminergic system in restless legs syndrome (RLS): plastic changes and neuroadaptations that may contribute to augmentation. *Sleep Med* (2017) 31:71–7. doi:10.1016/j.sleep.2016.06.003
41. Jellen LC, Beard JL, Jones BC. Systems genetics analysis of iron regulation in the brain. *Biochimie* (2009) 91:1255–9. doi:10.1016/j.biochi.2009.04.009
42. Gorges M, Rosskopf J, Müller H-P, Lindemann K, Hornyak M, Kassubek J. Patterns of increased intrinsic functional connectivity in patients with restless legs syndrome are associated with attentional control of sensory inputs. *Neurosci Lett* (2016) 617:264–9. doi:10.1016/j.neulet.2016.02.043

Conflict of Interest Statement: MH, BS, RR, AS, and UD have no conflicts of interest to disclose. For the conduction (2007–2014) of a study on the course of restless legs syndrome, KB has received unrestricted grants to the University of Münster from the German Restless Legs Society and Boehringer Ingelheim Pharma, Mundipharma Research, Neurobiotec, Roche Pharma, UCB Germany, UCB Switzerland, and Vifor Pharma.

frontiers in Neurology

BRIEF RESEARCH REPORT
published: 29 November 2018
doi: 10.3389/fneur.2018.01022

Imaging Individual Differences in the Response of the Human Suprachiasmatic Area to Light

Elise M. McGlashan[1], *Govinda R. Poudel*[1,2,3], *Parisa Vidafar*[1], *Sean P. A. Drummond*[1] *and Sean W. Cain*[1]*

[1] Monash Institute of Cognitive and Clinical Neurosciences and School of Psychological Sciences, Monash University, Melbourne, VIC, Australia, [2] Sydney Imaging, The University of Sydney, Camperdown, NSW, Australia, [3] Mary Mackillop Institute of Health Research, Australian Catholic University, Melbourne, VIC, Australia

Circadian disruption is associated with poor health outcomes, including sleep and mood disorders. The suprachiasmatic nucleus (SCN) of the anterior hypothalamus acts as the master biological clock in mammals, regulating circadian rhythms throughout the body. The clock is synchronized to the day/night cycle via retinal light exposure. The BOLD-fMRI response of the human suprachiasmatic area to light has been shown to be greater in the night than in the day, consistent with the known sensitivity of the clock to light at night. Whether the BOLD-fMRI response of the human suprachiasmatic area to light is related to a functional outcome has not been demonstrated. In a pilot study ($n = 10$), we investigated suprachiasmatic area activation in response to light in a 30 s block-paradigm of lights on (100 lux) and lights off (<1 lux) using the BOLD-fMRI response, compared to each participant's melatonin suppression response to moderate indoor light (100 lux). We found a significant correlation between activation in the suprachiasmatic area in response to light in the scanner and melatonin suppression, with increased melatonin suppression being associated with increased suprachiasmatic area activation in response to the same light level. These preliminary findings are a first step toward using imaging techniques to measure individual differences in circadian light sensitivity, a measure that may have clinical relevance in understanding vulnerability in disorders that are influenced by circadian disruption.

Keywords: melatonin suppression, light sensitivity, circadian rhythms, light exposure, BOLD-fMRI

OPEN ACCESS

Edited by:
Kai Spiegelhalder, Klinik für Psychiatrie und Psychotherapie, Universitätsklinikum Freiburg, Germany

Reviewed by:
Pablo Torterolo, Universidad de la República, Uruguay
Chiara Baglioni, University Hospital Freiburg, Germany

***Correspondence:**
Sean W. Cain
sean.cain@monash.edu

Specialty section:
This article was submitted to Sleep and Chronobiology, a section of the journal Frontiers in Neurology

Received: *27 July 2018*
Accepted: *13 November 2018*
Published: *29 November 2018*

Citation:
McGlashan EM, Poudel GR, Vidafar P, Drummond SPA and Cain SW (2018) Imaging Individual Differences in the Response of the Human Suprachiasmatic Area to Light. Front. Neurol. 9:1022. doi: 10.3389/fneur.2018.01022

INTRODUCTION

The human circadian system is responsible for regulating physiological processes across the 24-h day. This includes rhythms in alertness, sleep-wake behavior, metabolism, mood and cognitive function (1–3). The endogenous master clock (the suprachiasmatic nucleus, SCN) generates rhythms of ∼24 h, which are synchronized to the environmental light/dark cycle via retinal light exposure (4).

Disrupting the relationship between the light-dark cycle, behavior and internal rhythms has significant consequences for health. Circadian disruption is a factor in the etiology of mood disorders (5), cognitive decline (6), the onset of metabolic diseases such as diabetes (3, 7), cardiovascular health (8), and is associated with an increased risk for cancer (9). Although

these health concerns may arise from the uncoupling of rhythms with behavior (e.g., cross-meridian travel, engaging in shift-work), it has also been suggested that an abnormal response to environmental light may lead to the development of circadian disruption in the absence of, or in combination with, behavioral change (10, 11). Both hyper- and hypo- sensitivity to environmental light could lead to the development of abnormal circadian synchronization (10–12). Therefore, an abnormal response of the circadian system to light is a potentially important factor for disease vulnerability.

Better characterization of the function of the SCN (master circadian clock) in response to light cues may provide clinically relevant information, leading to improved interventions. However, our understanding of human SCN function in a clinical context to date has often relied on peripheral measurements of clock function. For example, the most common assessments of SCN function involve measuring the timing of melatonin onset (usually via dim-light melatonin onset; DLMO) for circadian timing [e.g., (13, 14)], and melatonin suppression to assess circadian light responsiveness [e.g., (11, 15)]. However, for patients taking beta-blockers, antidepressants, or sleeping aids such as exogenous melatonin, these assessments will be uninformative due to the pharmacological impact on endogenous melatonin levels, or cross reactivity with existing assays (16, 17). The ability to directly assess the activity of the SCN in response to light cues would overcome these limitations.

There is a substantial neuroimaging literature examining non-visual light responses in humans. For example, the BOLD-fMRI response of the suprachiasmatic area to light during the day, evening, and night has been imaged, showing differential activation across times of day which matches the known rhythm in the responsiveness of the circadian system to light (18). Studies have also shown enhancement of activity in brain areas associated with working memory, alertness and cognition [e.g., (19, 20)] and emotional processing (21) in response to blue light, compared to green. Further, the use of light stimuli which differentially stimulate melanopsin (high- or low-stimulation) during fMRI has been utilized to characterize the cerebral activation associated with non-visual light processes (22). However, the measurement of suprachiasmatic area function in humans has yet to be related to individual responsiveness using established laboratory techniques. In this study we examined, within individuals, the relationship between suprachiasmatic area activation in response to light in an fMRI scanner and melatonin suppression to light in the laboratory. We hypothesized increased activation of the suprachiasmatic area in response to light would be associated with increased melatonin suppression to light.

MATERIALS AND METHODS

Participants

Ten healthy young men and women (5 men, M_{age} = 20.80, SD = 1.87) were recruited. Participants were free of medical and psychiatric conditions and were not taking any medications at the time of the study. Women were naturally cycling (i.e., not using any hormonal contraception).

In-laboratory Circadian Assessments

All participants completed an in-laboratory assessment of circadian light sensitivity. This involved an assessment of dim-light melatonin levels and a subsequent light exposure of ∼100 lux. Sessions ran from ∼4 h prior to the participants' bedtime, until 1 h after, during which the participant remained awake and seated (other than for bathroom breaks). These two sessions were a minimum of 1 week apart, with the dim-light session occurring first. Participants maintained a strict 8:16 h sleep-wake dark-light schedule for at least 1 week prior to, and in between sessions, whereby >1 deviation of more than 30-min in 1 week would be exclusionary. Adherence to the schedule was monitored using wrist-worn actigraphy (Actiwatch Spectrum Plus or L, Philips Respironics, OR, USA) and sleep diaries. Schedules were selected to be in line with participants typical sleep-wake behavior, an example schedule, with an overview of the protocol is available in the **Supplementary Material**. During test-sessions, hourly saliva samples were taken using salivettes (Sarstedt, Germany), which were then assayed in duplicate for melatonin at the Adelaide Research Assay Facility using radioimmunoassay with the G280 antibody and the [1251]2-iodomelatonin radioligand (LOD 4.3 pMol).

In MRI Light Exposure and Imaging Procedure

Participants completed an fMRI scan beginning ∼1 h prior to habitual bedtime. For 1 h prior to this they were seated in dim-lighting conditions of <10 lux. Prior to their scan, participants provided a urine sample for toxicology to be conducted, with a positive result being exclusionary (n = 0, SureStep 6 Panel, Medvet, South Australia, Australia).

All subjects were imaged using a 3T Scanner (Siemens Magnetom Skyra) with 20 channel head coils. High-resolution anatomical images of the whole brain were acquired using T1-weighted anatomical scans (TE = 2.07 ms; TR = 2.3 s; field of view: 256 × 256 mm; slice thickness: 1 mm). Functional images were acquired using echo-planar-imaging (TR: 2.06 s; TE: 24 ms; field of view: 190 × 190 mm; slice thickness: 3 mm; number of slices: 41; flip angle = 90, number of volumes = 177). The first five images of each session were discarded to allow for T1 equilibration.

Participants were requested to lay supine in the MRI scanner, while an optic-fiber-based light delivery system was fitted on the MRI head coil. This device consisted of a halogen light source (DC950H, Dolan-Jenner Industries, MA, USA), which transmitted light through metal-free fiber optic cables (100 strand cable with 0.75 mm fibers, Optic Fiber Lighting, Sydney, AU) to two circular plastic diffusers (40 mm diameter) positioned ∼50 mm above each eye. The diffusers were designed to bathe each eye in light, achieving an even spread of illumination. Light stimuli had a CCT of ∼2800 K (λp = 650 nm), and was delivered at two intensities, ∼100 lux (42.73 $\mu W/cm^2$) and ∼1000 lux (392.28 $\mu W/cm^2$).

Each participant was exposed to a passive light stimulus paradigm in which they were requested to keep their eyes open (other than normal blinking). This was comprised of alternating periods of lights off (darkness, six 30 s epochs) and lights on at a moderate level (100 lux, six 30 s epochs) or bright level

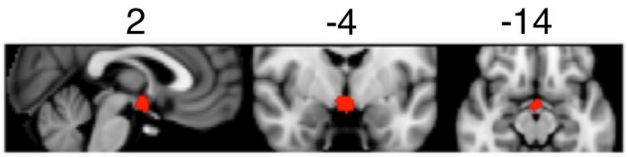

FIGURE 1 | Mask of the suprachiasmatic area used to determine BOLD activation during the light exposure paradigm.

(1000 lux, six 30 s epochs). Moderate and bright blocks (of 6 min total duration each) were delivered separately, with the moderate light exposure block always being presented first. Due to the aversive nature of the 1000 lux bright-light stimuli (which often led to significant eye closures), only data for the moderate light exposures are reported here.

Data Analysis

Melatonin Suppression

Area under the curve (AUC) was calculated for the final 2 h of each dim-light control, and each 100-lux light exposure (where melatonin levels were adequate in all participants in our protocol). Average percent suppression across the 2 h was then calculated by determining the percent change in AUC from baseline to the 100-lux light exposure for each individual.

MRI Data Processing

Detailed information regarding fMRI data processing and analysis can be found in the **Supplementary Material**. Briefly, MRI data were pre-processed using FSL (FMRIB's Software Library, www.fmrib.ox.ac.uk/fsl). For each participant, pre-processed fMRI data were analyzed using first-level general linear models. The linear models included regressors for light on blocks and standard motion parameters (six regressors). To focus our analysis on the suprachiasmatic area of the brain, we generated a mask covering hypothalamic area using a meta-analytic tool NeuroSynth (http://neurosynth.org/analyses/terms/hypothalamus/). This mask (see **Figure 1**) covered both the anterior and posterior hypothalamus including the suprachiasmatic area.

Statistical Analyses

A correlational analysis was used to assess the relationship between suprachiasmatic area function in response to light (100 lux relative to dark periods) and melatonin suppression. A Spearman's correlation was used due to the small sample size and potential non-normality of the BOLD response.

RESULTS

There was a significant, strong positive correlation between suprachiasmatic area activity during light exposure periods (relative to dark) and melatonin suppression (**Figure 2**). Increased suprachiasmatic area activation was associated with an increase in melatonin suppression (i.e., greater circadian light sensitivity).

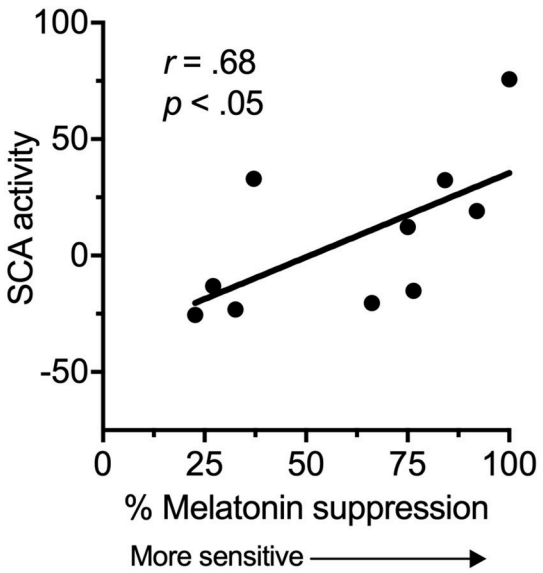

FIGURE 2 | Relationship between the fMRI BOLD response in the suprachiasmatic area (SCA) during 100 lux light exposures (relative to dark), and melatonin suppression.

DISCUSSION

This study provides preliminary evidence for a relationship between suprachiasmatic area activation in response to light and an established in-laboratory measure of circadian light sensitivity. We found a significant relationship between suprachiasmatic area activation and melatonin suppression, indicating that an increase in fMRI measured suprachiasmatic area activation in response to light related to an increase in circadian light sensitivity. Thus, these are the first data in humans to show a relationship between a proximal measure of activity in the anterior hypothalamus and a functional outcome.

An increase in melatonin suppression relates to larger shifts in circadian phase (23), and has been associated with disease states (10, 11). Our results suggest that increased melatonin suppression findings may reflect increased activation of the SCN in response to environmental light. Light information is received at the retina by intrinsically photosensitive retinal ganglion cells (iPRGCs), which then project to the SCN via the retinohypothalamic tract (RHT), and to other brain areas (24, 25). Light exposure leads to changes in circadian timing, amplitude, levels of alertness and mood (23, 26, 27). The magnitude of the impact of this light on the circadian system will be partly dependent on individual differences in light sensitivity, and our results demonstrate that this inter-individual variability may arise from functional differences in the ability of retinal light exposure to activate the SCN.

Circadian dysfunction has been associated with several chronic disease states, including mood disorders (10, 28), metabolic and cardiovascular disease (29) and sleep disorders

(11, 14, 30). Abnormalities in circadian light sensitivity may be a trait vulnerability for mood disorders with variable or decreased sensitivity being observed in seasonal affective disorder (12), while hypersensitivity to light has been observed in bipolar disorder (10, 28), and in some sleep disorders or disturbances (11, 31). Imaging of the response to moderate light as used in this study may reveal abnormal SCN function, which could lead to circadian dysfunction.

It should be noted that although a significant relationship was observed here between suprachiasmatic area activation and melatonin suppression, our sample was small, and these data do not indicate that an individual scan of the response to light can currently replace melatonin suppression as an indicator of circadian light sensitivity. The BOLD fMRI response to light in the suprachiasmatic area may instead prove a useful clinical tool for studying changes in light sensitivity associated with either a clinical diagnosis, or pharmacological intervention. Given suggestions that light sensitivity can change across a disease course (12), and may mediate treatment response in mood disorders (32, 33), this has important clinical implications. However, further characterization of the relationship between suprachiasmatic area activation and melatonin suppression is required in order to establish clinically meaningful ways of interpreting individual data.

This study has shown, in a small sample, evidence for a relationship between suprachiasmatic area BOLD-fMRI activation to light and an established measure of circadian light sensitivity. This is a first step in the development of imaging techniques for the assessment of individual differences in circadian function. This is critical given the pervasive nature of circadian dysfunction in disease states.

ETHICS AND DATA AVAILABILITY STATEMENT

All procedures were approved by the Monash University Human Research Ethics Committee (MUHREC) prior to commencement (Project 4760). Participants gave written, informed consent prior to participation and were reimbursed for their time. The raw data supporting the conclusions of this manuscript will be made available by the authors, without undue reservation, to any qualified researcher.

AUTHOR CONTRIBUTIONS

The study was conceived by SC. All authors contributed to the study design. GP was responsible for programing the light delivery device and MRI sequences, and completing fMRI data analysis. EM and PV were responsible for recruitment, data collection, and melatonin data processing. EM was responsible for the final data analysis and writing the manuscript. All authors reviewed and contributed to the manuscript prior to submission for publication.

FUNDING

This project was supported by a project grant from the National Health and Medical Research Council (NHMRC) awarded to SC (Project 1064231), and a Platform Access Grant (PAG) from the faculty of Medicine Nursing and Health Sciences at Monash University awarded to SC, SD and GP (15-0038). EM was supported by an Australian Government Research and Training Program (RTP) scholarship. PV was supported by a scholarship from the National Health and Medical Research Council (NHMRC), via the NeuroSleep Centre for Research Excellence.

ACKNOWLEDGMENTS

We would like to thank Gilles Vandewalle for his advice and consultation regarding the build of our custom light device, and the Monash Instrumentation Facility for their assistance designing and constructing the device. We would also like to acknowledge the radiographers and staff of the Monash Biomedical Imaging center (MBI) at Monash University for the use of their facilities, and assistance in running our studies out of business hours–in particular Richard McIntyre. Lastly, we would like to thank the staff and students of the Monash University Sleep and Circadian Medicine Laboratory for their assistance in the running of in-laboratory circadian assessments.

SUPPLEMENTARY MATERIAL

The Supplementary Material for this article can be found online at: https://www.frontiersin.org/articles/10.3389/fneur.2018.01022/full#supplementary-material

REFERENCES

1. Czeisler CA, Weitzman ED, Moore-Ede MC, Zimmerman JC, Knauer RS. Human sleep: its duration and organization depend on its circadian phase. *Science* (1980) 210:1264–7. doi: 10.1126/science.7434029
2. Dijk DJ, Duffy JF, Czeisler CA. Circadian and sleep/wake dependent aspects of subjective alertness and cognitive performance. *J Sleep Res.* (1992) 1:112–7. doi: 10.1111/j.1365-2869.1992.tb00021.x
3. Scheer FA, Hilton MF, Mantzoros CS, Shea SA. Adverse metabolic and cardiovascular consequences of circadian misalignment. *Proc Natl Acad Sci USA*. (2009) 106:4453–8. doi: 10.1073/pnas.0808180106
4. Pittendrigh C, Daan S. A functional analysis of circadian pacemakers in nocturnal rodents. *J Compar Physiol.* (1976) 106:223–52. doi: 10.1007/BF01417856
5. Harvey A. Sleep and circadian functioning: critical mechanisms in the mood disorders? *Ann Rev Clin Psychol.* (2011) 7:297–319. doi: 10.1146/annurev-clinpsy-032210-104550
6. Naismith SL, Hickie IB, Terpening Z, Rajaratnam SW, Hodges JR, Bolitho S, et al. Circadian misalignment and sleep disruption in mild cognitive impairment. *J Alzheimer's Dis.* (2014) 38:857–66. doi: 10.3233/JAD-131217
7. Buxton O, Cain S, O'connor S, Porter J, Duffy J, Wang CC, et al. Adverse metabolic consequences in humans of prolonged sleep restriction combined with circadian disruption. *Sci Transl Med.* (2012) 4:129ra143. doi: 10.1126/scitranslmed.3003200
8. Portaluppi F, Tiseo R, Smolensky MH, Hermida RC, Ayala DE, Fabbian F. Circadian rhythms and cardiovascular health. *Sleep Med Rev.* (2012) 16:151–66. doi: 10.1016/j.smrv.2011.04.003

9. Haus EL, Smolensky MH. Shift work and cancer risk: potential mechanistic roles of circadian disruption, light at night, and sleep deprivation. *Sleep Med Rev.* (2013) 17:273–84. doi: 10.1016/j.smrv.2012.08.003
10. Nathan PJ, Burrows GD, Norman TR. Melatonin sensitivity to dim white light in affective disorders. *Neuropsychopharmacology* (1999) 21:408–13. doi: 10.1016/S0893-133X(99)00018-4
11. Aoki H, Ozeki Y, Yamada N. Hypersensitivity of melatonin suppression in response to light in patients with delayed sleep phase syndrome. *Chronobiol Int.* (2001) 18:263–71. doi: 10.1081/CBI-100103190
12. Thompson C, Stinson D, Smith A. Seasonal affective disorder and season-dependent abnormalities of melatonin suppression by light. *Lancet* (1990) 336:703–6. doi: 10.1016/0140-6736(90)92202-S
13. Emens J, Lewy AJ, Mark J, Arntz D, Rough J. Circadian misalignment in major depressive disorder. *Psychiatry Res.* (2009) 168:259–61. doi: 10.1016/j.psychres.2009.04.009
14. Murray JM, Sletten TL, Magee M, Gordon C, Lovato N, Bartlett DJ, et al. Prevalence of circadian misalignment and its association with depressive symptoms in delayed sleep phase disorder. *Sleep* (2017) 40:zsw002. doi: 10.1093/sleep/zsw002
15. Hallam K, Begg D, Olver J, Norman TR. Abnormal dose-response melatonin suppression by light in bipolar type I patients compared with healthy adult subjects. *Acta Neuropsychiatrica* (2009) 21:246–55. doi: 10.1111/j.1601-5215.2009.00416.x
16. Stoschitzky K, Sakotnik A, Lercher P, Zweiker R, Maier R, Liebmann P, et al. Influence of beta-blockers on melatonin release. *Eur J Clin Pharmacol.* (1999) 55:111–5. doi: 10.1007/s002280050604
17. Carvalho L, Gorenstein C, Moreno R, Pariante C, Markus R. Effect of antidepressants on melatonin metabolite in depressed patients. *J Psychopharmacol.* (2009) 23:315–21. doi: 10.1177/0269881108089871
18. Vimal RLP, Pandey-Vimal MUC, Vimal LSP, Frederick BB, Stopa EG, Renshaw PF, et al. Activation of suprachiasmatic nuclei and primary visual cortex depends upon time of day. *Eur J Neurosci.* (2009) 29:399–410. doi: 10.1111/j.1460-9568.2008.06582.x
19. Vandewalle G, Balteau E, Phillips C, Degueldre C, Moreau V, Sterpenich V, et al. Daytime light exposure dynamically enhances brain responses. *Curr Biol.* (2006) 16:1616–21. doi: 10.1016/j.cub.2006.06.031
20. Vandewalle G, Gais S, Schabus M, Balteau E, Carrier J, Darsaud A, et al. Wavelength-dependent modulation of brain responses to a working memory task by daytime light exposure. *Cerebral Cortex* (2007) 17:2788–95. doi: 10.1093/cercor/bhm007
21. Vandewalle G, Schwartz S, Grandjean D, Wuillaume C, Balteau E, Degueldre C, et al. Spectral quality of light modulates emotional brain responses in humans. *Proc Natl Acad Sci USA.* (2010) 107:19549–54. doi: 10.1073/pnas.1010180107
22. Hung S-M, Milea D, Rukmini AV, Najjar RP, Tan JH, Viénot F, et al. Cerebral neural correlates of differential melanopic photic stimulation in humans. *NeuroImage* (2017) 146:763–9. doi: 10.1016/j.neuroimage.2016.09.061
23. Lockley SW, Brainard GC, Czeisler CA. High sensitivity of the human circadian melatonin rhythm to resetting by short wavelength light. *J Clin Endocrinol Metab.* (2003) 88:4502–5. doi: 10.1210/jc.2003-030570
24. Gooley JJ, Lu J, Chou TC, Scammell TE, Saper CB. Melanopsin in cells of origin of the retinohypothalamic tract. *Nat Neurosci.* (2001) 4:1165. doi: 10.1038/nn768
25. Hattar S, Liao HW, Takao M, Berson DM, Yau KW. Melanopsin-containing retinal ganglion cells: architecture, projections, and intrinsic photosensitivity. *Science* (2002) 295:1065–70. doi: 10.1126/science.1069609
26. Cajochen C, Zeitzer JM, Czeisler C, Dijk DJ. Dose-response relationship for light intensity and ocular and electroencephalographic correlates of human alertness. *Behav Brain Res.* (2000) 115:75–83. doi: 10.1016/S0166-4328(00)00236-9
27. Even C, Schröder CM, Friedman S, Rouillon F. Efficacy of light therapy in nonseasonal depression: a systematic review. *J Affective Disord.* (2008) 108:11–23. doi: 10.1016/j.jad.2007.09.008
28. Lewy A, Nurnberger JI, Wehr TA, Becker LE, Pack D, Powell R-L, et al. Supersensitivity to light: possible trait marker for manic-depressive illness. *Am J Psychiatry* (1985) 146:725–7.
29. Rajaratnam SM, Howard ME, Grunstein RR. Sleep loss and circadian disruption in shift work: health burden and management. *Med J Aust.* (2013) 199:S11–5. doi: 10.5694/mja13.10561
30. Flynn-Evans EE, Shekleton JA, Miller B, Epstein LJ, Kirsch D, Brogna LA, et al. Circadian phase and phase angle disorders in primary insomnia. *Sleep* (2017) 40:zsx163. doi: 10.1093/sleep/zsx163
31. Moderie C, Van Der Maren S, Dumont M. Circadian phase, dynamics of subjective sleepiness and sensitivity to blue light in young adults complaining of a delayed sleep schedule. *Sleep Med.* (2017) 34:148–55. doi: 10.1016/j.sleep.2017.03.021
32. Hallam KT, Olver JS, Horgan JE, Mcgrath C, Norman TR. Low doses of lithium carbonate reduce melatonin light sensitivity in healthy volunteers. *Int J Neuropsychopharmacol.* (2005) 8:255–9. doi: 10.1017/S1461145704004894
33. McGlashan EM, Nandam LS, Vidafar P, Mansfield DR, Rajaratnam SMW, Cain SW. The SSRI citalopram increases the sensitivity of the human circadian system to light in an acute dose. *Psychopharmacology* (2018) 235:3201–9. doi: 10.1007/s00213-018-5019-0

Conflict of Interest Statement: The authors declare that the research was conducted in the absence of any commercial or financial relationships that could be construed as a potential conflict of interest.

Advantages of publishing in Frontiers

OPEN ACCESS
Articles are free to read for greatest visibility and readership

FAST PUBLICATION
Around 90 days from submission to decision

HIGH QUALITY PEER-REVIEW
Rigorous, collaborative, and constructive peer-review

TRANSPARENT PEER-REVIEW
Editors and reviewers acknowledged by name on published articles

Frontiers
Avenue du Tribunal-Fédéral 34
1005 Lausanne | Switzerland

Visit us: www.frontiersin.org
Contact us: info@frontiersin.org | +41 21 510 17 00

REPRODUCIBILITY OF RESEARCH
Support open data and methods to enhance research reproducibility

DIGITAL PUBLISHING
Articles designed for optimal readership across devices

FOLLOW US
@frontiersin

IMPACT METRICS
Advanced article metrics track visibility across digital media

EXTENSIVE PROMOTION
Marketing and promotion of impactful research

LOOP RESEARCH NETWORK
Our network increases your article's readership